Puerto Rico 2012

Extended Abstracts

Editors:

Idalia Ramos
University of Puerto Rico at Humacao

Jorge J. Santiago Avilés
University of Pennsylvania

Ibersensor Permanent Committe

Mariano Aceves-Mejias, Instituto Nacional de Astrofísica, Óptica y Electrónica, México
Manuela Viera, Instituto Superior de Engeneharia de Lisboa, Portugal
Laura M. Lechuga, Research Center on Nanoscience and Nanotechnology, España
Marcelo Bariatto A. Fontes, Faculdade de Tecnologia de São Paulo, Brasil
Olimpia Arias de Fuentes, IMRE, Universidad de la Habana, Cuba
José Antonio Rodríguez Pérez, Universidad de la Habana, Cuba
Francisco Valdés Pérezgasga, Instituto Tecnológico de La Laguna, México
José A. Plaza, Centre Nacional de Microelectrònica, Barcelona, España
Julián Alonso Chamarro, GSB-Universidad Autònoma de Barcelona, España
Cecilia Jiménez Jorquera, Centre Nacional de Microelectrònica, Barcelona, España
Carlos Domínguez Horna, Centre Nacional de Microelectrònica, Barcelona, España
Héctor Gómez, Universidad de la República, Uruguay
Maria Teresa Seabra dos Reis Gomes, Universidade de Aveiro, Portugal
Salvador Alegret, Universidad Autònoma de Barcelona, España
Liliana Fraigi, Instituto Nacional de Tecnología Industrial, Argentina

Local Organizing Committe

Idalia Ramos, PREM, Universidad de Puerto Rico en Humacao
Jorge Santiago Avilés, University of Pennsylvania
José O. Sotero-Esteva, PREM, Universidad de Puerto Rico en Humacao
Rocío Cardona, University of Pennsylvania
Lynette Rivera, PREM, Universidad de Puerto Rico en Humacao
Ramón Rivera, PREM, Universidad de Puuerto Rico en Humacao
Anamaris Meléndez, PREM, Universidad de Puerto Rico en Humacao
Gilda Jiménez, PREM, Escuela Superior Petra Mercado, Humacao

Extended Abstracts of the 8th Ibero-American Congress on Sensors Ibersensor 2012

October 16-19, 2012

Editors:

Idalia Ramos
University of Puerto Rico at Humacao

Jorge J. Santiago Avilés
University of Pennsylvania

Introduction

The PREM-UPRH Partnership for Research and Education from the University of Puerto Rico at Humacao welcomes you to the 8th Ibero-American Congress on Sensors (Ibersensor 2012). Ibersensor is a forum of the Spanish and Portuguese speaking scientific community, working in the fields of development of sensors of every kind and their applications. Previous conferences series were successfully carried out in La Habana, Cuba (1998), Buenos Aires, Argentina (2000), Lima, Perú (2002), Puebla, México (2004), Montevideo, Uruguay (2006), Sao Paulo, Brasil (2008), and Lisboa, Portugal (2010).

We thank all the authors and reviewers for their scientific contributions. We would also like to acknowledge support from the following agencies and programs: NSF-PREM (DMR-0934195), NSF Nano-Bio Interface Center, and NASA Center for Advanced Nanoscale Materials.

Humacao, Carolina, and San Juan, Puerto Rico, October 2012

Idalia Ramos, Co-Chair Ibersensor 2012

Jorge J. Santiago-Avilés, Co-Chair Ibersensor 2012

Mariano Aceves-Mijares, President Ibersensor Permanent Committee

Table of Contents

Chapter 1: Nanosensors

Hydrogen Sensors with TiO_2 and TiO_xN_y nanotubes

K.F.Albertin[1*], T.C. Bohn[1], T.M Fraga[2] and I.Pereyra[2]
[1] CECS, Universidade Federal do ABC - UFABC, CEP 09.210-170, Santo André, SP, Brazil
[2] Universidade de São Paulo - LME/PSI/EPUSP, CEP 05508-900, São Paulo, SP, Brazil
*katia.torres@ufabc.edu.br

Abstract

Hydrogen sensors based on TiO_2 and TiO_xN_y nanotubes would be fabricated and characterized as function of temperature. TiO_2 and TiO_xN_y nanotubes are or were obtained by anodization of sputtered Ti and TiO_xN_y thin films and Ti/TiOxNy multilayers in a NHF_4 organic solution. Platinum contacts were deposited on nanotubes arrays in order to measure the resistance variation as function of hydrogen concentrations. These measurements are carried out at different temperatures (27, 100, 200 and 300°C) and the sensor response to the operation temperature is analyzed.

Keywords: TiO_2 nanotubes, TiO_xN_y nanotubes, hydrogen sensor

Introduction

Metal oxide semiconductors gas sensors can be promising candidates for monitoring H_2, NO, NO_2, CO, alcohol and other gases due to their simple manufacturing techniques, low cost fast response and recovery time among other advantages [1]. However in order to present high sensitivity most of these sensors have to operate at high temperatures values in the order of hundreds Celsius degrees. sensors fabricated with metal oxide semiconductors thin films present a limited sensitivity due to the low superficial area exposed to the gas, in this way, if metal oxide semiconductors nanostructures were utilized significant increase in sensitivity would be obtained leading to decreasing operation temperatures, size and cost [2].

Hydrogen is the strongest candidate for clean carbon free fuel. Its use or its undesirable presence when it is considered a contaminant requires precise monitoring in order to detect very low hydrogen concentrations. In some applications, concentrations on the order of ppm have to be detected. Hydrogen monitoring at high temperatures is undesirable in some environments, for example, inflammable environments, biomedical applications and low power circuits. In this way, research is directed to low temperature hydrogen sensors study. Another challenge is to avoid sensor contamination that promotes measurement errors and decreases sensors lifetime [2].

Hydrogen sensors fabricated with TiO_2 nanotube arrays present self-cleaning properties under UV irradiation [2,3]. Nanotube arrays a few microns thick, with mouth diameters ranging from 22 to 110 nm present extraordinary changes in their electrical resistance with low hydrogen levels at room temperature when compared with micro and macro structures. This ability to work with high sensitivity at room temperature makes viable the utilization of these sensors in the biomedical area for diagnosis and disease treatment monitoring since TiO_2 nanotubes are bio- compatible. Nanotubes with diameter of 22 nm present a resistance variation of five orders of magnitude when exposed to 500 ppm of hydrogen, 200 times higher than nanotubes with diameter of 76 nm [2].

In this work hydrogen sensors with TiO_2 nanotubes arrays are fabricated and characterized at different hydrogen concentrations and operation temperatures, intending to evaluate the viability of utilizing these sensors at room temperature. A new kind of sensor, utilizing TiO_xN_y nanotube arrays will be fabricated and characterized. Their sensitivity will be evaluated and compared to the TiO_2 nanotube arrays intending to obtain the same or high sensibilities but with the advantage, due the nitrogen presence and decrease in the material band gap energy, of self-cleaning with visible radiation.

Experimental Procedures

In figure 1 a scheme of the electrolytic cell utilized for the growth of the nanotubes is shown. The platinum cathode and the anodic substrates, where the TiO_2 and TiO_xN_y nanotubes arrays were grown, were polarized with a DC voltage source (Agilent E3649). As

anodes 0,5 and 1μm of Ti, for TiO_2 nanotubes, and of Ti/TiOxNy multilayers, for TiO_xN_y nanotubes, sputtered onto 1 x 0,5 in glass substrates . As bath a solution of NH_4F in ethylene glycol (0, 5 % in weight) and 2 % H_2O, magnetically stirred during the process, was utilized.

Ti films were obtained by r.f. magnetron sputtering utilizing a Ti target and Ar and O_2 gaseous mixture (60 and 40%), TiOxNy films were obtained through the Ar, O_2 and N_2 (60, 5 and 35%), both were obtained with r.f. power of 150 W a deposition pressure of 1 mTorr at environmental temperature.

In previous works the anodization conditions were investigated and in figure 2 the nanotubes diameter value as function of anodization voltage is shown.

It is possible to notice that the nanotubes diameter increases linearly with anodization voltage. In figure 3 is shown a SEM image of nanotubes grown from Ti foil with 10V, in this case, diameters of approximately 20 nm were obtained.

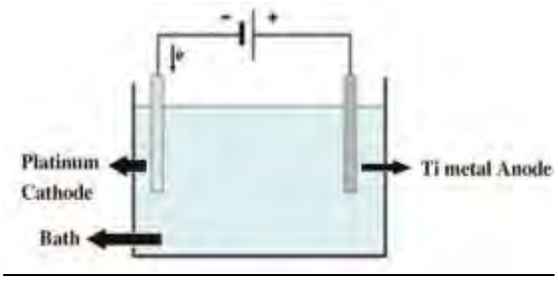

Figure 1. Electrolytic cell utilized for the anodization processes.

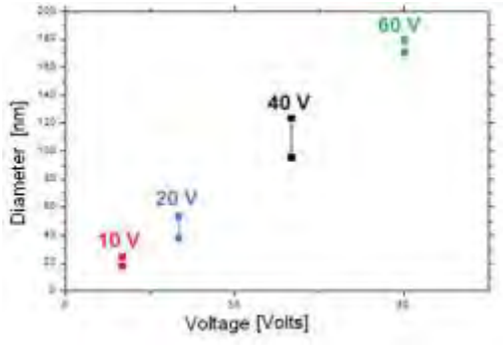

Figure 2 – Nanotubes diameter values as function of anodization voltage process.

For these reason the nanotubes arrays, for the hydrogen sensors, were grown with 10V. The nanotubes anodization processes were monitored by the I x V curve intending to determine the end process where the Ti film is totally transformed in nanotubes. In this point a null current value is expected. The process time to reach this point was 15 min. The nanotubes were annealed at 300°C for 2 hour in air for anatase crystalline phase formation. In figure 3 (b) is shown a TiO_2 nanotube arrays obtained with 60V by anodization of a thin Ti sputtered film, it is observed that the arrays on glass are much more uniform.

The obtained nanotubes were characterized by Scanning electron Microscopy (SEM) to analyse the tubes morphology (diameter and length) and Energy Dispersion Spectroscopy (EDS) measurements to determine the nanotubes chemical composition.

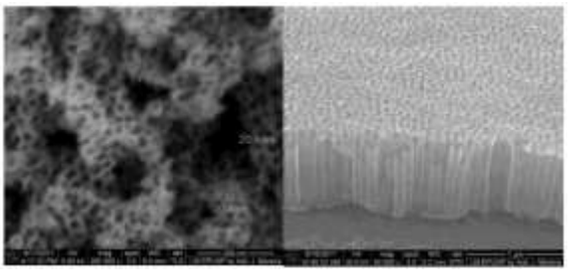

(a) (b)

Figure 3 – TiO_2 nanotubes arrays obtained by (a) Ti foil at 10V and (b) on glass with 60 V

The Platinum contacts are deposited by e-beam technique. The hydrogen sensors are characterized in a vacuum chamber and the sensor response to different hydrogen concentrations and as function of operation temperature (27, 100, 200 and 300°C) is analyzed.

.

References

[1] Hao Feng Lu et. Al. Nanotechnology ,19 pp. 405-504, 2008
[2] Craig A. Grimes, Gopal K. Mor. “TiO2 Nanotubes arrays: Synthesis, Properties and Applications” Springer, Chaper 3, 2009.
[3] G.K. Mor et. al., J. Mater. Res., Vol.19, No.2, pp. 628-634 2004.

Characterization of Aluminum Doped Zinc Oxide Thin films and Nanostructures for H_2 Gas Sensing Applications

Victor M. Pantojas, Laura Amadeo, Nelson Granda, Carlos Ortiz, Wilfredo Otaño
University of Puerto Rico at Cayey
Cayey, Puerto Rico, 00736
victor.pantojas@upr.edu

Abstract

Metal oxides, such as ZnO, are especially attractive as sensing elements synthesized in the form of thin films and nanostructures. The influence of Al doping on the gas sensing performance of ZnO films and fibers are explored with the hope of improving the sensitivity or the selectivity of the sensor. The objective is to obtain faster and more sensitive gas sensors by reducing the dimensions of the sensing elements and by doping. Zinc oxide fibers are formed by preparing a PVA solution containing zinc acetate which is deposited as a thin film by sol-gel or as fibers by electrospinning. A chamber was set up to test the sensitivity of the material to hydrogen gas.

Keywords: Zinc oxide, electrospinning, sol gel, hydrogen sensor

Introduction

Zinc oxide (ZnO) is a promising semiconductor for gas sensing applications because of its chemical sensitivity to volatile gases, high chemical stability, and non-toxicity. ZnO is also easily doped, transparent in the visible, has a high excitonic energy and high optical gain which promises interesting electro-optical applications. Many researchers have studied ZnO thin film and nanostructures for the detection of toxic gases, combustion gases, pollutants and organic vapors [1]. The use of ZnO nanostructures for the detection of hydrogen is of particular interests given its importance as a new energy source [2]. The influence of doping on the gas sensing performance of ZnO films have also been explored with the hope of improving the sensitivity or the selectivity of the sensor [3]. In this work we characterize Al-doped ZnO thin films and nanofibers, prepared by sol-gel and electrospinning respectively. Preliminary work on the influence of Al doping on the sensing of hydrogen will be presented.

Experimental

Aluminum doped zinc oxide thin films were prepared on fuse glass substrates by spin coating a solution containing zinc acetate dihydrate ($Zn(CH_3COO)_2$ •$2H_2O$), aluminum nitrate ($Al(NO_3)_3$•$9H_2O$), and a mixture of 2-methoxyethanol and monoethanolamine. Solutions with a concentration of Al ranging from 0 at.% to 10 at % with respect to zinc were prepared. The sol solution is dropped onto the substrate and rotated at 3,000 rpm for 30s. Just after deposition the film is placed on top of a pre-heated hot plate at 250^{o}C for 10 min to remove organics. Such rapid heating has been found to yield a homogeneous microstructure and reduces the possibility of formation of metastable intermediate phases. The coating and heating are repeated until obtaining the desired thickness. Finally, the films are annealed in air at a temperature of 700^{o}C for 1 h.

ZnO fibers are prepared by dissolving zinc acetate dehydrate ($AcZn*2H_2O$) and poly(vynil alcohol) (PVA) in de-ionized water. PVA is a semi-crystalline, hydrophilic polymer with good chemical and thermal stability, and water soluble. The required amount of aluminum nitrate ($Al(NO_3)_3$•$9H_2O$) is added to obtain 0.5, 1.0 and 1.5 at% Al. Acetic acid HOAc or ethanolamine was added to the aqueous solution. When the solution becomes clear it is cooled down to room temperature. Electrospinning is performed with a voltage of 17kV, at a distance of 18cm and a rate 0.05 mL/hr.

Samples are characterized by scanning electron microscopy (SEM), energy dispersive spectroscopy EDS, and optical transmittance. Electrical characterization is accomplished using a fully computerized I-V and C-V system. Metal contacts are deposited by sputtering.

Results

The surface morphology of Al-doped ZnO fibers and thin film studied by SEM are shown in Figure 1. The images present a distribution of pores along the fibers and on the surface of the film which is attributed to the evaporation of the solvent and the decomposition of the organic molecules that generate gases during heat treatment. High porosity and large surface area are desirable in gas sensing applications since the surface in where the gas is adsorbed and reactions occur.

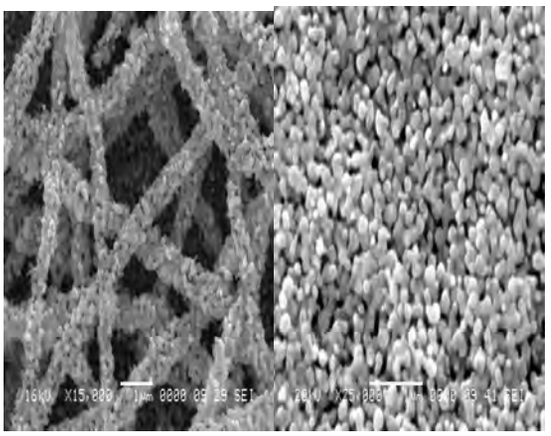

Fig. 1 SEM image of Al-doped ZnO fiber and thin film

Al-doped ZnO thin films show excess oxygen as determined by EDS which is typical of ZnO films prepared by chemical solution based methods such as sol-gel deposition. This zinc deficiency can be reduced by annealing the as-prepared films in an inert gas environment. The surface roughness appears to decrease with Al content until a minimum of 3.2 nm is reached at 3 at. % Al. This can be related to the known solubility limit of Al in ZnO which is around 2.0 at.%. The optical transmittance evaluated in the range of 400 to 800nm varied from 84.5 to 90.1%. The highest transmittance occurred for 2at. % Al. The optical band gap (Eg) as determined from the optical transmission slightly decreased with Al doping. This may be attributed to the fact that Al^{3+} ion occupies the divalent Zn^{2+} sites allowing electrons to move to the conduction band.

In the case of ZnO fibers, two different stabilizers were found to work well, monoethanolamine (MEA) and acetic acid (HOAc). Fibers prepared with acetic acid had an average diameter of 126 nm while for those prepared by MEA was 146 nm. Fibers are deposited on oxidized Si substrates and rectangular Au contacts were deposited 1mm apart. Figure 2 shows a typical experiment where a ZnO fiber mat is exposed to 1% H_2 gas in nitrogen. Characterization of the Al-doped fiber mats as sensor elements is underway.

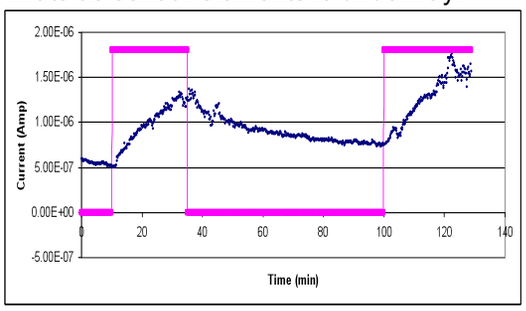

Fig. 2 Current as a function of time for a ZnO fiber mat hydrogen sensor.

Conclusions

Aluminum doped ZnO thin films and nanofibers were prepared by the sol-gel spin coating and electrospinning. Films with Al concentration ranging from 0 to 10 at. % were prepared. Compositional analysis shows an excess of oxygen as compared to zinc. The Rms roughness of films decreased with Al concentration showing a minimum for a doping concentration of 2.0%. Higher Al concentration produced films with higher Rms roughness. All doped films exhibited high transmittance in the visible range ranging with a maximum for a concentration of 2 %. Only a slight variation in the band gap energy was observed with Al concentration. Preliminary test of the films and fibers as hydrogen sensors were performed. Further improvement in sensitivity are been explored by controlling the size, orientation and morphology of the zinc oxide crystalline grains in the films and fibers.

Acknowledgement

This project was supported by DOE-EPSCoR Program grant DE-FG02-08ER46526, NSF-PREM grant NSF-DMR-0934195 and the Institute of Functional Nanomaterials funded by NSF-EPSCoR grant OIA-0701525.

References

[1] N.V. Hien, N.D. Chien, Physica B, Vol. 403, 50-56, 2008. M.-W. Ahn, K.-S. Park, J.-H. Heo, D.-W. Kim, K.J. Choi, J.-G Park, Sensors and Actuators B:Chemical, Vol. 138, 168-173, 2009

[2] O. Lupan, G. Chai, L. Chow, Microelectronics Journal, Vol. 38, 1211-1216, 2007

[3] F. Paraguay, M. Miki-Yoshida, J. Morales, J. Solis, W. Estrada, Thin Solid Films, Vol. 373, 137-140, 2000

Electrospun conducting polymer nanofibers as the active material in sensors and diodes

Nicholas J. Pinto
University of Puerto Rico - Humacao
Humacao, PR 00792, Puerto Rico
nicholas.pinto@upr.edu

Abstract

Polyaniline doped with camphorsulfonic acid (PANi-HCSA) and poly(3,4-ethylenedioxythiophene) doped with polystyrene sulfonic acid (PEDOT-PSSA) were electrospun separately to obtain individual nanofibers which were captured on Si/SiO_2 substrates and electrically characterized. The fiber resistance was recorded as a function of time in the presence of vapors of aliphatic alcohols of varying sizes. Due to the large surface to volume ratio, uniform diameter and small quantity of active material used in the construction, these sensor responses are comparable to or faster than those prepared from nanofiber mats of the same polymer. Sensors made from individual fibers also show true saturation upon exposure to and removal of the sensing gas A Schottky diode was also fabricated using a *n*-doped Si/SiO_2 substrate and a single PANi-HCSA fiber and tested in vacuum and in ammonia. The diode response was instantaneous upon exposure to ammonia with nearly complete recovery of the current upon pumping out the ammonia, thereby making it a reusable sensor with rectifying behavior.

Keywords: electrospinning, nanofibers, sensors, diode

Introduction

The rapid detection of minute traces of toxic gases in an inadequately ventilated environment is crucial to effectively reduce any widespread loss to life and property. This requires sensors capable of detecting small quantities of gas, such as those fabricated using nanofibers that possess enhanced surface to volume ratio Organic conducting polymers (CP's) are especially suited for use as gas sensors for a variety of reasons. In particular, the oxidation/reduction states of these polymers can be reversibly tuned by exposure to basic/acidic environments, resulting in several orders of magnitude change in the conductivity with no polymer degradation and that would extend the lifetime of sensors based on these polymers. Furthermore, CP's are cheap and easy to synthesize in bulk quantities, they are relatively stable under ambient conditions and can readily be processed as films or fibers.

Individual polyaniline (PANi-HCSA) and poly(3,4-ethylenedioxythiophene) (PEDOT-PSSA) nanofibers were electrospun and used separately to sense a variety of alcohols with response times that are faster than sensors made from thin films of the same material[1,2]. In addition we fabricated Schottky diodes based on these fibers and tested them in a gaseous environment with near complete recovery[3]. This leads to the possibility of fabricating multifunctional devices making them more versatile.

Experimental

Nanofibers of PANI-HCSA and PEDOT-PSSA were prepared via electrospinning and contacted using gold wire and silver paint. In order to fabricate a Schottky diode the fibers were captured on an n-doped Si/SiO_2 wafer with

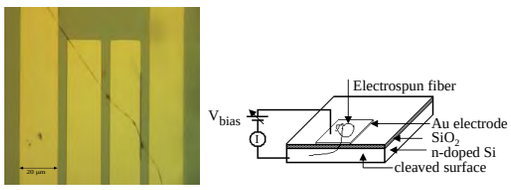

Figure 1: Optical microscope image of fiber and a schematic of the Schottky diode with external connections

prepatterned leads. Figure 1 shows an optical microscope image of a PANi-HCSA nanofiber crossing gold contact leads and also shows a schematic of the Schottky diode with external electrical connections. In all of the measurements the current in the sensor was

monitored at a fixed applied voltage, while an inert gas (N_2) and the sensing gas (N_2 bubbled into the alcohol) were switched in predetermined intervals over the sample.

Results and Discussion

Fig 2 (a), (b) and (c) show the time dependence of the change in the normalized resistance of single PANi-HCSA nanofibers and Fig 2 (d), (e) and (f) represent the same for PEDOT-PSSA nanofibers upon exposure to vapors of

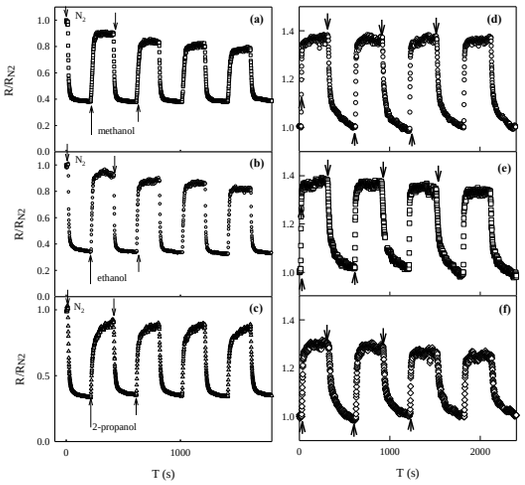

Figure 2: Time dependence of the normalized resistance of PANi-HCSA(left) and PEDOT-PSSA(right) nanofibers to vapors of methanol(a),(d), ethanol(b) (e) and 2-propanol (c) (f)[1,2].

methanol, ethanol and 2-propanol respectively, where RN_2 is the resistance of the fiber under a flow of dry N_2 gas. The responses are similar i.e. the flow of N_2 decreases the resistance while the flow of alcohol vapor increases the resistance. These results show true saturation and also faster response times when compared to thin films/fiber mats of the same material. The response is larger for larger molecules and the response time is shorter for smaller molecules. The response times were 32, 20 and>110s for PANi-HCSA and 8, 10 and 20 s for PEDOT-PSSA sensors for methanol, ethanol and 2-propanol respectively. PEDOT-PSSA are thus better sensors compared to PANi-HCSA. The increase in sensor resistance in the presence of the alcohol vapor is due to polymer swelling that leads to separation of polymer chains thereby increasing their resistance, while the flow of dry N_2 reverses this effect.

Figure 3 shows the I-V characteristic curve of a Schottky diode, which is seen to be asymmetrical with a turn on voltage in the range 0.4V - 0.6 V and a much reduced reverse bias current that did not tend to saturate. These devices exhibited rectifying behavior and the ratio of the forward to reverse current at a bias voltage of ±2V for this device was calculated to be ~100 which was limited in part due to the low fiber conductivity and the series resistance of the semiconductor. Since it is well known that the conductivity of polyaniline is

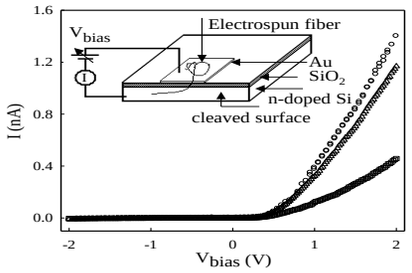

Figure 3: I-V characteristic curves for a Schottky nanodiode when used as a gas sensor (○) - as prepared sample measured in vacuum; (□) – a few seconds after exposure to ammonia vapor; (Δ) - after 5 hours of pumping. The inset shows the schematic of the diode construction[3].

affected by the dedoping effects ammonia this motivated us to test the diode response when exposed to ammonia gas. Figure 3 also shows the results of this experiment in an as prepared device measured in vacuum, after ammonia exposure and after pumping out the ammonia. Due to the large surface to volume ratio of the fiber, the change in the diode response was instantaneous upon exposure to ammonia with near compete recovery of the current upon ammonia removal The diode turn on voltage is not affected by the sensing action and attests to its robust nature.

Conclusion

We successfully fabricated true conducting polymer nanfibers using the electrospinning technique and tested them in the presence of various alcohol vapors and also tested a Schottky diode in vacuum and in an ammoinia vapor. Nanofiber sensors are faster than thin film sensors and have the potential to be used in detecting small amount of gases. They can also be used in diodes that are reusable and are multifunctional.

This work was funded by NSFPREM 0934195.

References

[1]N.J. Pinto et al. Sens. and Actuators, Vol. 129, No. 2, pp. 621-627, February 2008.

[2]N.J. Pinto et al. Sens. and Actuators, Vol. 156, No. 2, pp. 849-853, August 2011.

[3]N.J. Pinto et al. Appl. Phys. Lett. Vol. 89, No. 3, pp 033505(3) July 2006.

Palladium Nanoshells for Ultrasensitive Hydrogen Sensors

Diego Rodríguez-Vindas[1], Carlos Ortiz[2], Víctor Pantojas[2] and Wilfredo Otaño[2,3]
1 University of Puerto Rico at Río Piedras, 2 University of Puerto Rico at Cayey and 3 Institute for Functional Nanomaterials, Cayey, PR 00737
wilfredo.otano@upr.edu

Abstract

Ultrasensititive hydrogen sensors are required in several applications such as fuel cell systems and aerospace environments. One method to improve the sensitivity is using new nanoscale morphologies that provide larger surface areas for adsorption, and smaller crystallite size that reduces the time needed for "bulk" diffusion. In this project, Pd nanoshells are prepared by magnetron sputtering deposition on top of polymer fibers mats, which act as a template that shapes the morphology of the material being deposited while providing support to the metallic scaffold that is created. The sensitivity shown to 1% or less of hydrogen in nitrogen is excellent, as measured from the conductance changes with hydrogen concentration that result from the competing mechanisms of percolation and scattering. Process parameters such as target material, deposition time, sputtering pressure, and power can be used to produce nanoshells with different composition, thickness and crystallinity and, in consequence, to tailor their sensing properties.

Keywords: Palladium, sensors, ultrasensitive, nanotechnology, sputtering, electrospinning

Introduction

Palladium (Pd) metal is one of the most prominent materials studied for the detection of hydrogen gas.[1-3] Hydrogen rapidly dissociates on its surface and diffuses into subsurface layers forming palladium hydride with consequent changes in optical, mechanical and electrical properties that are easily detected [4]. Sputtering of Pd in a nanoscale morphologies is a promising way to improve sensor performance by provid*ng* larger surface areas for adsorption, and smaller crystallite size that reduces the time needed for "bulk" diffusion. The amount of sites available for hydrogen adsorption per Pd atom is also higher in the surface and subsurface layers resulting in higher sensitivity.

Experiments and Results

Pd nanoribbons and nanoshells were prepared by magnetron sputtering deposition on top of a mat of poly(ethylene oxide) (PEO) fibers, which acted as a template shaping the morphology of the metal deposited and providing support to the scaffold created.[5] Sputtering is a line-of-sight deposition process and a larger amount of palladium is deposited on top of the fiber compared to the sides. The top and sides of the fibers shadow their bottom parts closer to the substrate preventing any substantial deposition there. The end result of the deposition is the formation of Pd nanoshells, thicker in the middle region, and with a larger void network toward the thinner edges.

The samples were prepared by electrospinning a mat of fibers on top of an oxidized silicon substrate followed by 10-50 s sputtering deposition of Pd and deposition of gold contacts. The samples were introduced in a stainless steel chamber where argon and hydrogen flows were controlled using MKS mass flow controllers. A total flow of 300 sccm was used in all measurements with 1% hydrogen. A Keithley multimeter controlled using the LabView software was used to supply a voltage and measure the current.

Figure 1 (top) shows the current as a function of time for a mat of 10nm thick Pd nanoshells on top of PEO fibers. The introduction of hydrogen in the flowing gas produced a decrease in current that is the typical response of bulk Pd.[6-8] In the bottom of Figure 1 is shown the response of another sample where a dramatic increase in current is observed when the hydrogen is introduced in

the flowing gas. This response is an effect of the improvement in percolation paths through the mat of nanoshells that results from the lattice expansion of the Pd as consequence of the formation of the hydride.[9,10]

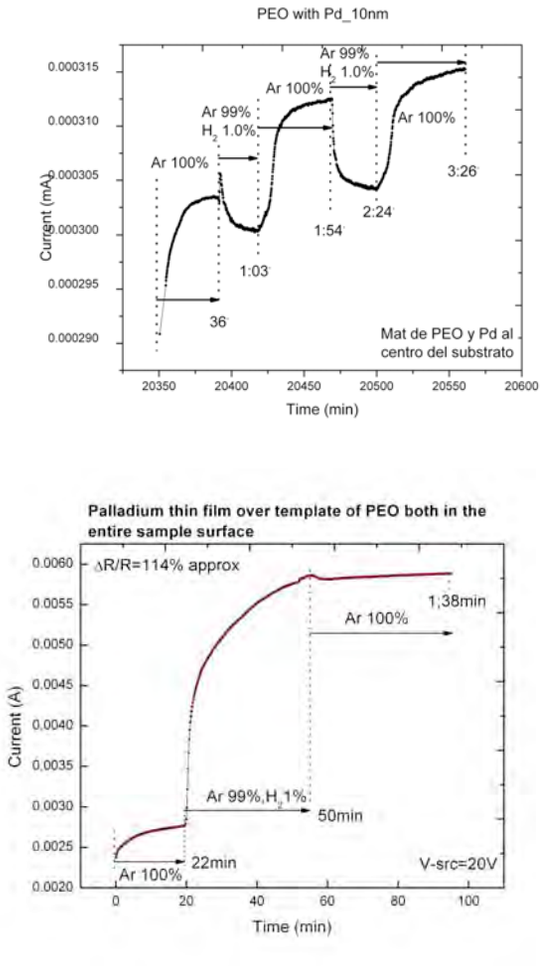

Figure 1: *Sensor response to 1% hydrogen in argon. Bulk (top) and percolation modes (bottom).*

Both modes, bulk and percolation, can be present simultaneously in a non-continuous film. In Figure 1 (top) a small peak, corresponding to an increase in current is observed the first time that the sample is exposed to hydrogen. The initial expansion of the lattice reduces the contact resistance of the film producing the initial spike in current. After that, the bulk mode scattering of the electrons produce the subsequent reduction in current. The response of the sensor is then a competition between both, the bulk and percolation modes. The percolation mode is more sensible but will not recover completely after removing the hydrogen, as seen at the bottom of Figure 1.

Conclusions

Sputtering process parameters such as deposition time, deposition pressure, and power can be used to produce nanoshells with different thickness and crystallinity. The high sensitivity shown to 1% or less of hydrogen in nitrogen is understood to result from the reduced dimensions combined with this unique nanostructure. Two competing effects are observed to affect the current in the sensor corresponding to percolation and scattering of electrons as a function of hydrogen adsorption. Understanding of these phenomena is important to develop better ultrasensitive sensors.

Acknowledgements

This project was supported by NASA-URC grant NNX08BA48A and by NASA-PREM grant NSF-DMR-0934195**.**

References

[1] G. W. Hunter, J. C. Xu, L. Evans, A. Biaggi-Labiosa, B. J. Ward, S. Rowe, D. B. Makel, C. C. Liu, P. Dutta, G. M. Berger, and R. L. Vander Wal. The Development of Micro/Nano Chemical Sensor Systems for Aerospace Applications, *SPIE Newsroom, 10.1117/2.1201006.002984*, *June (2010)*.

[2] J. F. Patton, Hunter, S. R., Sepaniak, M. J., Daskos, P. G., and Barton, D. *Sensors and Actuators A: Physical* 163 (2), pp. 464-446 (2010).

[3] W. J Buttner,. Post, M. B., Burgess, R.T. and C. Rivkin, *International Journal of Hydrogen Energy* 36 (3), pp. 2462-2470 (2010).

[4]] P. Zoltowski, Electrochem.Act. 55, pp. 6274-6282(2010).

[5] V. M. Pantojas, Rodríguez-Vindas, D., Morell, G., Rivera, A., Ortiz, C., Santiago-Aviles, J. J. and Otaño, W., J. Nanophoton. Vol. 2, pp. 021920 (2008).

[6] T. Xu, Zach, M. P.; Xiao, Z. L.; Rosenmann, D.; Welp, U.; Kwok, W. K. and Crabtree, G. W., Applied Physics Letters 86 (20), pp. 203104 (2005).

[7] J. Zou, Hubble, L. J., Iyer, K. S. and Raston, C. L., S*ensors and Actuators B: Chemical15 (1)*, pp. 291-295 (*2010*).

[8] E. C. Walter, Ng, K., Zach, M. P., Penner, R. M. And Favier, F., *Microelectronic Engineering* 61-62, pp. 555-561 (2002).

[9] O. Dankert and Pundt, A., Appl. Phys. Lett. 81 (9), pp. 1618-1620 (2002).

[10] F. Favier, Nanogaps for Sensing, *Procedia Chemistry* 1 (1), pp. 746-749 (2009).

Devices and sensors based on PVDF-TrFE/SWNT's composites

Manuel Bonilla, Idalia Ramos, and Nicholas Pinto
University of Puerto Rico-Humacao
Humacao PR 00972
manuel.bonilla@upr.edu

Abstract

Sensor devices were prepared using PVDF-TrFE/SWNT's composite and compared with a pure SWNT's sensor. Current as function of time measurements at room temperature shows an improved sensitivity and faster response time in the presence of acetone for the composite resistor device that was fabricated putting the composite solution between two gold electrodes on an *n* doped Si/SiO_2 substrate. The pure SWNT's resistor produced a faster response time that the composite in the presence of NO_2. Schottky diodes were prepared with the PVDF-TrFE/SWNT's composite and the *n* doped Si/SiO_2 substrate. Successful rectification was obtained and changes in the turn on voltage and in the I_{on}/I_{off} ratio were observed as the diode was in the environments of different gases. The composite improved the sensitivity of the devices that are faster and can be used to prepare a device with both diode and resistor functionalities. These sensor and the diodes can be reused after the removal of the gases.

Keywords: PVDF-TrFE, SWNT's, diode, sensor

Introduction

Nanofibers and nanotubes have a large surface to volume ratio. This feature is especially useful in sensor technology as the sensor response will be rapid. Single walled carbon nanotubes (SWNT) have been used to sense various gases and show high sensitivity [1]. We have focused our research on the composite ferroelectric co-polymer poly (vinylidene fluoride-trifluoroethylene)-PVDF-TrFE (75/25) with SWNT's. Sensors and a Schottky diode were fabricated using cast films of this composite material and tested in the presence of acetone and NO_2. The sensor response was rapid and reversible. The ability to sense NO_2 at room temperature is particularly useful as many ceramic sensors can only sense this gas at elevated temperatures. The diodes show rectification that was tunable in the presence of the gas and was reusable upon removal of the sensing gas.

Experimental

Devices were prepared using a 1 wt% solution of SWNT's dispersed in N,N-Dimethylformamide (DMF) and a solution of 1 wt% PVDF-TrFE in DMF for the composite devices. These solutions were drop cast on *n*-doped Si/SiO_2 wafer (<0 0 1>, 0.1-1.0 Ω cm) with a 200nm thermally grown oxide layer. The PVDF-TrEF/SWNT's composite was a mixture of 0.5 ml of SWNT's in DMF and 4.5 ml of 1 wt% PVDF-TrFE in DMF For sensor measurements, the current at fixed voltage was measured as a function of time for resistor devices of pure SWNT's and the composites. These measurements were taken in the presence of NO_2 and in the presence of acetone using N_2 as the inert carrier gas. Schottky diodes consisting of pure SWNT'S/*n*-Si and also of the composite/*n*-Si were prepared and electrically characterized under the same gaseous conditions

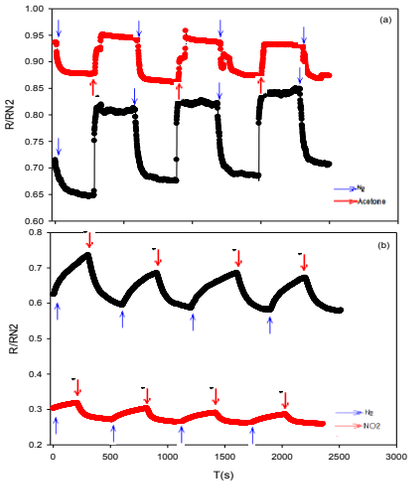

Fig. 1.Normalized resistance of individual sensors switching the gas ambience between (a) N_2 and acetone (b) N_2 and NO_2. PVDF-TrFE/ SWNT's *is in black and* SWNT's. *in red. The arrows indicate the moment when the specified gas was introduced*

Table 1
Composite and pure SWNT's sensors response time and recovery time

Sample	PVDF-TrFE/SWNT's		SWNT's	
Sensing gas	Acetone	NO_2	Acetone	NO_2
Response time(s)	5	200	15	180
Recovery time (s)	100	235	120	200

Results and discussion

Figure 1 shows the normalized resistance of the pure SWNT and the composite PVDF-TrFE/SWNT sensors in the presence of acetone and NO_2 gases. The response to acetone is rapid and true saturation can be observed, while for NO_2 the sensor does not appear to saturate in the 300s time interval of the measurements. Nevertheless, in the four cycles presented in Figure 1, there is reproducibility. The response times of these sensors is presented in Table 1 and shows that composite sensors are much faster than pure SWNT sensor for acetone. This could be due the presence of the polymer that speeds gas entry into the fiber. From Figure 1 we see that acetone increases the resistance due to polymer swelling while NO_2 decreases it and could be related to the doping effect that NO_2 has on organic materials eg. graphene [2].

Figures 2(a) and (b) show the I-V characteristic curves for the Schottky diode made of composite PVDF-TrFE/SWNT's in the presence of acetone and NO_2 respectively and Figures 2(c) and (d) show the same for the pure SWNT's under the same conditions. In all these figures we notice the asymmetric rectifying behavior. Consistent with the sensor measurements in Figure 1, acetone reduces the on state current, the effect of NO_2 is more pronounced in the reverse bias direction. In all cases however we notice the diode recovers after the sensing gas is removed making useful as a reusable diode cum gas sensor. The performance of the diode was analyzed using the standard thermionic emission model of a Schottky junction via the equations above and device parameters are tabulated in Table 2.

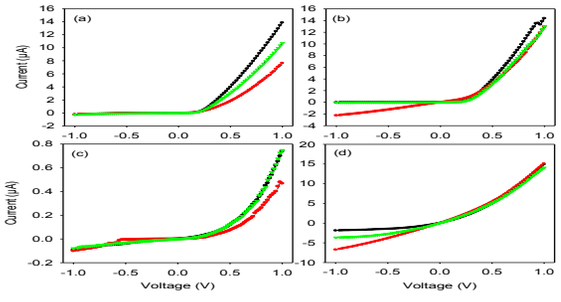

Fig. 2.Current-voltage characteristic of the Schottky diodes. The black plots are under the presence of N_2.The red plots corresponds to a ambience of (a) acetone (b) $N0_2$ for the composite diode and (c) acetone (d) NO_2 for the CNT's diode. The green plots are after the removal of the gas.

$$J = J_S[\exp\left(\frac{qV_B}{kT}\right) - 1]$$

$$J_s = A^*T^2\exp\left(-\frac{q\Phi_B}{kT}\right)$$

$$n = \frac{q}{KT}\left(\frac{\partial V_B}{\partial lnJ}\right)$$

Table 2
The turn on voltage (V_{on}), I_{on}/I_{off} ratio, the diode ideality factor and the barrier height

Sensing gas	V_{on}	I_{on}/I_{off}	n	Φ_B (eV)
PVDF-TrFE/CNT's in Acetone				
N_2	0.30	57	1.7	0.46
Acetone	0.39	34	1.6	0.45
PVDF-TrFE/CNT's in NO_2				
N_2	0.37	550	2.3518	0.44
NO_2	0.27	6	4.462	0.35
CNT's in Acetone				
N_2	0.55	8	4.5	0.4453
Acetone	0.56	5	2.4	0.5065
CNT's in NO_2				
N_2	0.31	8	3.3	0.34
NO_2	0.27	2	5.0	0.32

Conclusion

Sensors based on pure SWNT's and PVDF-TrFE/SWNT were fabricated and tested in acetone and NO_2. The composite sensors had a faster response time in acetone compared to NO_2. A Schottky diode was also prepared using these same materials and the device retained its rectifying behavior in the presence of the sensing gas and there is recovery upon gas removal.

Acknowledgments

This work was funded by NSF under grants PREM 0934195 and RUI 0965023.

References

[1]C. Staii, A.T. Johnson, Jr., M. Chen, A. Gelperin Nano Lett. Vol. 5, No. 9, pp. 1774-1778 August 2005.

[2] F. Schedin , A. K. Geim , S. V. Morozov, E. W. Hill , P. Blake, M. I. Katsnelson & K. S. Novoselov, Nature Materials, Vol.6, pp. 652 – 655 July2007

New Synthesis Pathways of Silicon Oxide Containing Silicon Nanostructures

C. Fernández-Sánchez[1], J.A. Rodríguez[2], J. Juvert[1], V. Auzelyte[3], J. Brügger[3], C. Domínguez[1]
[1] Instituto de Microelectrónica de Barcelona (IMB-CNM, CSIC)
08193, Bellaterra, Barcelona, España
[2] Facultad de Física - IMRE, University of Habana
10400, Ciudad Habana, Cuba Cuba
[3] École Polytechnique Fédérale de Lausanne
1015, Lausanne, Switzerland
Carlos.Dominguez@imb-cnm.csic.es

Abstract

Motivated by the desire to develop efficient and low-cost light emitters operating at room temperature whose production is fully compatible with existing Silicon integrated circuit technology, several approaches to fabricate Si-based light emitting devices (LED) have been explored and, accordingly, a variety of materials have been developed. In this work materials containing Si-nanostructures (Si-nc) embedded in a SiO_2 matrix have been obtained and their photoluminescence characteristics measured, as the first step to fabricate low cost light emitting devices based on Si-nc obtained by non-conventional precursors/processes.

Keywords: Sol-gel, alkoxydisilanes, hydrogen silsesquioxane, photoluminescence, Si-nc

Introduction

The field of optical chemical sensing has been a growing research area over the last three decades. The most widely used techniques employed in optical chemical sensors are optical absorption and luminescence, but sensors based on other spectroscopic techniques as well as on optical parameters, such as refractive index and reflectivity, have also been developed.

The successful development of an optical chemical sensor is intrinsically linked to the nature of the applied physical platform [1]. If silicon is used, integrated optical sensors that combine light delivery/collection with intrinsic sensing functionality, are more flexible to design and can integrate multiple functionalities onto a single sensor chip. Unfortunately, silicon is badly suited to operate as a light emitter, thus the main drawback of integrated optical sensors is the difficulty to include the light source in the same substrate as the transducer and the detector, hence monolithic integration can hardly be obtained.

Nevertheless, in the last few years the development of silicon-based optoelectronics has received a decisive improvement with the fabrication of the first Si-nc/SiO_2-based light emitting diode (LED). Si-nc embedded in a SiO_2 matrix may be obtained through a variety of techniques such as implantation of Si in thermal SiO_2, co-sputtering, chemical vapor deposition, laser ablation etc.

In the present work we report on the synthesis of bulk silicon oxide containing silicon nanostructures by sol-gel technology and spin-coating processes using non-conventional precursors like alkoxydisilanes and hydrogen silsesquioxane.

Experimental

By using the sol-gel technique, the starting material was obtained by the combined hydrolysis and condensation reactions of one of the basic precursors, hexaethoxydisilane ($C_{12}H_{30}O_6Si_2$; Hexaet) or hexamethoxydisilane ($C_6H_{18}O_6Si_2$; Hexamet), dissolved in ethanol (EtOH/Hexaet(Hexamet), 2/1 in volume) and further diluted in acidic water (pH= 5; H_2O/Hexaet(Hexamet), 2/1 in volume). The resulting *sol* solution was left to gel and cure at room temperature for a week until a translucent and quite brittle solid is obtained. Some experiments by using a mixture of both precursors were also carried out.

Hydrogen Silsesquioxane (HSQ) is an electron-beam negative resist similar to siloxane

compounds used to obtain Spin-on-Glass dielectrics. HSQ belongs to a family of ordered three-dimensional polymers that do not contain carbon bonds. Continuous 100 nm thick HSQ films were deposited by spin-coating at 7000 rpm on 100 nm-thick silicon oxide on silicon substrates.

The resulting bulk (sol-gel) and thin film (spin-coated) materials were annealed in a N_2 atmosphere for one hour at temperatures in the range 950 - 1150 ºC. As-obtained and annealed samples were analyzed by photoluminescence (PL) technique with a He-Cd laser (excitation line at 325 nm). The integration time was 10 seconds and light was recorded using a QE65000 Ocean Optics spectrophotometer.

Results

For sol-gel obtained samples the PL spectra showed important differences for both of the applied precursors. For samples obtained with Hexamet (Fig. 1a) a unique, wide and very intense band, picking somewhere in the spectral range 400-600 nm, depending on the annealing temperature, is observed. This behavior is typical of oxide matrix defects-related recombination. On the contrary, for samples synthesized with Hexaet (Fig. 1b), a narrower, unique and less intense band, picking in the range 750-850 nm for the different annealing temperatures and typical of quantum confinement effect in Si-nc of a few nm size embedded in a silicon oxide matrix, is obtained.

The spectra recorded from the HSQ samples (Fig. 2) shown an intense emission band in the range 600-900 nm, which increases its intensity with the annealing temperature.

The reasons of these different behaviors are analyzed in the work and verified by other structural characterization techniques (XPS) used.

Acknowledgments

Authors thanks CSIC (PIE 201150E055), and MINECO (project ref. TEC2010-17274) for the economic support.

References

[1] C. McDonagh, C. S. Burke, B. D. MacCraith, Chem. Rev., vol. 108, No. 2, pp. 400-422, 2008.

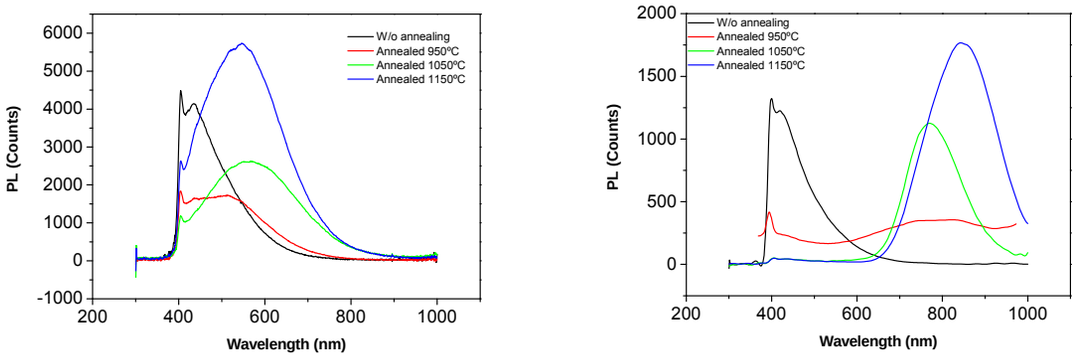

Figure 1. Photoluminescence spectra for sol-gel samples annealed at different temperatures and obtained from hexamethoxydisilane (a) and hexaethoxydisilane (b).

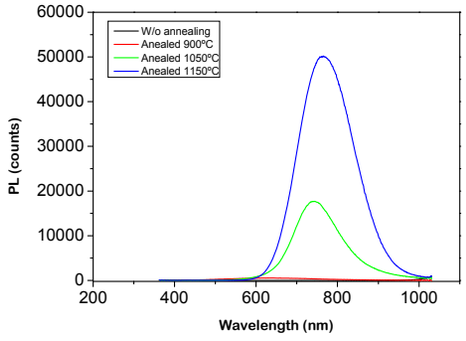

Figure 2. Photoluminescence spectra of HQS samples annealed at different temperatures.

Synthesis of ZnO fibers doped with Al for gas sensors

Laura Amadeo Sanchez and Victor Pantojas
Universidad de Puerto Rico at Cayey
laura.amadeo@upr.edu

Abstract

Synthesis of ZnO fibers doped with Al for gas sensors Zinc Oxide (ZnO) is an n-type semiconductor with the potential to be used as gas sensing element because of its favorable properties such as good transparency and high electron mobility. We produced ZnO fibers by electrospinning a mixture containing zinc acetate (ZnAc), poly(vinyl alcohol)(PVA), acetic acid (HOAC) and aluminum nitrate (AlNO3). Aluminum Nitrate was used to deliver the Al dopant to the fibers and improve their conductivity. The fibers where characterized by Scanning Electron Microscopy (SEM), Energy Dispersive Spectroscopy (EDS), X-ray diffraction (XRD) and electrical characterization.

Keywords: Nanofibers, Al doping, Electrospinning, Sensors

Introduction

Zinc Oxide is an n-type semi-conductor, his hight capacity of electron mobility, the wide band gap (3.37 eV) this great properties make the ZnO so much interesting for the fabrication of nanomaterial. Also investigations show that doped ZnO nanomaterial will improve the electrical and optical properties, this time we use Aluminum because it can be an electron donor in a ZnO lattice and increase de carrier concentration in the material[1-2]. The electrospinning is a simple and economical method to make uniform and long nanofibers in one dimensional (1D).

Experimental

The ZnO fibers doped with Al were prepared by electrospinning technique with a sol-gel aqueous solution. First, a solution of poly(vinyl alcohol) (PVA) is prepared at 10% (in deionized water). The ZnO precursor is Zinc acetate and the doping precursor is aluminum nitrate we make the solution making variations on the percent of AlNO3 (0.5%, 1.0%) the amount of ZnAc is the same, also we add acetic acid and water to help dissolve the ZnAc. Then the solutions were heated at 60°C-70°C under magnetic stirring to make an homogeneous solution. After heated for 2.5 hours, we let it cool for an hour with the magnetic stirring. For electrospinning apparatus we put the solution in a plastic syringe (1ml), a stainless (0.5mm, diameter), DC voltage source, and a ground with the fibers collector. The parameters for the electrospinning process the distance between the needle and the fiber collector were 18cm. The nanofibers were collected in oxidized silicon substrates then we put them in air treatment at 600°C and 700°C for 6 hours to decompose the polymer PVA. The SEM was used to characterize the morphologies of the fiber. The composition was evaluated by Energy Dispersive Spectroscopy (EDS). The electrical characterizations were performed at Professor's Kikkawa laboratory at UPENN.

Result and discussion

ZnO fibers were obtained by electrospinning. SEM micrographs indicate that the fibers are composed of crystalline grains. Long and thin fibers appears with high porosity are obtained.

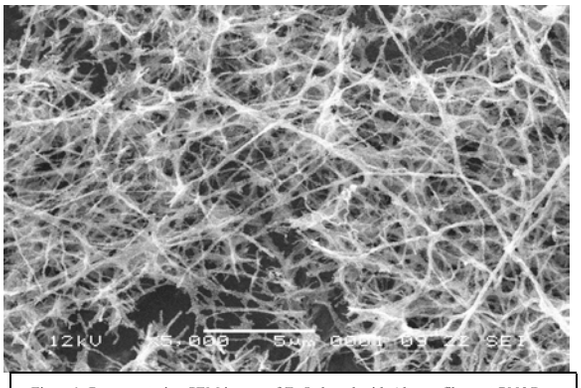

Figure1: Representative SEM image of ZnO doped with Al nanofibers at 700°C

Also a lot of ramifications along the fiber are observed which can be beneficial for sensing applications. High porosity increases the surface area which is exposed to the gas which is expected to increases the sensitivity of the

sensor. Fiber diameters were measured by analyzing the SEM images.

The composition of the fibers and the amount of Al incorporated into the fibers was obtained. Figure 2 shows the results from the EDS showing the presence of O, Zn and Al. The samples contain between 0.5% and 1.0% of Al. The ratio of O/Zn at. percent is less than 1 indicating the deficiency of oxygen. Oxygen vacancies in ZnO are known to be donor type defects which contribute to the n-type conductivity of the material.

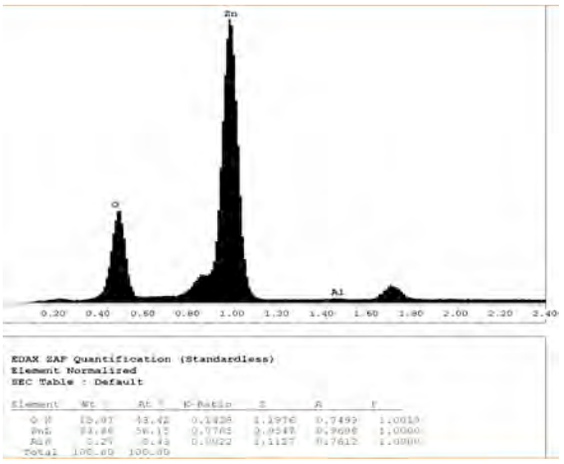

Figure2: Results of the EDS analysis; showing the presence O, Zn, Al

Electrical measurements were performed by 2 point probe technique at room temperature. The distance between points was about 2 cm. No detectable current was observed. Thus, the current vs voltage measurements indicate a very high resistance even with the addition of Al. Either the samples are very insulating or there is no passage for the current through the fibers connections. To improve the measurements we will change the substrates to glass in order to avoid leakage currents. Also, the atomic percent of Aluminum will be increased.

Conclusions

Aluminum doped ZnO thin films and nanofibers were prepared by electrospinning. The fibers contain an Al concentration ranging from 0.5 and 1.0 at. %. Compositional analysis shows a deficiency of oxygen as compared to zinc. The morphology of the fibers indicate high porosity and high degree of ramification along the fibers after heat treatment. Preliminary test of the fibers mats as gas sensors are underway.

Acknowledgements

This project was supported by DOE-EPSCoR Program grant DE-FG02-08ER46526 and NSF-PREM grant NSF-DMR-0934195.

References.

[1] X. Zi-qiang, D. Hong, L. Yan, C. Hang, Al-doping effects on structure, electrical and optical properties of c-axis-oriented ZnO:Al thin films, Mat. Science. in Semic. Process. 9 (2006) 132-135.

[2] Caglar Y., Caglar M., Saliha Ilican, Microstructural, optical and electrical studies on sol gel derived ZnO and ZnO:Al films, Current Appl. Phys. 12 (2012) 963-968]

Label-free impedimetric detection of copper based on DNAzyme biosensor

Cristina Ocaña[1], Natalia Malashikhina[2], Valery Pavlov[2] and Manel del Valle[1]**
[1]Sensors and Biosensors Group, Department of Chemistry, Universitat Autònoma de Barcelona, Edifici Cn,08193 Bellaterra, Barcelona, SPAIN.

[2]Biofunctional Nanomaterials Department, CIC biomaGUNE, Parque Tecnológico de San Sebastian, Donostia, San Sebastian, SPAIN

manel.delvalle@uab.es

Abstract

In this work, we report a sensitive and selective Cu^{2+} detection method based on the use of specific DNAzyme. DNAzymes are single stranded DNA molecules that exhibit catalytic activity. With the employed DNAzyme, the presence of ascorbic acid and Cu^{2+} ions catalyzes the breakdown of the specific hairpin DNAzyme. The detection principle is labeless, based on changes of interfacial properties of the electrode; these were probed in the presence of the reversible redox couple $[Fe(CN)_6]^{3-}$/ $[Fe(CN)_6]^{4-}$ as marker using the electrochemical impedance spectroscopy (EIS) technique. In the catalytic event, the electrode surface was partially blocked due to catalytic action of DNAzyme accompanied by the adsorption of oxidation products on the electrode surface, resulting in an increase of the interfacial electron-transfer resistance detected by EIS. .

Keywords: Impedance, DNAzyme, copper, ascorbic acid, labeless.

Introduction

DNAzymes are single stranded DNA molecules that exhibit catalytic activity which are exploited in medicine, material sciences and biosensing. Developments in these areas are related to the many advantages of DNAzymes over conventional protein enzymes, such as their thermal stability or simpler preparation[1,2]. One of the typical applications of DNAzymes in chemical analysis is for the low level determination of metals, although most of them are based on spectrophotometric or fluorimetric techniques.

In the present communication, we report the application a label-free electrochemical DNAzyme biosensor for the detection of copper using avidin graphite-epoxy composite electrodes[3]. This platform is of general use in our laboratories and has been already extensively studied and applied for amperometric, enzymatic, immuno and genosensing assays[4,5].

Experimental

The scheme of the experimental procedure is represented in Figure 1.

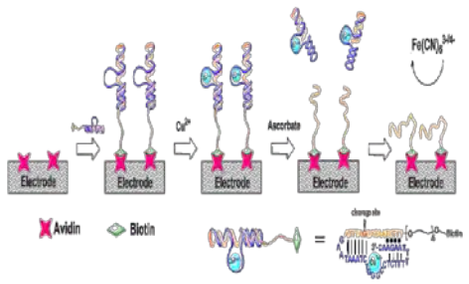

Figure 1. Steps of the biosensing procedure

In order to compare the results obtained from the different electrodes used, and to obtain independent and reproducible results, relative signals are needed[6]. Thus, the Δ_{ratio} value was defined according to the following equations:

$$\Delta_{ratio} = \Delta_s / \Delta_p$$

$$\Delta_s = R_{ct\ (DNAzyme\text{-}AA\text{-}Cu)} - R_{ct\ (electrode\text{-}buffer)}$$

$$\Delta_p = R_{ct\ (DNAzyme)} - R_{ct\ (electrode\text{-}buffer)}$$

where $R_{ct(DNAZyme\text{-}AA\text{-}Cu)}$ was the electron transfer resistance value measured after incubation with ascorbic acid and copper; $R_{ct\ (DNAzyme)}$ was the electron transfer resistance value measured after DNAzyme inmobilitation on the electrode, and $R_{ct\ (electrode\text{-}buffer)}$ was the

electron transfer resistance of the blank electrode and buffer.

Results

First of all, the concentration of DNAzyme immobilized onto the electrode surface was optimized by building it response curve. After that, and following the above experimental protocol for the detection of copper, the biosensor response was initially evaluated. The presence of ascorbic acid and Cu^{2+} ions catalyzes the breakdown of the specific hairpin DNAzyme and the electrode surface was partially blocked due to catalytic action of DNAzyme accompanied by the adsorption of oxidation products on t he electrode surface, resulting in an i ncrease of the interfacial electron-transfer resistance, figure 2 .

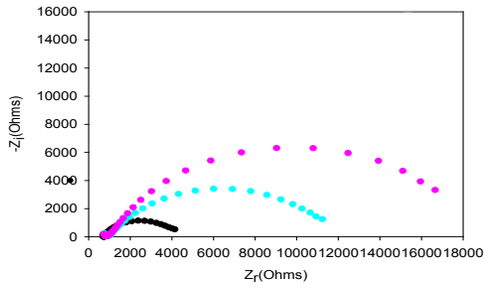

Figure 2. Nyquist Diagram of: (a) Electrode-buffer ●, (b) DNAzyme ● , and (c) Ascorbic acid and Cu^{2+} 30 μM ● .

Performing new experiments with solutions containing different amount of cupper, the calibration curve was built. Figure 3 shows this calibration curve. After adding 40 μ M of Cu^{2+} DNAzyme is saturated and Rct drecreases.

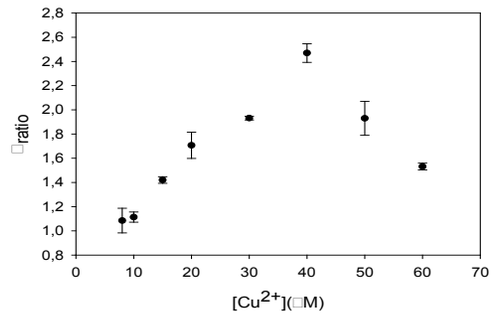

Figure 3. Calibration curve versus Cu^{2+} concentration.Uncertainty values corresponding to replicated experiments (n = 5).

The system presented a linear response range of 10 μM to 40μM Cu^{2+} , a sensitivity of $4 \cdot 10^{-2}$ $\mu M^{-1}$and a detection limit of 6.5 μM.

To study the specificity of the system, we evaluated the response of different divalent metals such as nickel, cadmium and l ead. As can be seen in figure 4, the interference to these metals can be considered negligible.

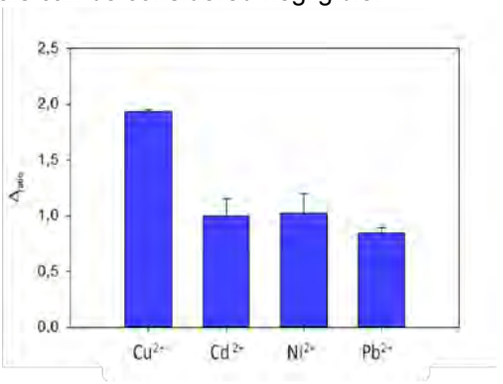

Figure 4. Bar charts of different metals assayed at the same concentration (30 μM). *Uncertainty values corresponding to replicated experiments (n = 5).*

Conclusions

In conclusion, we have described a s imple biosensor for the determination of copper(II) based on its DNAzyme immobilized by simple affinity avidin-biotin on the electrode surface. The presence of Cu^{2+} and ascorbic acid catalyses the breakdown of hairpin DNAzyme. The immobilization step and the catalytic event difficult the electron-transfer kinetics of the redox probe at the electrode interface, which have been reported by labeless electrochemical impedance spectroscopy. The DNAzyme biosensor shows a linear response range of 10 μM to 40μM Cu^{2+} and a detection limit of 6.5 μM. Interference to some related metals can be considered negligible. Advantages of the reported label-free method for Cu^{2+} detection are together with the labeless detection, its simplicity, sensitivity and high selectivity.

References

[1] J. Liu; Y.Lu, Angewandte Chemie, Vol.46, pp.7587–7590, 2007.

[2] I. Willner; B. Shlyahovsky; M . Zayats B. Willner, Chemistry Society Reviews, Vol. 37, pp.1153, 2008.

[3] E. Zacco; MI. Pividori; S. Alegret, Biosensors and Biolectronics, Vol.21, No. 7, pp. 1291-1301, 2006.

[4] A.Merkoçi.;M. Aldaver; S. Marín; S. Alegret,TrAC Trends in Analytical Chemistry , Vol.24, No.4, pp.341-349, 2005.

[5] M. Pumera,; M. Aldavert; C. Mill.; A. Merkoci; S. Alegret, Electrochimica Acta, Vol. 50, No.18, pp.3702-3707, 2005.

[6] A. Bonanni; M.J. Esplandiu; M.I. Pividori; S. Alegret; M. del Valle, *Analytical and Bioanalytical Chemistry*, Vol. 385, No.7,pp. 1195-1201, 2007.

Electrospun Nanobridges Towards Self-Heated Gas Sensors with Enhanced Sensitivity

C.J. Camargo[1], A. Melendez[2], J. Robles[2], J. Esteve[1], H. Campanella[1] and I. Ramos[2]
[1] Instituto de Microelectrónica de Barcelona IMB-CNM (CSIC), 08193, Barcelona, Spain
[2] Department of Physics and Electronics, University of Puerto Rico at Humacao, Humacao, PR 00791, Puerto Rico.
E-mail: carlos.camargo@csic.es

Abstract

This paper presents the fabrication process of ZnO and GaN nanobridges by electrospinning. The main purpose of these structures is obtaining fibers with larger area exposed to the gas to be sensed and consequently obtaining an enhanced sensitivity. In addition, the substrate where the fibers are deposited is favorable for a well-controlled current setting and therefore, take advantage of self-heating effects to set appropriate temperatures for gas sensing.

Keywords: Electrospining, nanofibers, gas sensor, self-heating, GaN, ZnO.

Introduction

Semiconductors-based gas sensors have wide applications in medical diagnosis, environmental sensing and control applications. Gas sensing is possible thanks to the convection of electrical conductivity due to surface reaction such as oxidation or reduction caused by different gas exposures. Since these surface reactions depend on the active centers and the defects existing on the surface layer of the materials, the sensor response is usually determined by the surface-to-volume ratio of materials. [1]

Compared with conventional materials like bulk or thin films applied to gas sensors, one-dimensional nanostructures such as electrospun nanofibers, have a high gas sensitivity due to the ultra-high surface-to-volume ratio. It also implies that transport quality could be strongly modified by reactions at grain boundaries and depletion of carriers in grains. [2]

In this regard, our proposal for deposition of individual nanofibers as a bridge leads to the enhancement of gas sensitivity since the exposed area is probably doubled in comparison with those fibers electrospun on a solid substrate.

In addition, the small dimensions of our structures are responsible for self-heating effects caused by dissipated power while operating in electrical devices. This leads to temperature gradients, which significantly reduce the lifetime of these components. However, effective temperatures for gas sensing applications could be settled by applying a well-controlled current value to the nanobridge. This concept has already been proved by Prades, et al. [3]

In this work, we reported the fabrication process of Zinc Oxide (ZnO) and Gallium Nitride (GaN) nanobridges, leading to self-heated gas sensors with enhanced sensitivity.

Experimental Procedures

In order to fabricate nanobridges by electrospinning, firstly the substrate where the fibers are collected is micro-machined. Conventional silicon wafers were covered by deposition of 400 nm of thermal SiO_2 as electrical insulating layer. Then, the oxide and the substrate were etched by reactive ion etching to make 10 μm-height structures with rectangular and squared patterns (as Picture 1 shows). The gaps between patterns are in the range from 2 to 50 μm. Post-processing of nanobridges involves the deposition of a metal layer over the high-relief regions to serve as electrical pads. This procedure is carried out by stenciling.

GaN and ZnO nanofibers are deposited using conventional electrospinning technique. First, a polymeric solution based on cellulose acetate (CA) was prepared to be used as carrier of the Zinc Choride ($ZnCl_2$) and Gallium Nitrate. The CA is dissolved in a 1:2 molecular weight ratio mixture of Dymethylacetamide (DMA) and Acetone. The final solution of CA is 20% wt.

Parallel to this, a 30% wt $ZnCl_2$ solution is prepared, using acetone as solvent (for ZnO), and 20% wt gallium nitrate solution was made using DMA instead acetone (for GaN). Each

solution was mixed several hours in a volume ratio of 1:2 with the polymeric solution. More details about precursor solution are presented in [4].

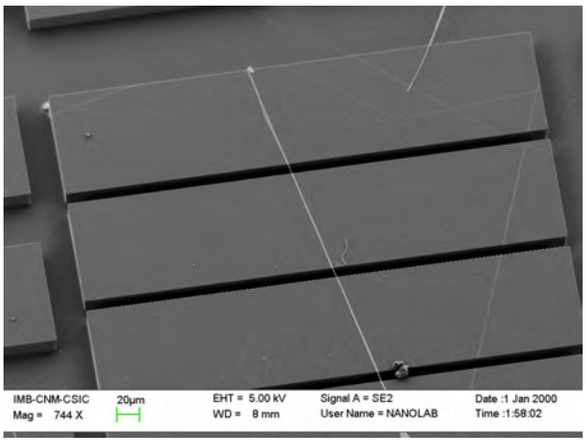

Picture 1. Rectangular patterns used for deposition of nanofibers by electrospinning. It is clearly showed a ZnO fiber crossing several patterns and making bridges between them.

Finally, once the fibers are deposited, the ZnO bridges are obtained by sintering of the fibers at 600 ºC in air for two hours, with a previous temperature ramp of 5 ºC/min.

The GaN process has two stages: calcination and nitridation. The first is made in nitrogen ambient at 500 ºC with a previous ramp of 2.5 ºC/min. Then, the temperature is increased up to 1000 ºC at ratio 2.5 ºC/min. The nitridation is carried out under ammonia atmosphere flowing at 40 sccm during 4 hours.

Results and future work

Different nanobridges are shown in next pictures. ZnO bridges are highly granulated, which is favorable for gas sensing applications since the gas penetrates the structure and larger area is exposed, however it also makes the bridges structurally weak and easy to break during process. It gives a major value to the achieved results. The structures present a mean diameter of 700 nm. On the other hand, GaN bridges are thinner since the sintering process is longer. Contrary to ZnO structures, they are not granulated, therefore are suitable to make longer bridges. Future work involves the electrical and thermal characterization under different atmospheres.

Acknowledgements

This research is partially funded by PENN-UPRH PREM (NSF-DMR-0934195).

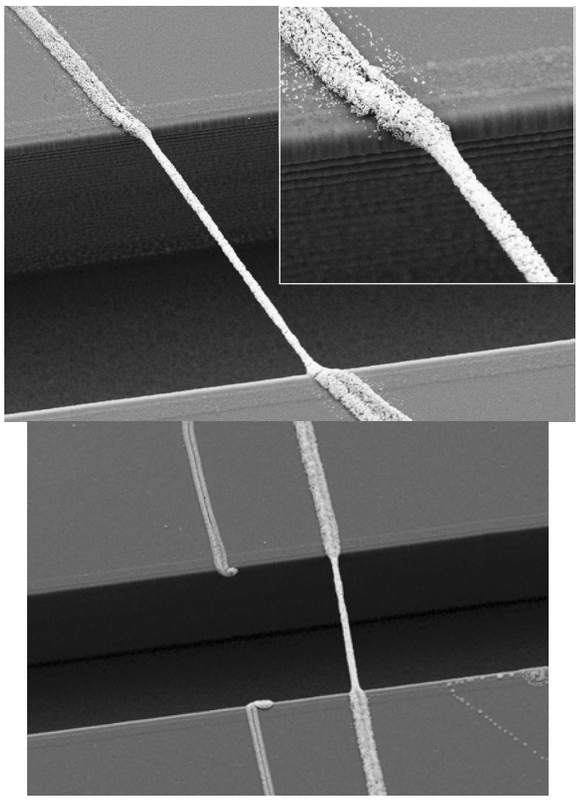

Picture 2. ZnO nanobridges. Up: A 20 µm-long nanobridge is depicted. Inset is a zoom in, which describes the high granulation of the structure. Down: The suspended fibers are structurally weak which makes more valuable the results achieved.

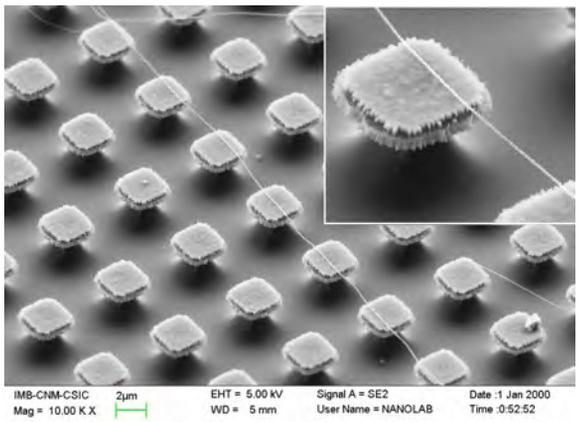

Picture 3. GaN nanobridges. A different pattern is used in this case to obtain several nanobridges suspended between squared islands.

References

[1] A. Ponzoni, E. Comini, G. Sberveglieri. *Appl. Phys. Lett. 88,* 203101, 2006.
[2] H. Huang, Q.K. Tang, Y.C. Lee, T.D. Tran, M.S. Tse. *Appl. Phys. Lett. 87,* 163123, 2005.
[3] J.D. Prades, R. Jimenez-Diaz, F. Hernandez-Ramirez, S. Barth, A. Cirera, A. Romano-Rodriguez, S. Mathur, J.R. Morante. *Appl. Phys. Lett. 93,* 123110, 2008.
[4] A. Melendez, K. Morales, I. Ramos, E. Campo, J. Santiago-Avilés. Proc. of SPIE, Vol. 7402, 740210-2, August 2-6, 2009.

Chapter 2: Chemical Sensors

CARACTERIZACIÓN DE FIBRAS A BASE DE OXIDO DE ESTAÑO EN LA ESTEQUIOMETRÍA $Sn_{1-x}Fe_xO_2$ PARA APLICACIONES COMO SENSOR DE GASES

J. Rodríguez[2], Abrego[1], A. Watson[1], I. E. Ching[1]
[1]Departamento de Ciencias Naturales; Facultad de Ciencias y Tecnología, Universidad Tecnológica de Panamá.
[2]Departamento de Física; Facultad de Ciencias Naturales, Exactas y Tecnología, Universidad de Panamá.
Panamá, Ciudad de Panamá
juan.rodriguez8@utp.ac.pa, ildeman.abrego@utp.ac.pa,
amanda.watson@utp.ac.pa, eleicer.ching@utp.ac.pa

Abstract

Se prepararon fibras de óxido de estaño mediante la técnica de electrospinning a partir de una solución precursora a base de $SnCl_4$ y $FeCl_3 \cdot 6H_2O$ en distintas relaciones molares, las cuales fueron tratadas térmicamente y luego caracterizadas física y morfológicamente. Su caracterización mediante SEM evidenció la formación fibras bastante cilíndricas y homogéneas con diámetros de 1 a 20 μm. Pruebas sensoras en presencia de vapor de agua, mostraron variaciones de hasta 10^3 Ω en su resistencia eléctrica. Por pruebas de impedancia eléctrica se evidenció un comportamiento capacitivo con un ligero comportamiento inductivo. Por otra parte, en las pruebas de corriente-voltaje a diversas temperaturas, se obtuvo valores mayores de conductividad eléctrica a temperaturas más elevadas, además de otros resultados que serán posteriormente discutidos.

Palabras claves: electrospinning, sensor de gases, dopaje con Fe.

Introducción

El óxido de estaño (SnO_2) es un material semiconductor, transparente y de gran estabilidad química y mecánica. El interés que ha tenido su estudio, está motivado fundamentalmente por las múltiples aplicaciones que posibilitan sus propiedades físico-químicas. Cabe destacar especialmente su extendido uso como sensor de gases, conductor transparente y catalizador. Sin embargo, la aplicación más extendida del SnO_2 se basa en su capacidad de detección de gases. Durante las últimas décadas, ha sido uno de los materiales más ampliamente empleado como sensor de gases, con múltiples aplicaciones a nivel industrial y doméstico, en dispositivos de alarmas o detectores de gases contaminantes como es el caso del CO, CO_2, H_2, H_2O, NH_3, O_2 y NO_X entre otros [1].

La sensibilidad, así como la selectividad del SnO_2 ante diferentes gases, dependerán de las condiciones a las que ocurra la reacción. Además, la sensibilidad de detección puede incrementarse disminuyendo el tamaño de partícula, dopando con elementos metálicos, como en el caso del hierro [2], o modificándola temperatura a la que se encuentre el detector.

En el presente trabajo de investigación se caracterizan fibras de SnO_2 dopadas con hierro. En este sentido, se prepararon muestras a base de una solución precursora de $SnCl_4$ con distintas cantidades de $FeCl_3 \cdot 6H_2O$, por la técnica de electrospinning, para obtener muestras que mantuvieran relaciones molares fijas de Sn:Fe y poder obtener, mediante tratamiento térmico, fibras con la estructura $Sn_{1-x}Fe_xO_2$ para $0 \leq x \leq 1.0$. El polímero utilizado como medio para la técnica de electrospinning fue poli-óxido de etileno (PEO) de Aldrich. Se presentarán a continuación los primeros resultados que ha arrojado el desarrollo de este trabajo de investigación.

Caracterización morfológica

Micrografías tomadas mediante SEM muestran la formación de fibras con simetría casi cilíndrica con diámetros bastante uniformes que varían entre $(1-20)\,\mu m$. La superficie de estas fibras se observa bastante uniforme sin formación de poros, ni fases diferenciables a lo largo de la estructura, hasta la magnificación que se muestra (figura 1).

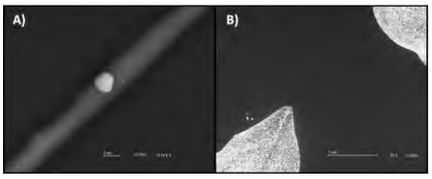

Figura 1. Imágenes mediante SEM de la superficie de una fibra (A) dopada con Fe al 0.3 molar y de sus contactos (B).

Medidas de impedancia

Las pruebas de impedancia eléctrica fueron realizadas con un puente de impedancia Agilent E4980A. Los primeros resultados obtenidos dan indicios de un comportamiento capacitivo de las muestras evidenciado por un patrón de dos semicírculos (figura 2), uno a frecuencias de entre 20 Hz a 8.5 kHz, y otro a frecuencias de entre 9.5 kHz a 130 kHz, según la información disponible en la literatura [3]. Sumado a esto, se pudo observar en las muestras analizadas un leve comportamiento inductivo evidenciado por un pequeño rizo a frecuencias cerca de 11 kHz, resultado que se discutirá en más detalle.

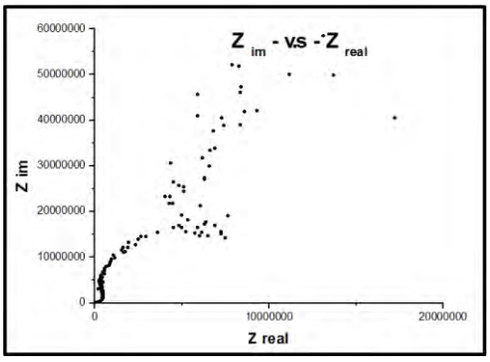

Figura 2. Espectro de impedancia para muestra con dopaje a 0.3 molar.

Medidas de resistencia versus tiempo en presencia de vapor de agua

La resistividad eléctrica de las muestras dopadas a 0.3 molar, en condiciones de humedad relativa entre $(60-65)\,\%$ presentan valores de en el orden de $10^3\,\Omega\cdot m$. Estas muestras fueron sometidas a pruebas sensoras con volúmenes de agua de $(25-200)\,\mu L$ inyectados mediante flujos de aire seco (figura 3). Se observó una disminución de su resistividad eléctrica hasta valores en el orden de $10^1\Omega\cdot\mathrm{m}$, sin presentarse para ninguno de los volúmenes un punto de saturación, al igual que otros resultados que serán discutidos en más detalle.

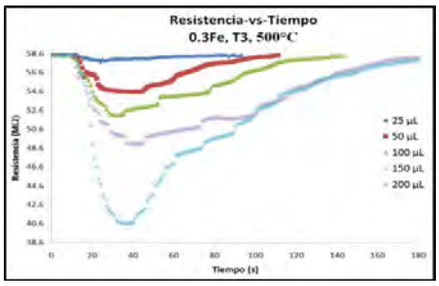

Figura 2. Respuesta sensora ante distintos volúmenes de vapor de agua para una muestra con dopaje de Fe a 0.3 molar.

Medidas de voltaje-corriente

Las medidas de voltaje-corriente fueron realizadas en un rango de temperatura de $(25\text{-}500)\,℃$ en condiciones de humedad relativa de entre $(60-65)\,\%$. Ensayos preliminares muestran una mayor conductividad eléctrica a temperaturas más elevadas, resultados que serán ampliados y discutidos en más detalle, mediante mediciones realizadas con la adquisición de un electrómetro Keithley modelo 6517B.

Referencias

[1] D. Maestre, "CRECIMIENTO Y CARACTERIZACIÓN MEDIANTE TÉCNICAS DE MICROSCOPÍA, DE NANO- Y MICROESTRUCTURAS DE SnO_2 y TiO_2", tesis de doctorado, Madrid, Facultad de Ciencias Físicas, Departamento de Fisica de Materiales.

[2] K. Galatis, et al., "p- and n- type Fe-doped SnO_2 gas sensors fabricated by the mechanochemical processing technique" Sensors and Actuators B 93, 2003, pp. 562-565.

[3] A. Conde, et al., "Corrosión de la aleación 8090 en medios salinos de agresividad moderada" en *Revista de metalurgia* [*En línea*], *Mayo de 1998.*

Caracterização de filmes finos de SnO_2 obtidos por oxidação térmica do estanho

Luis da S. Zambom[1], Marcelo Bariatto A. Fontes[1], Francisco T. Degasperi[1], Ronaldo D. Mansano[2]
[1] MPCE/DSE – FATEC-SP – CEETEPS, 01124-060, São Paulo, Brasil
[2] DEE – PSI – EPUSP, São Paulo, SP, Brasil
zambom@fatecsp.br, bariatto@fatecsp.br, ftd@fatecsp.br

Abstract

Filmes finos de estanho foram obtidos a partir da técnica de evaporação térmica. Os filmes de estanho obtidos passaram por processos de oxidação em ambiente de oxigênio atmosférico na temperatura de 300 °C com o objetivo de se obter filmes finos de óxido de estanho. A partir desses filmes, estruturas elétricas foram feitas e verificou-se a sua sensibilidade na presença de gás oxigênio. Além da análise elétrica, foram obtidos valores de espessura, índice de refração, resisitividade e composição química. Por meio dos resultados elétricos verificou-se que os filmes de óxido de estanho obtidos por essa técnica mostraram sensibilidade ao gás oxigênio.

Palavras-chave: Evaporação, filme fino, SnO_2, sensor, gás

Introdução

Filmes finos de óxido de estanho (SnO_2) são utilizados como sensores químicos para detecção de diferentes gases. A resposta do sensor de SnO_2 para um determinado gás é obtido pela variação de resistência do sensor, para gases oxidantes (NO_2, O_2, SO_2, H_2S etc.) [1,2} para gases redutores (CO, etc.) [2,3] e vapores orgânicos (C_2H_5OH, CH_3OH, tolueno, benzeno, etc.) [3,4]. Dependendo do tipo de gás adsorvido (oxidante ou redutor), medindo-se em atmosfera controlada e temperatura entre 100 °C a 350 °C, na superfície do óxido de estanho, uma região espaço-carga de depleção ou acumulação é produzida. Filmes finos de óxido de estanho podem ser obtidos por meio de diferentes técnicas, que incluem sputtering reativo, spray pirólises, evaporação, sol-gel e deposição química a vapor assistida por plasma entre outras. Cada uma dessas técnicas permite obter óxido de estanho com propriedades particulares que são dependentes da uniformidade de espessura, cristalinidade, tamanho de grão e área de crescimento. O objetivo deste trabalho foi de obter filmes finos de óxido de estanho e utilizá-los na detecção de gás oxigênio, por não ser tóxico nas condições normais de uso e, também, por não ser necessário um ambiente isolado. Os testes de desempenho, para diferentes concentrações de O_2, são realizados em sistema de vácuo apropriado com controle das variáveis envolvidas.

Parte Experimental

Para a obtenção de filmes de óxido de estanho foram utilizadas lâminas de silício ((100), tipo-p, (1,0 - 10) MΩ.cm, diâmetro de 7,5 cm). Todas as lâminas passaram pela seguinte limpeza: 10 minutos em solução de ácido sulfúrico e peróxido de hidrogênio, 5 minutos de enxágue em água deionizada de 18 MΩ.cm e 1 minuto em solução de ácido fluorídrico. O processo consistiu em evaporar amostras, massa variando entre 38,5 mg a 92,4 mg de estanho, em pressão de $1{,}0.10^{-5}$ torr. As amostras de estanho foram oxidadas, com o oxigênio do ar, sobre um prato quente na temperatura de 300 °C. Os filmes de óxido de estanho foram caracterizados pelas seguintes técnicas: a) elipsometria - índice de refração, perfilometria – espessura, quatro pontas – resistividade, Rutherford Backscattering – para determinação de Sn e O e análise IV – para detecção do gás oxigênio. As conexões elétricas sobre o de óxido de estanho foram obtidas utilizando-se evaporação direta de alumínio, com 0,88 mm de diâmetro e 500 nm de espessura. A distância entre cada par de contatos varia entre 0,4 mm e 0,7 mm, figura 1.

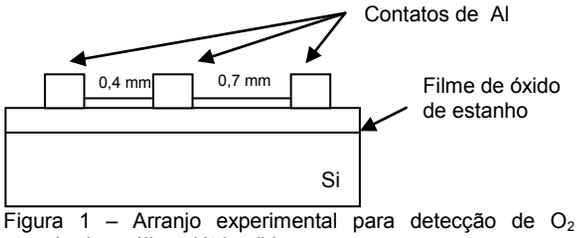

Figura 1 – Arranjo experimental para detecção de O_2 através da análise elétrica IV.

Entre os contatos de Al, um ambiente de gás oxigênio, 99,999 %, foi mantido constante, na temperatura ambiente.

Resultados e Discussão

A tabela 1 mostra que os filmes de óxido de estanho estão mais resistivos quando comparados com o de estanho da literatura.

Tabela 1 – Resultados da oxidação do estanho.

Esp. Sn (nm)	Tempo oxidação (min)	Esp. SnO_2 (nm)	*Resistividade SnO_2 (Ω.cm)
98	14	153	$6{,}06\ 10^{-3}$
116	14	193	$4{,}72\ 10^{-3}$
98	29	194	-
116	29	191	$1{,}39\ 10^{-3}$

Literatura [5]:
* Sn = $1.09\ 10^{-6}\ \Omega$.cm
SnO_2 = ($5\ 10^{-2}$ – $5\ 10^{-5}$) Ω.cm

O índice de refração, figura 2, varia de 1,64 a 3,16, indicando que para o menor valor tem-se maior concentração de oxigênio presente no filme e, para o maior valor, tem-se maior concentração de estanho no filme. Diferentemente da literatura, os valores de índice de refração variam significativamente com o comprimento de onda utilizado na elipsometria. O espectro de RBS, figura 3, mostra a presença de Sn e O no filme, no entanto, a concentração de oxigênio é baixa, indicando uma baixa oxidação do estanho.

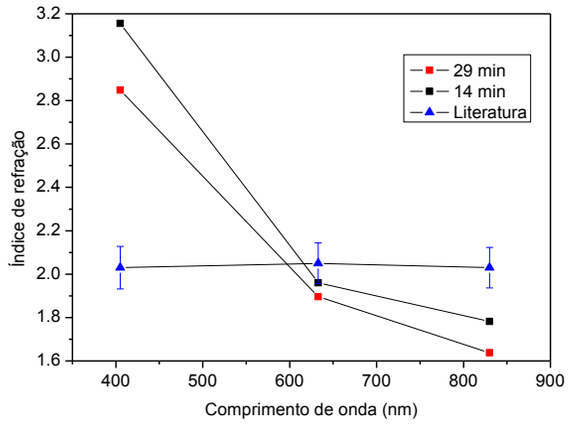

Figura 2 – Índice de refração versus comprimento de onda.

A figura 4 mostra um resultado típico de curva IV para a detecção de oxigênio, em temperatura ambiente, para os filmes de óxido de estanho obtidos por oxidação térmica do estanho. A presença do gás oxigênio produziu um aumento de corrente elétrica entre os contatos de alumínio em comparação com o gás nitrogênio.

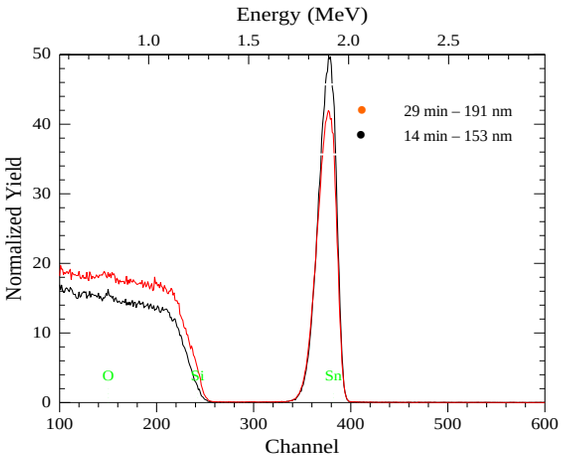

Figura 3 – Espectros RBS de SnO_2.

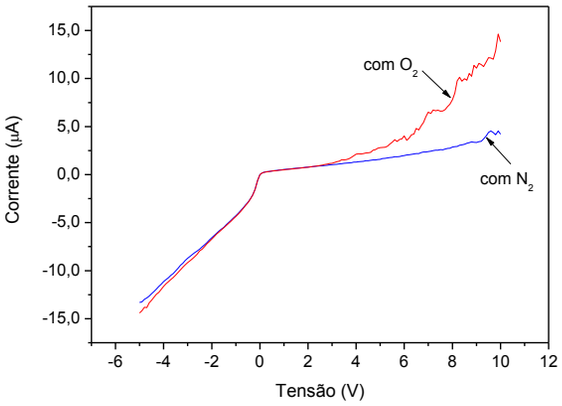

Figura 4 – Detecção de oxigeno através da Curva IV.

Conclusão

Filmes finos de óxido de estanho, obtidos pela oxidação térmica do estanho, apresentaram grande variação na concentração de oxigênio, como pode ser visto pelos valores de índice de refração. Esses filmes mostram-se sensíveis quando expostos ao gás oxigênio.

Agradecimentos

Os autores agradecem ao CNPq pela ajuda financeira e ao LAMFI-IFUSP pela análise RBS.

Referências

[1] W. Hellmich et al, Thin Solid Films, Vol. 263, pp. 231-237, 1995.
[2] P. Serrini et al, Thin Solid Films, Vol. 304, pp. 113-122, 1997.
[3] G. Sberveglieri et al, Sensors and Actuators B, Vol. 7 pp. 721-726, 1992.
[4] T. Yama et al, Analytical Chemistry, Vol. 34, No. 11, pp. 1502-1503, 1962.
[5] S. Reddaway, D. A. Wright, J. Appl. Phys., vol. 16, pp. 195-196, 1965.

Monitorização das Propriedades Viscoelásticas de uma Suspensão de Amido com um Sensor Acústico

M. D. Santos, M. T. S. R. Gomes*
CESAM & Departamento de Química, Universidade de Aveiro
3810-193 Aveiro, Portugal
*mtgomes@ua.pt

Resumo

Um cristal piezoeléctrico de quartzo foi utilizado para seguir a gelatinização do amido de milho. Através da observação das variações da frequência em série do cristal foi possível detectar alterações nas propriedades viscoelásticas do amido. Essas alterações foram analisadas à luz do conhecimento existente sobre o comportamento dos grãos de amido sob acção do aquecimento. O máximo da frequência (mínimo da viscosidade) ocorreu aos 73,5±0,5 ºC, temperatura esta que coincidiu com a perda total de birrefringência observada por microscopia de luz polarizada.

Palavras-chave: Amido, Sensor Acústico, Cristal Piezoeléctrico de Quartzo, Gelatinização.

1. Introdução

Actualmente, o amido está presente em muitos dos alimentos consumidos pelo ser humano, contribuindo com 50% a 70% da energia necessária na dieta humana (fonte directa de glucose) [1].

O amido para além de essencial à alimentação, tem grande importância como matéria-prima para diversas indústrias, sendo extraídas anualmente 60 milhões de toneladas em todo o mundo [1]. De todo o amido extraído, 60% é utilizado na área alimentar, enquanto que os restantes 40% são utilizados na indústria farmacêutica, assim como indústrias não alimentares [2].

A gelatinização do amido é geralmente vista como um conjunto de processos que ocorrem durante o aquecimento do amido na presença de água: inchamento do grânulo, saída de amilose, fusão da amilopectina e formação de gel ou massa tipo pasta [3]. Este processo é acompanhado pela perda de cristalinidade, perda de birrefringência, destruição da ordem molecular [4, 5] e aumento da viscosidade [5].

Diversas técnicas têm sido usadas no estudo deste processo, contando-se entre elas, a calorimetria diferencial de varrimento (DSC), a microscopia e a reologia. Como alternativa iremos utilizar neste trabalho um sensor acústico, baseado na utilização de um cristal de quartzo piezoeléctrico. Os sensores acústicos, que são geralmente vistos como sensores de massa, quando estão em contacto com um meio líquido, vêm a sua frequência mudar drasticamente com as propriedades do mesmo [6].

.

2. Material e Métodos

2.1. Amido

Foi analisado amido de milho comercial da marca Maizena, em suspensão 2,5%.

2.2. Microscopia Electrónica de Varrimento (SEM)

As imagens foram obtidas através de um microscópio Hitachi SU-70.

2.3. Microscopia Luz Polarizada

Foi utilizado um microscópio Olympus BH2-UMA, com um “Hot Stage” Mettler FP82HT e Processador Central Mettler FP90. A suspensão de amido foi aquecida a uma velocidade de 2,0ºC/minuto.

2.4 Sensor Acústico

Foram utilizados cristais de quartzo piezoeléctrico de 9 MHz, corte AT, HC-6/U, polidos, com eléctrodos de ouro (ICM).

Foi montado o sistema apresentado na fig. 1. Introduziram-se 1,00 ml da suspensão de amido na célula de teflon, tendo ficado em contacto com uma das faces do cristal piezoeléctrico.

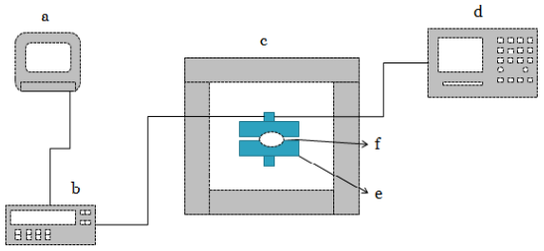

Fig. 1 – Sistema utilizado: (a) computador, (b) multímetro digital, (c) câmara termostática, (d) analisador de rede/espectro /impedância, (e) célula de teflon, (f) cristal de quartzo.

A temperatura foi monitorizada com recurso a uma sonda Pt100, que se encontra mergulhada na suspensão. O cristal de quartzo encontrava-se ligado a um analisador de rede/espectro/impedância, Hewlett-Packard 4395A. A frequência em serie foi lida em intervalos de 0,5 ºC.

3. Resultados e Discussão

Através da imagem obtida por Microscopia electrónica de varrimento (fig. 2), foi possível ver que os grânulos de amido de milho apresentam uma forma irregular com tamanho que variava entre 7 e 15 µm.

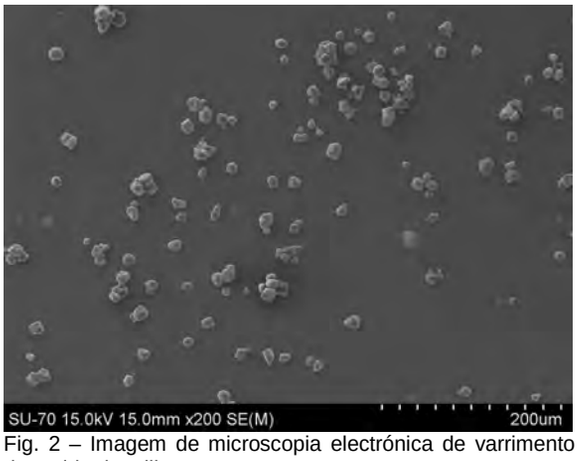

Fig. 2 – Imagem de microscopia electrónica de varrimento de amido de milho.

Através da microscopia de luz polarizada foi possível monitorizar a perda de birrefringência dos grânulos de amido durante o aquecimento. Verificou-se que aos 74,0 ºC já não existia qualquer cruz de malta, o que revela a perda total de birrefringência do material, que é um indicador da perda da ordem molecular.

A mesma suspensão de amido quando analisada no sensor acústico mostrou ter o comportamento apresentado na fig. 3.

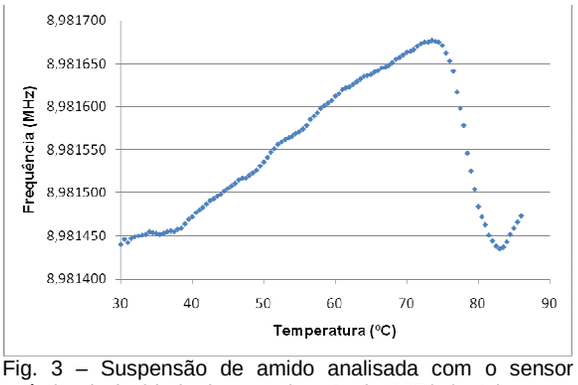

Fig. 3 – Suspensão de amido analisada com o sensor acústico (velocidade de aquecimento de 2 ºC/minuto).

Através do resultado obtido é possível concluir que a viscosidade da suspensão de amido diminui (aumento da frequência) até à temperatura de 73,5±0,5 ºC. Durante esta fase de aquecimento, a água entrou para o interior do grânulo de amido, existindo saída de água e amilose do seu interior [3]. A temperatura a que se verificou a perda total da birrefringência (ordem molecular) dos grânulos, 74,0 ºC (microscopia de luz polarizada) coincide com a a temperatura a partir da qual se verifica um aumento da viscosidade (diminuição da frequência) da suspensão no sensor acústico. O aumento da viscosidade deve-se possivelmente à saída de uma quantidade significativa da amilose que se encontrava aprisionada no interior do grânulo e ao contínuo inchamento do mesmo [3]. A viscosidade aumenta até aos 83,0ºC, máximo de viscosidade, onde os grânulos se encontram inchados ao máximo [1]. A partir desta temperatura, verifica-se uma diminuição da viscosidade (aumento da frequência) devido à ruptura total dos grânulos de amido [1].

4. Conclusão

A utilização de um cristal piezoeléctrico de quartzo permitiu seguir a gelatinização do amido. A temperatura à qual a frequência atingiu um máximo (mínimo da viscosidade) foi concordante com a perda de birrefringência, detectada pela microscopia de luz polarizada.

Bibliografia

1. L. Copeland, et al.,Food Hydrocolloids, vol.: 23, No. 6: pp. 1527-1534, 2009.
2. M.M. Burrell,Journal of Experimental Botany, vol.: 54, No. 382: pp. 451-456, 2003.
3. S. Brouillet-Fourmann, et al.,Rheologica Acta, vol.: 42, No. 1-2: pp. 110-117, 2003.
4. R. Hoover,Carbohydrate Polymers, vol.: 45, No. 3: pp. 253-267, 2001.
5. E.M. Nelles, et al.,Journal of Cereal Science, vol.: 31, No. 3: pp. 287-294, 2000.
6. M.I.S. Verissimo, et al.,Carbohydrate Polymers, vol.: 82, No. 2: pp. 363-369, 2010.

Effect of Organic Vapor in Porphyrin Devices

L. E. G. Armas[a], M. F. G. Huila[b], H. E. M. Peres[c], F. J. R. Fernandez[c], M. A. Valle[c], K. Araki[b], H. E. Toma[b], A. D. Santos[d] and A. C. Seabra[a]

[a] Laboratório de Sistemas Integráveis do Departamento de Engenharia de Sistemas Eletrônicos da Escola Politécnica da USP (LSI-PSI/EPUSP), São Paulo, SP, Brazil

[b]Departamento de Química Fundamental, IQ, da Universidade de São Paulo, USP, São Paulo, SP, Brazil

[c] Laboratorio de Microeletrônica do Departamento de Engenharia de Sistemas Eletrônicos da Escola Politécnica da USP (LME-PSI/EPUSP)

[d] Instituto de Física, IF, Departamento dos Materiais e Mecânica da Universidade de São Paulo, USP, São Paulo, SP, Brazil

e-mail: legarmas@gmail.com

Abstract

We have studied the effect of ethanol vapor on meso (3 and 4 pyridyl) porphyrin cobalt (III) species coordinated to four $[Ru(bipy)_2Cl]^+$ film devices (Pfd) applying positive and negative gate voltage. These devices have not an ohmic behavior on the Source drain current and voltage. For this purpose three different gases were used, Nitrogen (N_2), Air (Ar) and ethanol vapor which passed through the sample. To produce the organic vapor (ethanol) a flux of N_2 was passed for a litle botlle (chamber) of ethanol with the aim of being mixture at different ethanol vapor concentrations (EVCs). We have observed a strong shift on the source drain current, for positive and negative back gate voltage for pure ethanol than for EVCs.

Keywords: porphyrin devices, organic transistors, ethanol sensors.

Introduction

It is well known that organic transistors are the most promising electronic devices when they are fabricated from well ordered thin films as the charge-transporting layers [1–2]. In particular, soluble organic semiconductors are attracting much attention for the development of low-cost, large-scale, and practical devices [3,4]. Among them, porphyrin derivatives are of much interest due to their unique properties in photonics and electronics [5]. Since wide range of properties can be expected by derivatizing with various metals and substituents in a large and flat conjugated macrocyclic ring, porphyrins have often found in the use of solar energy conversion, electron transfer, and artificial photosynthesis [6], but they have been relatively less exploited as building blocks for the fabrication of organic field-effect transistors and sensor devices [7].

In this work we report the effect of pure ethanol vapour and EVCs on the source-drain current and voltage measurements of porphyrin film devices, for positive and negative gate voltage. For comparison this device was exposed to others gases, such as N_2, Ar and EVCs. Showing a strong effect at the presence of pure ethanol.

Samples and experimental details

To fabricate the porphyrin film devices, heavely n doped (100) wafers with dopant concentration of $N_A = 10^{15}$ cm^3 and resistivity 0.002 – 0.005 Ω.cm were used as substrates as well as the back gate electrode with a thermally grown oxide layer of thickness of 280 nm, which acts as the dielectric. Then, the films were generated by direct deposition of the nanocomposite aqueous suspensions over the surface of the prefabricated electrical contacts. For electrical measurements the device were placed in a small chamber connected by a tube to a container of vapor mixture. Concentration of organic vapors was controlled by mixing N_2 gas and measured by gas detector. All electrical measurements were carried out by using DC supply at atmospheric pressure.

Results and discussions

Fig. 1 shows the output characteristics of the Pfd device at the presence of N_2 atmosphere, for negative, zero and positive gate voltage (-5.0 V, 0.0 V, 5.0 V). We observe

not ohmic and similar behaviour for the three different applied gate voltage, as a current of the order of picoampere (pA*).*

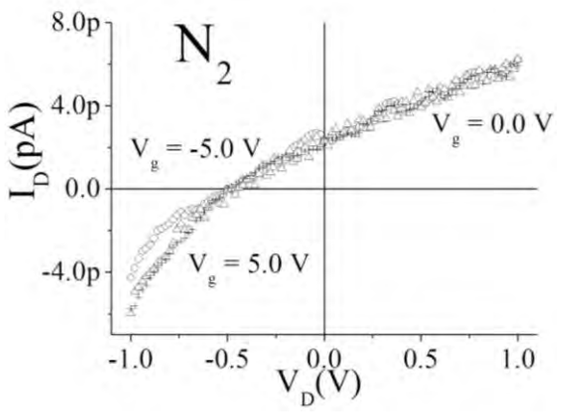

Fig.1- Electrical measurements of source-drain current as a function of source-drain voltage (-1.0 V to 1.0 V) at the presence of N_2 gas and negative, zero and positive gate voltage (-5.0 V, 0.0 V and 5.0 V).

For comparison the same samples were exposed at the presence of pure ethanol and the same gate voltage when the sample was in N_2 (-5.0 V, 0.0 V, 5.0 V). These results are shown in Fig. 2. From this Figure we can observe an ohmic behaviour for zero gate voltage, and a shift of the current for positive and negative gate voltage, being higher for positive than for negative gate voltage. These kind of measurements were performed at the presence of Ar gas, having a little shift on the source-drain current.

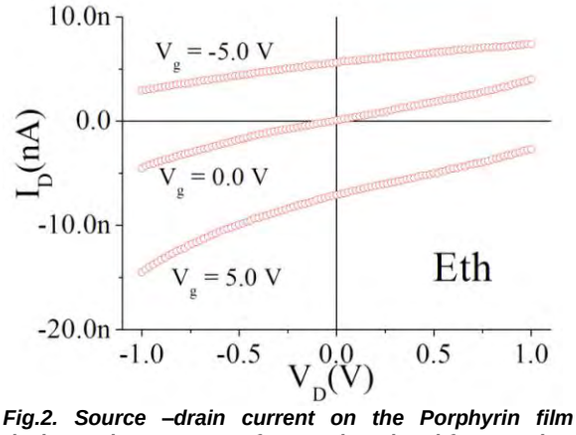

Fig.2. Source –drain current on the Porphyrin film device at the presence of pure ethanol and for negative, zero and positive gate voltage (-5.0 V, 0.0 V, 5.0 V). It is possible to see a shift on the current for this gate voltage.

Fig. 3 shows source-drain current as a function of the bias voltage (V_D) for a fixed gate voltage, -5.0 V, at the presence of different atmospheres (N_2, Ar, E_{th} and EVC of 3500 ppm). We can observe that the current is higher when ethanol vapor pass through the sample than when others gases are absorved by the sample. Similar measurements for positive gate voltage (5.0 V) were performed, showing negative increasing of the current at the presence of ethanol. On the other hand, for zero voltage (not shown here) the current behaviour has a small shift as in Fig. 1 but from – 400.0 pA to 800.0 pA.

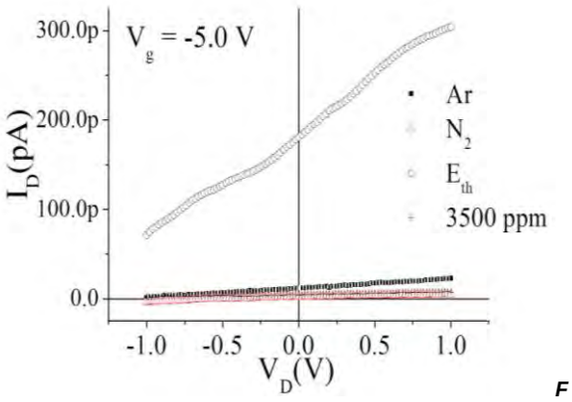

Fig.3. Source –drain current for a fixed gate voltage (- 5.0 V) at the presence of different gases (Ar, N_2, E_{th} and EVCs).

Conclusions

In Conclusion we reported that porphyrin films have a higher sensitivity in ethanol than in N_2, Ar and EVCs. Then, this films could be used as gas sensors.

Acknowledgments

FAPESP for financial support and LME-PSI/EPUSP for facility measurements.

References

[1] P. Gao, D. Beckmann, H.N. Tsao, X. Feng, V. Enkelmann, M. Baumgarten, W. Pisula, K. Müllen, Adv. Mater. Vol. 21, pp. 213, 2009.

[2] L. Jiang, W. Hu, Z. Wei, W. Xu, H. Meng, Adv. Mater. Vol. 21, pp. 3649, 2009.

[3]Y. Zhou, T. Lei, L. Wang, J. Pei, Y. Cao, J. Wang, Adv. Mater., Vol. 22, pp. 1484, 2010.

[4] F. Silvestri, A. Marrocchi, M. Seri, C. Kim, T.J. Marks, A. Facchetti, A. Taticchi, J. Am. Chem. Soc. , Vol. 132, pp. 6108, 2010 .

[5] Z. Wei, W. Hong, H. Geng, C. Wang, Y. Liu, R. Li, W. Xu, Z. Shuai, W. Hu, Q. Wang, D. Zhu, Adv. Mater., Vol. 22, pp. 2458, 2010.

[6] (a) A.J. Jiang, D.K.P. Ng, Acc. Chem. Res., Vol. 42, pp. 79, 2009; (b) G. Lu, Y. Chen, Y. Zhang, M. Bao, Y. Bian, X. Li, J. Jiang, J. Am. Chem. Soc., Vol. 130, pp. 11623, 2008.

[7] (a) C.M. Drain, A. Varotto, I. Radivojevic, Chem. Rev., Vol. 109, 1630, 2009; (b) S.M. Vlaming, R. Augulis, M.C.A. Stuart, J. Knoester, P.H.M. van Loosdrecht, J. Phys. Chem. B, Vol. 113, pp. 2273, 2009; (c) Z. Wang, L.E. Lybarger, W. Wang, C.J. Medforth, J.E. Miller, J.A. Shelnutt, Nanotechnology, Vol. 19, pp. 395604, 2009.

Effect of Gate Voltage in Porphyrin Film Sensors

M. F. G. Huila[b], L. E. G. Armas[a], H. E. M. Peres[c], F. J. R. Fernandez[c], M. A. Valle[c], K. Araki[b], H. E. Toma[b], A. D. Santos[d] and A. C. Seabra[a]

[a] Laboratório de Sistemas Integráveis do Departamento de Engenharia de Sistemas Eletrônicos da Escola Politécnica da USP (LSI-PSI/EPUSP), São Paulo, SP, Brazil

[b]Departamento de Química Fundamental, IQ, da Universidade de São Paulo, USP, São Paulo, SP, Brazil

[c] Laboratorio de Microeletrônica do Departamento de Engenharia de Sistemas Eletrônicos da Escola Politécnica da USP (LME-PSI/EPUSP)

[d] Instituto de Física, IF, Departamento dos Materiais e Mecânica da Universidade de São Paulo, USP, São Paulo, SP, Brazil

e-mail: legarmas@gmail.com

Abstract

In this work we have studied the effect of different ethanol vapor concentrations (EVCs) and gate voltage on meso (3 and 4 pyridyl) porphyrin cobalt (III) species coordinated to four $[Ru(bipy)_2Cl]^+$ film sensors (Pfs). For this purpose Nitrogen (N_2), Air (Ar) and different EVCs were passed through the sample, and to produce the organic vapor concentration a flux of N_2 was passed for a litle botlle (chamber) of ethanol. We have observed a strong positive (negative) shifting on the source drain current for negative (positive) back gate voltage for pure ethanol than for EVCs. On the other hand, a high sensivity to different EVCs, positive and negative gate voltage has been observed by the porphyrin film sensors.

Keywords: porphyrin sensors, organic transistors, ethanol sensors.

Introduction

It is well known that the use of porphyrins layers as the sensing elements in technical applications as the electronic nose [1] and the electronic tongue [2] has anticipated the real comprehension of the mechanisms determining at a microscopic level the interaction between the analyte molecules and the layer itself. A huge bulk of phenomenological data has been accumulated [3], showing the high efficiency of these organic materials versus specific gaseous particles. Experimental research has shown that porphyrins offer a fascinating opportunity, since they couple a very high reactivity to the possibility of tuning their gas sensing properties by simple modifications of their structure: this can be obtained by choosing suitably the metal at the centre of the ring and/or the peripheral substituents [4]. It has been also reported that the sensitivity to gas would be higher for highly disordered layers [5].

In this work we report the effect of pure ethanol vapour on the source-drain current when positive and negative gate voltage is applied to the device. On the other hand, porphyrin film sensors have shown a high sensivity to different EVCs when positive and negative gate voltage is applied.

Samples and experimental details

To fabricate the porphyrin film sensors, heavely n doped (100) wafers with dopant concentration of $N_A = 10^{15}$ cm^3 and resistivity 0.002 – 0.005 Ω.cm were used as substrates as well as the back gate electrode with a thermally grown oxide layer of thickness of 280 nm, which acts as the dielectric. Then, the films were generated by direct deposition of the nanocomposite aqueous suspensions over the surface of the prefabricated electrical contacts. For electrical measurements the devices were placed in a small chamber connected by a tube to a little bottle of ethanol. Concentration of organic vapors was controlled by mixing N_2 gas and measured by gas detector. All electrical measurements were carried out by using DC supply at atmospheric pressure.

Results and discussions

Fig. 1 shows a strong shift on the source-drain current as a function of the bias voltage, at the presence of N_2 atmosphere, Ar, 50 ppm ethanol vapour concentration

and pure ethanol, when negative gate voltage was applied to the device. We observe not ohmic behaviour and high current, in the order of pico-Ampere (pA*).*

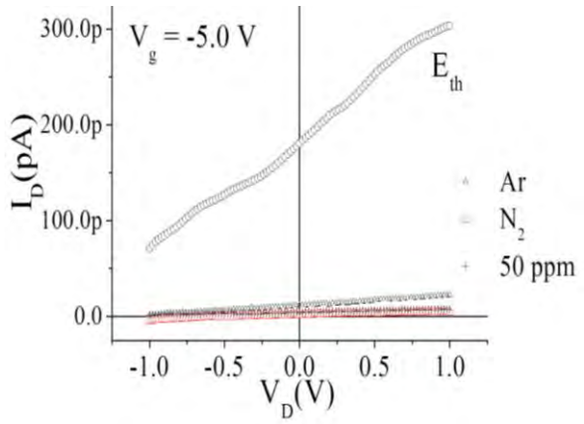

Fig.1- Source-drain current as a function of source-drain voltage (-1.0 V to 1.0 V) at the presence of N_2, Ar, 50 ppm ethanol vapour and pure E_{th}.

For comparison the same samples were exposed to the presence of the same gases as in Fig. 1 and positive gate voltage. The results are shown in Fig. 2, from this figure it is possible to observe a strong negative shifting on the source-drain current for the positive gate voltage.

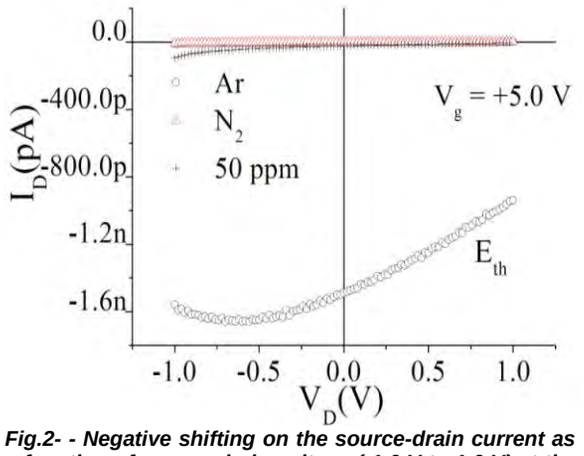

Fig.2- - Negative shifting on the source-drain current as a function of source-drain voltage (-1.0 V to 1.0 V) at the presence of N_2, Ar, 50 ppm ethanol vapour and pure E_{th}, for a positive gate voltage applied.

Finally, Fig. 3 shows source-drain current as a function of time of the device upon exposure to different ethanol vapour concentrations for negative (a) and positive (b) gate voltage at room temperature. We can observe a positive (negative) increasing of the source-drain current as the EVCs increase, as well as a rapid response and recovery time for the applied gate voltage. Someya at. al [6] characterized the influence of alcohols adsorption on the resistance of Single Wall Carbon Nanotubes (SWCNTs).

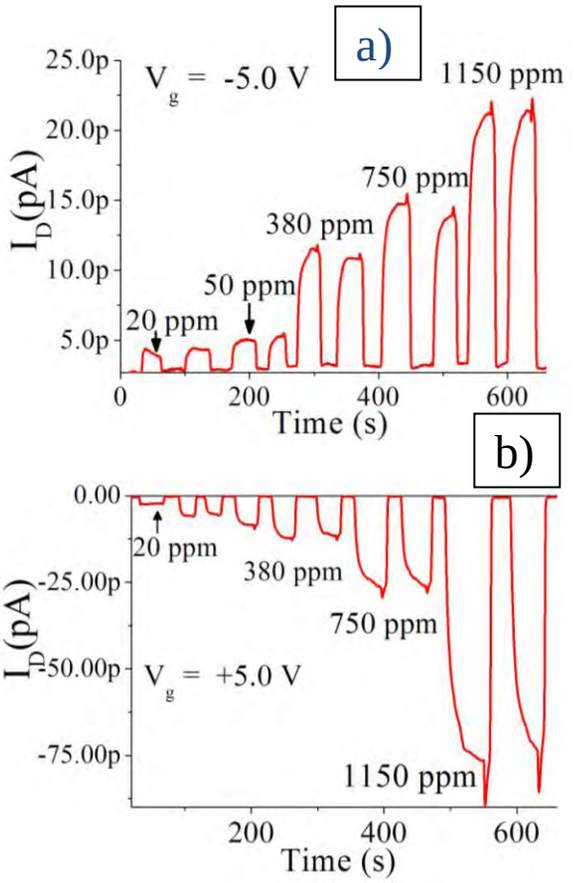

Fig.3. Drain current for a fixed source- drain voltage (V_D= -0.5 V) at the presence of different ethanol concentrations (20 ppm, 50 ppm, 380 ppm, 750 pp and 1150 ppm), for negative (a) and positive (b) gate voltage.

Conclusions

In Conclusion we reported that porphyrin films sesnors have a high sensitivity to different ethanol vapour concentrations at positive and negative gate voltage.

Acknowledgments

FAPESP for financial support and LME-PSI/EPUSP for facility measurements.

References

[1]A. D'Amico, C. Di Natale, A. Macagnano, F. Davide, and A. Mantini, Biosens. Bioelectron. Vol. 13, pp. 711 , 1998.

[2]A. Legin, A. Rudnitskaya, Yu. Vlasov, C. Di Natale, E. Mazzone, and A. D'Amico, Sens. Actuators Vol. 65, pp. 232, 2000.

[3]R. Paolesse, C. Di Natale, A. Macagnano, F. Davide, T. Boschi, and A. D'Amico, Sens. Actuators B Vol. 47, pp. 70, 1998.

[4]K. M. Kadish, K. M. Smith, and R. Guilard (eds.), The Porphyrin Handbook, Vol. 6 (Academic Press, New York, 2000).

[5] T. H. Richardson, C. M. Dooling, O. Worsfold, L. T. Jones, K. Kato, K. Shinbo, F. Kaneko, R. Tregonning, M. O. Vysotsky, and C. A. Hunter, Colloids Surf. A Vol. 198, pp. 843, 2002.

[6] T. Someya et al. Nano Letters, Vol. 3, pp. 877, 2003.

Caracterización de un sensor de pH en fibra óptica con análisis de componentes principales

Sergio Rosete-Meléndez[1], Georgina Beltrán-Pérez[2], Juan Castillo-Mixcóatl[2], Severino Muñoz-Aguirre[2]
[1]Fac. Cs. de la Electrónica, [2]Facultad de Ciencias Físico-Matemáticas, Benemérita Universidad Autónoma de Puebla.
Av. San Claudio y 18 Sur, San Manuel CU, CP. 72570, Puebla, Puebla, México
e-mail: gbeltran@fcfm.buap.mx, smunoz@fcfm.buap.mx

Abstract

Se presenta un sensor de pH basado en una película sensible de TiO_2 dopada con un colorante orgánico y depositada sobre una LPFG en fibra óptica. El sensor se pone en contacto con una solución acuosa cuyo pH ha sido previamente ajustado utilizando HNO3 para las soluciones ácidas y KOH para las alcalinas. Se midió el espectro de transmisión y el resultado se estudió utilizando el método de análisis de componentes principales. Los resultados mostraron que las variaciones del espectro en función del pH, las cuales no son evidentes a simple vista, se pueden observar claramente utilizando este método.

Keywords: sensor de pH, fibra óptica, LPFG, Análisis de Componentes Principales

Introducción

La medición de niveles de pH es importante puesto que existen una gran variedad de procesos biológicos que pueden ser monitoreados o analizados por medio de dicho parámetro. Por lo tanto, se requieren sensores adecuados. Aun cuando ha habido una extensiva investigación acerca de sensores de pH, aquellos basados en fibras ópticas son todavía muy pocos a pesar de ofrecer una variedad de potenciales ventajas [1], tales como, inmunidad a interferencia electromagnética, diámetro pequeño o detección remota, entre otras. En este trabajo se presenta un sensor basado en una película sensible de TiO_2 dopada con un colorante orgánico y depositada sobre una rejilla de periodo largo en fibra óptica (LPFG) [2]. El espectro de transmisión se analiza utilizando el método de análisis de componentes principales (PCA por sus siglas en inglés). Dicho método tiene la ventaja de utilizar la información del espectro de transmisión completo, cosa que no es posible midiendo en potencia óptica o en longitud de onda. Los resultados muestran que es posible cuantificar el pH en soluciones acuosas en un amplio rango de valores.

Análisis de componentes principales

El análisis de componentes principales (PCA) involucra un procedimiento matemático que transforma un número de variables posiblemente correlacionadas en un pequeño número de variables no correlacionadas llamadas componentes principales [3]. El primer componente principal *Z1* contiene la mayor cantidad posible de varianza de los datos y cada sucesivo componente principal contiene la mayor varianza de aquella varianza remanente. La operación de PCA puede pensarse como una proyección del conjunto de datos en *n* dimensiones a un número menor de dimensiones (generalmente 2 ó 3), como se muestra en la Figura 1.

Experimento

La LPFG se fabricó por la técnica punto a punto usando arcos eléctricos aplicados a una empalmadora de fusión. La película sensible fue depositada por el método de sol-gel por la técnica de dip-coating. Se realizaron diferentes películas sensibles dopadas con diferentes colorantes orgánicos tales como rodamina 6G, coumarin y azul de bromofenol. Las películas se doparon con diferentes concentraciones. La respuesta del sensor se midió con el arreglo que se muestra en la Figura 2. El sensor se colocó en la solución acuosa la cual tiene un pH determinado, se utilizó HNO_3 para preparar soluciones ácidas, mientras que las alcalinas se prepararon con KOH. El espectro de transmisión se obtuvo realizando un barrido en longitud de onda usando un láser sintonizable en un

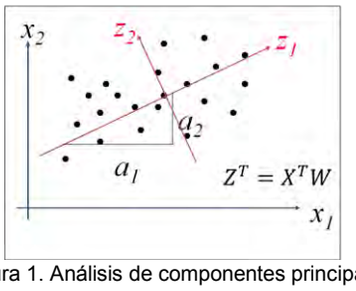

Figura 1. Análisis de componentes principales

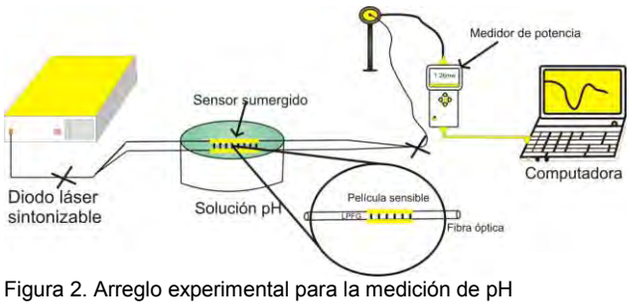

Figura 2. Arreglo experimental para la medición de pH

rango de 1520 a 1620 nm. La salida del sensor se midió con un fotodetector convencional y los datos se almacenaron en una PC.

Resultados y discusión

El espectro de transmisión se midió para varios niveles de pH. El caso de las LPFG cubiertas con coumarin se muestra en la Figura 3a. Como se puede observar, aun cuando hay ligeras variaciones del espectro conforme cambia el pH, tales variaciones no son muy evidentes a primera vista. En la Figura 3b, se muestra una gráfica del primer contra el segundo componente principal (PCA1 vs. PCA2). En esta gráfica, cada punto corresponde a un espectro de la LPFG. La distribución de puntos es regular conforme cambian los valores de pH. Puesto que la varianza contenida en el PCA1 fue 84.4%, se puede decir que los datos pueden ser explicados usando sólo este parámetro (PCA1). Por lo tanto, en la figura 3c se muestra una gráfica de PCA1 en función de los valores de pH. Se puede observar un comportamiento regular para un rango de valores de pH 2 a pH 12. El comportamiento es similar para el sensor con Rodamina 6G.

Conclusiones

Se construyó un sensor de pH depositando una película sensible sobre una LPFG. Se realizó la caracterización utilizando análisis de componentes principales. Como resultado, se encontró que dicho método puede discriminar ligeras variaciones de los espectros de transmisión de las LPFG. Se pudo cuantificar valores de pH en un rango de 2 a 12, para diferentes colorantes orgánicos, obteniéndose el mejor resultado con coumarin.

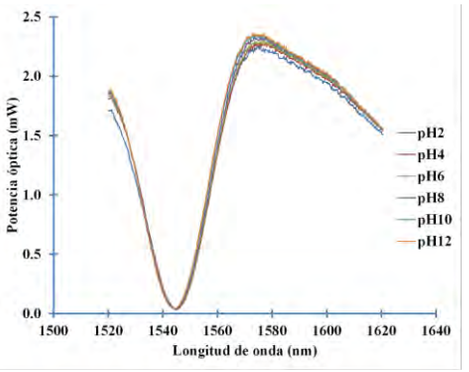

a

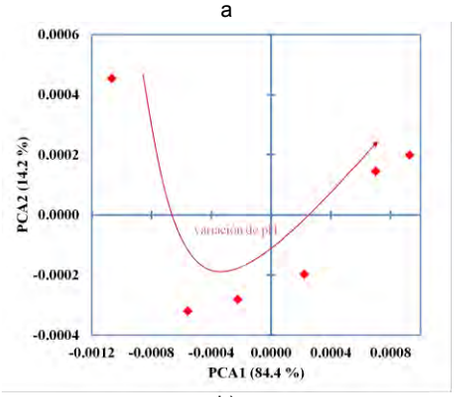

b)

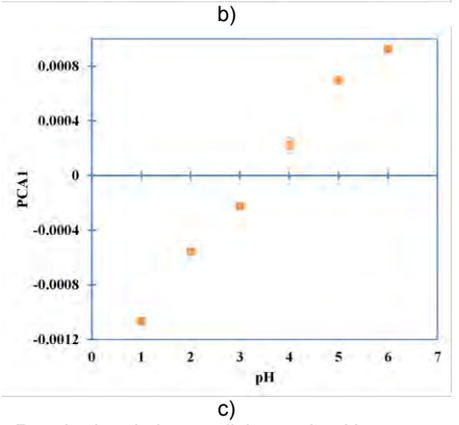

c)

Figura 3. Resultados de las mediciones de pH para un sensor con una película sensible de coumarin. a) Espectros de la LPFG con la variación de pH, b) Gráfica de PCA1 vs. PCA2 y c) Gráfica de PCA1 en función de los valores de pH

Referencias

[1] G. Beltrán-Pérez, F. López-Huerta, S. Muñoz Aguirre, J. Castillo-Mixcóatl, R. Palomino-Merino, R. Lozada-Morales, O. Portillo-Moreno, Sensors And Actuators B, Vol. 120 (2006) pp. 74-78.

[2] G. Beltrán-Pérez, R. Agustín-Serrano, S. Muñoz-Aguirre, J. Castillo-Mixcóatl, III encuentro Participación De La Mujer En La Ciencia, Mayo 2006.

[3] Y. Tanaka and K. Wakimoto, Tahenryo Tokei Kaisekiho (Statistical Methods of Multivariate Analysis), Ed. Gendai Sugaku. Tokyo 1983. In Japanese.

Ochratoxin A Detection: Aptatools and Aptasensors

C. Yang[1, 2], X. Yang[2], and J-L. Marty[1]
[1] Laboratoire IMAGES EA 4218, Université de Perpignan Via Domitia (UPVD), Bâtiment S, 52 avenue Paul Alduy, 66860 Perpignan Cedex, France
[2] State Key Laboratory of Electroanalytical Chemistry, Changchun Institute of Applied Chemistry, Chinese Academy of Sciences, Changchun, Jilin 130022, China
jlmarty@univ-perp.fr

Abstract

In the search of inexpensive, fast and sensitive methods, we reported a new approach using aptamers as bioreceptor for Ochratoxin A (OTA) detection. As a further development of enzyme-linked colorimetric aptamer assay, an electrochemical aptasensor, based on disposable screen-printed electrode was developed to increase the sensitivity of system. Taking into account the advantages of gold nanoparticles and OTA's aptamer which could fold into antiparallel G-quadruplex after its binding with OTA, a colorimetric aptamer based assay using unmodified gold nanoparticles (AuNPs) as indicator was also developed for OTA detection.

Keywords: Ochratoxin A, Aptamer, Colorimetric, Amperometric, Gold nanoparticles, magnetic beads

Introduction

OTA is the most common naturally occurring mycotoxin. It is produced mainly by *Aspergillus ochraceus* and *Penicillium verrucosum*. OTA can be found in a large variety of commodities, such as cereals, beans, dried fruits, coffee, wine, *etc.* [1]. A variety of toxicity of OTA, like nephrotoxicity, hepatotoxicity, teratogenicity, immunotoxicity, and carcinogenicity have been noticed [2-3]. To avoid the risk of OTA consumption, the detection and quantitation of OTA level in contaminated raw materials are of great significance.

Aptamers are functional oligonucleotides selected in vitro by the systematic evolution of the ligand by the exponential enrichment (SELEX) process from random-sequence nucleic acids libraries. They possess high binding-affinity to specific targets. Aptamer has many advantages over antibodies in terms of biosensing [4].

The color of solution depends not only on the diameter of the gold nanoparticles, but also on the interparticle distance. In general, for two gold nanoparticles, when the interparticle distance decreases below the particle diameter, the resonance peak red-shifts. So colorimetric sensors based on gold nanoparticles are usually realized by the drastic color change caused by aggregation of nanoparticles.

In this work, a colorimetric detection method of OTA using unmodified AuNPs as indicator and its aptamer as specific recognition element was developed.

Principle of biosensing of OTA using unmodified AuNPs

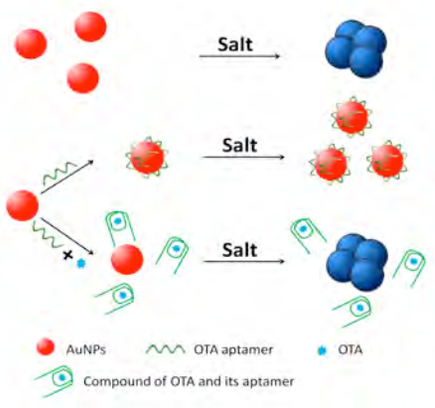

Fig. 1 Principle of biosensing OTA using unmodified AuNPs.

OTA's aptamer could be easily adsorbed onto the surface of AuNPs, thus enhanced the stability of AuNPs against salt-induced aggregation. In the presence of OTA, however, the conformation of OTA's aptamer changed from random coil structure to G-quadruplex structure, and thus lost the ability to protect AuNPs. Upon the addition of salt, electrostatic repulsion between AuNPs was screened,

resulting in the aggregation of AuNPs. The detection could be realized by monitoring the colour change of the AuNPs even with naked eyes.

Characterized the structure of aptamer by Circular Dichroism (CD) spectra

In this work, the conformation variations of OTA's aptamer were confirmed by CD spectra. It is well known that G-quadruplexes exhibit characteristic CD signals depending on their strand composition. Antiparallel G-quadruplex has a CD spectrum characterized by a positive ellipticity maximum around 296 nm, a negative minimum around 264 nm and a crossover around 278 nm. CD spectroscopic data showed that the addition of OTA facilitated the formation of antiparallel G-quadruplex structure. The ratio of antiparallel G-quadruplexes structure increased with the increase of the concentration of OTA (Fig. 2). This suggested that OTA possessed the ability of inducing the formation of antiparallel G-quadruplexes structure.

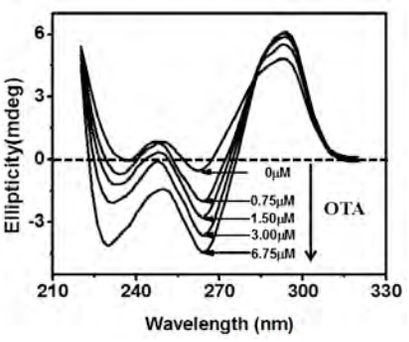

Fig. 2 CD spectra of 13.5 μM OTA's aptamer in PBS buffer (10 mM, pH 8.5) containing 20 mM Mg^{2+}, 150 mM NaCl with different concentrations of OTA.

Spectral characteristics

UV-visible spectra of the AuNPs solution under different experimental conditions are shown as Fig. 3A. Correspondingly, the color change of solution is shown in the photograph as Fig. 3B. In the presence of aptamer and OTA, the absorbance at higher wavelength increases. This suggests particle aggregation. As it can be seen, the change in the solution color corresponds to the change in the optical spectra. Control experiments using RDNA instead of aptamer and using warfarin instead of OTA under similar condition were performed. As we can see, there wasn't any noticeable change in absorbance spectrum of gold nanoparticles solution, and the color of solution remained red. This demonstrated the selectivity of this aptasensor towards OTA.

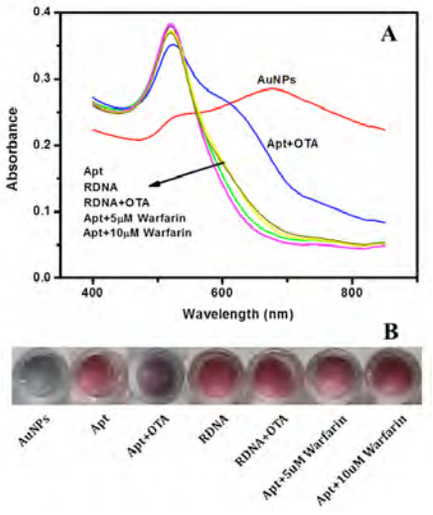

Fig. 3 (A) UV-visible absorption spectra of AuNPs after addition of 170 mM NaCl under different experimental conditions. Other experimental condition are c_{OTA} = 500 nM, c_{apt} =c_{RDNA} =200 nM. (B) The photographs corresponding to the spectra. of Fig. 3A

Colorimetric biosensing of OTA

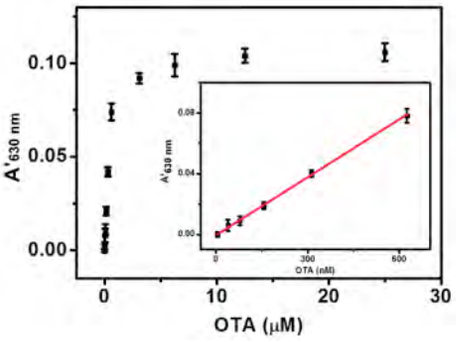

Fig 4 Absorbance value at 630 nm vs. OTA concentration Inset: derived calibration curve. The error bars represent the standard deviation of three measurements.

Under the optimized experimental conditions, UV-visible spectra of AuNPs with different concentration of OTA in the range of 0-25 μM were recorded (Fig. 4). As can be seen in Fig. 4, a linear correlation was obtained between A_{630nm} and the concentration of OTA from 20 to 625 nM, and a limit of detection of 20 nM (3σ) was obtained. The regression equation is A_{630nm} = 1.3×10^{-4} c_{OTA} (nM) with the correlation coefficient of 0.997.

References

[1]. L Monaci,F Palmisano, Determination of ochratoxin A in foods: state-of-the-art and analytical challenges. Analytical and Bioanalytical Chemistry, 2004, 378(1): 96-103.

[2]. A Pfohl-Leszkowicz,R A Manderville, Ochratoxin A: An overview on toxicity and carcinogenicity in animals and humans. Molecular Nutrition & Food Research, 2007, 51(1): 61-99.

[3]. H Tsubouchi,K Yamamoto,K Hisadaet al., Effect of Roasting On Ochratoxin-A Level In Green Coffee Beans Inoculated With Aspergillus-Ochraceus. Mycopathologia, 1987, 97(2): 111-115.

[4]. M Mascini, Aptamers in bioanalysis. Wiley Online Library. 2009.

Effect of Ethanol Concentrations on Few Layer Schottky graphene Transistors

L. E. G. Armas[a], M. F. G. Huila[b], M. Pojar[a], H. E. M. Peres[c], F. J. R. Fernandez[c], K. Araki[b], H. E. Toma[b], A. D. Santos[d] and A. C. Seabra[a]

[a] Laboratório de Sistemas Integráveis do Departamento de Engenharia de Sistemas Eletrônicos da Escola Politécnica da USP (LSI-PSI/EPUSP), São Paulo, SP, Brazil

[b]Departamento de Química Fundamental, IQ, da Universidade de São Paulo, USP, São Paulo, SP, Brazil

[c] Laboratorio de Microeletrônica do Departamento de Engenharia de Sistemas Eletrônicos da Escola Politécnica da USP (LME-PSI/EPUSP)

[d] Instituto de Física, IF, Departamento dos Materiais e Mecânica da Universidade de São Paulo, USP, São Paulo, SP, Brazil

e-mail: legarmas@gmail.com

Abstract

We have studied the effect of ethanol vapor concentration on the few layer graphene transistors (devices) applying positive and negative gate voltage. These devices have a Schottky behavior on the Source drain current and voltage. For this purpose Nitrogen (N_2) gás was used as base gas, passing through the sample, then the flux of this gas was passed for a litle botlle (chamber) of ethanol with the aim of being mixture at 20 ppm, 750 ppm and 3800 ppm ethanol vapor concentrations. We have observed a shift on the source drain current, for positive and negative back gate voltage, as the ethanol vapor concentration increase.

Keywords: graphene transistors, Schottky transistors, ethanol sensors.

Introduction

Carbon-based Nanomaterials promise to be alternative candidates to replace silicon in device technology [1-2]. Carbon nanotubes have been investigated widely for their field-effect properties and these transistors have found some applications as well [3]. Graphene, the two-dimensional hexagonal lattice arranged in a dense honeycomb structure is a zero-gap material with high electron mobility and is an attractive material for fabrication of FETs. The first field-effect device with single-layer graphene was prepared using a sample obtained by micromechanical cleavage of pyrolytic graphite [4].

In this work we report the effect of different ethanol vapour concentrations (EVC) on the source-drain current and voltage measurements as the EVC increase. We observed a shift (not ohmic behavior) on the source- drain current for low source-drain voltage (V_D). This shift occurs for negative and positive gate voltage, whereas for zero gate voltage there is an ohmic behaviour. We must emphasize that this shift increase as the EVC increase

Samples and experimental details

To fabricate the FLG transistors devices, heavely n doped (100) wafers with dopant concentration of $N_A = 10^{15}$ cm^3 and resistivity 0.002 – 0.005 Ω.cm were used as substrates as well as the back gate electrode with a thermally grown oxide layer of thickness of 280 nm, which acts as the dielectric, Ti/Au contacts were evaporated after optical lithography and structured by the lit-off technique. After the device was fabricated, it was placed in a small chamber connected by a tube to a container of vapor mixture. Concentration of organic vapors was controlled by mixing N_2 gas and measured by gas detector. All electrical measurements were carried out by using DC supply at atmospheric pressure.

Results and discussions

Fig. 1 shows the output characteristics of the device, which is based on FLG graphene and shows a Schottky behaviour on the source-drain current as the V_D voltage is swept from – 2.0 V to 2.0 V, and for zero back gate voltage. We observe that for this bias voltage (V_D) there is no difference between

N_2 gas and 20 ppm, 750 ppm and 3800 ppm EVC.

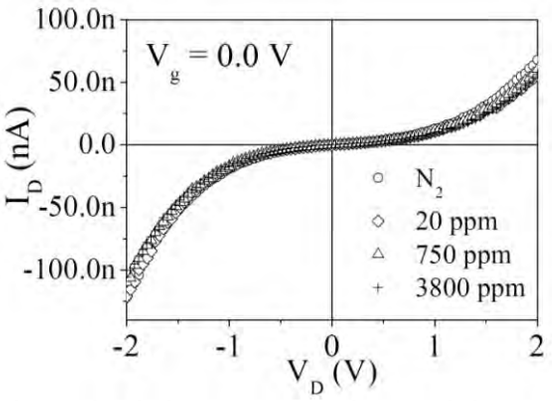

Fig.1- . Electrical measurements of source-drain current as a function of source-drain voltage (-2.0 V to 2.0 V) at the presence of N_2 gas and different concentrations of ethanol vapor (20 ppm, 750 ppm and 3800 ppm).

In order to have a better information of the device, we measured the output characteristic of the source drain current at low V_D voltage, swept from -0.5 V to 0.5 V for -40.0 V gate voltage, which is shown in Fig. 2. In this Fig. we observe a little shift and increase of the current for high EVC (3800 ppm), whereas for N_2 gas, 20 ppm and 750 ppm the current is almost the same.

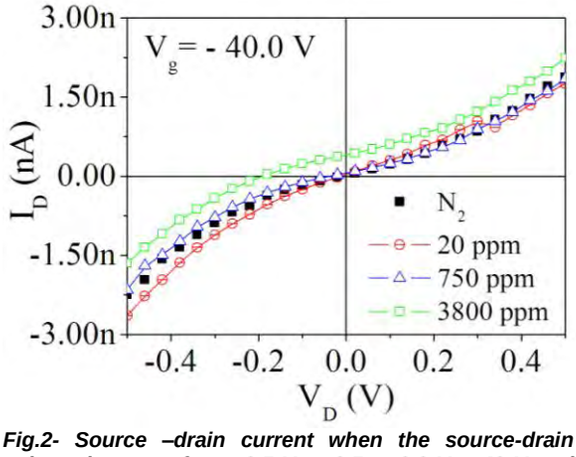

Fig.2- Source –drain current when the source-drain voltage is swept from -0.5 V to 0.5 at 0.0 V, - 40 V and 40.0 back gate voltage.

Finally, Fig. 3 shows the source drain current as function of the V_D voltage (-10.0 mV to 10.0 mV), when the gate voltage is zero, - 40.0 V and 40.0 V, and for a fixed 20 ppm EVC. From this figure we observe a positive (negative) shift of the current for negative (positive) gate voltage. The measurements were performed at 750 ppm and 3800 ppm of EVC, observing higher shift on the source drain current (not shown here). Several samples were measurements obtaining similar results in all the samples.

Source-drain current as a function of the back gate voltage show p type behaviour (not shown here) in all the graphene samples, for low EVC concentrations, and the electron mobility and other parameters varying from sample to sample. For example, from Fig. 3 we can see that for positive (negative) gate voltage the current decrease (increase), being this kind of behaviour typically of ambipolar graphene devices, where the electron mobility increase as the trasconductance increase. Additional measurements have shown that for high EVC and high gate voltage the current increase. This means that it is possible to pass from unipolar to ambipolar conduction increasing the EVC.

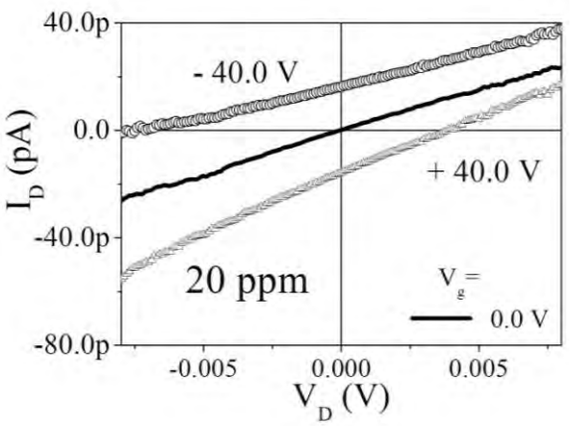

Fig.3. Source –drain current as a function of the source-drain voltage, when it is swept from - 10.0 mV to10.0 mV, and at fixed 20 ppm EVC.

Conclusions

In conclusion, we report positive (negative) shifting on the source drain current, at low source-drain voltage as the ethanol vapour concentration increase, for negative (positive) gate voltage. In other words it could be possible to change from unipolar to ambipolar conduction increasing the EVC and gate voltage.

Acknowledgments

FAPESP for financial support and LME-PSI/EPUSP for facility measurements.

References

[1] S.J. Wind, J. Appenzeller, R. Martel, V. Derycke, P. Avouris, Appl. Phys. Lett. 80 (2002) pp. 3817.
[2] A. Javey, G. Jing, W. Qian, M. Lundstrom, H. Dai, Nature 424 (2003) 654.
[3] A. Javey, J. Guo, D.B. Farmer, Q. Wang, E. Yenilmez, R.G. Gordon, M. Lundstrom, H. Dai, Nano Lett. 4 (2004), pp. 1319.
[4] K.S. Novoselov, A.K. Geim, S.V. Morozov, D. Jiang, Y. Zhang, S.V. Dubonos, I.V. Grigorieva, A.A. Firsov, Science 306 (2004), pp. 666.

Uso de transistores de porta suspensa para medidas de pH.

B. da Silva Rodrigues[a,b], O. De Sagazan[a], S. Crand[a], T. Mohammed-Brahim[a], N.I. Morimoto[b]

[a]GM-IETR UMR-CNRS 6164, Universidade de RENNES I, 35042 Rennes Cedex, France
[b]LSI, Universidade de São Paulo, Av. Prof. Luciano Gualberto, trav. 3 nº158, São Paulo, Brasil
bruno@lsi.usp.br

Resumo

Este trabalho apresentará um novo sensor de pH baseado na tecnologia de transistores de porta suspensa (SGFET). Nesta nova tecnologia a variação de pH será detectada a partir da influência dos íons de H^+ e OH^- na tensão de limiar dos transistores SGFET o que possibilitará a obtenção de valores de sensibilidade superiores 59 mV/pH, valor de sensibilidade dos medidores de pH existente em produção industrial.

Palavras-chave: SGFET, sensores, pH

Introdução

Atualmente a medida da variação de pH em soluções é dada principalmente pelo uso de dois sensores: eletrodos duplos e ISFET's onde em ambos os casos a sensibilidade máxima é de 59 mV/pH à 20 ºC (sensibilidade Nerstiniana). Esta sensibilidade limitada pelo potencial de Nernst[1] motiva o estudo e desenvolvimento de novos dispositivos que alcance sensibilidade superiores a 59 mV/pH.

Visando aumentar a sensibilidade das medidas de pH, foram desenvolvidos os sensores baseados na tecnologia SGFET. A figura 1 apresenta uma foto MEV do dispositivo SGFET.

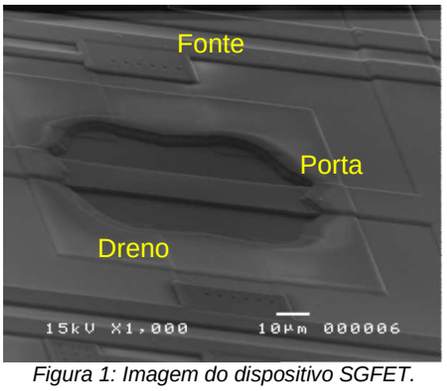

Figura 1: Imagem do dispositivo SGFET.

Os SGFET's possuem o mesmo principio de funcionamento dos transistores MOS, no entanto, entre a região de canal e a porta do dispositivo temos um vão livre (GAP) que servirá como região ativa do sensor. A figura 2 apresenta um perfil da estrutura SGFET.

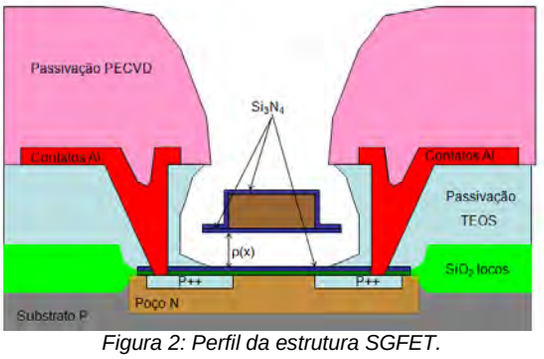

Figura 2: Perfil da estrutura SGFET.

Quando imerso em soluções onde deseja-se obter o valor do seu pH, a tensão de limiar do transistor será influenciada pelos íons H^+ e OH^- do analito conforme apresenta a equação 1 [2].

$$V_T = \phi_{MS} + 2\phi_F + \frac{Qss}{C_{ox}} - \frac{1}{Ce_{ox}} \int_0^{e_{ox}} x\rho(x)dx \quad (1)$$

Resultados experimentais

Considerado a influencia do pH das soluções na tensão de limiar dos transistores SGFET a figura 3 apresenta a evolução da curva de transferência do transistor SGFET e as respectivas transcondutâncias para medidas em soluções de pH 4 de acido bórico (H_3BO_3) e soluções de NaOH de pH 8. Neste teste obtivemos uma sensibilidade de aproximadamente 610 mV/pH, valor 10 vezes superior as sensibilidades obtidas usando sensores baseados no principio de Nernst.

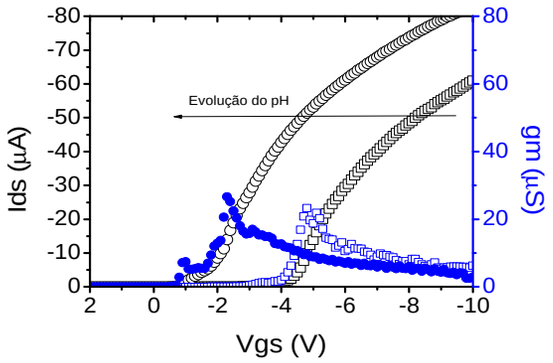

Figura 3: Curva Ids=f(Vgs) e transcondutancia para soluções de pH 4 e pH 8 para Vds= -100 mV.

Num segundo teste foram realizadas medidas Ids=f(Vgs) em soluções com diferentes valores de pH. Esta sequencia de medidas foram iniciadas em soluções de pH 3,84 de H_3BO_3. A partir da solução de H_3BO_3 pH 3,84, o pH da solução foi aumentado gradativamente com a adição de uma de NaOH de pH 10,até o valor de pH 7,40. A figura 4 apresenta as medidas Ids-f(Vgs) para soluções com diferentes valores de pH.

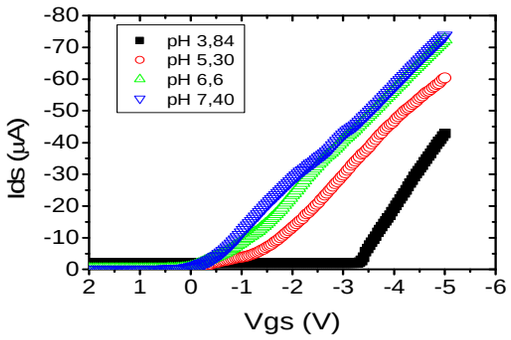

Figura 4: Curva de transferência do transistor SGFET durante medidas em soluções com diferentes valores de pH para Vds= -300 mV.

A partir dos valores da curva de transferência do transistor SGFET em soluções com pH diferenciado, foram extraídas as curvas de transcondutância conforme apresenta a figura 5.

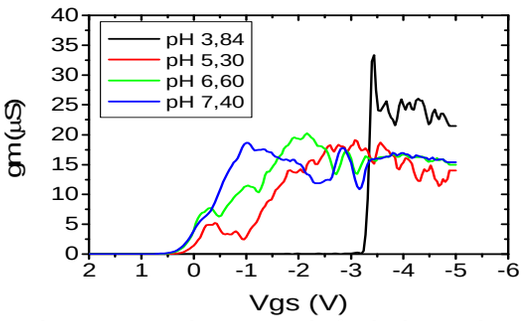

Figura 5 Curva de transcondutância do transistor SGFET durante medidas em soluções com diferentes valores de pH para Vds= -300 mV.

A partir da figura 5, os valores de Vgs para a transcondutância máxima (Gm=gm_{max}) de cada medida de pH foram extraídos para traçar a curva de Vgs=f(pH) conforme apresenta a figura 6.

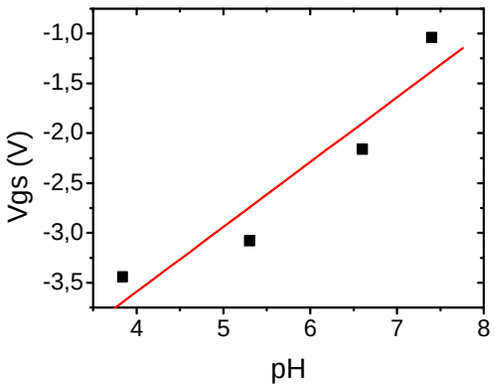

Figura 6: Curva Vgs em função do pH para diferentes valores de pH.

A sensibilidade obtida através da medida apresenta na figura 6 foi de 650 mV/pH valor próximo a sensibilidade calculada na figura 3.

O sensores de pH baseados na tecnologia SGFET que foram apresentados neste artigo mostraram-se promissores. Obtivemos em teste experimentais valores de sensibilidade em torno de 600 mV/pH, valor 10 vezes superior ao potencial de Nernst e boa reprodutibilidade.

Referencias

[1] Carvalho, Geraldo Camardo de. “Química moderna”. : Scipione, São Paulo 1997. 85-262-3020-4

[2] T. Mohammed-Brahim, A.-C. Salaün, F. Le Bihan Sensors & Transducers Vol. 90, pp. 11-26, April 2008

Electrochemical Characterization of poly-(3,4 propylenedioxythiophene) Pseudo-Capacitor

JaeWan Park, Hitesh Sahoo, Timothy Jones, Rocío del A. Cardona,
and Jorge J. Santiago-Avilés*
Electrical and Systems Engineering Department
University of Pennsylvania, Philadelphia, PA 19104
santiago@seas.upenn.edu*

Abstract

Every day use appliances relies mostly in lithium-ion batteries to satisfy their energy requirements. However, these batteries' desirability is limited by the materials utilized and its lower power density. An alternative to batteries are the supercapacitors, which are capable of storing energy in the electrical double layer (EDL) formed between the electrode material and the electrolyte. To reduce the gap in terms on energy anf power density between batteries and EDL supercapacitor, pseudocapacitors has been used. In pseudo-capacitors amaterial that is capable of storing faradaic charge, such as metal oxides and conducting polymers, is deposited in the electrode surface, but its charge / discharge behavior is like one of the EDL supercapacitor. Therefore, energy density is gained even though the faradaic nature of the process makes its power density decreases.

In this paper, we use the conducting polymer, poly-(3,4 propylene-dioxythiophene) for the assembling of a pseudo-capacirtor. We present the electrochemical characterization of the devices as a function of the amount of material accumulated in the platinum current collector, in terms of the energy and power density, and capacitance.

Keywords: poly-(3,4 propylene-dioxythiophene), pseudo-capacitor, electropolymerization, capacitance

Introduction

Energy consumption worldwide went from 495 kWh in 2007 with a projected increasing to 739 kWh by 2035 (1). From this a 50 % (~ 230 kWh) consumed currently by the countries belonging to the OECD (Organization for Economic Co-operation and Development). However, when this number is estimated to not change for OECD's countries by 2035, the countries from emerging economies will be accountable for the total increment in global energy consumption. This panorama calls for actions to improve the managing of electrical energy resources and it usage.

In the USA, nearly 41 % of the energy produced goes into electric power form which nearly a % 50 percent it used to provide electricity to residential and commercial purposes (2). Regardless of the challenges to obtain energy from renewable sources, one existing challenge is how to storage the electric energy that is non-used during low load requirement periods during the day effectively. Energy storage devices (ESD) can present an alternative for the managing of electric energy. Also, ESD are important for the miniaturization of technologies such as house hold electrical appliances, smart phones, personal computers, biomedical applications (peacemakers), and electric vehicles.

Supercapacitors are just one of the approaches to storage energy, among others as Li-ion batteries, and fuel cells. Super-capacitors rely on the formation of the EDL between the material deposited in the electrode (regularly carbon based materials) and the electrolyte (3).

Different from batteries, no chemical reaction is going on therefore, the cyclability of these ESD are higher as well as its power density. However, energy density is lower than that of the batteries which limits it uses in some applications. Pseudo-capacitors, have appeared as alternative to reduce the gap between super-capcitor and Li-ion batteries by combining chemical phenomena and surface phenomena. In pseudo-capacitor an electroactive material is placed in the electrode in a configuration that permits the formation of the double-layer phenomena (3).

In this study we present the use of electro-active polymer poly-(3,4 propylene-dioxythiophene) (**Figure 1**), which upon immobilization over the electrode can be oxidized or neutralized to create a charge difference between electrodes. We explore how the amount of materials immobilized initially at

electrode surface affect parameter such as energy, power density, and capacitance.

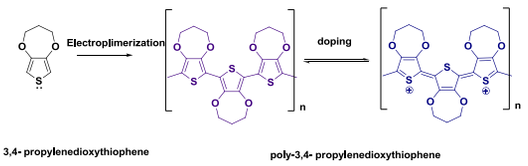

Figure 1. Structure of poly-(3,4 propylene-dioxythiophene)

Materials and Instrumentation

Tetrabutylammonium perchlorate (TBAP), 99% was obtained from Fluka, propylene carbonate, 99.7 %, and 3,4-propulenedioxythiphene were obtained from Aldrich, poly-propylene separator paper (China Lake), polishing michrocloth, metadii fluid, and Metadi II diamond polishing compound were obtained from Buehler, acetone (HPLC grade),and DIUF water were obtained from Fisher Scientific.

Biopotentiostat (AFCBP1) from PINE Instruments Company was used for all electrochemical experiments unless stated otherwise. Potentiostat/galvanostat (273 A) was used for electrode area determination experiments. All experiments were conducted inside the glove-box (LC Technology Solution Inc.) under N_2(g) atmosphere.

Methods

The area of the working electrode (Pt) were determined by using potassium ferricyanide as standard using a three electrode cell configuration, were Pt, nichrome and Ag/AgCl (3 M NaCl) were the working, reference and auxilarly electrode respectively.

After area determination, a $5x10^{-3}$ M PEDOT/0.1 M TBAP/PC solution was use in a three electrode configuration cell to grow the poly-PEDOT over the Pt electrodes. The elctropolymerization was carried in a potential window of (-1000-1500) mV at a 100 mv/s scan rate. Different time of polymerization (cycles) were carried (10,20,30,40, and 50) cycles. After polymerization electrodes were place in a cell in a solution of 0.1 M TBAP/PC with a similar cell configuration and different scan rates were ran (25-10,000)mV/s to confirm the deposition of the polymer. Also, coulombic efficiency was determined for the electrodes that were used to ensemble the device.

For device assembling, the configuration presented in **Figure 2** was used. The device test was performed for three different potential's windows at different scan rate. From the device test energy and power density was determined as well as capacitance for the devices as a function of the amount of material deposited.

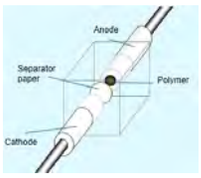

Figure 2. Device configuration

Results

Calculated Pt electrodes' area ranged from (0.018-0.020) cm^2. As expected the amount of material deposited over the surface of the electrode increases (**Figure 3**) with the number of polymerization cycles (2.27-8.39) $x10^{-5}$ g/cm2. However, from our results showed that after 30 cycles there we reach the limit of the amount of material that can be deposited over the electrode surface.

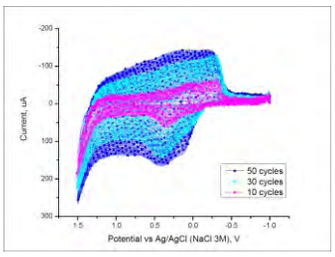

Figure 3. Cyclic voltammetry for the electropolymerization of 3,4 propylene-dioxythiophene

The device test showed that the average capacitance increases as a function of material in the electrode (0.06 mF or 3.37 mF/cm^2) – (0.41 mF or 21.87 mF/cm^2). The same, as expected, occur for the average current (2.78-2067.50) μA and power densities (1.39-2067.50) μW.

Conclusions

We have show the dependence of pseudo-capacitor's properties upon the amount of material immobilized at electrode surface. Where a polymerization conditions of 30 cycles present the optimal polymerization conditions

References

1. EIA *Annual Energy Review 2009. http://205.254.135.24/totalenergy/data/annual/pdf/aer.pdf accessed 5/7/2012*
2. Ibrahim, H.; Ilinca, A.; Perron, J. *Renewable & Sustainable energy Reviews*. **2008**. 12, 1221-1250.
3. Abruña, H.D.; Kiya, Y.; Henderson, J.C.. *Physics Today*. **2008**. 43-47.

Synthesis, Characterization and use of Ru-Fc Intercalation Complex as an Electrochemical Label for the Detection of Pathogen-DNA

Madeline Díaz-Serrano[1], Arelys Rosado[1], Dianicha Santana[2], Esther Z. Vega[2], Ana R. Guadalupe[1]
[1]Department of Chemistry, P.O. Box 23346, University of Puerto Rico, Río Piedras Campus, San Juan, Puerto Rico, 00931-3346
[2]Department of Biology, P.O. Box CUH 100 Rd 908, University of Puerto Rico, Humacao Campus, Humacao, Puerto Rico, 00791
diazmadeline@yahoo.com

Abstract

This report describes the synthesis of $[Ru(Fe\text{-}Phen)_2dppz](PF_6)_2$ (Ru-Fe complex) for a label-free approach to detect DNA hybridization. The binding constant of Ru-Fe complex with CT-DNA obtained by UV-vis and OSWV were 8.0 $x10^4$ M^{-1} and 6.5 x 10^5 M^{-1} respectively. We used the Ru-Fe complex and the Ferrocene covalently attached to the target to monitor the hybridization event of a 70-mer oligo immobilized in 10.3KD NHS-PS-NHS. We also measured the hybridization event of a PCR amplified biotinylated *Omp*C gene of *Salmonella* using only the Ru-Fe complex. The lowest target detectable concentration for both DNA fragments was above 0.4 µM.

Keywords: *Salmonella*, DNA Biosensor, Electrochemical Label, Ruthenium-Ferrocene Complex

Waterborne and foodborne diseases are one of the principal public health problems worldwide. Our particular interest is the development of nucleic acid biosensors (NAB) for the detection of pathogenic microorganisms in food and water samples. In a NAB, a ss-nucleic acid sequence is used as a probe to identify a complementary target sequence (the analyte) [1]. In this research, we report on the development of a NAB prototype using a polymer modified electrode surface together with sequences of different lengths for the OmpC gene from Salmonella as probes and Ruthenium-Ferrocene (Ru-Fc) bi-metallic complex as a label (Scheme 1).

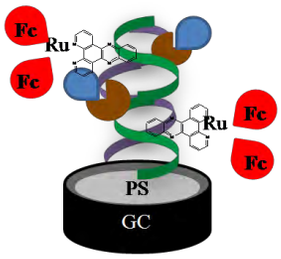

Scheme 1: Ru-Fc bimetallic intercalator and sandwich design of the DNA hybridization detection.

We have optimized several PS films and anchored nucleic acid sequences with different lengths at gold and carbon surfaces. Non contact mode AFM and XPS were used to monitor each step of the NAB preparation, from polymer modification to oligos hybridization (conventional design). The hybridization event has been detected electrochemically by the conventional method, which is modifying the target with Fc-NHS. We observed a small current at the potential for the Fc oxidation without signal amplification [2]. Calibration plots were constructed using the 12K g/mol-43Kg/mol polymer range modified glassy carbon electrode. A 15-mer, 35-mer and 70-mer probes were attached to the surface and hybridized with its complementary sequences.

We synthesized a $Ru(Fcphen)_2dppz$ complex to use as an electrochemical intercalator [3]. The electrochemical behavior of 1.3 mM Fe-Phen and 68.0 mM Ru-Fe complex was studied in CH_3CN/0.101M TBAP with OSWV. The Ru-Fe complex showed oxidation signals at +608 mV and +1192 mV corresponding to the $Ru^{II/III}$ and $Fe^{II/III}$ centers, respectively. The Fe-Phen ligand showed an oxidation potential at +548 mV. We study the binding affinity of the Ru-Fc complex to calf thymus (CT) DNA via an intercalation mode. On the addition of the CT-DNA, the complex bands at 283, 376 and 519 nm shifted slightly toward the red by a corresponding 4, 3 and 7 nm. The Ru-Fe complex absorption at the same wavelengths also decreased by 43%, 47% and 36%, respectively. These changes suggest that the complex interacts with CT-DNA.

To show that the Ru-Fe complex could be used to detect a target oligo sequence from a *Salmonella* genome fragment, our collaborators Vega and Santana prepared and characterized a PCR amplified biotinylated 158 bp probe.

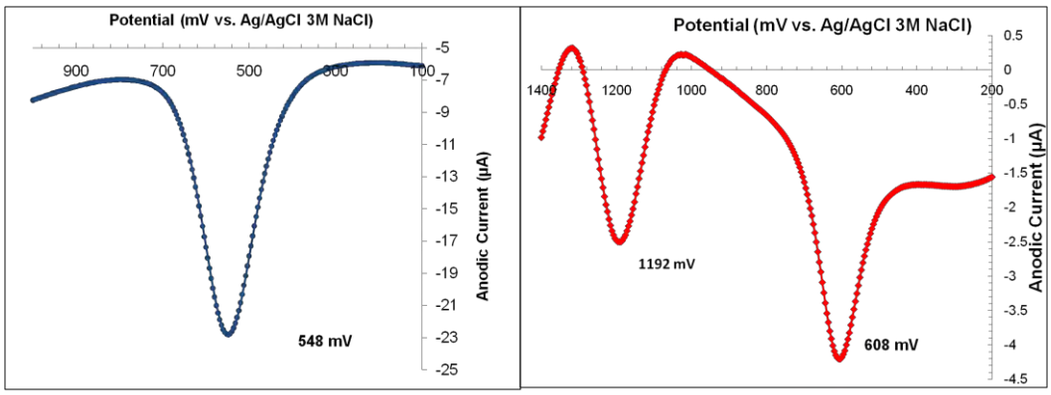

Figure 1. Square Wave Voltammetry of (A) 1.3 mM Fc-Phen and (B) 0.68 mM [Ru(Fc-phen)$_2$dppz](PF$_6$)$_2$ between 100 and 1400 mV in acetonitrile 0.101 M TBAP.

Kwang and collaborators (1996) showed that it was possible by PCR to identify Salmonella among other enterobacterias.

This probe represents an oligo sequence found in the *OmpC* gene of *Salmonella* that selectively discriminates this bacterium from *Shigella*, *E.coli* and *Enterobacter aerogenenes*. To achieve our goal, we immobilized this probe to 10.3KD NHS-PS-NHS modified glassy carbon electrode. A 158 bp ds-DNA fragment from the *Salmonella* genome was used as the target. The hybridization event was detected with the Ru-Fe complex in 0.070 M PBS/NaCl (µ = 0.271 M; pH 6.9) as the redox label. After the hybridization, the sensor was exposed to GOx-avidin for 4 h at RT. CC and OSWV were done at each step in the presence and absence of glucose. CC was done in a potential window from 800 mV to 1300 mV with a pulse width of 250 msec.

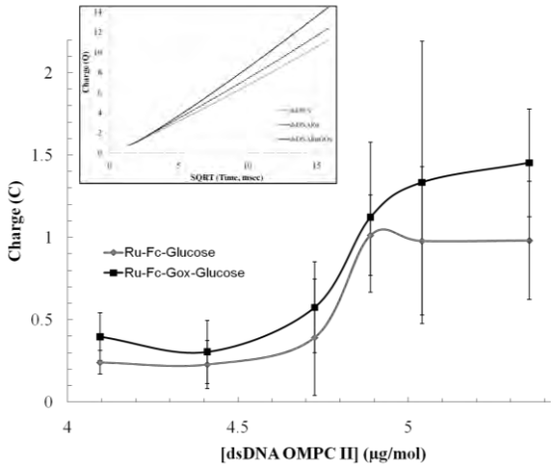

Figure 2. Calibration curve of the NHS-PS-NHS 10.3 KD modified glassy carbon electrode with biotinylated-dsDNA Probe-Target Hybridization using Ru-Fe redox intercalator, before (black curve) and after (gray curve) adding 52 mM glucose to the PBS buffer. The target concentration varied from 5.36 µM to 4.10 µM. Inset: CC voltammogram of 4.10 µM dsDNA-biotinylated probe-target hybridization before and after the electrode was exposed to 0.114 mM Ru-Fe and 0.25 mg/mL GOx-avidin in 52 mM glucose/ PBS.

Figure 2, shows the calibration curve corresponding to the Ru (II) oxidation in response in the absence and presence of GOx-avidin/glucose. Analyte solutions with different concentrations of target dsDNA varied from 6.3 µM to 4.1 µM. OSWV results also confirmed the current amplification by GOx-avidin/glucose. The charge density amplification of Ru(II) in the absence and and presence of GOx-avidin/glucose ranged from 32% to 73%.

In summary, we synthesized and successfully characterized the ligands (Fe-phen and dppz) and the bimetallic Ru-Fe complex. The Fc-Phen showed the characteristic $Fe^{II/III}$ process of ferrocene. Ru-Fe complex showed the expected $Ru^{II/III}$ and $Fe^{II/III}$ redox processes. A *Salmonella* DNA biosensor was also done using a biotinylated 158 bp DNA fragment from the *Omp*C gene of the bacterium. A calibration curve was constructed using CC data and measuring the charge density at the Ru(II) oxidation potential, the lowest target detectable concentration was above 0.41 µM. This sensor could be used to study the hybridization of complementary oligo sequences of once optimized and their detection in real samples.

Acknowledgements

PENN-UPRH Partnership for Research and Education (NSF-DMR- 0934195)

References

1. Muñoz, L.; Guadalupe, A. R.; Vega, E. Journal of Biotechnology, Vol. 118, pp. 233-245, 2005.
2. Díaz, M. *et al.* Polymeric Materials Science and Engineering, Vol. 98, pp. 448-449, 2008.
3. Díaz, M. *et al.* Biosensor & Bioelectronics, Submitted 2012.

FIA-automated System Used to Electrochemically Measure Nitrite and Interfering Chemicals through a 1-2 DAB / Au Electrode: Gain of Sensitivity at Upper Potentials

F. L. Ameida[1*], S. G. dos Santos Filho[2], and M. B. A. Fontes[3]

[1,2]Laboratório de Sistema Integráveis, Universidade de São Paulo, São Paulo, SP, Brazil.
[3]Faculdade de Tecnologia de São Paulo – FATEC-SP/CEETEPS, São Paulo, SP, Brazil.

*Corresponding author: falmeida@lsi.usp.br

Abstract

In the present work, it is presented nitrite analysis, electrochemically measured, using a Flow-injection Analysis (FIA) system. The presented electrochemical planar sensor uses silk-screen technology and has a measuring electrode covered with 1-2 Diaminobenzene (DAB) that allowed good selectivity, linearity, repeatability, stability and gain of sensitivity at 0.5 $V_{Ag/AgCl\ Nafion^{®}\ 117}$ in relation to 0.3 $V_{Ag/AgCl\ Nafion^{®}\ 117}$. It was noteworthy that nitrite response adds to the response of the studied interfering chemicals (paracetamol, ascorbic acid and uric acid).

Keywords: nitrite measurement, 1-2 DAB, amperometric sensor and electrochemical potential

Introduction

From the 70's and 80's until currently the microfabrication, silkscreen and microelectronic technologies can been employed in nitrite biosensor and electrochemical sensor [1,2]. Actually, the amperometric technique has been largely worn in sensors due to easy setup of electrodes, surface modification and direct measurement [2]

The 1-2 Diaminobenzene (DAB) film was chosen due to previous studies [2,3] which show increment of selectivity to nitrite and decreasing interfering-composts signal of the uric acid (UA), ascorbic acid (AA) and paracetamol (PA) [4].

In addition, we have studied the conduct film integrated to the Flow-injection Analysis Automated (FIA-automated) System in order to improve repeatability and stability.

Procedures and Methods

1) Fabrication of the Sensor

The sensor composed by three electrodes was silk-screened onto alumina substrate of 17 x 43 mm: measuring electrode (Au, DuPont® 5142), reference electrode (Ag/AgCl, DuPont® 6146, recovered with Nafion® 117) and auxiliary electrode (Pt, ESL 5545-LS) with areas of 4.5 ± 0.2, 4.2 ± 0.7 and 59.8 ± 0.7 mm^2; respectively. The Au past and DuPont® 9615 were utilized to define connection lines / contacts and electric isolation, respectively.

2) Characterization

The characterization of the electrodes determines the relation between functionally and response for measuring current. The Cyclic Voltammetry using solution 0.1 mol l^{-1} potassium ferrocyanide in 0.5 mol l^{-1} KCl was employed to obtain the effective area of the working electrode and to verify the its stability. The solution 3 mol l^{-1} NaCl was employed to perform the reversibility test of the reference electrode (both not shown).

2) FIA-automated System

The system was arranged for the items: solenoid valve, discard, analysis-cell, air-pump, electrical and fluidic connections, PalmSens voltammetric and analytes. The experimental

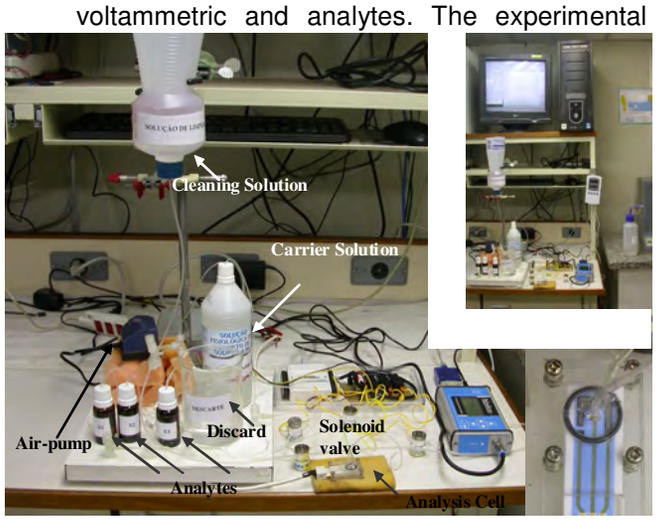

Figure 1. *FIA-automated: detail analysis-cell and control computer*

analysis-cell (at the lower right corner) and control computer (at the upper left corner).

The physiologic serum (NaCl 0.9 % and pH = 7.3) was employed as solvent or as cleaning or carrier solution during the measurement. The used concentrations for **Nitrite** were 50, 250 and 500 µmol l^{-1}. The **Interfering chemicals** were UA (0.55 mmol l^{-1} diluted in 0.1 mol l^{-1} NaOH), AA (0.11 mmol l^{-1}) and PA (0.17 mmol l^{-1}) - maximum therapeutic doses in blood of a patient [4].

3) Surface Modification of the gold electrode

5 mmol l^{-1} DAB was prepared to 0.05 mol l^{-1} phosphate buffer (pH = 7.2) and after purging during 30 min in nitrogen gas. In following, the film was electrodeposited over the gold surface by Cyclic Voltammetry technique using PalmSens (50 cycles in 0 to +0.65 $V_{Ag/AgCl\ 3M\ KCl}$ with scanning velocity = 0.1 V s^{-1}).

4) Study of the Electrochemical Potentials

Empirically, electrochemical response potentials were extracted by DPV technique (*Differential Pulse Voltammetry*). The table 2 systematizes them according to metabolite concentrations and room temperature (25 ºC).

Table 2. *Electrochemical Response Potentials obtained*

Metabolites	Concentration mmol l^{-1}	Peak Potential $V_{Ag/AgCl\ Nafion®\ 117}$	Start Potential of Electrochemical Reaction $V_{Ag/AgCl\ Nafion®\ 117}$
Nitrite	2.00	0.880	0.500
Ascorbic Acid (AA)	0.44	0.292	0.172
Uric Acid (UA)	2.00	0.472	0.352
Paracetamol (PA)	0.68	0.602	0.372

In this work, two different potentials were chose. 0.3 $V_{Ag/AgCl\ Nafion®\ 117}$, where nitrite response can be negligible (figure 2 "c"), on the other hand, interfering-composts' little influence has been checked (below 1 nA) and 0.5 $V_{Ag/AgCl\ Nafion®\ 117}$, nitrite signal is added to interfering responses.

Results and Discussion

In the figure 2, graphic "a" and "b" correspondent to interfering chemicals response. AA and paracetamol presented signals nearly equal in 0.3 $V_{Ag/AgCl\ Nafion®\ 117}$. For 0.5 $V_{Ag/AgCl\ Nafion®\ 117}$, the PA and UA signals were upper the single signal nitrite. This is to say, it was masked from 2 nA, comparing signals exhibited in "b", interfering and "d", nitrite.

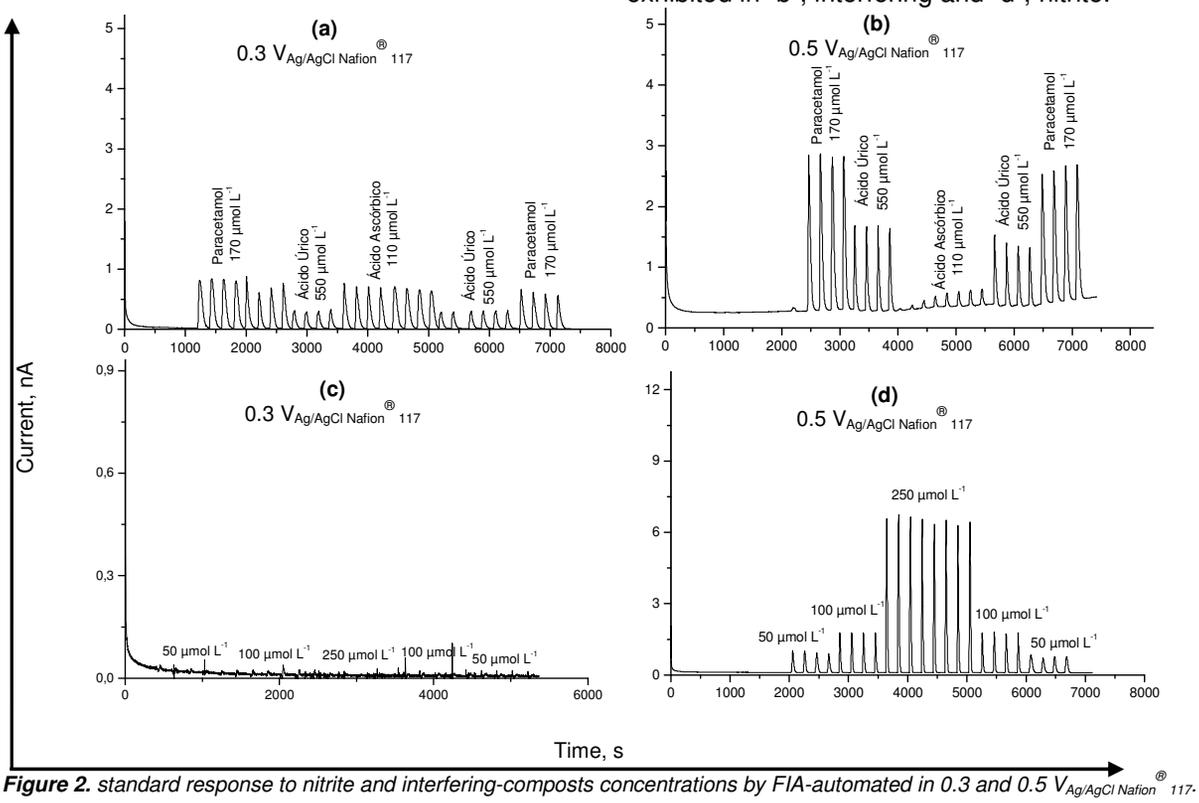

Figure 2. *standard response to nitrite and interfering-composts concentrations by FIA-automated in 0.3 and 0.5* $V_{Ag/AgCl\ Nafion®\ 117}$.

Conclusions

The presented results indicated linearity, repeatability, stability and selectivity for nitrite detection. The calculated sensitivity for nitrite specimens was on order of 6.67 µA mol^{-1} L mm^{-2} and 6.35 nA mol^{-1} L mm^{-2} for 0.5 $V_{Ag/AgCl\ Nafion®\ 117}$ and 0.3 $V_{Ag/AgCl\ Nafion®\ 117}$ potentials, respectively.

References

[1]. H. SUZUKI, **J. Electrochem. Soc.,** Vol. 12, pp. 468-474, 2001.

[2]. B. ADHIKARI, ***Prog. Polym. Sci.***, Vol. 29, pp. 699-766, 2004.

[3]. L. MATTOS, ***Química Nova***, pp. 200-205, 2001.

[4]. S. LASCHI, **Medical Engineering & Physics,** no. 28, pp. 934–943, 2006.

pH sensors based on TiO_2 nanotubes

M.Z. Mielli [1], K.F. Albertin[2], A.T. Lopes[1], M.N.P. Carreño[1] and I. Pereyra[1]
[1] Universidade de São Paulo - LME/PSI/EPUSP, CEP 05508-900, São Paulo, SP, Brazil
[2] CECS, Universidade Federal do ABC - UFABC, CEP 09.210-170, Santo André, SP, Brazil
*katia.torres@ufabc.edu.br

Abstract

pH sensors based on TiO_2 nanotubes are described, fabricated and characterized. The TiO_2 nanotubes are obtained by anodization of Ti foil in a NHF_4 organic solution at different polarization voltages, as grown and thermal annealed samples are utilized in this work. The nanotubes morphology and crystalline phase are characterized by SEM and XRD measurements. The relationship between pH sensitivity with nanotubes diameter and crystalline phase is investigated. Preliminary results show that nanotubes obtained with higher anodization voltage present better sensitivity, probably due to the higher nanotubes diameter obtained in this condition that permit a better solution penetration inside the tubes, thus leading to a larger superficial effective contact area.

Keywords: TiO_2 nanotubes, TiO_xN_y nanotubes, hydrogen sensor

Introduction

The development of miniaturized and high sensitive sensors is of special importance for biosensors and "Lab on a Chip" development [1]. In this context and due to its n-type semiconductor character and high chemical stability, TiO_2 thin films have been proposed for application as pH and H sensors [2]. Even more, taking advantage of their high specific surface, TiO_2 nanotube arrays have been also considered as natural candidates for application in pH detection [3].

Due to its high refractive index, photo-stability and biocompatibility, TiO_2 is an extremely versatile material. Of special importance here, TiO_2 also changes its electrical and/or optical properties upon adsorption of specific molecules on its surface. In this way, TiO_2 can be utilized in photocatalysis, photo-splitting of water, photovoltaic devices and gas sensing devices among others [1,2,3]. Even more, due to its large specific surface area, TiO_2 nanotubes instead of bulk or thin TiO_2 films can be utilized in electrochemical devices. Besides, TiO_2 nanotube arrays also present self-cleaning properties under UV irradiation [4].

Titanium dioxide nanotubes can be obtained through several processes. In particular, the anodization of metallic Ti foil in fluorinated solutions has been demonstrated to lead to highly ordered nanotube arrays and this is the process utilized here to produce the nanotubes.

In this work pH sensors with TiO_2 nanotube arrays, with different nanotube diameter and crystalline phase are fabricated and characterized.

Experimental Procedures

In figure 1 a scheme of the electrolytic cell utilized for the growth of the nanotubes is shown. The platinum cathode and the anodic substrates (1x1 cm of 0,5 mm Ti foil), where the TiO_2 nanotube arrays were grown, were polarized with a DC voltage source (Agilent E3649). As bath a solution of NH_4F in ethylene glycol (0,5 % in weight) and 2 % H_2O, magnetically stirred during the process, was utilized. Anodization voltages of 20 and 60 V were utilized. TiO_2 nanotubes were annealed treated at 300^oC for 2 hour to obtain the anatase crystalline phase. The obtained nanotubes were characterized by scanning electron microscopy (SEM) to analyse the tubes morphology (diameter and length) and X-ray diffraction spectroscopy (XRD) to measure the crystalline phase before and after annealing treatment.

Preliminary tests were performed using the TiO_2 nanotubes as the working electrode of a bench pH meter (HI 221, Hanna Instruments). A neutral pH solution (deionized water) and an acid solution (HCl 0,26 M) were used as test solutions and the electrical response, in milivolts, of the nanotubes versus Ag/AgCl reference electrode were obtained. Prior the tests, the Ti foils containing the nanotubes were coated with PDMS (polydimethylsiloxane), defining a small window through which the test solution could contact the electrode, as ilustrated in figure 2.

Results

In figure 3 the nanotubes diameter value as function of anodization voltage is shown. It is observed that the nanotubes diameter increases linearly with anodization voltage. In figure 4 is shown a SEM image of the nanotubes grown from Ti foil with 20V and 60V, in this case, diameters of approximately 30 nm and 120 nm were obtained.

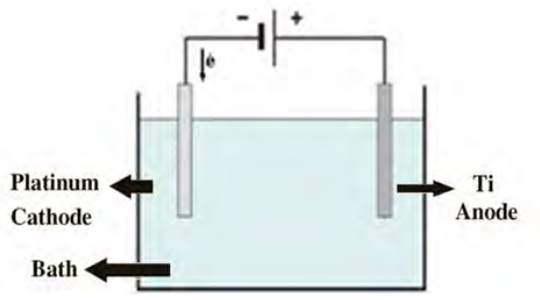

Figure 1. Electrolytic cell utilized for the anodization processes.

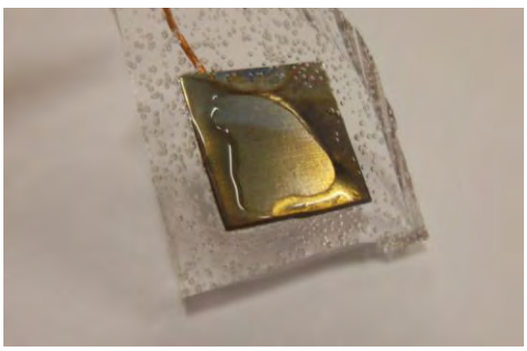

Figure 2. Test device used as working electrode.

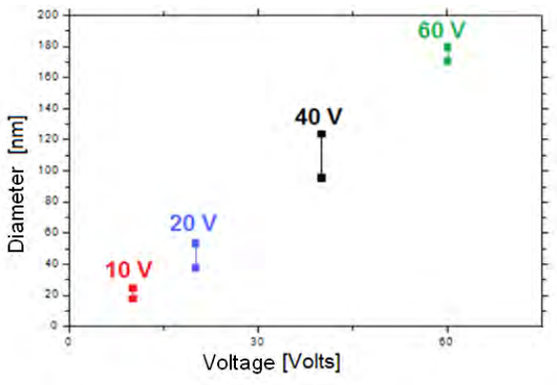

Figure 3 – Nanotubes diameter values as function of anodization polarization voltage.

pH measurements were performed, using the TiO_2 nanotubes as the working electrode, on DI water (pH=7) and on an acid solution of 0,26 mol/L of HCl in water (pH=3). Preliminary results for the test working electrodes are discussed.

(a)

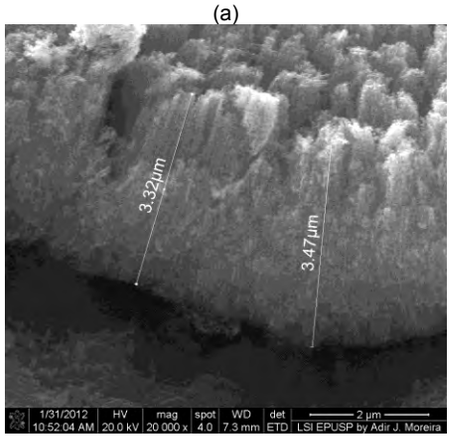

(b)

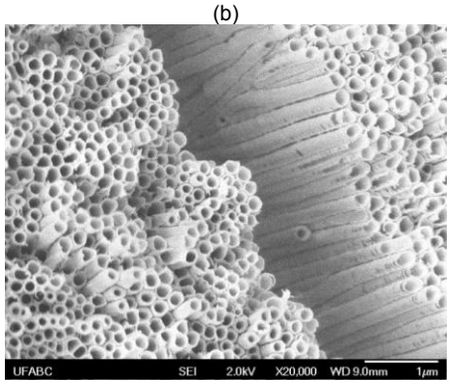

Figure 4. Nanotubes obtained with (a) 20V/4h and (b) 60V/45min

The electrode fabricated with 20V grown nanotubes did not present significant changes on ΔV values, for DI water approximately 466 mV and for HCl solution 469 mV. On the other hand utilizing the electrode fabricated with 60 V grown nanotubes, values of 320 mV and 529 mV respectively were obtained. In this way better sensitivity was obtained for the pH sensor utilizing the electrode fabricated with 60 V grown nanotubes. This result is attributed to the larger nanotube diameter allowing solution penetration inside the tubes and thus promoting a larger surface contact area. The effect of anodization time, nanotube crystallization phase and UV radiation are also studied.

References

[1] T. Pan, J. Lin, Sens. Actuators B: Chem. 138 (2009) 474

[2] G. Yu, X.J. Zhao, Q.N. Zhao, Mater. Chem. Phys. 69 (2001) 25.

[3] R. Zhao, M. Xu, J. Wang, G. Chen, Electrochimica Acta 55 (2010) 5647–5651.

[4] G.K. Mor et. al., J. Mater. Res., Vol.19, No.2, pp. 628-634 2004.

Chapter 3: Optical Sensors

Reconfigurable photonic structures based on a-Si/C devices

M. Vieira[1,2,3], M. A. Vieira[1,2], P. Louro[1,2], V. Silva[1,2], A. Fantoni[1,2]

[1]Electronics Telecommunication and Computer Dept. ISEL, Lisboa, Portugal, mv@isel.ipl.pt.
[2] CTS-UNINOVA, Quinta da Torre, Monte da Caparica, 2829-516, Caparica, Portugal.
[3] DEE-FCT-UNL, Quinta da Torre, Monte da Caparica, 2829-516, Caparica, Portugal.

Abstract

This paper shows that a double SiC/Si pin photodiode can be de-composed into two photonic active filters changeable in function. Reconfiguration is provided by optical control signals to the optoelectronic front and back pin building blocks. Depending on the wavelength and irradiation side of the external optical bias the device acts either as a short- and a long- pass band filter or as a band-stop filter, amplifying or rejecting a specific wavelength range.

Keywords: Optical filters, Si/C devices, MUX/DEMUX,

Introduction

Multilayered structures based on amorphous silicon technology are expected to become reconfigurable to perform WDM optoelectronic logic functions and provide photonic functions such as signal amplification and switching. The basic operating principle is the exploitation of the physical properties of a nonlinear element to perform a logic function, with the potential to be rapidly biasing tuned. Amplification and amplitude change are two key functionality properties, Any change in any of these factors will result in filter readjustments.

Deposition and operation

The active device consists of a p-i'(a-SiC:H)-n/p-i(a-Si:H)-n heterostructure with low conductivity doped layers (Fig.1).

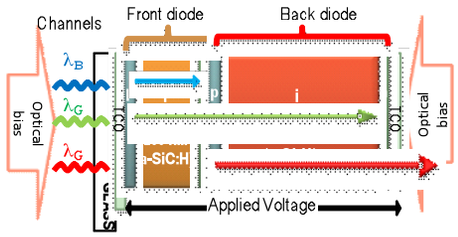

Fig. 1 *Device configuration and operation.*

Transfer function characteristics

The transfer function magnitude (or gain) allows determining the ability of the optical filter to distinguish between signals at different wavelengths. In Fig. 2, at 500 Hz, the spectral photocurrent (symbols) is displayed under red, green, blue and violet background and without it.

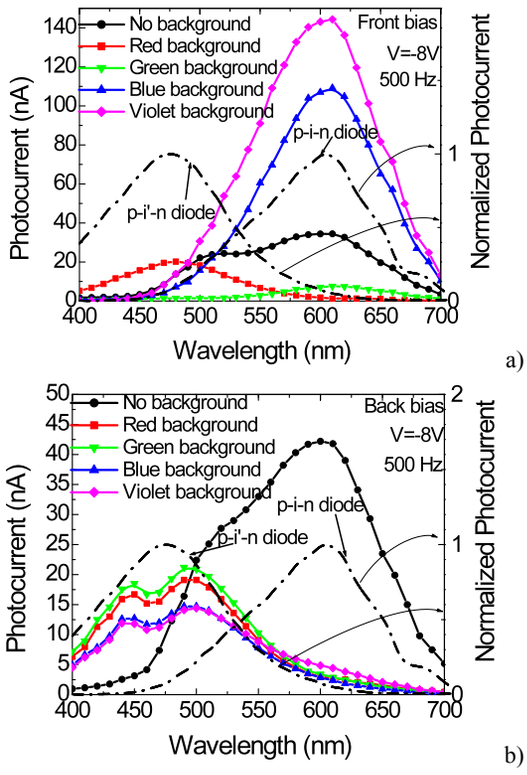

Fig. 2 *Photocurrent without and with front (a) and back (b) backgrounds.The current of the individual photodiodes are superimposed (dash lines)*

Data shows that the front and back building blocks, separately, presents the typical response of single p-i-n cells with intrinsic layers based on a-SiC:H or a-Si:H materials, respectively. Results show that under front irradiation the sensitivity is much higher than

under back irradiation. Under front irradiation (Fig.2a) the violet background amplifies the spectral sensitivity in the visible range while the blue optical bias only enhances the spectral sensitivity in the long wavelength range (>550 nm) and quenches it in the others. Under red bias, the photocurrent is strongly enhanced at short wavelengths and disappears for wavelengths higher than 550 nm. Under green the sensitivity is strongly reduced in all the visible spectra. In Fig. 2b, whatever the wavelength of the backgrounds, the back irradiation strongly quenches the sensitivity in the long wavelength range (> 550nm) and enhances the short wavelength range. So, back irradiation, tunes the front diode while front irradiation, depending on the wavelength used, tunes the back one.

Encoder and decoder device

Three monochromatic pulsed lights separately (red, green and blue input channels, Fig. 3a) or combined (multiplexed signal, Fig. 3b) illuminated the device at 6000 bps. Steady state violet optical bias was superimposed separately from the front (solid lies, pin_1) and the back (dash lines, pin_2) sides and the photocurrent generated measured at -8 V.

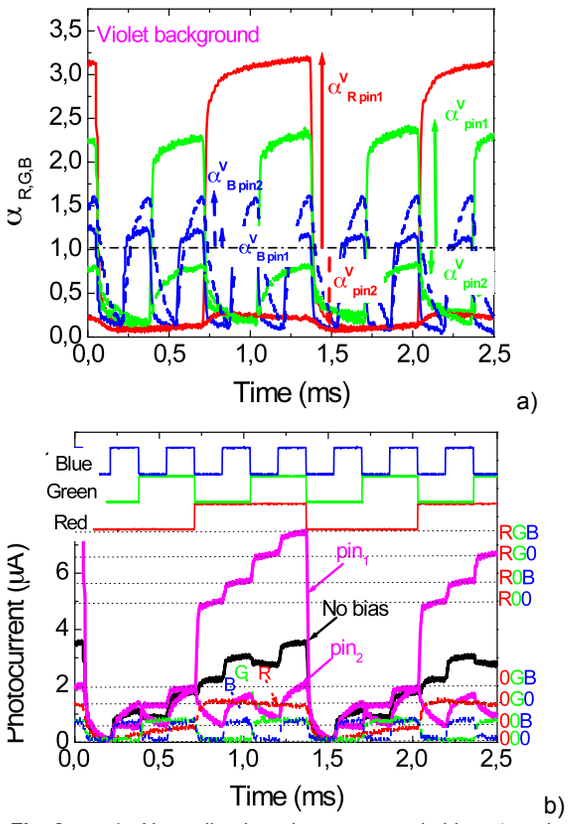

Fig. 3 *a) Normalized red, green and blue transient signals at -8V with violet (400 nm) steady state optical bias from the front side and from the back side. b) Input R,G,B channels and multiplexed output without (no bias) and under front (pin1) and back (pin2) irradiation.*

Under front irradiation, the encoded multiplexed signal presents eight separate levels (2^3) each one related with an RGB bit sequence (right side of the Fig. 3b). Under back irradiation, the red channel is suppressed, the blue enhanced and the green reduced, so the encoded multiplexed signal presents only four main separate levels (2^2). We have used this simple algorithm to decode the multiplex signal. The results are displayed in Fig. 4. An excellent fit was obtained

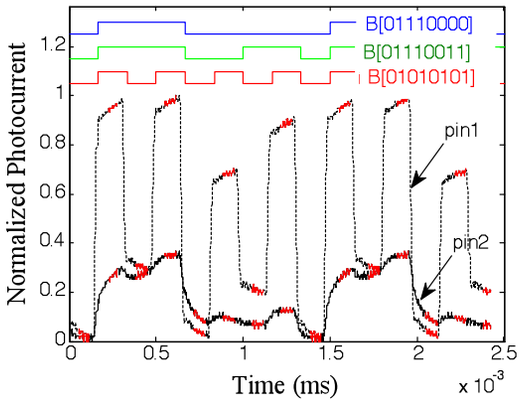

Fig. 4 *MUX signal under front and back irradiation. On the top the DEMUX signals obtained using the decoder algorithm is displayed as well as the binary bit sequences.*

Results show that the pinpi´n multilayered structure become reconfigurable under front and back irradiation. They perform WDM optoelectronic logic functions providing photonic functions such as signal amplification, filtering and switching. So, by means of optical control applied to the front or back diodes, the photonic function is modified from a long- to a short-pass filter, giving a step reconfiguration of the device.

Conclusions

Combined tunable converters based on SiC multilayer photonics active filters are analyzed. Results show that the light-activated pi'n/pin a-SiC:H devices combine the demultiplexing operation with the simultaneous photodetection and self amplification of an optical signal. The output waveform presents a nonlinear amplitude-dependent response to the wavelengths of the input channels. Depending on the wavelength of the external background it acts either as a short- or a long- pass band filter or as a band-stop filter. A two stage active circuit is presented and gives insight into the physics of the device.

Acknowledgements

This work was supported by FCT (CTS multi annual funding) through the PIDDAC Program funds and PTDC/EEA-ELC/111854/2009 and PTDC/EEA-ELC/120539/2010.

Photodetector with integrated optical thin film filters

M. A. Vieira[1,3], M. Vieira[1,2], P. Louro[1,2], V. Silva[1,2], A. S. Garção[2,3]

[1]Electronics Telecommunication and Computer Dept. ISEL, Lisboa, Portugal, mv@isel.ipl.pt.
[2] CTS-UNINOVA, Quinta da Torre, Monte da Caparica, 2829-516, Caparica, Portugal.
[3] DEE-FCT-UNL, Quinta da Torre, Monte da Caparica, 2829-516, Caparica, Portugal.

Abstract

This paper reports on optical filters based on a-SiC:H tandem pi´n/pin heterostructures. The spectral sensitivity is analyzed. Steady state optical bias with different wavelengths, are applied from each front and back sides and the photocurrent is measured. Results show that it is possible to control the sensitivity of the device and to tune a specific wavelength range by combining radiations with complementary light penetration depths. The transfer characteristics effects due to changes in the front and back optical bias wavelength are discussed.

Keywords: Optical filters, Si/C devices, MUX/DEMUX,

Introduction

Multilayered Si/C structures based on amorphous silicon technology are expected to become reconfigurable to perform WDM optoelectronic logic functions. Filters are used to emphasize signals in a certain wavelength range and to reject signals in other ranges. They have a nonlinear magnitude-dependent response to each incident light wave. This nonlinearity provides the possibility for selectively removing and adding wavelength and can be used to boost signal after multiplexing or before demultiplexing.

Deposition and operation

The sensor element is a multilayered heterostructure based on a-Si:H and a-SiC:H. The configuration shown in Fig. 1. The thicknesses and optical gap of the front í'- (200nm; 2.1 eV) and back i- (1000nm; 1.8eV) layers are optimized for light absorption in the blue and red ranges, respectively.

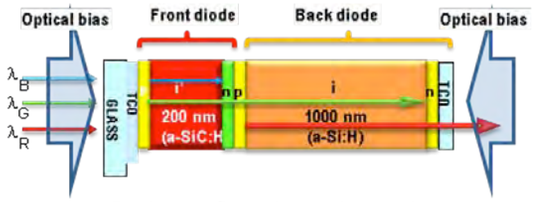

Fig. 1 *Device configuration and operation.*

In Fig. 2 it is displayed the ratio between the photocurrent under different optical bias and without it (gain) under front (symbols) and back (lines) irradiations: 624 nm (α^R), green (α^G), blue (α^B), violet (α^V). Results show that under controlled wavelength backgrounds the device sensitivity is enhanced in a specific wavelength range and quenched in the others, tuning or suppressing a specific band. Under back irradiation the transfer function does not depend on the wavelength background and the device acts as a short-pass filter. Under front red irradiation the transfer function has a high gain at short wavelengths acting as a short-pass filter. Under blue and violet irradiation the transfer function presents an enhanced gain in the long wavelength range acting as a long-pass filter.

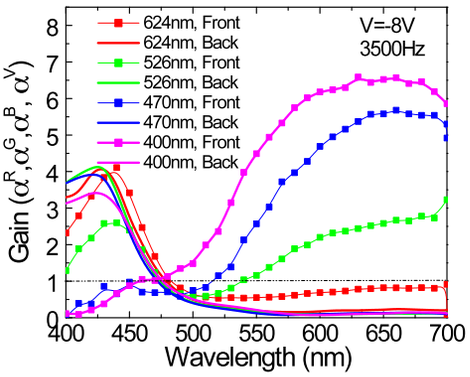

Fig. 2 *Gain under front (symbols) and back (lines) irradiations: 624 nm (α^R), green(α^G), blue (α^B), violet (α^V).*

Under front green background the device is a band-rejection active filter that works to screen out wavelengths that are within the medium range (475nm-550nm), giving easy passage at all wavelengths below and above. Thus the pass-band characteristic of the optical short-

and long-pass filters, under green irradiation, is transformed, respectively, into the lower and the upper pass-band of the optical band-rejection filter. The sensor is a wavelength current-Results show that self optical bias amplification or quenching under uniform irradiation is achieved. By using background lights with complementary light penetration depths across the pi´n/pin device and changing the irradiation side, it is possible to control the spectral response and to filter a specific wavelength band.

Light filtering effects

A polychromatic combination of red, green and blue input channels, in different bit sequences, was used to generate a multiplexed (MUX) signal. In Fig. 3 the filtered signals under red, green blue and violet light control are displayed. The signals were normalized to the maximum intensity under violet (Fig. 3a) and red (Fig. 3b) front irradiations to suppress the dependence on sensor and LEDs positioning. The bit sequences used to transmit the information are shown at the top of the figures.

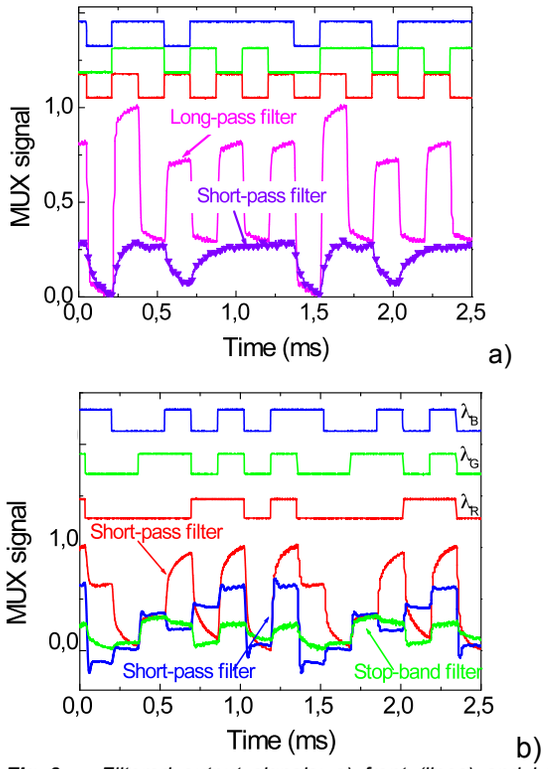

Fig. 3 *Filtered output signals: a) front (lines) and back (symbols) violet irradiation. b) Front red, green and blue background.*

Photonic active filters

Three monochromatic pulsed lights (input channels): red (R_{Ch}), green (G_{Ch}) and blue (B_{Ch}) illuminate the device. Steady state red, green, blue and violet optical bias was superimposed separately from the front and the back sides (see Fig. 1), and the generated photocurrent measured at -8V.

Under front violet irradiation the magnitude of the red and green channels are amplified and the blue reduced (see solid arrows). Violet back irradiation cuts the red channel and slightly influences the magnitude of the green and blue ones.

In Fig. 4 an output MUX signal under front violet irradiation is displayed. On the top the signals used to drive the input channels are displayed showing the presence of all the possible 2^3 on/off states (x_0….x_7).

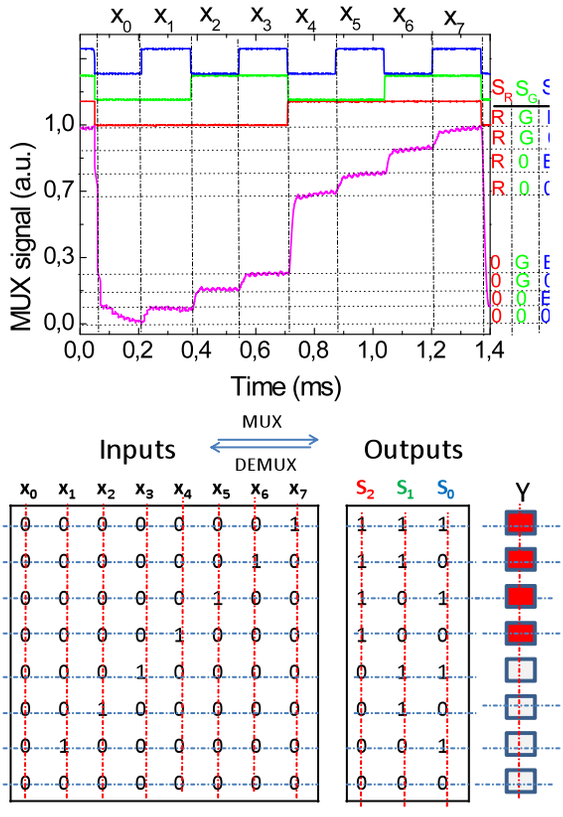

Fig. 4 *MUX signal outputs and truth table of the encoders that perform 8-to-1 multiplexer (MUX) function, under front violet irradiations.*

Under front violet irradiation, $\alpha^V_R >> 1$, $\alpha^V_G > 1$ and $\alpha^V_B \sim 1$ (Fig. 3). So, the correspondence between the outputs S_2, S_1, S_0 and the *on/off* state of the input channels, S_R, S_G, S_B, is obvious.

Conclusions

Tandem a-SiC:H pi'n/pin active filters are analyzed under different back and front optical bias wavelengths. An optoelectronic band-pass filter model supports the experimental data. A truth table of an encoder that performs 8-to-1 multiplexer (MUX) function is presented.

Detección Colorimétrica de Cobalto Utilizando Micro-Sistemas de Análisis

O.N. Bustos López[1]*, C.S. Martínez Cisneros[2], J. Alonso Chamarro[2], F. Valdés Perezgasga[1], H. A. Moreno Casillas[1]
[1]División de Estudios de Posgrado e Investigación, Instituto Tecnológico de La Laguna
C.P. 27000, Torreón, Coahuila, México
[2]Universidad Autónoma de Barcelona, España
*Corresponding autor: bustosolga@yahoo.com.mx

Resumen

Los avances logrados en los últimos años en el área de micro-sistemas de análisis total (μ-TAS), han permitido el desarrollo de instrumentos analíticos para medición y determinación de variables que anteriormente requerían de instrumental de laboratorio para tales fines. El presente trabajo detalla el proceso mediante el cual se han adaptado metodologías colorimétricas clásicas, utilizadas en los sistemas de análisis discontinuos, a sistemas de flujo continuo para la determinación de cobalto en soluciones acuosas en tiempo real, este tipo de metodologías brindan una alta sensibilidad además de ser sencillas y costeables. La finalidad de esta adaptación es la posterior miniaturización del sistema usando cerámicas de cocimiento conjunto a bajas temperaturas o LTCC (Low-temperature co-fired ceramics).

Palabras Clave: Cobalto, LTCC, Flujo continuo, Colorimetría.

Introducción

En las últimas décadas ha aumentado la necesidad de determinar concentraciones cada vez más pequeñas en espacios más cortos de tiempo, con una mayor precisión y exactitud.[1] Con esta finalidad, se requiere instrumentación que permita realizar análisis cuantitativos y cualitativos para obtener medidas *in-situ* con una alta selectividad. Lo que ha dado lugar a los llamados *Lab-on-a-chip* o microsistemas de análisis total (*μTAS*) [2].

Los métodos colorimétricos figuran entre los procedimientos analíticos de mayor sensibilidad. Así, puede procederse con estas técnicas, en general, a la determinación de iones metálicos en el campo de concentración de 10^{-4} a 10^{-5} g/L. Además muchos de los reactivos utilizados en el trabajo colorimétrico presentan un grado notable de selectividad, como resultado, el análisis de un ión dado se puede realizar frecuentemente en presencia de concentraciones muy elevadas de otros iones [3]. El método de tiocianato es adecuado para la determinación de cantidades relativamente grandes de cobalto, sin embargo, los métodos con nitroso-naftoles o nitroso-R sal son mucho más específicos [4].

Nitroso-R sal es un derivado de 1-nitroso-2-naftol. Ambos reactivos son específicos para el cobalto. Los grupos sulfonato en la molécula de nitroso-R sal hacen que este reactivo y su complejo de cobalto sea soluble en agua pero insoluble en solventes no polares. Por lo tanto, nitroso-R sal se utiliza para determinar espectrofotométricamente cobalto en un medio acuoso. [5,6].

Metodología

La metodología desarrollada para la micro-determinación colorimétrica de cobalto, emplea como reactivo el Nitroso-R sal, en un medio de acetato y citrato de sodio, que favorece la reacción. La solución portadora de la muestra se prepara con ácido sulfúrico, lo que permite un equilibrio en la reacción en caso de posibles interferencias de otros metales [7].

La absorbancia del complejo formado fue medida a 540 nm, el sistema utiliza una bomba peristáltica para mantener el flujo, una válvula de 6 vías para la inyección de la muestra, una estructura micro-fluidica en LTCC, un foto-emisor y un foto-detector, así como una aplicación basada en la *suite* de programación LABVIEW que muestra la medición de las absorbancias para un rango de concentraciones entre 0.1 y 10 ppm.

Para la detección colorimétrica se dispuso como foto-emisor un LED color verde con longitud de onda a 540 nm, la luz incidente en el dispositivo

cerámico recorre un camino óptico de 1 mm, y se transmite mediante una fibra óptica hacia el foto-transductor que convierte la variable física a un voltaje proporcional. Un circuito de acondicionamiento de señal permite la adecuación del voltaje de dicho sensor hacia la tarjeta de adquisición de datos, como se aprecia en la figura 1.

.

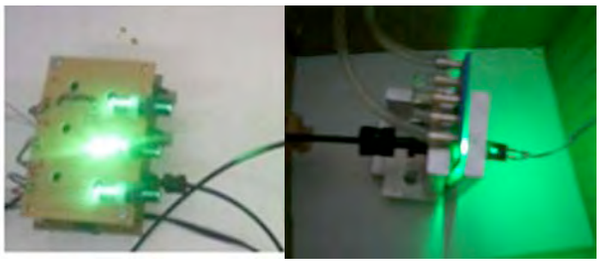

Fig.2. Montaje del sistema opto-electrónico.

Resultados

Los resultados obtenidos validan la adaptación del método empleado mediante los coeficientes de correlación lineal, cuyos valores oscilan entre 0.92 y 0.99 cumpliendo con la Ley de Beer, lo cual hace posible su aplicación para la miniaturización completa del análisis de cobalto, como lo muestran las figuras 3 y 4, donde se muestra la respuesta del sistema para diferentes concentraciones patrón de cobalto.

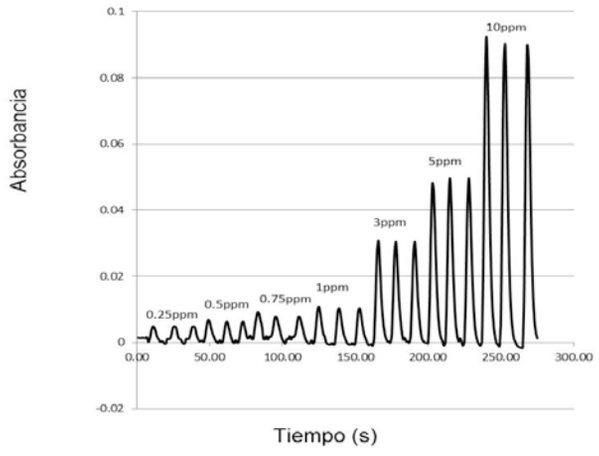

Fig.3. Absorbancias obtenidas en patrones de cobalto desde 0.25-10ppm.

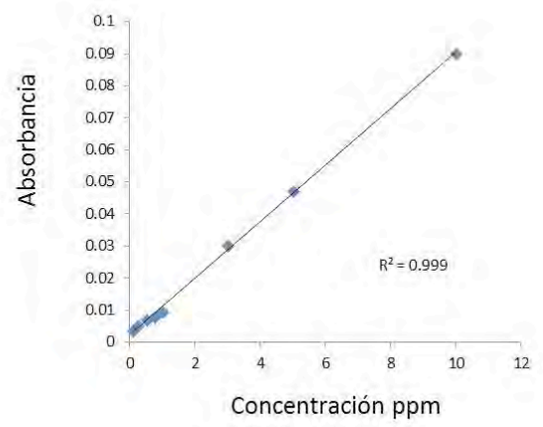

Fig.4. Regresión lineal y coeficiente de correlación.

Referencias

[1] Dewey D.W., Marston H.R., *Anal. Chim. Acta*, Vol.57, pp. 45-49 , November 1971..

[2] Harris, D.C. "Quantitative Chemical Analysis". WH Freeman and Company. Pp. 155-165, 2003.

[3]. Wursch G., *Talanta*, 26,177 (1979).

[4] Pyrzynska K., Janiszewska Z., "*Determination of Trace Amounts of Cobalt by Flow Injection With Spectrophotometric Detection", Analyst,* Vol.119, pp. 45-47, July 1994.

[5] Villalobos A., *"Diseño de Sensores para Metales Pesados",* Tesis Doctoral, pp. 85-90, 2006.

[6] J. Růžička, E.H. Hansen. Flow Injection Analysis. Jonh Wiley & Sons, Inc. Pittsburgh, PA. pp. 6, 1981.

[7] Hayashibe et al " Method, for measung imputiy concentration and removing impurities from electrolytic solution for electrowinning of zinc." U.S. Patent 5,178,771, January 12, 1993.

Wavelength Division Multiplexing device based on a-SiC:H

P. Louro[1,2], M. Vieira[1,2,3], M. A. Vieira[1,2], V. Silva[1,2], A. Fantoni[1,2]

[1]Electronics Telecommunication and Computer Dept. ISEL, Lisboa, Portugal, mv@isel.ipl.pt.
[2] CTS-UNINOVA, Quinta da Torre, Monte da Caparica, 2829-516, Caparica, Portugal.
[3] DEE-FCT-UNL, Quinta da Torre, Monte da Caparica, 2829-516, Caparica, Portugal.

Abstract

In this paper we report the use of a device based on two multilayered a-SiC:H/a-Si:H stacked heterostructures to photodetect and demultiplex optical signals of the visible spectrum. Both heterostructures were optimized for the detection of short and long wavelengths within the visible range. The optoelectronic characterization of the device includes spectral response measurements under reverse bias and using different optical steady state light conditions to soak the device. Results show that the device photocurrent signal measured using appropriate steady state optical bias, allows the separate detection of the input transmitted signals which enables the demultiplexing task. A numerical simulation, gives insight into the transduction mechanism to explain the device wavelength selective behavior.

Keywords: Optoelectronics, Si/C devices, MUX/DEMUX,

Introduction

The capacity of an optical communication system can be increased using the Wavelength Division Multiplexing (WDM) technique [i]. Multiplex is the operation of combining several optical signals and transmit all of them along the same transmission medium. At the reception end it is necessary to carry out the reverse operation for separating the combined signal into each individual component, i.e., to demultiplex the signal. In this paper we report the use of an integrated photodetector and demultiplexer device based on two stacked mutilayered a-SiC:H/a-Si:H structures that act as optical filters in the visible range [ii, iii]. The possibility of tuning the spectral device sensitivity is analyzed and discussed using several optical bias conditions. The use of light to soak the device induces different modulations of the electrical field along both front and back heterostructures, which amplifies or cuts specific wavelengths [iv]. This enables the identification of the transmitted individual input channels and implements the demultiplexing operation in the visible spectrum,

Device operation

Fig. 1 shows the simplified schematic diagram of the structure of the device, that has in the front side a very thin pin photodiode based on a-SiC:H and on the back side a thick photodiode of a-Si:H. Both front and back photodiodes are coated with a transparent electrode (indium tin oxide – ITO) to allow photons to enter the device from the front and back sides.

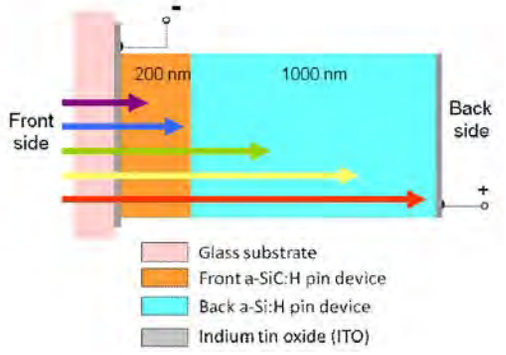

Fig. 1 *Device configuration.*

Numerical simulation

We used a device simulation program ASCA-2D to analyze the generation rate profiles in the device. The generation rate is calculated following a Urbach-Tauc-Lorentz model [v] for the absorption coefficient. Resuklts show that the depth of light penetration within the device depends on the wavelength. If the light in the background is a short wavelength radiation, the photogeneration profile is strongly influenced by the choice of the device side for light incidence. Under back irradiation the generation in the

back photodiode increases for short/medium wavelengths due to the light penetration depth of the violet light across the bottom of the a-Si:H intrinsic layer.

Spectral sensitivity

Fig. 2 displays the spectral photocurrent, measured along the visible spectrum, without and with optical light bias focusing the device from the front side and back sides.

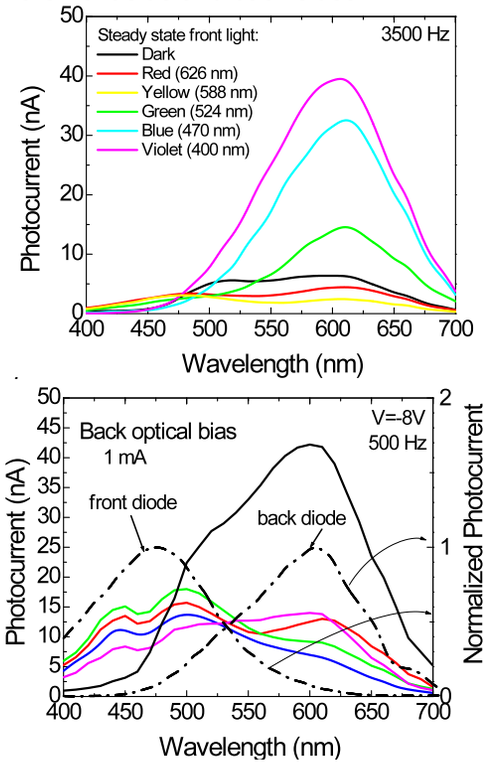

Fig. 2 *Device spectral photocurrent under: a) front and b) back steady state illumination.*

Transient mux signal

In order to test the decoding performance of the device using violet (400 nm) front and back optical bias, different combined red, green and blue optical waveform signals were used. Fig. 3 displays the transient multiplexed signal under reverse bias using different optical bias conditions during the signal acquisition process: no optical bias (dark line), and front violet (magenta line) and back violet light (violet line) for the steady state light. The output multiplexed signal, obtained with the combination of the three optical sources, depends on the side of the background illumination and on the ON-OFF state of each input optical channel. In order to decode the input channels both multiplexed signals measured with back and front steady state illumination were divided into eight time slots, each corresponding to a different optical state.

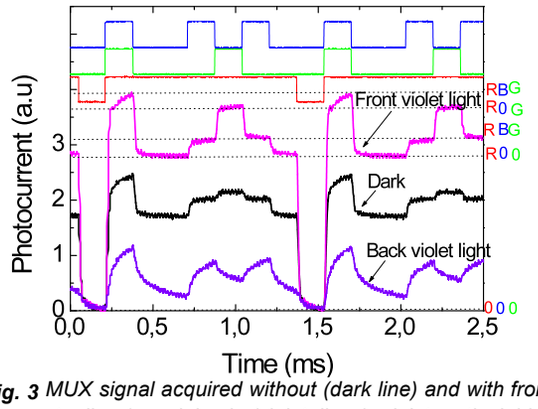

Fig. 3 *MUX signal acquired without (dark line) and with front (magenta lines) and back (violet lines) violet optical bias using different combinations of the red, green and blue optical signals. On the top the input optical signals are displayed*

Conclusions

A double pi'n/pin a-SiC:H WDM device was presented. Spectral response characterization was done using different optical biasing conditions to change the absorption mechanism. A numerical simulation to model the device generation rate profile was used to explain the optical filtering properties. Multiple monochromatic pulsed communication channels, in the visible range, were transmitted together, each one with a specific bit sequence. The combined optical signal was analyzed by reading out, under front and back steady state illumination the generated photocurrent across the device. Results show that the use of short range (400 nm, violet) wavelength steady state optical bias focusing the device from its front and back side allow the decoding of each input channels.

i M.Bas, Fiber Optics Handbook, Fiber, Dev.and Syst. for Opt. Comm., Chap, 13, Mc Graw-Hill, 2002.

ii M. Vieira, M. Fernandes, P. Louro, A. Fantoni, Y. Vygranenko, G. Lavareda, C. Nunes de Carvalho, Mat. Res. Soc. Symp. Proc., Vol. 862 (2005) A13.4.

iii M. Vieira, A. Fantoni, M. Fernandes, P. Louro, G. Lavareda, C.N. Carvalho, J. Nanosci. Nanotechn., 9 (7), (2009) 4022-4027. DOI: 10.1166/jnn.2009.M05.

iv P. Louro, A. Fantoni, M. Fernandes, A. Maçarico, R. Schwarz, M. Vieira, J. Non Cryst. Solids, 338-340 (2004) 345-348. DOI: 10.1016/j.jnoncrysol.2004.02.070.

v A.S. Ferlauto , G.M. Ferreira , J.M. Pearce, C.R. Wronski, R.W. Collins, X. Deng, G. Ganguly, Thin Solid Films 455–456 , 388 (2004)

Determination of the Generation Time in Optical Sensors Based on Metal-Oxide-Semiconductor Capacitors

O. Malik, F. J. De la Hidalga-W.
Electronics Department of National Institute for Astrophysics, Optics, and Electronics (INAOE)
P.O. 51 and 216 Puebla, 72000 Mexico
amalik@inaoep.mx

Abstract

In this work we present a simple technique for the determination of the generation time in optical sensors with giant signal amplification based on MOS capacitors fabricated on high-resistive silicon. The results are compared with other known methods. This technique may be considered as an express instrumentation method using lower cost equipments. The generation time is one of the most important parameter that determines the lowest level of optical signals recorded by sensors based on silicon MOS capacitors.

Keywords: Silicon, MOS capacitor, carriers generation time, measurement technique.

MOS Capacitor as Optical Sensor with Giant Signal Amplification

In our previous articles [1, 2] we presented a detailed analysis of optical sensors based on MOS capacitors. Such sensors operate in non-equilibrium mode. Under the charge storing mode, when a voltage step is applied to the capacitor gate, a potential well is formed at the semiconductor surface. The width of the depletion layer changes with time due to the carriers' thermal generation. For a long value of the generation time, the filling of the potential well by thermo-generated minority carriers occurs slowly. Under such conditions, a low optical signal can be recorded through the integration of the electrical signal (photocurrent) during the storage time. The integrated charge can be obtained as a narrow current peak by changing the voltage to the initial value (readout mode). The giant internal current amplification (10^4-10^6) comes from the parametric amplification due to the time "compression". The readout charge is about the same as the stored one, and both charges are obtained as the time integrals of the current flowing during the charge storing and readout processes, respectively. However, the output current presents a peak because of the short duration of the readout process and the recombination process in the silicon substrate.

Generation Time as an Important Parameter

The current flowing in the charge storing process consists of two parts: the dark current and the photocurrent. The optimal condition for the sensor operating under low illumination level, requires a small value of the dark current in comparison with photocurrent. This condition can be obtained for a long value of the generation time. Thus, the knowledge of this value is quite important for the optimal operation of the sensors optical. The traditional methods require specialized equipment. We propose an express method based on non-equilibrium processes in MOS capacitor when a voltage ramp is applied to the capacitor gate. The generation time can be estimated from the signal recorded by a digital oscilloscope.

Mathematical Model

The time-dependent gate voltage (a) and the current (b) flowing through the circuit are shown in Figure 1.

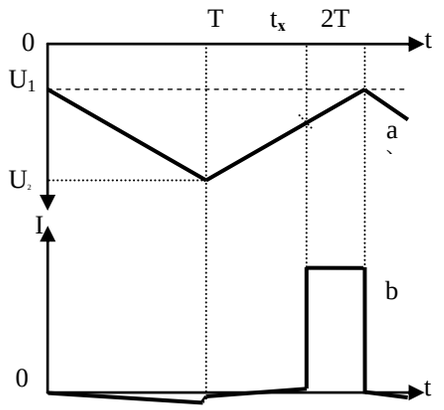

Figure 1. Time-dependent gate voltage (a) and the current (b) flowing through the circuit.

From the second Kirchhoff's law for the circuit containing the MOS capacitor connected in series with the function generator and a load resistor R_L, the basic equations are:

$$U(t) = \frac{Q_p}{C_{ox}} + U_p + U_n + \frac{qN_d w^2(t)}{2\varepsilon_0 \varepsilon_s}$$

Here, Q_p is the charge of the inversion layer at the voltage U_1; U_p and U_n are the voltage drops in the inversion and depletion layers at the voltage U_1, respectively, $C_{ox}=\varepsilon_0\varepsilon_{ox}A/d_{ox}$, ε_0 , ε_{ox} , ε_s are permittivity of vacuum, oxide, and substrate, d_{ox} is the oxide thickness, and N_d is a donor concentration in the substrate. The voltage drops U_p, U_n and on the load resistor for $R_L<$ 50 kΩ are very low for a current level below 10^{-5} A when compared to U(t)-U_1>5 V. This equation and the equation for the time variation of the inversion layer charge dive us time dependence of the depletion layer $w(t)$.

Filling the potential well by thermo generated carriers continues until that moment at which this well is completely filled by the minority carriers. At that moment, the value of $w(t)$ will decrease down to zero at the time $t=t_x$, and the capacitance leads to the value of C_{ox} as it is shown on Figure 1.

The generation time (τ_g) may be obtained from the equation for the charge balance at $t=t_x$:

$$C_{ox}\Delta U\,\frac{2T-t_x}{T} = \frac{en_i A w_0}{\tau_g}\left[\int_0^T \left(\frac{t}{T}\right)^{1/2} dt + \int_T^{t_x}\left(\frac{2T-t}{T}\right)^{1/2} dt\right],$$

where

$$w_0 = \left(\frac{2\varepsilon_0\varepsilon_s\Delta U}{eN_d}\right)^{1/2}$$

After integrating, the equation for τ_g is:

$$\tau_g = en_i w_0 A \frac{4T^2 - \left(2/T^{1/2}\right)\left(2T-t_x\right)^{3/2}}{3C_{ox}\Delta U\left(2T-t_x\right)}$$

Experimental Results

From Figure 2, the experimental data used for the determination of the generation time with the proposed method is shown. Using the results obtained experimentally for 2T=1.964 s, ΔU=17.31 V, t_x=1.932 s, n_i=5.1x109 cm-3 (at a measured temperature of 15.5^{0}C), and using the next parameters for the MOS capacitor: area A=0.06 mm^2, C_{ox}=1.9 nF, ε_s=11.8, ε_{ox}=4.7, N_d=2x10^{12} cm^{-3}, the value obtained for the generation time τ_g is 0.517 ± 0.04 ms.

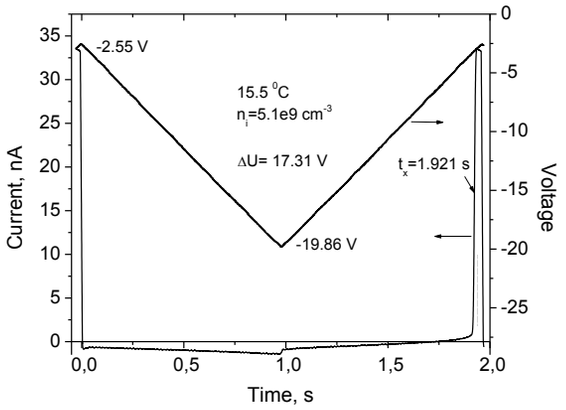

Figure 2. Experimental data (oscilograms) used for the determination of the generation time with the proposed method.

Our results for the value of the generated time were compared with that obtained with a standard current-capacitance technique [3]. This method gives us a close value of 0.530 ms.

Conclusions

A new express method is proposed for determining experimentally the generation time in MOS capacitors. Results obtained with this method agree with a well known standard method based on the measurement of capacitance-current characteristics of MOS capacitor under non-equilibrium conditions.

The knowledge of the generation time allows for improving the fabrication process to obtain more efficient optical sensors based on MOS capacitors for the detection of small optical signals.

References

[1] A. Malik, V. Grimalsky, M.C. Tsou, D. Durini, Chi-Tang Lo, Proc. of 33-rd European Solid-State Device Research Conference (ESSDERC), Estorial, Portugal, September 16-18, pp. 67-70, 2003.

[2] A. Malik, V. Grimalsky, Sensors and Actuators A, Vol.110, pp. 310-317, 2004.

[3] J.S. Kang, D.K. Schroder, Phys. Stat. Sol., Vol. 89a, pp. 13-43, May, 1985.

Caracterización de un sensor laser empleando la frecuencia de batido fundamental

O. Méndez-Zepeda, S. Muñoz-Aguirre, G. Beltrán-Pérez and J. Castillo-Mixcóatl
Facultad de Ciencias Físico-Matemáticas, Benemérita Universidad Autónoma de Puebla
Av. San Claudio y 18 Sur, San Manuel CU, CP. 72570, Puebla, Puebla, México
mezeos9@yahoo.com, smunoz@fcfm.buap.mx

Resumen

Se presentan el análisis teórico y resultados experimentales preliminares de un sensor multipunto basado en dos cavidades Fabry-Perot, conformadas por una FBG de referencia y otra como elemento sensor. Se discuten las condiciones de operación del sistema y finalmente se exponen algunos resultados para una cavidad donde se analiza la señal de salida del sensor en el dominio de la frecuencia, demostrándose que existe una dependencia de la intensidad del espectro de la señal de salida del sensor respecto de los estiramientos que sufre la rejilla sensora.

Palabras clave: Interferómetro Fabry-Perot, rejillas de Bragg, frecuencia de batido fundamental

Introducción

Los métodos empleados para medir variables físicas con sensores basados en rejillas de Bragg (FBG) usan equipos costosos como el analizador de espectros ópticos que mide los corrimientos que sufre la longitud de onda de Bragg (λ_B) cuando la FBG esta bajo la influencia de alguna variable [1]. Por otro lado se emplean técnicas complejas como la multiplexión de FBGs cubiertas con diferentes polímeros que modifican la λ_B cuando el polímero detecta temperatura o salinidad [2]. Por lo anterior, se requieren técnicas más simples y económicas.

En un trabajo previo se mostró teóricamente que es posible medir al menos dos variables en un mismo arreglo a partir de la frecuencia de batido fundamental (FBF) a través del análisis en el dominio de la frecuencia utilizando la transformada rápida de Fourier (FFT), detectando y midiendo la variable a partir de la cuantificación del valor y de la intensidad espectral de la FBF, respectivamente. La amplitud espectral del pico de la FBF depende del numero de modos que se amplifican, los cuales a su vez dependen del traslape de los espectros de las FBGs [3], por lo que en el actual trabajo, se presentan resultados experimentales para una cavidad, al medir el estiramiento de una FBG, utilizando este método.

La FBF depende de la longitud de la cavidad y esta dada por (1).

$$\Delta\nu = \frac{c_0}{2nd} \qquad (1)$$

donde c_0/n es la velocidad de la luz en la cavidad, n es el índice de refracción y d es la longitud de la cavidad [4].

Arreglo experimental

El arreglo se muestra en la Fig. 1 y consiste de un diodo de bombeo a 980 nm, acoplado a una fibra dopada con erbio (7 m) a través de un WDM. La cavidad con longitud de 314 m esta conformada por dos FBGs (FBG-S con λ_B=1534 nm y FBG-R con λ_B=1536 nm). La FBG-S se estiro con un tornillo micrométrico en un rango de 0 a 120 μm, en pasos de 20 μm. La salida se digitaliza con la tarjeta PCI-1712 y es analizada con la FFT.

Resultados experimentales y discusión

Para verificar lo mencionado anteriormente, se midió la señal del arreglo de la Fig. 1 durante 16 s a una taza de muestreo de 1 MS/s. Posteriormente se obtuvo el espectro de esta señal al aplicarle la FFT, localizando un pico centrado a 328 kHz que corresponde a una cavidad de longitud de 314m, lo cual concuerda con el valor calculado de la Ec. 1.

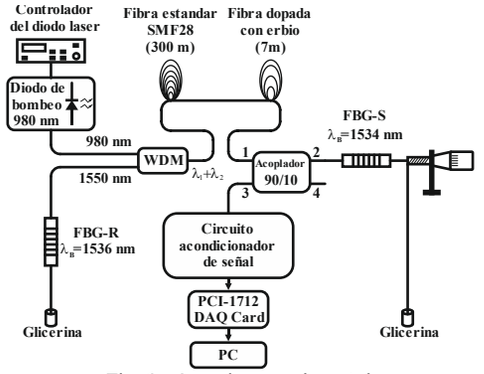

Fig. 1. Arreglo experimental.

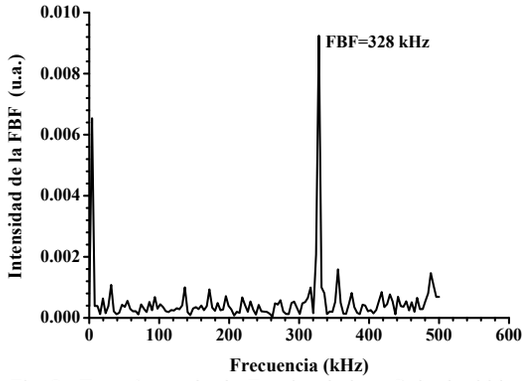

Fig. 2. Transformada de Fourier de la señal adquirida.

Por lo que es posible identificar la FBG-s a partir del valor de la FBF.

Para comprobar que la intensidad del pico de la FBF varia en función de los estiramientos de la FBG-S se graficaron distintos picos correspondientes para diferentes estiramientos, lo cual se puede observar en la Fig. 3.

A su vez, para determinar el comportamiento de la intensidad del pico de la FBF respecto del traslape de las FBGs, se graficaron los cambios que sufren los picos conforme la FBG-S se estira en un rango de 0 a 140 μm con incrementos de 20 μm (Fig. 4). Se observa un comportamiento bastante lineal ya que se obtuvo un coeficiente de correlación de R^2=0.9703. La sensibilidad calculada del sensor fue de 1.17×10-4 μm^{-1} y la resolución de aprox. 17 μm.

Finalmente para determinar la estabilidad de la respuesta del sensor, se realizaron cinco mediciones por cada estiramiento de la FBG-S en

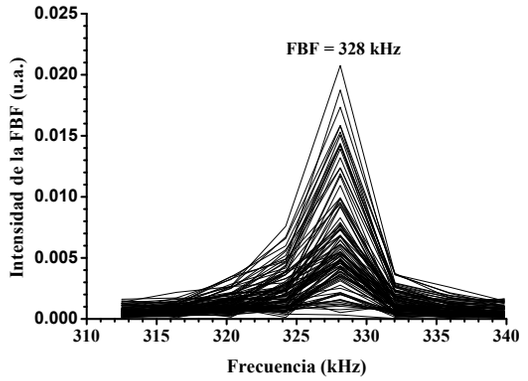

Fig. 3. Cambios en la Intensidad de la FBF por efecto de los estiramientos.

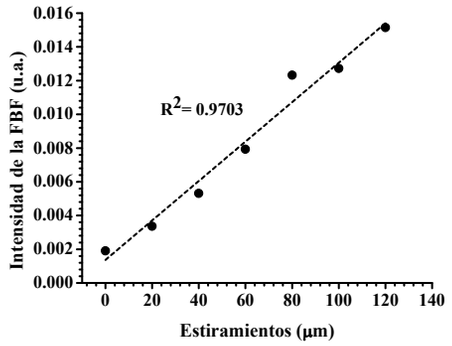

Fig. 4. Comportamiento de la intensidad de la FBF en función de estiramiento de la FBG-S.

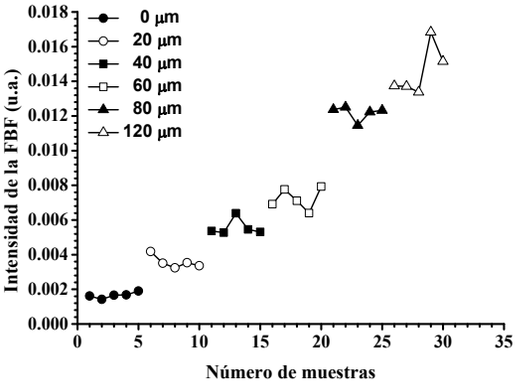

Fig. 5. Estabilidad de la respuesta del sensor para diferentes valores de estiramiento (cinco mediciones para cada estiramiento).

un rango de 0 a 120 μm. Los resultados obtenidos se muestran en la grafica de la Fig. 5, obteniéndose fluctuaciones del orden del ± 15%.

Conclusiones

En este trabajo se comprobó el método de cuantificación de estiramientos de una FBG-S a partir de la medición de la intensidad del pico de la FBF, obteniendo un comportamiento lineal con un factor de correlación de R^2=0.9703. Por otro lado se evaluaron los estiramientos en un rango de 0-140 μm y se obtuvo una resolución de aprox. 17 μm con una sensibilidad de 1.17×10-4 μm^{-1}.

Referencias

[1] Yasukazu Sano and Toshihiko Yoshino, J Lightwave Technol 21 (2003) 132-139.

[2] Ping Lu, Liqiu Men, and Qiying Chen, Appl Phys Lett 92, 171112 (2008).

[3] O. Méndez-Zepeda, S. Muñoz-Aguirre, G Beltrán-Pérez and J. Castillo-Mixcóatl, Analysis of a multipoint sensor based on two Fabry-Perot cavities employing fiber Bragg gratings, Proc. of SPIE Vol. 8011 (2011) 80114T

[4] Bahaa E. A. Saleh, Malvin Carl Teich, Fundamentals of Photonics, John Wiley & Sons 1991.

Laser de fibra con longitud de onda dual empleado como sensor

M. Durán-Sánchez[a], E. A. Kuzin[b], B. Ibarra-Escamilla[b], R. I. Álvarez-Tamayo[C], A. González-García[b]
[a]Universidad Tecnológica de Puebla
Antiguo Camino a la Resurrección N°1002-A Parque Industrial, Puebla, Pue.72300,
México, Tel/fax +52 222 3098825
[b]Instituto Nacional de Astrofísica, Óptica y Electrónica, Óptica,
Luis Enrique Erro No. 1, Puebla, Pue. 72000, México, Tel/fax +52 222 2472940
Benemérita Universidad Autónoma de Puebla, FCFM, Av. San Claudio y Rio Verde s/n Col.,
San Manuel, C.P. 72570 Puebla, México
e-mail: mdurans.utp@gmail.com

Abstract

Presentamos resultados experimentales de un láser de fibra óptica con doble longitud de onda y doble longitud de onda seleccionable utilizando fibra dopada con erbio basado en dos rejillas de Bragg (FBG) y un lazo de Sagnac el cual funge como espejo. Controlando las perdidas en la cavidad se pueden obtener una o doble longitud de onda mediante el lazo de Sagnac. Al modificar la longitud de onda de cualquiera de las rejillas de Bragg las cuales fingen como sensores; es posible estimar los cambios mediante ajustes en las perdidas de la cavidad utilizando el Interferómetro de Sagnac.

Keywords: Optical fiber sensor, Dual wavelength fiber laser, Interferometer of Sagnac

Introducción

Láseres con longitud doble longitud de onda y sintonizable son muy atractivo para la gran variedad de aplicaciones en sensores, multiplexación de longitud de onda, generación de microondas fotónicas, entre otras aplicaciones. Una fibra dopada con erbio (EDF) muestra una ganancia homogénea a temperatura ambiente. Debido a la competencia de ganancia entre las dos longitudes de onda de emisión láser, es difícil producir un láser de fibra óptica utilizando fibra dopada con erbio. Varias técnicas se han propuesto para superar la limitación del uso de una fibra dopada con erbio como medio de ganancia. Un número de láseres de fibra de doble longitud de onda usados como sensores se han reportado utilizando fibras dopada con erbio [1-4]. En la mayoría de los láseres con doble longitud de onda utilizan una fibra dopada con erbio, las longitudes de onda de emisión láser se ajustan a través de controladores de polarización PC. En trabajos anteriores hemos reportado algunas configuraciones para la generación de emisión láser con doble longitud de onda [5-8].

En este trabajo, nosotros demostramos una sencilla técnica para generar un láser de fibra óptica con doble longitud de onda, una o ambas longitudes de onda pueden ser seleccionadas mediante una ajuste apropiado en el interferómetro de Sagnac el cual se puede utilizar como sensor de dos variables físicas.

Arreglo Experimental

En la Fig. 1 se muestra el arreglo experimental del láser propuesto. El láser de cavidad lineal consiste de un lazo de Sagnac (SFL) el cual funge como espejo, un acoplador multiplexador por división de longitud de onda (WDM-980/1550), 1 m de EDF, y dos FBG. Las FBGs actúan como espejos reflectores (sensores) y el SFL se utiliza para para ajustar las perdidas en la cavidad. La EDF es bombeada a través del acoplador WDM por mediante un diodo láser a una longitud de onda de 980 nm con una potencia de 50 mW. El lazo de SFL se fabrica con un acoplador direccional de fibra monomodo, donde dos de sus puertos están conectados entre sí por medio de 28 cm de fibra de alta birrefringencia (Hi-BiF) formando un lazo de fibra óptica. Es bien conocido que estos dispositivos son altamente sensibles a cambios de temperatura, los cuales ocasionan un desplazamiento en la longitud de onda del SFL, por lo cual la fibra de Hi-Bi es colocada en un Peltier, dispositivo con el cual inducimos cambios de temperatura. Este efecto es utilizado para alcanzar la conmutación oscilante de la longitud de onda y para controlarla mediante un laseo simultáneo. Las características espectrales se miden usando un monocromador, posteriormente se detectan con

un fotodetector y finalmente se monitorea la salida láser con un osciloscopio digital.

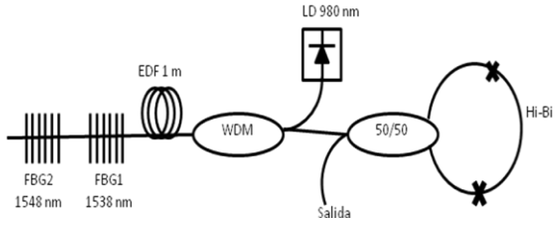

Fig. 1 Arreglo Experimental

Resultados y discusiones

Las dos rejillas FBGs con reflectividades de 55.4 % (FBG1 = 1537.9 nm) y 59.75 % (FBG2 = 1547.8 nm) para las cavidades 1 y 2, respectivamente, fueron conectadas en forma serial. Entonces la conmutación oscilante de la longitud de onda se observó ajustando las pérdidas en la cavidad con el SFL. Obtuvimos con éxito el funcionamiento oscilante de la selección de la longitud de onda controlando la temperatura del Peltier y con esto la longitud de onda del SFL. Cuando la temperatura en la fibra de Hi-Bi es de 16 °C, logramos obtener emisión laser con doble longitud de onda, esto se generó al conseguir igualar las pérdidas en las dos cavidades con el SFL, tal como se muestra en la Figura 2.

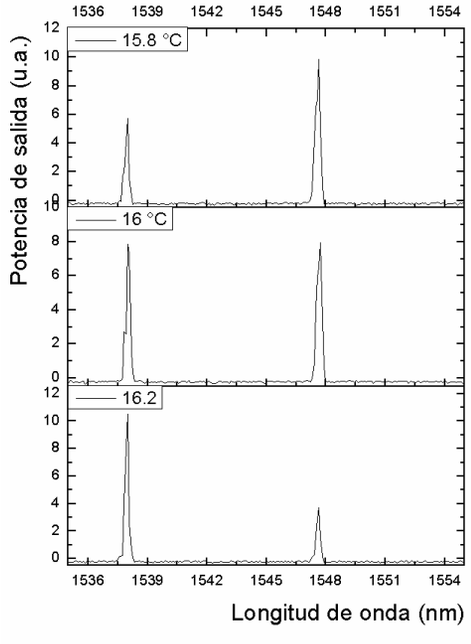

Fig.2 Laser con doble longitud de onda

De acuerdo con la figura 2, cuando la temperatura se cambia a 16.2 °C, se genera una longitud de onda de emisión laser a 1539 nm y este efecto en la cavidad 2 se ve disminuido debido a que las pérdidas en la cavidad son mayores. El efecto contrario ocurre cuando se cambia la temperatura a 15.8 °C, ahora la longitud de onda de emisión laser es a 1547.7 nm y consecuentemente la cavidad 1 se bloquea. Es importante notar que tanto para las temperaturas de 16.2 °C y 15.8 °C, solo se observa una línea de emisión láser, lo cual significa que se puede considerar como un conmutador.

Cuando se modifica la longitud de onda de FBG1 por alguna variable física existe la posibilidad de obtener nuevamente emisión laser con doble longitud de onda, modificando la temperatura en el SFL. En la Figura 3 se muestra el espectro de emisión laser con doble longitud de onda cuando FBG1 se modificó a 1534.8 nm mediante un ajuste en temperatura en el SFL la cual fue de 16.9 °C.

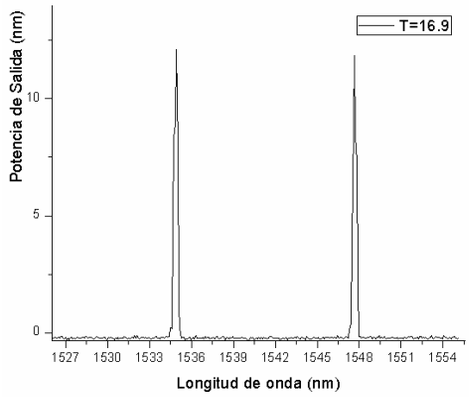

Fig.4 Laser con doble longitud de onda

Los resultados muestran que al modificar la longitud de onda de cualquiera de las dos FBG podemos obtener nuevamente emisión laser con doble longitud de onda mediante el ajuste de la temperatura y esta diferencia puede estimar el valor de la variable física aplicada.

Este trabajo es soportado por Proyecto Conacyt 151434

Referencias

[1] W. W. Morey, et. al. “SPIE Fiber Optic and Laser Sensor VII”, Vol. 1169, 1989.
[2] A. D. Kersey, et. al, “Lightwave. Technol.” Vol. 15, pp. 1442-1463, 1997.
[3] A. D. Kersey et. al., “Electron, Lett.”, Vol. 29, pp. 112-114, 1993.
[4] Duan Liu, et. al., “PTL”, Vol. 19, pp. 1148-1150, August. 2007
[5] R. I. Alvarez Tamayo, et. al., Laser Physics, Vol. 21, pp. 1932-1935, 2011.
[6] M. Duran Sánchez, et. al., Laser Physics, Vol. 20, pp. 1270-1273, January 2011.
[7] R. I. Alvarez Tamayo, et. al., Applied Optics, Vol. 50, pp. 253-260, January 2011.
[8] M. Duran Sánchez, et. al., “Revista Mexicana de Física”, Vol. 55, pp. 73-76, Febrero, 2009.

Limite de Sensibilidad en la Detección Entre un Interferómetro de Michelson y un Dispositivo Basado en la Reflexión del Haz Óptico

G. E. Sandoval-Romero*
E. González-Espinosa
E. F. Pinzón-Escobar
Centro de Ciencias Aplicadas y Desarrollo Tecnológico
Universidad Nacional Autónoma de México
A.P. 70-186, México D. F., 04510, México.
*e-mail: eduardo.sandoval@ccadet.unam.mx

Abstract

In this paper, we do a comparison of the maximum sensitivity between a Michelson interferometer and a device that uses reflection optical beam, registering the lowest displacement. The devices are compared by means of the minimum shift register that performs a piezoelectric device under effect of the electric field is made to circulate, this piezoelectric has a mirror which serves to reflect a light signal incident, on the other hand, this light signal is directed to a photo-detector, where its intensity is measured implemented in two configurations: one is the Michelson interferometer and the other optical beam reflection.

Resumen

En este trabajo se realiza una comparación de la sensibilidad máxima, entre un interferómetro de Michelson y un dispositivo que utiliza la reflexión del haz óptico, registrando mínimos desplazamientos. Los dispositivos son comparados por medio del registro del desplazamiento mínimo que realiza un dispositivo piezoeléctrico bajo el efecto del campo eléctrico que se le hace circular; este piezoeléctrico tiene un espejo el cual sirve para reflejar una señal luminosa que incide en él, por otro lado, esta señal luminosa es dirigida hacia un fotodetector, en donde su intensidad es medida en dos configuraciones implementadas; una es el interferómetro de Michelson y la otra de reflexión del haz óptico.

Keywords: Sensitivity, interferometer, Michelsonm piezoelectric, reflexion

Introducción

En el área de la instrumentación científica y tecnológica, existe la necesidad de medir desplazamientos muy pequeños producidos, a veces por la presencia de algún fenómeno externo que se convierte en una magnitud física que es necesaria cuantificar. Para realizar esta medición, es necesario tener los dispositivos adecuados, que permitan realizar una cuantificación verás de la magnitud física que indirectamente está presente, cuando el registro correcto de esos diminutos desplazamientos.

En este trabajo se proponen dos dispositivos implementados en el laboratorio, que nos permitan realizar esas mediciones con una gran exactitud, los cuales entre ellos difieren, básicamente en la complejidad de su construcción; el primero dispositivo implementado es un interferómetro de Michelson en óptica de volumen [1] y el segundo es un dispositivo que utiliza la técnica de la reflexión del haz láser [2].

Por otro lado, se utiliza como actuador a un piezoeléctrico el cual reacciona con el estimulo de una corriente eléctrica que se propaga en este dispositivo, su forma de manifestarse externamente, es notoria ya que emite una vibración regular y constante que depende de la frecuencia y voltaje de alimentación [3].

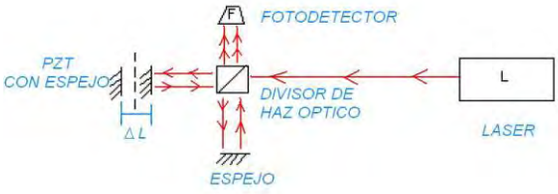

Figura 1. Implementación del interferómetro de Michelson utilizada.

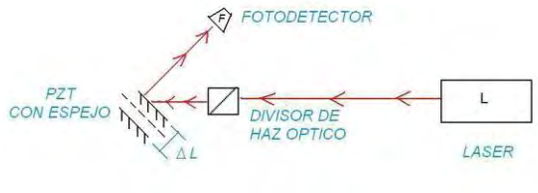

Figura 2. Implementación del dispositivo de reflexión del haz láser.

El objetivo principal de este trabajo, radica en la comparación de los resultados de medición entre los dos dispositivos implementados (interferómetro de Michelson y el que utiliza la reflexión del haz óptico), medir el desplazamiento provocado en un piezoeléctrico, cuando en la superficie de este existe un cambio en la posición provocada por el cambio del voltaje y de la frecuencia, según el experimento lo requiera. Comparar la máxima sensibilidad que se puede alcanzar en las mediciones realizadas; en este caso la sensibilidad está relacionada con el mínimo desplazamiento que puede realizar el piezoeléctrico cuando, la frecuencia y el voltaje con el que se excita son mínimos; a partir de como se muestran en las respectivas configuraciones, Figura 1) implementación del interferómetro de Michelson, Figura 2) implementación del dispositivo de reflexión del haz láser [4, 5].

Formato de Trabajo

El trabajo esta dividido en dos partes experimentales, las cuales se desarrollan de la siguiente forma; utilizando la implementación del interferómetro de Michelson, en la Figura 1; este arreglo nos permite sensar desplazamientos muy pequeños, que son imposible de percibir a simple vista; estos desplazamientos son producidos en un dispositivo piezoeléctrico, implementado de tal forma que el movimiento (vibración) que este dispositivo experimenta al hacerle pasar a través de él una corriente eléctrica, bajo dos condiciones que se mantienen a lo largo del desarrollo del experimento, con un voltaje de pico a pico constante cambiando la frecuencia de alimentación de esta corriente y con una frecuencia constante haciendo variable el voltaje pico a pico de esta alimentación.

En la Figura 2, se presenta una imagen del arreglo del dispositivo que utiliza la reflexión del haz láser, este arreglo nos sirve para detectar los movimientos que se presenten en el piezoeléctrico y son registrados por el fotodetector que a su vez lo envía al osciloscopio.

Estos dos arreglos implementados nos permiten identificar los desplazamientos que realiza el piezoeléctrico, definiendo dos diferentes condiciones de trabajo, idénticos para ambos arreglos; el primer caso se tiene cuando, el voltaje pico a pico es constante y se varía la frecuencia de este voltaje aplicado, la señal es registrada en el fotodetector y mostrada en el osciloscopio; el segundo caso se tiene cuando, la frecuencia se mantienen constante y el voltaje pico es variable. En las Figuras 3 y 4, contienen mediciones de laboratorio con resultados experimentales, que se realizaron bajo las condiciones anteriormente descritas, en donde podemos ver las diferencias de sensado que existen en los arreglos.

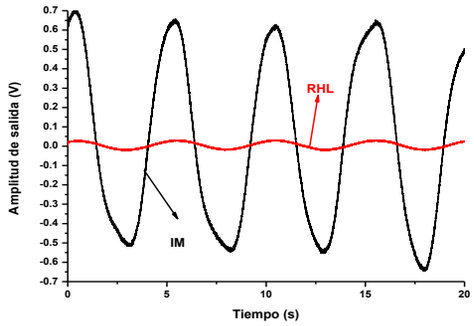

Figura 3. Comportamiento de los arreglos IM y HRL cuando se tiene un voltaje pico constante de 0.5 [V] y 0.2 [Hz] en la frecuencia.

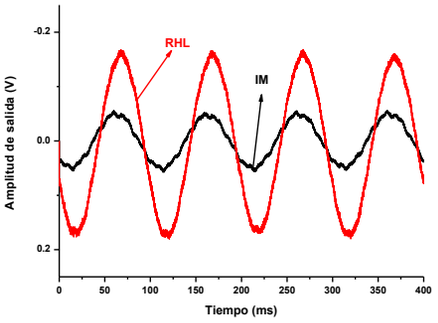

Figura 4. Comportamiento de los arreglos IM y HRL cuando se tiene una frecuencia constante de 10 [Hz] y el voltaje pico a pico de 1 [V].

Agradecimientos

Trabajo apoyado por DGAPA-UNAM, en el proyecto IT101712.

Referencias

[1] Eugene Hecht, Alfred Zajac. Optics. Massachusetts: Addison-Wesley Publishing Co. 1974.

[2] Constant A. J. Putman, Bart G. De Grooth, Niek F. Van Hulst, and Jan Greve. A detailed analysis of the optical beam deflection technique for use in atomic force microscopy. J. Appl. Phys. 72, 6 (1992).

[3] Raoul Enning, Dominik Ziegler, Adrian Nievergelt, Ralph Friedlos, Krithika Venkataramani et al. A high frequency sensor for optical beam deflection atomic force microscopy. Rev. Sci. Instrum. 82, 043705 (2011).

[4] A. García-Valenzuela, R. Díaz-uribe, “Approach to improve the angle sensitivity and resolution of the optical beam deflection method using a passive interferometer and Ronchi grating”. Optical Engineering, 36, 1770-1778 (1997).

[5] A. García-Valenzuela, “Limits of different detection schemes use in the optical beam deflection method”, J. Appl. Phys. 82 (3), 985-988, (1997).

Use of a Laser Fiber Source Implemented With a Resonator Sagnac, for Fiber Optic Sensors

G. E. Sandoval-Romero*
E. F. Pinzón-Escobar
Centro de Ciencias Aplicadas y Desarrollo Tecnológico
Universidad Nacional Autónoma de México
A.P.70-186, México D. F., 04510, México
*E-mail: eduardo.sandoval@ccadet.unam.mx

Abstract

In this work the authors present a simple laser source is implemented using erbium-doped fiber [1, 2] and a Sagnac fiber resonator [3,4] to generate emission in the wavelength at 1550 nm. The pumping source this carried out with a erbium-doped fiber that serves from feeding to the Sagnac fiber resonator-a simple fiber ring resonator, this it generates a quite stable sign, but a problem exists in the output, who has an polarization in the resonator.

Keywords: Doped fiber optic, erbium, Sagnac Interferometer, fiber optic.

Introduction

The work that here we present is a work with preliminary results where we develop a laser source using Sagnac's resonator and polarizer plates. Here the active element is an optical doped fiber with erbium.

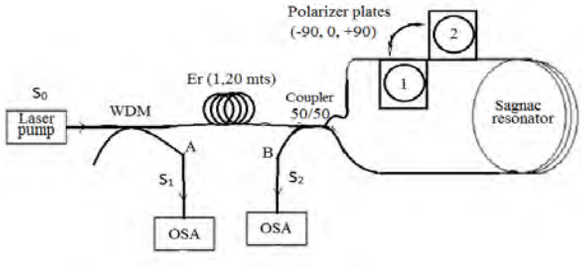

Figure 1. General schema of the proposed fiber laser source.

In this set up, we used a laser diode in wavelength 980 [nm] like pump, 1,20 meters of fiber doped with erbium like a active element, the Sagnac resonator we do with 65 meters of standard single mode fiber; and the polarizer plates.

In the development of this work, we want to determine the dependence of the output signal of the position of the polarizing plates. For this, we choose the output signal measured when the polarizer is positioned at 90 degrees to between the plates.

First Case

In the first case Fig. 2, measurements are made after the wavelength-division-multiplexing (WDM); in this case there are seven different combinations between the positions of the polarizer plates, in this paper we show peculiar cases where the positions of the polarizer plates are at 0, 90 and 180 degrees between them, as show in the figures 3, 4 and 5.

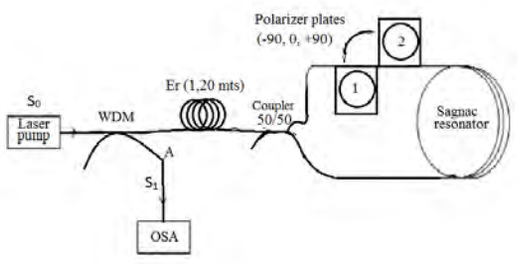

Figure 2. First case.

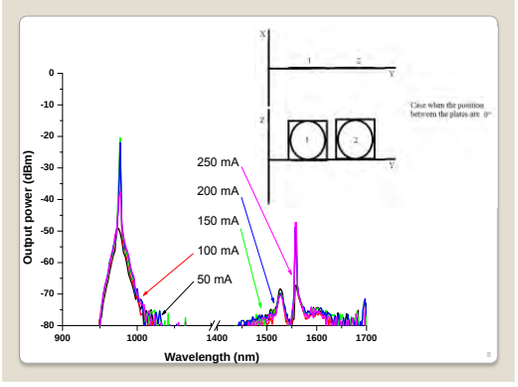

Figure 3. The position between the plates are 0°.

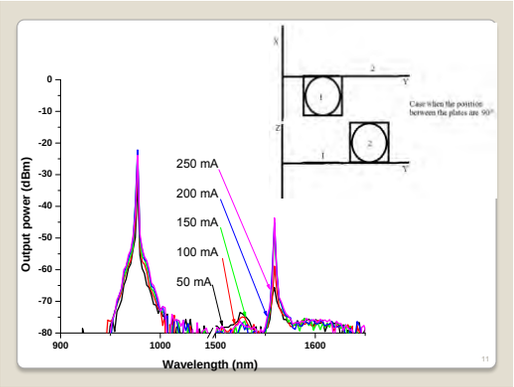

Figure 4. The position between the plates are 90°.

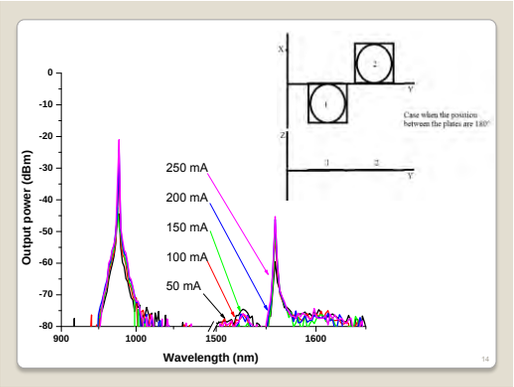

Figure 5. The position between the plates are 180°.

Second case

In the second case figure 6, measurements were carried out at the output coupler 50/50, when the output signal is generated by the Sagnac resonator.

Also as in the previous case, measurements are more representative when the position between the polarizer´s plates are at 0, 90 and 180 degrees between them, as show in the figures 7, 8 and 9.

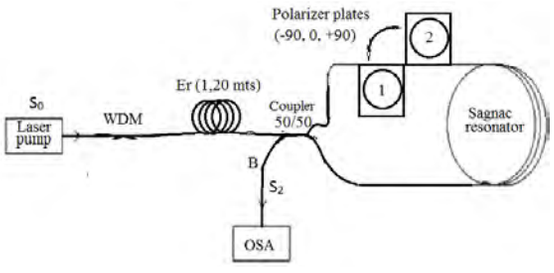

Figure 6. Second case.

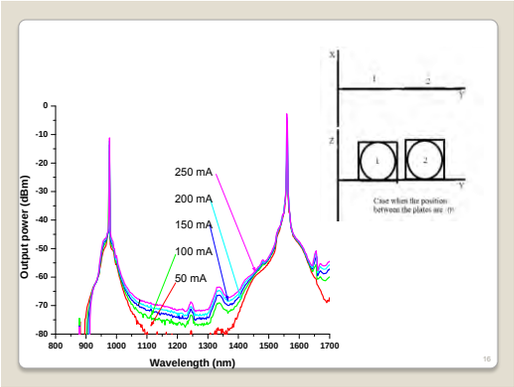

Figure 7. The position between the plates are 0°.

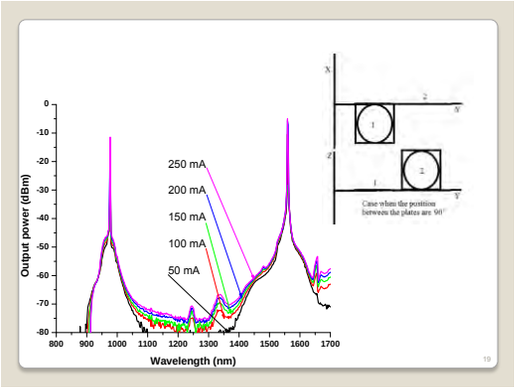

Figure 8. The position between the plates are 90°.

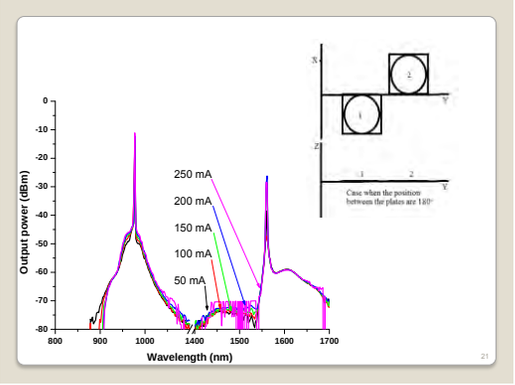

Figure 9. The position between the plates are 180°.

Conclusions

From the previous analysis, it can be deduced that there is a mixed source, wherein simultaneously the obtained output signals, are in the regimen of laser and superluminescent.

Acknowledgments

The authors acknowledge support from the UNAM-PAPIIT (IT101712).

References

[1] G. E. Sandoval-Romero, *J. Opt. Technol.* 74(8), (2007) 573.
[2] X. Fang, L.O. Claus, *Opt. Lett*. 20 (1995) 2146.
[3] C. S. Kim, J. U. Kang, *Appl. Opt.* 43 (2004) 3151.
[4] K. Hotate, T. Ito, *Electron. Lett.* 32 (1996) 923.

Comparative Broadband Fiber Amplifier

E. F. Pinzón-Escobar*
G. E. Sandoval-Romero
Centro de Ciencias Aplicadas y Desarrollo Tecnológico
Universidad Nacional Autónoma de México
A. P. 70-186, México D. F., 04510, México
E-mail: enrique.pinzon@ccadet.unam.mx

Abstract

We present an experimental work of a broadband amplifier centered at 1550 nm using erbium doped fiber and ytterbium doped fiber pumped at 976.8 nm. The experimental results show that the gain is practically independent of the state of polarization of the pump and the signal. We propose that the Ytterbium doped fiber could be used as an option to filter the pump power. These amplifiers are based on the telecommunications amplifiers and could have direct application in wavelength multiplexed arrangements of fiber sensors, fiber gyroscopes or in general, in any sensors in which a broad wavelength and stable light source is required.

Keywords: fiber amplifier, doped fiber optic, erbium, ytterbium, sensors of physical magnitudes, fiber optic.

Introduction

The invention of the erbium-doped fiber attracted many interest especially like communication amplifier systems and superfluorescent fiber sources for several industries mainly for fiber optic gyroscope (FOG). The typical gain bandwidth of Erbium doped fiber amplifier (EDFA) is from 1520 nm to 1570 nm, and the typically values of gain for small signal are 30-40 dB [1], on the other hand Erbium-doped fiber has weak absorption at 980 nm for this reason is co-doped with Ytterbium to increases the absorption and transfers the absorbed energy to Er3+. However this work focuses to report the spectral characteristics when use Ytterbium-doped fiber at the output of an EDFA.

Experimental Setup

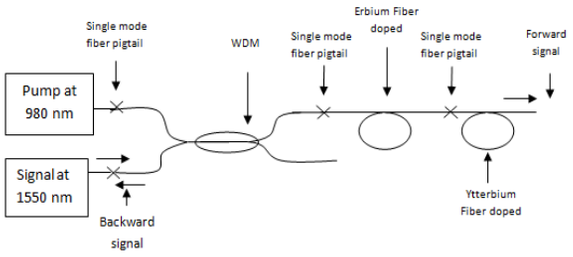

Figure1. Experimental setup.

The experiment was developed in two parts, the first part consisted in the measurement of a common EDFA amplifier for a laser signal and for a superluminiscent signal and in the second part was included the ytterbium-doped fiber for the same signals. In the experimental setup we used a laser diode pump at 980 nm, a WDM 980/1550 nm, 3 m of erbium-doped fiber, 24 cm of ytterbium doped fiber. It tested with two different signals at 1550 nm, one a laser diode and the other a superluminescent diode. In this experiment the EDFA works in small signal regime.

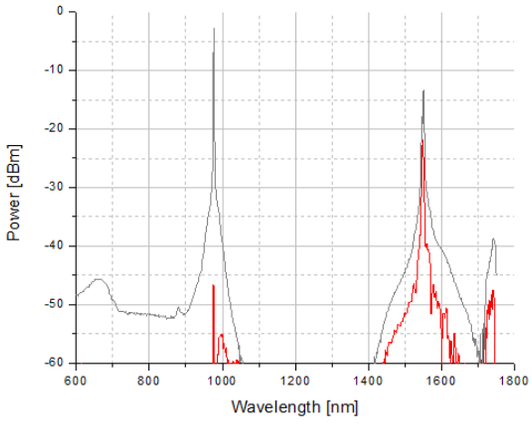

Figure 2. Spectra of EDFA amplifying the laser signal.

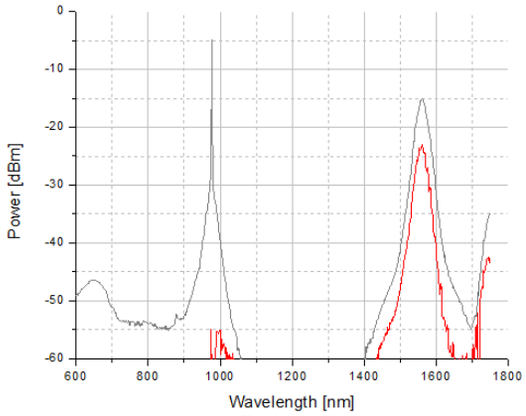

Figure 3. Spectra of EDFA amplifying the superluminiscent signal.

In the Figure 2 and figure 3 the gray spectra are the behavior of the EDFA amplifying the laser signal and the superluminiscent signal respectively, and the red spectra are the output of the ytterbium doped fiber connected at the end of the EDFA. For both cases we can see the same behavior, when is used the ytterbium-doped fiber the pump signal (signal at 980nm) is strongly absorbed, for some sensors this characteristic is useful to filtering the pump signal and avoid damages in the detectors, on the other hand, the amplified signal is also attenuated. For the amplified signals the use of the ytterbium doped fiber reduce the spectral width, particularly for the laser case this is an advantage because the ytterbium fiber helps to remove the ASE signal.

Acknowledgments

The authors acknowledge support from the UNAM-PAPIIT (IT101712)

References

[1] Marcello Potenza, “Optical Fiber Amplifiers for Telecommunication Systems”, IEEE Communications Magazine, pp. 96-102, August 1996.

[2] Paschotta, J. Nilsson, A. C. Tropper, and D. C. Hanna, "Ytterbium-doped fiber amplifiers", IEEE J. Quantum Electron., v. 33, pp. 1049-1056, 1997.

[3] M.J. Digonet, “Rare-Earth-Doped Fiber Laser and Amplifiers”, Marcel Dekker Inc. Second Edition. U.S.A. 2001.

Chapter 4: Materials, Fabrication, and Packaging Techniques for Sensors

Optoelectronic logic architecture based on SiC multilayer structures

M. Vieira[1,2], M. A. Vieira[1,3], P. Louro[1,2], V. Silva[1,2], M. Barata[1,2]

[1]Electronics Telecommunication and Computer Dept. ISEL, Lisboa, Portugal, mv@isel.ipl.pt.
[2] CTS-UNINOVA, Quinta da Torre, Monte da Caparica, 2829-516, Caparica, Portugal.
[3] DEE-FCT-UNL, Quinta da Torre, Monte da Caparica, 2829-516, Caparica, Portugal.

Abstract

Tunable WDM converters based on amorphous SiC multilayer photonic active filters are analyzed. The manipulation of the magnitude is achieved through appropriated front and back backgrounds. Transfer function characteristics are studied. Results show that the light-activated device combines the demultiplexing operation with the simultaneous photodetection and self amplification of an optical signal. A combinational logic function is mapped onto an active two stage optoelectronic logic circuit.. An optoelectronic model supports the optoelectronic logic architecture.

Keywords: Optical filters, logic architecture, MUX/DEMUX,

Introduction

Data transmission can be improved using the wavelength division multiplexing-demultiplexing technique, WDM. In digital hardware, it corresponds to a building block named multiplexer (MUX). Logic theory shows that all digital operations may be reduced to elementary logic functions. A digital system can be seen as a collection of AND, OR, and NOT circuits.

Deposition characterization and operation

The active device consists of a p-i'(a-SiC:H)-n/p-i(a-Si:H)-n heterostructure with low conductivity doped layers (Fig.1).

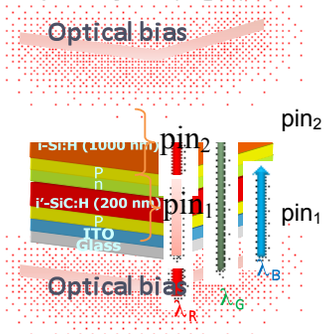

Fig. 1 *Device configuration and operation.*

In Fig.2, the spectral photocurrent, normalized to its value without background is displayed, under front (a) and back (b) violet irradiations and different intensities. A peak fit adjustment to the data was performed (lines) with peaks centered around 630 nm (solid), 520 nm (dash) and 430 nm (dot).

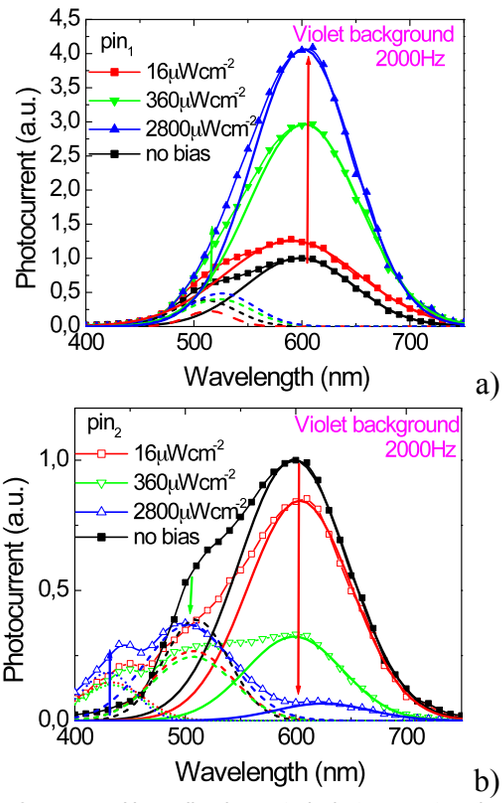

Fig.2 *Normalized spectral photocurrent under front (a) and back (b) violet irradiations with different intensities.*

Results show that under violet irradiation, as the background intensity increases, the peak centered at 630 nm (red range) strongly increases while under back light an opposite

behavior is observed and the red peak is strongly reduced (see arrows). Under front and back side irradiation, the peak at 520 nm (green range) increases slightly with the intensity. Under back irradiation, a new peak centered at 430 nm appears and increases with the background intensity. So, under front illumination the reddish part of the spectrum is strongly enhanced with the intensity while under back illumination the main enhancement occurs at the blue region.

Opto-Electronic Conversion

Fig.3 displays the normalized MUX signals, under front Fig. 4 under back violet irradiations. On the top the signals used to drive the input channels are displayed showing the presence of all the possible 2^3 *on/off* states. The truth tables of both encoders, that perform 8-to-1 MUX function, are also shown. The MUX device selects, through the violet background, one of the eight input logic signals and sends it to the output ($y=x_S$). The output is a three-bit [$S_2S_1S_0$] binary RGB number that may identify one of eight possible inputs. Those OR gates are expressed, respectively, as: $S_2=x_7+x_6+x_5+x_4$ and $S_2=x_7+x_3+x_5+x_1$.

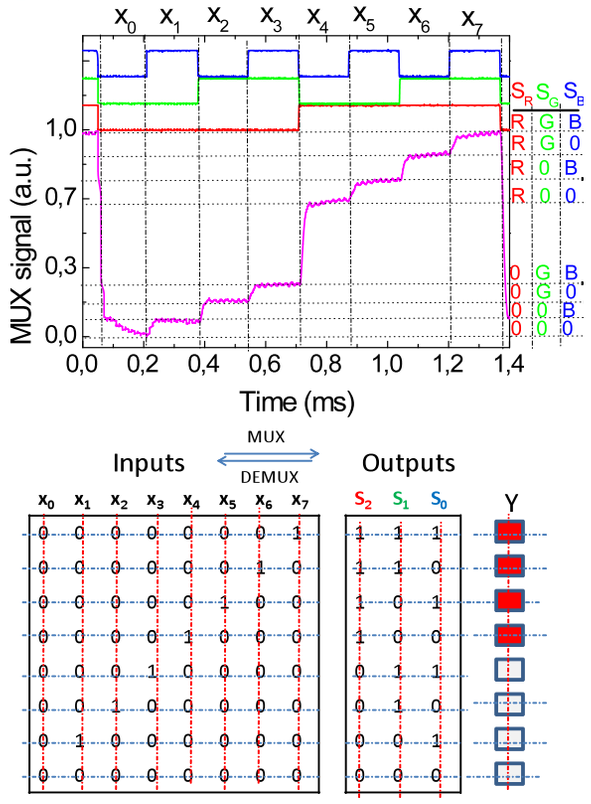

Fig. 3 *MUX signal outputs and truth tables of the encoders that perform 8-to-1 multiplexer (MUX) function, under front violet irradiations (x means " not significant").*

Violet irradiation is applied from the front (pin_1; $\alpha^V_{Rpin1}>>1$, $\alpha^V_{Gpin1}>1$ and $\alpha^V_{Bpin}\sim1$) and back (pin_2; $\alpha^V_{Rpin2}<<1$, $\alpha^V_{Gpin2}<1$ and $\alpha^V_{Bpin2}>1$) sides. Under front irradiation (Fig. 3) the 2^3 levels can be grouped into two main classes due to the high amplification of the red channel. The upper four levels are ascribed to the presence of the red channel ON, and the lower four to its absence, allowing the red channel decoder (4-to-1 multiplexer; long-pass filter function). Since under front irradiation the green channel is amplified the two highest levels, in both classes, are ascribed to the presence of the green channel and the two lower ones to its lack. So, the correspondence between the outputs S_2, S_1, S_0, and the on/off state of the input channels, S_R, S_G, S_B, is obvious.

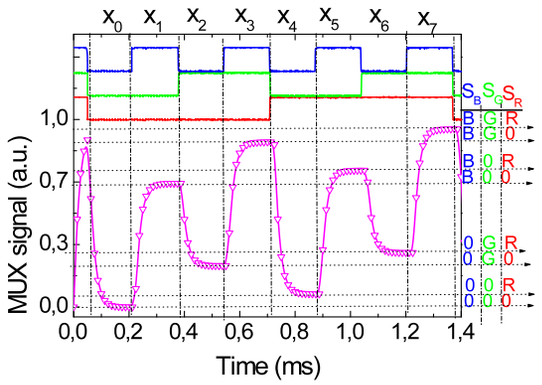

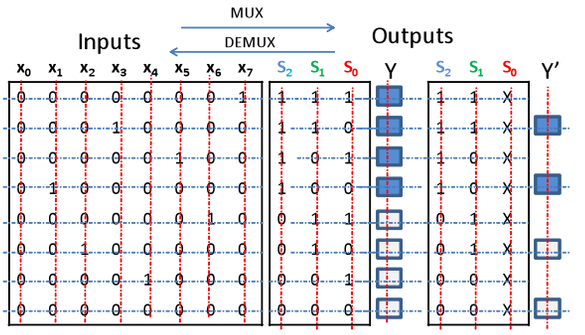

Fig. 4 *MUX signal outputs and truth tables of the encoders that perform 8-to-1 multiplexer (MUX) function, under front violet irradiations (x means " not significant").*

Under back irradiation the encoded multiplexed signal is grouped in two main classes, the uppers four where the blue channel is ON and the others where it is OFF (S_B) (4-to-1 multiplexer; short-pass filter function. If we consider the red output bit “not significant” only four separate levels (2^2) are considered and the logic MUX function is converted into a logic filter function. The blue channel is then decoded.

Conclusions

WDM converters were analyzed. Results show that depending on the wavelength of the external background and irradiation side, it acts either as a short- or a long- pass band filter or as a band-stop filter. MUX signals that perform 8-to-1 MUX function and truth tables lookup are compared.

Adsorbent Composites Used on Mixing in Miniaturized Structures

Leonardo F. Hernandez[1], Alisson R. Leite[2], Roberto R. Lima[1*], Maria Lúcia P. Silva[1,4], Estevão R. Fachini[3]
[1] Polytechnic School, University of São Paulo, Av. Luciano Gualberto, 158, SP, 05508010, Brazil
[2] Institute of Physics, University of São Paulo, Brazil
[3] College of General Studies, University of Puerto Rico at Río Piedras, Puerto Rico
[4] Faculty of Technology of São Paulo, CEETEPS, Brazil
malu@lsi.usp.br , rrlima@if.usp.br

Abstract

Adsorbent plasma thin films were designed to perform as passive mixers or adsorptive layers in sensors. Clustered films from tetraethoxysilane (TEOS) and nonafluoro(iso)butyl ether (HFE®) precursors were prepared in an in-built plasma reactor. Chemical characterization points out a silicone like structure, sensible to the presence of humidity, and a fluorinated surface that protects against ultraviolet radiation (UVC). The optimized structures were built and tested. The results point out the utility of these films in humidity sensors or as passive layers for mixing.

Keywords: adsorbent films, plasma thin films, passive mixers, humidity presence, TEOS.

Introduction

TEOS (tetraethoxysilane) derivative plasma films present a hydrophobic silicone-like structure that can be changed by ultraviolet radiation. These films are also sensitive to water presence. Both film properties suggest the use of TEOS films in sensor development [1].

HFE® (nonafluoro(iso)butyl ether) derivative plasma films are permeable for organic compounds and they resist harsh environments [2].

Three-dimensional micro-channels are useful as pre-columns in chromatographic micro-systems. The channel surface can be modified to accomplish several functions, useful in spray or micro-reactor systems [3]. Micro-channels with alternated hydrophobic/ hydrophilic regions promotes of the formation of a drop with two immiscible phases [4].

This work directs the production and characterization of composites films from TEOS and HFE precursors. These composites were used: 1) in miniaturized structures (3D-microchannels) for gas mixing or heterogeneous drop formation; 2) for humidity detection or 3) as passive layers on sensors.

Experimental

The adsorbent thin films from HFE and TEOS precursors were deposited on silicon, acrylic and glass substrates [2]. The thickness and refractive indexes of the films were determined by profilometry and ellipsometry measurements, respectively. The chemical properties of the films were inferred from infrared (FTIR) and x-ray photoelectron (XPS) spectra. The resistance toward base/acid aqueous solutions was evaluated by optical microscopy. The cluster formation was followed by scanning electron microscopy (SEM). The hydrophobic/hydrophilic character and the adsorption of volatile organic compounds (VOCs) in the films were evaluated using contact angle measurements.

Figure 1A presents the 3D-microchannels machined on acrylic which surface was modified by a plasma film; a mask (Fig. 1B) was used to expose the surface to UVC. This structure was used for mixing or spray formation purposes. The fluid behavior in such a structure was simulated using FEMLAB® 3.2 software. Capacitance-Voltage (CV) analysis determined the electric behavior in the presence of water.

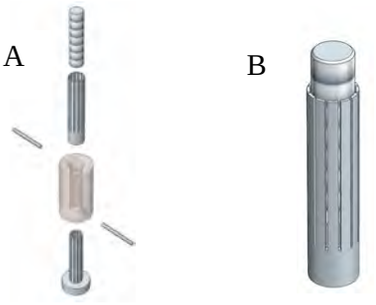

Fig. 1: Schematics of (A) 3-D-micro-channels and (B) mask for UVC exposure.

Results and Discussion

The home-made plasma instrument allows the use of incompatible monomers in plasma, i.e., monomers that do not polymerize simultaneously. Because of that, the equipment favors the formation of composites [2]. It was observed the following tendencies: a) auxiliary electrode grounded: homogeneous TEOS/HFE film; b) lowering the pressure in chamber: carbon and silicone clusters formed; c) lowering HFE flux near the surface: carbon clusters is favored; d) electrode near the sample is grounded: silicone clusters deposited. Deposition rates of 20 nm/min can be achieved in the system. The refractive index of films will not change markedly. Representative numbers for the cluster size and density are 0.6 μm and 40,000 cluster/mm^2, respectively.

FTIR and XPS analysis revealed that species from TEOS and HFE are incorporated in the films [1,2]: the composite showed a silicone-like structure with fluorine and carboxyl groups. XPS analysis suggested the presence of graphite, C-Si and C-OH species. If TEOS and HFE act as film precursors, CF species in FTIR spectra are detected. XPS data indicated low amount of fluorine. Raman microscopy revealed that the clusters are amorphous carbon. All films had a water contact angle close to 90º but they were organophilic, being wetted by n-hexane and 2-propanol. Six hr of UVC exposure increased the amount of oxygen in TEOS films by 7% (XPS data) and the water contact angle decreased to 80º. The exposed area had a different color compared to a pristine surface. Possibly the UVC exposure favors crosslink and/or oxidation of organic radicals in the TEOS/HFE composite, which agrees with data for pure TEOS films [1]. Films made just from HFE did not degrade after a 24 hr UVC treatment.

TEOS films are sensitive to acid/base solutions. The color and thickness of the films changed due to chemical attack, as revealed by profilometer measurements. The composite film was not damaged by those solutions after several minutes.

The 3D-microchannel surface covered or not with the composite film was exposed to UVC, some areas being protected by a mask. If a liquid sample is introduced in the channel, its dispersion can be followed by optical microscopy; asymmetric drops were formed due to differences on surface hydrophobicity. Such differences favor sudden variation in velocity profile and vorticity as inferred from simulation [5]. Because of that, the dispositive can be used for removal of water drops and/or mixing.

Although composite materials resist corrosive aqueous solutions, the thin film is still sensitive to water and polar organic compounds (VOC's). Thus, organic compounds and water can change CV curve profiles. These curves were obtained using a setup described elsewhere [6] and show a good saturation response to 2-propanol vapors (Fig. 2B), without expressive difference if the non-polar n-hexane is admitted (Fig. 2A).

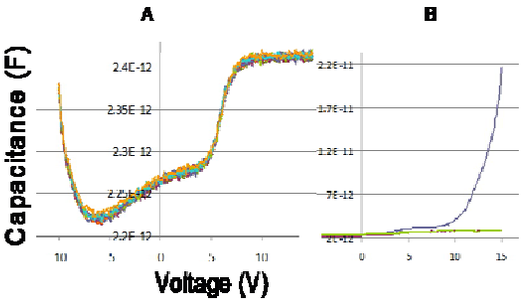

Fig. 2 - CV measurement for TEOS/HFE composites films exposed to 5 μL saturated vapor injections of (A) n-hexane or (B) 2-propanol.

Conclusions

This work proposes the use of a new TEOS/HFE derivative composite in micro-devices. These composite thin films are environment-friendly and can be used as UV protective layers, as adsorptive layers in a humidity sensor or as a mixer in technological applications.

Acknowledgments

Work supported by FAPESP and CNPq. We thankfully appreciate the generosity of Dr. Carlos R. Cabrera (UPRRP) to permit us using the XPS instrument.

References

[1] R. A. M. Carvalho, R. R. Lima, A. P. Nascimento Filho, M. L. P. Silva, N. R. Demarquette, Sensors and Actuators B: Chemical, Vol. 108, No. 1-2 Spec. Issue, pp. 955-963, 2005.
[2] R. R. Lima, L. F. Hernandez, A. T. Carvalho, R. A. M. Carvalho, M. L. P. da Silva, Sensors and Actuators B: Chemical, Vol. 141, pp.349-360, 2009.
[3] L. M. Silva, R. R. Lima, E. W. Simões, M. L. P. da Silva, Int. Review of Chemical Eng., Vol. 2, pp.134-141, 2010.
[4] Y. Yamasaki, A. Kariyazaki, S. Morooka, Int. Journal of Chemical Reactor Eng., Vol. 8, article A 140, 2010.
[5] L. C. Santos, F. P. Beraldo, E. W. Simões, A. T. Carvalho, M. L. P. da Silva, Sensors and Actuators B: Chemical Vol. 130, pp. 310–319, 2008.
[6] R. R. Lima, M. Y. Ieiri, E. Y. Matsuy, E. S. Ferreira, L. M. Silva, M. L. P. da Silva, Revista Brasileira de Aplicações de Vácuo, Vol. 28, No. 1-2, pp. 7-13, 2009.

Small and Simple Devices to Increase Mixing on Detector Surfaces

Leonardo F. Hernandez[1], Alexandre A. Jesus[1], Roberto R. Lima[1,2], Estevão R. Fachini[3], Maria Lúcia P. Silva[1*,2]
[1] Polytechnic School, University of São Paulo, Av. Luciano Gualberto, 158, SP, 05508010, Brazil
[2] Institute of Physics, University of São Paulo, Brazil
[3] College of General Studies, University of Puerto Rico at Río Piedras, Puerto Rico
[4] Faculty of Technology of São Paulo, CEETEPS, Brazil
malu@lsi.usp.br , rrlima@if.usp.br

Abstract

Analyte adsorption on the detector surface can be hindered by transport phenomena, increasing the detection limit. The proposed device has a tailored surface which improves its performance as a passive mixer. The film on the device surface was a hexamethyldisilazane (HMDS), nonafluoro(iso)butyl ether (HFE) and co-deposited HMDS/HFE plasma film modified by ultraviolet (UVC) or beta radiation exposure. All films were hydrophobic and adsorbent. HMDS films exposed to ultraviolet form a silicone-like structure whereas beta radiation exposure leads to carbon nodules formation. HFE films act as passive layer, even for beta radiation. Best design to surface modification has approximately a sinoidal shape.

Keywords: HMDS, HFE, miniaturized structure, mixing, plasma films.

Introduction

Plasma thin films are quite useful for sensor development; they can be used as a protective or a sensitive layer. The application of two or more consecutive layers of these films changes dramatically the surface properties and allows the production of different devices, such as preconcentrators, detectors, etc [1,2]. Using an inert layer is desirable in harsh environments, but decreases the diffusion rate of analytes to the inner volume. Consequently, the response of the device will broad and the detection limit will increase.

A compromise solution can be achieved using composite materials, i.e., a material that is not so resistant to the environment but more sensitive to the analyte [3]. Nonetheless, this composite material also presents some limitations because, due to limiting layer effect, some areas of the detector surface might be permanently covered by the sample. Consequently, a strategy is to modify the surface properties in order to promote variations of fluid velocity or vorticity, which can diminish the limiting layer and/or increase the transfer of material between the fluid streams. This strategy, as far as we know, it was not tested yet. This conception is somewhat similar to the passive mixer devices development [4].

Adsorbent thin films can be produced by plasma polymerization of silicon organic compounds, specifically hexamethyldisilazane – HMDS, or eventually fluorinated films, such as methyl nonafluoro(iso)butyl ether – HFE®. Both films are hydrophobic and sensible for volatile organic compounds (VOCs), which make them appropriate to be used with aqueous samples; nonetheless, HMDS films are not resistant to basic solution whereas HFE films are.

Therefore, this work aims the simulation, production and tests of a simple miniaturized structure that favors fluid mixing on detector surfaces.

Experimental

Plasma polymerization of HMDS, HFE and co-deposited HMDS/HFE were obtained on silicon, acrylics and piezoelectric quartz crystal (PQC) substrates. Polymerization occurs in DC-plasma equipment optimized for composite material formation [1,2]. The produced thin films were characterized by profilometry and ellipsometry. Raman, infrared (FTIR) and x-ray photoelectron (XPS) spectroscopy provided film chemical information. Optical, scanning electron (SEM) and atomic force (AFM) microscopies evaluated the film resistance toward ultraviolet light (UVC; 1.8 W/m^2, 10 cm apart) or beta radiation (electron beam, 2 MeV, from 10 nA to 100 nA). Cluster sizes were evaluated using ImageJ software. Hydrophobicity and the adsorption of volatile organic compounds (VOCs) were tested by contact angle measurements. Simulations of surface behavior were done using the FEMLAB

3.2 software. The flow of water was filmed to get insights of fluid mechanisms and/or dispersion phenomena on the surface. Methylene blue and Sudan black B dyes (1% w/w) were used as tracer in water or glycerin/mineral oil (43 cSt), respectively.

Results and Discussion

After 6 hours exposure to UVC light, FTIR spectra change in the 1500-1000 cm^{-1} region. Figure 1A shows typical data for HMDS films before and after this exposition. It suggests that UVC exposure leads to silicone-like structure formation, probably due to cross-linking. Optical microscopy shows a remarkable difference on exposed/non-exposed areas (Fig. 1A). The exposed film remains hydrophobic, the water contact angles decreasing from 90º to 80º. This does not occur on expenses of adsorption: UVC treated film is still wetted by polar and non-polar organic compounds.

Treatment of the HFE derivative films did not change severely their properties; FTIR spectra being similar after 24 hours of UVC exposure. Optical microscopy does not reveal any surface change and water contact angle values remains approximately 90º, being the adsorption of VOCs the same. Similar results are obtained with beta radiation. From XPS data and the visual unchanged surface of HFE films (Fig. 1B) it is supposed that fluorine is the outmost element on the surface, being responsible for the increase of resistance to UVC exposure. The FTIR spectra showed a significant increment on Si-O band (Fig. 1B) and suggest a strained film due to strong interactions with fluorine species. HMDS films remain adsorbent and hydrophobic. Whereas HMDS generated clustered films, HFE films were smooth. Co-deposited films were smoothed by UVC treatment, probably due to cross-linking formation in the HMDS clusters.

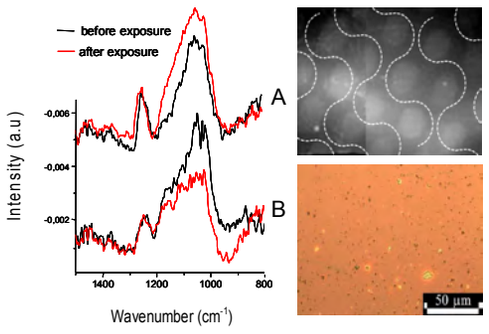

Fig. 1 – FTIR spectra and optical images of (A) HMDS and (B) HMDS/HFE derivative films.

The simulation considered the detector as a thick cavity [2] with hydrophobic/hydrophilic regions. The theoretical model to explain such modifications is described elsewhere [5]. If the sensor surface changes, the water path will be slightly changed whereas vorticity will be quite different and will improve the mass transfer near the sensor surface. The experimental results agreed with the theoretical model.

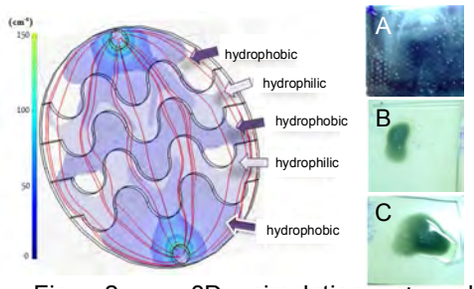

Fig. 2 – 3D simulation of velocity (streamline) and vorticity (color) for a 5 ml/min water flow. Photos of a real system showing hydrophilic areas (white spots) (A), a mixture of mineral oil and water on untreated (B) and treated (C) surfaces.

Mineral oil was easier to be dispersed on a cavity with treated surface than in a non-modified structure. The surface treatment could decrease the limiting layer and favor detection; although a preferential adsorption mechanism occurring on the UVC exposed regions cannot be ruled out. The presence of carbon nodules, noted on surfaces exposure to electron impact, could be used to increase adsorption, helping to decrease the detection limit.

Conclusions

HMDS, HFE and composites films can be used for simultaneously surface protection and analyte adsorption. Detection limit can be improved tailoring the surface properties with proper UVC exposition.

Acknowledgments

Work supported by FAPESP and CNPq. We thank Dr. Carlos R. Cabrera (UPRRP) to permit us using the XPS instrument.

References

[1] R.R. Lima, R.A.M. Carvalho, A.T. Carvalho, E.W. Simões, M.L.P. da Silva, Sensors and Actuators B: Vol. 137, pp. 185-194, 2009.
[2] R. R. Lima, L. F. Hernandez, A. T. Carvalho, R. A. M. Carvalho, M. L. P. da Silva, Sensors and Actuators B: Chemical, Vol. 141, pp. 349-360, 2009.
[3] M.R. Plata, A.M. Contento, A. Ríos, Sensors, Vol. 10, pp. 2511-2576, 2010.
[4] J.J. Chen, C.H. Chen, Modelling and Simulation in Engineering, Vol. 2011, Article ID 259401, 15 pages, 2011.
[5] L. C. Santos, F. P. Beraldo, E, W. Simões, A. T. Carvalho, M. L. P. Silva, Sensors and Actuators. B: Chemical, Vol. 130, pp. 310-319, 2008.

Influencia de la granulometría en la síntesis de cerámicos AZO

Claudia Vera, Silvia Maioco, Natan Rajchenberg y Ricardo Aragón*

Laboratorio de Películas Delgadas. Facultad de Ingeniería. Universidad de Buenos Aires. Paseo Colón 850. (1063) Ciudad Autónoma de Buenos Aires. Argentina y *CINSO-CITEDEF-CONICET. Juan Bautista Lasalle 4397. Villa Martelli. Buenos Aires. Argentina

e-mail: cvera@fi.uba.ar

Abstract

El ZnO dopado con aluminio es un óxido transparente conductor, cuya densidad y movilidad de portadores esta mediada por vacancias de oxígeno. Dada la baja difusividad de oxígeno la influencia de tratamientos térmicos reductores depende fuertemente de la granulometría. Medidas de resistividad y coeficiente Seebeck sugieren que cambios en la movilidad dominan el aumento de la conductividad por templado en atmósferas reductoras.

Keywords: Óxidos conductores transparentes; sensores óptoelectrónicos; AZO, vacancias.

Introducción

Los óxidos conductores transparentes (TCO) son semiconductores (Eg>3 eV) con resistividad del orden de 10^{-3} Ωcm y transmitancias mayores al 80%, en la banda de luz visible. Encuentran aplicación como electrodos en pantallas de cristal líquido (LCD), así como en múltiples dispositivos optoelectrónicos. Está ampliamente difundido el uso de óxidos de indio dopados con zinc (IZO) o estaño (ITO) [1,2], cuyo costo y escasez ha motivado la búsqueda de sucedáneos. Una alternativa que ha sido objeto de creciente atención en los últimos años, por la baja toxicidad de sus componentes, relativa abundancia, que media bajo costo, así como favorables propiedades es el óxido de zinc dopado con aluminio (AZO) [2]. Los dispositivos optoelectrónicos requieren películas delgadas de TCO, usualmente depositadas por "sputtering", ya sea a partir de blancos cerámicos ó metálicos en atmósfera reactiva. La calidad de las películas en cuanto a sus propiedades eléctricas y ópticas depende sustancialmente de la conductividad del cerámico [3] y las condiciones de proceso. En el presente trabajo se estudian comparativamente las propiedades físicas de cerámicos obtenidos por reacción en fase sólida y por coprecipitación química.

Parte Experimental

Se sintetizó AZO por reacción en fase sólida a partir de una mezcla de los óxidos: ZnO y Al_2O_3 (ambos Marca Merck, grado analítico) en proporción estequiométrica, con 3.2 % atómico de Al en Zn. Los óxidos se suspendieron en acetona, se molieron en mortero de ágata y se cernieron en tamiz N° 270 (53 µ) ASTM. El material se compactó en forma de pastillas de 12 mm de diámetro, mediante una prensa hidráulica (P = 98 MPa) y se sinterizó durante 48 h, a 1400 °C.

Para la preparación de la muestra por coprecipitación, se disolvió la aleación comercial (ZAMAC-3) en ácido nítrico (65 % m/m), que fue subsecuentemente tratada con NH_3 (28% m/m), manteniendo el pH entre 6 y 7, consistentemente con condiciones óptimas de solubilidad mínima [4].

Se emplearon tratamientos reductores a 1000°C, controlando la fugacidad de O_2 mediante un buffer reactivo de mezclas CO/CO_2, en un horno de reactor tubular, con provisión para revenido de la muestra en el extremo frío del reactor, en la misma atmósfera del templado. Los rótulos S6-0h, S6-2h, S6-4h identifican muestras representativas, obtenidas por reacción en fase sólida, con tratamiento reductor de distinta duración, mientras que los códigos Z11-0h, Z11-2h y Z11-4h, designan aquellas obtenidas por coprecipitación.

Para las medidas eléctricas, se cortaron prismas de 1.2 x 0.25 x 0.2 cm, en los que se depositaron electrodos de aluminio de 100 nm de espesor, por "sputtering" de magnetrón en corriente continua, sobre los que se conectaron termocuplas de cobre constantan, para medir resistividad eléctrica por el método Kelvin y coeficiente Seebeck, por subtracción análoga en relajación [5], con gradientes inferiores a 0.25 grados.

La morfología se examinó por microscopía electrónica de barrido (SEM).

Resultados y Discusión

La muestra obtenida por reacción en fase sólida tiene menor resistividad (Tabla 1). Los valores negativos del coeficiente Seebeck confirman el comportamiento de semiconductor tipo n y una magnitud creciente es inversamente proporcional a la densidad de portadores.

Tabla 1.- Resistividad y coeficiente Seebeck para las muestras obtenidas por reacción en fase sólida y por coprecipitación química.

Muestra	Al/Zn (% at.)	Resistividad (Ω cm)	S (μVK^{-1})
S6	3.2	0.43	-73.04
Z11	3.2	78700	Muy resistiva

Como la conducción electrónica en estos semiconductores tipo n es sensible a la concentración de vacancias de oxígeno [6], se implementaron tratamientos reductores de 2 y 4 horas, a 1000ºC y $f_{O2} = 10^{-16}$ atm. Las muestras coprecipitadas mostraron extrema sensibilidad a este proceso que disminuyó su resistividad en cinco órdenes de magnitud en las primeras 2 horas (Fig.1).

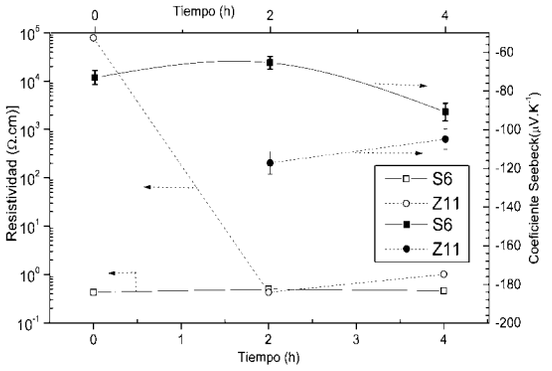

Fig.1.- Resistividad y coeficiente Seebeck de las muestras obtenidas por reacción en fase sólida (S6) y coprecipitación química (Z11), para distintos tiempos de tratamiento reductor.

En marcado contraste, las muestras obtenidas por reacción en fase sólida son prácticamente insensibles al tratamiento reductor, consistentemente con un tamaño de grano promedio del orden de 10 μm (Fig.2a), mientras que la granulometría de la muestra coprecipitada (Fig.2b) está claramente por debajo de la resolución (~1 μm).

Ensayos preliminares en muestras sinterizadas a 1200 °C, durante 24 h, resultaron en resistividades del orden del kΩ.cm. Una mayor temperatura y duración del sinterizado no solo contribuye a la homogeneidad de distribución del Al^{3+} dopante, sino que aumenta significativamente el tamaño de grano. La textura obtenida por coprecipitación, con menor tamaño de grano y elevada porosidad promueve mayor superficie específica y por ende mayor eficacia del tratamiento reductor, consistentemente con la baja difusividad intracristalina del oxígeno en la estructura de la wurtzita [7]. Es evidente que el mayor efecto sobre la resistividad, proporcional al producto de la movilidad y la densidad de portadores, ocurre durante las primeras dos horas de proceso cf. Fig.3, mientras que el aumento de la densidad de portadores, proporcional a la disminución del coeficiente Seebeck, es mucho más gradual, consistentemente con la influencia dominante de un aumento de la movilidad antes que de la densidad de portadores.

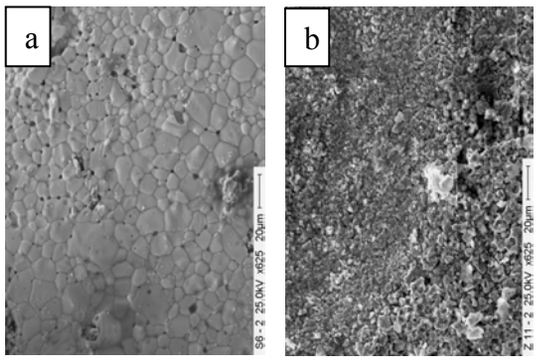

Fig.2.- SEM de muestras obtenidas por a) reacción en fase sólida (S6) y b) coprecipitación química (Z11).

Conclusiones

Para el material coprecipitado la sinterización no es suficiente para disminuir la resistividad en forma significativa. Tratamientos reductores para optimizar la estequiometría metal-oxígeno, pueden emplearse para mejorar las propiedades eléctricas. Dado que las aplicaciones prácticas de los TCO requieren películas delgadas de granulometría nanométrica, el tratamiento reductor puede proveer mejores condiciones de proceso.

Referencias

[1] E.Fortunato, D.Ginley, H.Hosono, D.C.Paine, MRS Bulletin, Vol. 32, pp. 242-247, March, 2007.

[2] T.Minami, Semicond.Sci.Technol.,Vol. 20, pp. S35-S44, March, 2005.

[3] T.Minami, J.Oda, J.Nomoto, T. Miyata, Thin Solid Films, Vol. 519, pp. 385-390, August, 2010.

[4] K.H.Gayer, L.C.Thompson, O.T.Zajicek, Can.J.Chem., Vol. 36, pp. 1268-1271,April, 1958.

[5] P. C. Eklundt and A. K. Mabatah ,Rev. Sci. Instrum., Vol. 48, No.7, pp.775-777,July 1977

[6] G.J.Exarhos, X-D.Shou, Thin Solid Films, Vol.515, pp. 7025-7052, March, 2007.

[7] A.C. Soares Sabioni, M.J. Ferreira Ramos, W. BarbosaFerraz, Materials Research, Vol. 6, N°2, pp. 173-178, March, 2003.

Encapsulation Procedure of ISFETs For Integration In LTCC Substrates

Massaki de O. Igarashi[1], Valtemar F. Cardoso[1], Zaira M. da Rocha[1], Sebastião G. dos Santos Filho[1], Cecilia Jimenez-Jorquera[2], Antonio Carlos Seabra[1]
Departamento de Sistemas Eletrônicos, Universidade de São Paulo, São Paulo, Brazil
Instituto de Microelectrónica de Barcelona IMB-CNM (CSIC), Bellaterra, Barcelona, Spain
05508-900, São Paulo, SP, Brazil
massaki.igarashi@usp.br

Abstract

The integration of ISFET based sensors in microfluidic structures offers a good alternative for the so called Lab on a Chip (LoC) systems. This work shows the preliminary results of ISFET encapsulation for integration in a LTTC ("Low Temperature Co-fired Ceramics") substrate. For that a metallization process using gold (Au) over the Aluminum contacts (Al) has been developed. This process permits the easy welding of contact ISFETs in LTCC substrates.

Keywords: Microsystem, microsensor, ISFET, Integration, Metallization, LTCC.

Introduction

In some of the analytical methods for phosphorous analysis [1, 2] the reactions are realized under an acid medium, demanding pH correction, mainly when the sample is a waste water effluent. In molybdenum blue method the intensity of color complex formation increases gradually with increasing acidification of the medium [3, 4]. Besides it, the adjustment of pH is very important for phosphorous removal [1-3].

For pH measurement, the ISFET microsensor is very attractive due to its robustness, its small size, rapid response and facility of integration with automated and flow systems [5, 6].

The design of microfluidic systems enables faster and more efficient analyzers. In this context the use of Low Temperature Cofired Ceramics– (LTCC) is a promissing technique [7, 8]. This work discusses the encapsulation and integration of ISFETs to LTCC substrates.

Methods and devices

ISFETS were fabricated according to NMOS technology at the Instituto de Microelectrónica de Barcelona (IMB-CNM). The chips are 3x3 mm and the gate contains a Si_2N_3 dielectric.

The LTCC substrate can contain silver-paste electrical tracks. On the other hand traditional ISFETs have their electrical contacts (PADs) made by aluminum thin-films. To efficiently solder the ISFET PADs to the LTCC tracks has been evaluated a procedure which uses interlayer metals for obtaining good solderability. The metal of choice in this case is gold. Our process uses the electroless technique [9] to grow a gold layer on the aluminum PADs.

A cement layer of palladium was deposited over the aluminum PADs to promote gold electroless deposition onto aluminum. To obtain the cement layer of palladium, reagents chloride palladium (II) ($PdCl_2$) and Potassium Tetrachloro-aurate (III) 99.995% were used.

The process started by preparing a dilute solution of hydrofluoric acid (HF, 49%) in water (ratio 1:50) followed by the preparation of the $PdCl_2$ solution, 3.10^{-3}M, in the diluted HF solution (1:50). Then, the gold solution, 3.10^{-3}M. was also prepared in diluted HF solution (1:50).

The sensitive layer of the sensor was coated with an adhesive polymer, leaving only the exposed pads; that avoided contact of the plating solution and damage throughout the process.

The metallization process basically consists in to form an intermediate layer of sacrificial oxide followed by a palladium layer to promote adhesion and finally gold layer for facilitating tin soldering.

Results

First the microsensor was put under 150°C during 15 minutes to form an oxide layer on aluminum and prevent etching by the hydrofluoric acid.

After the oxide formation, the microsensor received a 10 second dip process in PdCl

solution. Durign this process the PADs of the microsensor showed a dark color. Then a new dip process was done, into Au solution, during 15 seconds. The gold coloration, indicating Au deposition, was checked by an optical microscope (Figure 1).

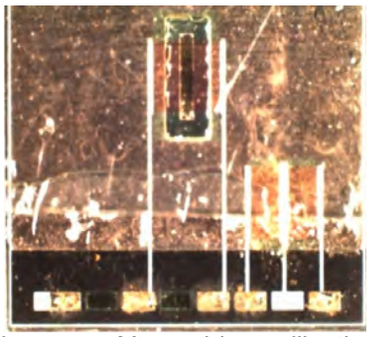

Figure 1 – After gold metallization.

After the gold pads metallization the adhesion of tin metal to PADs was tested, which demonstrated that, following a slight pressure with a laboratory clamp, tin adhered to PADs efficiently.

Figure 2 depicts the chip already encapsulated with the LTCC structure and wire bonded. Tests were made to integrate the ISFET microsensor (Figure 3) into LTCC substrate.

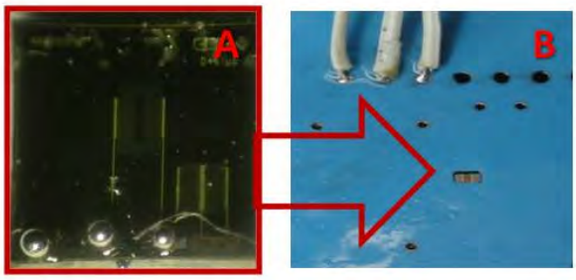

Figure 2 – First integrated prototype. A) Stained Chip PADs and b) Integrated ISFET Chip on LTCC substrate.

Conclusions

The gold metallization onto aluminum pads of the microsensor allowed one to solve an important problem, this is to say, the solderability over aluminum pads of microsensors integrated in green ceramics to measure and to adjust pH in flow. For better integration between pH sensor and the LTCC substrate it is still necessary to improve the process for the formation of thicker layers and also improvements in the repeatability and reproducibility of process for the full integration of the microsensor.

Acknowledgments

The authors would like to thank the financial support received from CAPES, Laboratory of Integrated Systems and the CYTED project P509AC0376 funding.

References

1. Turner, B.L., E. Frossard, and D.S. Baldwin. *Organic Phosphorus in the Environment*. in *Organic Phosphorus Workshop* 2003. Ascoa, Switzerland: CABI Publishing.

2. Andrew D. Eaton, et al., *Standard Methods for the Examination of Water & Wastewater: Centennial Edition*. 21st ed. Vol. 1. 2005: American Public Health Association.

3. Andrew, K.N., et al., *Flow injection techniques for water monitoring.* Analytical Chemistry, 1994. **66**(18): p. 916A-922A.

4. Mullerr, A., et al., *ChemInform Abstract: Molybdenum Blue: A 200-Year-Old Mystery Unveiled.* ChemInform, 1996. **27**(37): p. no-no.

5. Igarashi, M.d.O., et al., *Circuit for pH measurement in a LTCC substrate*, in *Conference on Electronics, Telecommunications and Computers - CETC2011*, P.i.E.E.R.S. Paulo Marques and P.i.M.S.E.M.a.O. Alessandro Fantoni, Editors. 2011, Department of Electronics, Telecommunications and Computer Engineering, at the High Institute of Engineering of Lisbon: Lisbon, Portugal.

6. Jimenez-Jorquera, C., J. Orozco, and A. Baldi, *ISFET Based Microsensors for Environmental Monitoring.* Sensors, 2009. **10**(1): p. 61-83.

7.da Rocha, Z.M., *Microlaboratórios autônomos para monitoramento de parâmetros de qualidade da água*, in *Departamento de Engenharia de Sistemas Eletrônicos da EPUSP* 2009, Universidade de São Paulo - USP: SãoPaulo.

8.da Rocha, Z.M., et al., *Compact and autonomous multiwavelength microanalyzer for in-line and in situ colorimetric determinations.* Lab on a Chip, 2012. **12**(1): p. 109-117.

9. Mallory, G.O. and J.B. Haber, *Electroless plating: fundamentals and applications*, ed. A.E.a.S.F.S.I.-. AESF. Vol. 1. 1990, Orlando, USA: Noyes Publications/William Andrew Publishing, LLC. 538.

Chapter 5: Signal Conditioning and Instrumentation

Diseño de un frecuencímetro de alto desempeño para sensores de gas basados en resonador de cuarzo

J. L. Muñoz-Mata, S. Muñoz-Aguirre, G. Beltrán-Pérez, J. Castillo-Mixcóatl
Facultad de Ciencias Físico Matemáticas, Benemérita Universidad Autónoma de Puebla
Av. San Claudio y Rio Verde. Col. San Manuel C.U., C.P. 72570, Puebla, Puebla, Mexico
josephm_7@yahoo.com.mx, smunoz@fcfm.buap.mx

Abstract

Las narices electrónicas son dispositivos que tratan de imitar la nariz humana; algunos de estos dispositivos utilizan sensores de gas a base de resonador de cuarzo para lo cual es esencial el uso de un frecuencímetro. Aunque ya existen frecuencímetros comerciales, generalmente solo tienen uno o dos canales, mientras que la nariz electrónica utiliza un arreglo de ocho o más sensores. Por otro lado, se han desarrollado sistemas para éste propósito pero están limitados en la velocidad de la generación de datos, lo cual afecta directamente la resolución de las respuestas del sensor medidas. El presente trabajo muestra el desarrollo de un frecuencímetro de alto desempeño y resolución utilizando un FPGA, el cual tiene la capacidad de generar un incremento significativo en la velocidad de la generación de datos (5 datos por segundo) sin afectar la resolución del mismo (1 Hz).

Keywords: FPGA, frecuencímetro, nariz electrónica, sensor QCM

1. Introducción

Las aplicaciones con sensores de microbalanza de cristal de cuarzo (QCM) son utilizados para la nariz electrónica (NE) debido a su correlación con la nariz humana [1]. El principio de funcionamiento del sensor está basado en que cuando las moléculas del gas interactúan con la película sensible provoca un decremento en la frecuencia de resonancia por el efecto de carga de masa [2].

Por lo tanto, para medir la respuesta de este tipo de sensores es esencial el uso de un frecuencímetro. Los frecuencímetros comerciales tienen precios elevados, además de que tienen uno o a lo más dos canales y en la nariz electrónica es necesario utilizar un arreglo de ocho o más sensores. En un trabajo previo, hemos reportado el desarrollo de un sistema para medir la respuesta de sensores QCM [3], pero la velocidad de este sistema está directamente relacionada con la base de tiempo del frecuencímetro, es decir, aumentar la velocidad en la generación de datos sería a expensas de una baja resolución. Por lo tanto es deseable un frecuencímetro que cuente con la capacidad de generar una mayor cantidad de datos por unidad de tiempo sin afectar la resolución.

En este trabajo se presenta el desarrollo de un frecuencímetro de alto desempeño y resolución para medir sensores QCM utilizando un dispositivo de compuertas programables en el campo (FPGA, por sus siglas en inglés), el cual tiene la capacidad de generar datos cada 200 ms manteniendo una resolución de 1 Hz, se obtuvieron resultados experimentales utilizando como patrón un generador de funciones.

2. Arreglo experimental

El frecuencímetro fue desarrollado utilizando un FPGA (Cyclone II-Altera), con un reloj de 50 MHz. Se utilizó un generador de funciones (AFG3102, Tektronix) para comprobar el desempeño del frecuencímetro. La adquisición de datos se realizó a través de una tarjeta (USB-DAQ) diseñada con un microcontrolador (PIC18F4455, Microchip). El desarrollo de software se realizó utilizando LabVIEW.

Diseño del frecuencímetro

El arreglo experimental se muestra en la Figura 1. Se utilizó el método de conteo de frecuencia directa para el desarrollo del frecuencímetro (figura 2). El principio de

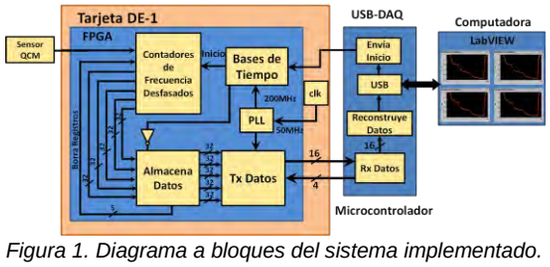

Figura 1. Diagrama a bloques del sistema implementado.

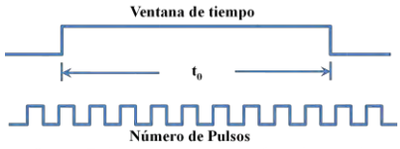

Figura 2. Principio de funcionamiento del frecuencímetro.

operación se muestra en la ecuación 1.

$$Frecuencia = \frac{Número\ de\ Pulsos}{t_0}. \qquad (1)$$

Donde sí la ventana de tiempo es de un segundo, la frecuencia es igual al número de pulsos de entrada.

Para el desarrollo del frecuencímetro de alto desempeño y obtener una generación de varios datos por segundo con una resolución de 1 Hz, se generaron ventanas de tiempo subsecuentes con duración de un segundo, es decir se utilizan contadores desfasados, teniendo la misma entrada en común proveniente del sensor QCM, como se muestra en la Figura 3. De esta manera se generan datos cada 200 ms sin afectar la resolución de 1 Hz. Los datos se almacenan en registros de 32 bits para cada contador. La trasferencia de datos a la computadora es a través de la tarjeta USB-DAQ. Los datos son enviados desde el FPGA en bloques de 16 bits para ser reconstruidos por el software de adquisición, en el cual se puede visualizar y almacenar la información.

3. Resultados y discusión

Para comprobar la efectividad en la generación de datos con la resolución de 1 Hz y en el incremento en la velocidad de generación de datos del frecuencímetro, se realizó una comparación entre los datos obtenidos con el sistema anteriormente desarrollado [3] y con el nuevo frecuencímetro usando como patrón el generador de funciones. Estos resultados se muestran en la figura 4. En la figura 4a se muestran datos en un periodo de tiempo de 100 segundos con incrementos de 1 Hz. La

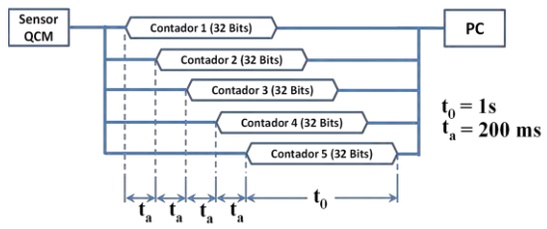

Figura 3. Diagrama a bloques de la generación de datos cada 200ms con una resolución de 1 Hz.

resolución se mantiene en ambos frecuencímetros, y además se puede observar en la gráfica del nuevo frecuencímetro una mayor densidad de datos dado que se han generado más puntos a diferencia del frecuencímetro anterior que solo genera un dato por segundo. En la Figura 4b se muestra un acercamiento a dichas gráficas para observar la generación de puntos en un periodo de 10 segundos. Es fácilmente observable la generación de puntos cada 200 ms por el frecuencímetro nuevo. Por lo tanto se comprueba la efectividad y la estabilidad en el instrumento.

4. Conclusiones

Se ha desarrollado un frecuencímetro de alta resolución y desempeño con un tiempo de generación de datos de 200 ms a una alta resolución (1 Hz). Se realizó una comparación en el desempeño entre el frecuencímetro anteriormente desarrollado y el frecuencímetro actual, comprobando la efectividad del sistema.

5. Referencias

[1] H. Troy Nagle R. Gutierrez O., S. Schiffman, IEEE Spectrum, Vol 35, No. 9 pp 22-34,Septiembre 1998.
[2] S. Muñoz-Aguirre, S. Nakamoto, T Moriizumi Sensors an Actuators B, Vol. 105, pp 144-149, Mayo.
[3] J. L. Muñoz M, S. Muñoz, H. González S., G. Beltrán P., J. Castillo M., Meas. Sci. Technol, Aceptado para su publicación, Marzo 2012

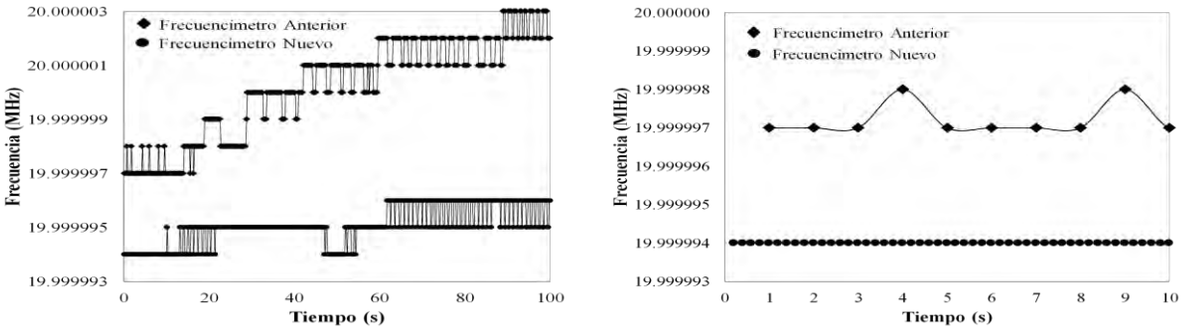

a) b)

Figura 4 Resultados obtenidos de comparación entre frecuencímetros con resolución de 1Hz. a) Datos obtenidos en 100 seg. b) Acercamiento de los datos obtenidos en un periodo de 10 seg.

Sistema portable de medición para microsensores tipo FETs basado en un microcontrolador PSoC

D. Garnier Fernández[1], O. Arias de Fuentes[2§], A. Blanco[2], A. Durán[2], C. Jiménez[3]
[1]Instituto Superior Politécnico "José Antonio Echeverría" (ISPJAE)
Calle 114 #11901, e/ 119 y 127 CP 19390, C. Habana, Cuba
[2]Instituto de Ciencia y Tecnología de Materiales, Universidad de La Habana
Zapata y G, Vedado CP 10400, C. Habana, Cuba
[3]Instituto de Microelectrónica de Barcelona, Campus-UAB, 08193 Bellaterra, Barcelona, España
§ E-mail: oarias@imre.oc.uh.cu; oarias@fisica.uh.cu

Abstract

En este trabajo se presenta el diseño e implementación de un sistema de instrumentación portable basado en un microcontrolador CY8C29466 (PSoC) para la caracterización y el empleo de microsensores ISFETs y CHEMFETs a fin de poder realizar controles en muestras líquidas, que posibilitarán la cuantificación de diversos iones contaminantes y nocivos para la salud. El sistema permite realizar mediciones que, además de ser mostradas en pantalla, pueden ser almacenadas para su posterior recuperación y análisis mediante su acople a una PC.

Keywords: ISFET, CHEMFET, PSoC, microsensor, instrumentación.

Introducción

En la actualidad los problemas medioambientales que afectan la salud de los seres vivos constituyen un importante centro de atención de la comunidad científica internacional. Tal es así, que se han desarrollado diversos sistemas para el control de la calidad del agua, otros destinados a apoyar el diagnóstico y la rehabilitación de personas con padecimientos médicos, así como otros que han permitido mejorar la calidad de vida de muchas personas.

Una rama muy vinculada a esto, que en las últimas décadas ha sufrido un acelerado desarrollo, ha sido la de los transductores y sensores. Con los avances de esta rama y los adelantos de la ciencia y la tecnología, es que surgen los microsensores basados en FETs (Transistores de Efecto de Campo).

Los microsensores basados en FETs han ganado una importancia cada vez mayor en diferentes aplicaciones dado sus ventajas sobre sensores convencionales en cuanto a tamaño, posibilidades de integración, bajos costos, tiempos de respuesta rápidos y necesidad de pequeños volúmenes de muestra para su utilización [1, 2].

El objetivo de este trabajo está dirigido hacia el diseño e implementación de un sistema portable con el empleo de un PSoC (Sistema Programable sobre un Dispositivo), asociado a microsensores basados en FETs. Con él será posible realizar mediciones que, además de ser mostradas en una pantalla de cristal líquido (LCD) que forma parte del sistema portable, podrán ser almacenadas por el PSoC para su posterior recuperación y análisis en el laboratorio mediante su acople a una PC.

Diseño general del sistema

El sistema se compone, básicamente, por una etapa acondicionadora de señal y otra encargada del procesamiento, visualización, almacenamiento y transmisión de los datos adquiridos por el sensor.

En el período de diseño se seleccionó cuidadosamente el circuito de polarización (etapa acondicionadora de señal), necesario para imponer el punto de operación del microsensor. Con él se fijó un valor constante para V_{DS} e I_{DS}, siendo estos 500mV y 100uA respectivamente. Para ello, se empleó el circuito amplificador con realimentación de voltaje al electrodo de referencia [3].

Como unidad básica de procesamiento se hizo uso del microcontrolador CY8C29466 [4], perteneciente a la familia de los PSoC. Lo más notable en él, es su capacidad para integrar componentes analógicos en la sección digital de un sistema. Esta característica permitió la implementación parcial del circuito de polarización en el PSoC. Con ello se favoreció la integración y la portabilidad del sistema.

En la Fig. 1 se muestra el diseño esquemático del sistema desarrollado.

Delay-Convolution-Modulation (DCM)

The first model is the DCM model whose result is a signal $y_a \in l^2(\mathbb{Z}_D)$:

$$y_a = g_a * \delta_{m_{a,b}}, \tag{3}$$

where $g_a \in l^2(\mathbb{Z}_D)$

$$g_a = T_{h_{a,b}}(f_b), \tag{4}$$

where $f_b \in l^2(\mathbb{Z}_D)$

$$f_b = x_b \odot_D X_{k_{a,b}}. \tag{5}$$

Composing these 3 equations give us a the following equation

$$y_a = H_{a,b}(x_b) = (T_{h_{a,b}}(x_b \odot_D X_{k_{a,b}})) * \delta_{m_{a,b}} \tag{6}$$

Modulation-Convolution-Delay (MCD)

The second model is the MCD model whose result is a signal $y_a \in l^2(\mathbb{Z}_D)$. A similar procedure where modulation is the first step, gives us the following equation

$$y_a = (T_{h_{a,b}}(x_b * \delta_{m_{a,b}})) \odot_D X_{k_{a,b}} \tag{7}$$

Finally, we have two general equations for a MIMO system:

$$y_a = \sum_{b=0}^{M-1} (T_{h_{a,b}}(x_b \odot_D X_{k_{a,b}})) * \delta_{m_{a,b}} \tag{8}$$

$$y_a = \sum_{b=0}^{M-1} (T_{h_{a,b}}(x_b * \delta_{m_{a,b}})) \odot_D X_{k_{a,b}} \tag{9}$$

GNURadio

According to its developer, Gnuradio is a free and open-source software development toolkit. Gnuradio was originally created for digital signal processing. Its main characteristics are: Signal processing blocks, Can be used readily with low cost external RF hardware, It can be used as a simulation environment, It is widely supported among hobbyist, academic, and commercial environments.

Gnuradio applications are primarily written using Python programming language. The critical performance signal processing is implemented in C++. The developer is able to implement real-time, high-throughput, signal processing paths in a simple to use development environment called gnuradio companion.

Gnuradio has several modules. These modules have blocks. All the blocks are bind together with the python language.

Physical Testbed

An accoustic environment is set. First, we place several objects into a room. Second, an array of speakers are set to transmit a given signal. Finally, an array of microphones receives the signals and feed a computational system. The computational system takes measures and estimations with the received signals.

Other approaches have determined the effect of indoor environment modeling precision on MIMO channel characterization when dealing with a 3D raytracing with electromagnetic wave propagation[4]. In [5] the problem is how to make measurements over a multipath simulator. Finally, the problem addressed in [6] is how to build a software radio with commercial over-the-shelf components. This ensures the capabilities and long term support for the propossed framework.

References

[1] J. Winters. Optimum combining for indoor radio systems with multiple users. *Communications, IEEE Transactions on*, 35(11):1222 – 1230, nov 1987.

[2] J. Mitola. The software radio architecture. *Communications Magazine, IEEE*, 33(5):26 – 38, may 1995.

[3] L. Cohen. *Time-Frequency Analysis*. Prentice Hall PTR, 1995.

[4] P. Carlos, P. Yannis, V. Rodolphe, and C. Pierre. Sensitivity of the mimo channel characterization to the modeling of the environment. *Antennas and Propagation, IEEE Transactions on*, 57(4):1218 –1227, april 2009.

[5] P. Hallbjorner, J.D. Sanchez-Heredia, P. Lindberg, A.M. Martinez-Gonzalez, and T. Bolin. Multipath simulator measurements of handset dual antenna performance with limited number of signal paths. *Antennas and Propagation, IEEE Transactions on*, 60(2):682 –688, feb. 2012.

[6] M. Dickens, B. Dunn, and L.J. Nicholas. Design and implementation of a portable software radio. *Communications Magazine, IEEE*, 46(8):58 –66, august 2008.

Low Temperature Co-fired Ceramic for Self-packaged EDL Super Capacitors Applications

H. K. Sahoo[*], T.S. Jones[#], M. Smith[%] and J.J. Santiago-Aviles[#]

[#] University of Pennsylvania, Electrical and Systems Engineering Department, Philadelphia, PA, 19104

- University of Pennsylvania, Materials Science and Engineering Department, Philadelphia, PA, 19104

[%] DuPont Micro Circuits Materials, RTP, NC. 27709

Abstract

Low temperature co-fired ceramics, LTCC or green tapes, form a series of alumina-based materials of substantial relevance in hybrid micro-electronics and growing importance in the field of micro-chemical reactors and micro-electro-mechanical systems. Powering these small systems often requires dedicated supplies and / or batteries. For portability and energy density, batteries often surpass other energy storage systems. If secondary batteries (rechargeable) are utilized, kinetics considerations often prevent the quick charging required for expeditious utilization. To obviate chemical kinetic problems, super-capacitors, capable of providing substantial power density (quick charging and discharging) are often utilized. In this work we report the utilization of LTCC for the fabrication of self packaged electrical double layer super-capacitors and the device characterization.

Keywords: super-capacitors, LTCC

Introduction

Powering distributed sensing / actuating systems often requires portable, light, high energy and power density devices. Batteries, in particular Li based systems, often satisfy the first two requirements, but fail in providing the high power density needed for fast charging / discharging applications. Super-capacitors, devices where a high specific surface area electrodes immersed in an electrolyte, allows for the formation of an electrical double layer often excel in this respect. In these layers, mobile charges in the electrolyte, interact with high electrical conductivity electrodes possessing the myriad of pores characteristic of high specific surface area (in our case approximately 2700 m^2/gm) [1]. From these interactions involving charged chemical species (ions) and atomic distances (nm), large capacitances are often obtained, some of the order of several hundred Farads. (Remember the expression for a parallel plate capacitor, where

$$C = \varepsilon\varepsilon_\circ A / d$$

Is the capacitance for a media with dielectric constant equal to $\varepsilon\varepsilon_\circ$, area A and d the separation between the charges.

These super-capacitors possess in common with batteries, a low series resistance, allowing them to behave as low impedance sources. As such they can be charged / discharged quickly, much quicker than batteries as they do not sustain chemical reactions and are not limited by kinetics considerations. Super-capacitors are mostly packaged in expensive metallic enclosures of complex fabrication and sensitive to chemical attacks such as corrosion.

Results and discussion:

The LTCC ceramic tapes are inexpensive, easy to fabricate and chemically stable. In the green (before firing) they consist fundamentally of alumina powder (Al_2O_3), a glass frit to enhance sintering and a organic vehicle to reduce the rheological demands during tape casting. In the green, this material is compliant and easy to machine. Metal conductors and vias are often screen printed on these tapes, using compatible

metal containing paste. After firing at approx. 850 C. these materials become rigid, impermeable, and hard.
In this work a simple super-capacitor (see figure 1) was designed, fabricated and electrochemically characterized as to monitor its performance. The two-capacitor plates are LTCC co-fired with Ag paste defining the current collectors (square cavity in the center). On top the screen-printed current collectors, carbide derived carbons were placed as electrodes.

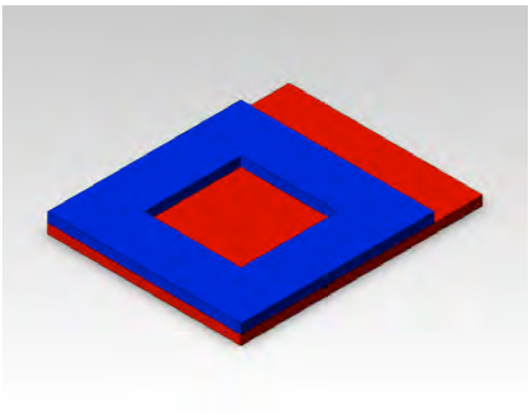

Figure 1, Solid works diagram of EDL super-capacitor.

Carbide derived carbons are high electrical conductivity [2] , high specific surface area materials obtained by the Cl_2 reduction of metal / metalloid carbides, in our case TiC. The chlorination temperature correlates with the electrical conductivity. The CDC material was mixed with 5 W/o PTFE (Teflon) as a binder. The electrolyte utilized is a 1 M aqueous solution of sulfuric acid. Between the two electrically identical sides of the super-capacitor, a separating membrane consisting of a polymer fabric loaded with stretched PTFE (GoreTex^{TM}) was used. The super-capacitor was characterized using a Pine Potentiostat, through the utilization of cyclic voltametry measurements (C-V).
The potentiostat trace is presented as figure 2. That trace shows that for the parameters used for the room temperature measurements of the capacitor characteristics, namely:

Scan rate :	250 mV /s
Anodic Charge:	87 mC
Cathodic charge	65.62 mC
Coulombic Efficiency	75.43

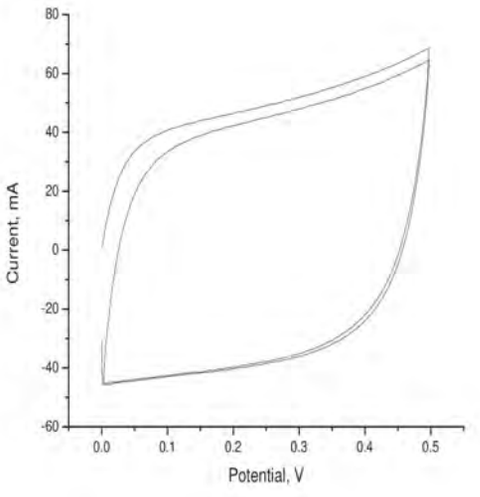

Figure 2. Current – voltage characteristics of an LTCC super-capacitor.

And analyzing the above trace one can obtain using straight forward application of the capacitor definition, namely charge per unit voltage, that the average capacitance for the device, with an area of 1 cm^2, and combined thickness of 150 μm, is 131.43 mF.

Conclusions:

Self packaged LTCC based EDL super-capacitors were design, fabricated and characterized. The average capacitance value obtained, 131.43 mF showing high capacity potential of metal encased devices and the low cost of the ceramic self-packaged ones.

References:

1
C.Portet, G. Yushin, and Y. Gogotsi "Effect of Carbon Particle Size on the Electrochemical Performance of EDLC" *Journal of the Electrochemical Society,* **155**(7), A521-A536 (2008).
2
P.M.Vora, P.Gopu,M. Rosario-Canales, C.R. Perez, Y. Gogotsi, J.J.Santiago-Aviles, J.M.Kikkawa "Correlating magnetotransport and diamagnetisms of sp^2 bonded carbon networks through the metal-insulator transition" *Phys Revs B* **84,** 155114 (2011).

Chapter 6: Ultrasonic Sensors

Análisis del elemento piezoeléctrico mediante el Método de los Elementos Finitos (MEF), cuando se ve modificada el área efectiva del elemento.

Israel Sánchez Domínguez[1,2], Pedro Acevedo Contla[1], Fabián García Nocetti[1], Manuel Recuero López[2]
Universidad Nacional Autónoma de México, Instituto de Investigaciones en Matemáticas Aplicadas y en Sistemas.
04510, México, D.F., México

Universidad Politécnica de Madrid, Escuela Técnica Superior de Ingenieros Industriales

Madrid, España

israel@uxdea4.iimas.unam.mx

Abstract

El presente trabajo, muestra la simulación y comparación sobre el desempeño del principal elemento que constituye el transductor, la cerámica piezoeléctrica, este estudio se basa en conocer como se ve afectada la respuesta de una cerámica piezoeléctrica durante el proceso de construcción de un transductor ultrasónico para aplicaciones médicas. Las simulaciones fueron realizadas empleando el Método de los Elementos Finitos (MEF), a partir de esta simulación se obtuvieron las respuestas en frecuencia cuando se cuenta con el elemento cerámico únicamente y con presencia de los electrodos, los cuales modifican la frecuencia natural del la cerámica, comparando estos resultados versus mediciones experimentales, para un transductor a 8MHz de operación. Demostrando que existe un corrimiento en la frecuencia durante el proceso de construcción de un transductor, modificando con esto el desempeño del transductor.

Keywords: Elemento cerámico, Método de los Elementos Finitos, Transductor ultrasónico, Frecuencia.

Introducción

En la actualidad los transductores ultrasónicos ocupan un lugar importante en el día a día, dichos dispositivos son empleados en diversas actividades que van desde el área industrial hasta aplicaciones médicas. Sin embargo el proceso de construcción puede afectar el desempeño de estos transductores, un problema fundamental se presenta en el elemento principal que conforma al transductor, es decir la cerámica piezoeléctrica.

Esta presenta cambios en su frecuencia y por ende en el funcionamiento de todo el transductor; este cambio en la frecuencia es originado principalmente al momento de colocar las conexiones eléctricas (electrodos) a la cerámica.

El presente trabajo reporta el análisis del elemento piezoeléctrico mediante el Método de los Elementos Finitos (MEF), cuando se ve modificada el área efectiva de la cerámica al momento de soldar los electrodos a la misma. Realizando comparaciones de las simulaciones versus mediciones experimentales.

Desarrollo y Metodología

La cerámica de estudio es fabricada por Piceramics, hecha de Titanato Zircanato de Plomo (PZT) con una frecuencia de trabajo a 8MHz con geometría cuadrada. Los electrodos

son realizados con cable coaxial, procurando no ocupar más del 10% área de la cerámica.

Se realizó la simulación de la cerámica usando el MEF, obteniendo la respuesta en frecuencia, para posteriormente realizar la simulación con presencia de los electrodos lo cual representa una reducción del área efectiva de la cerámica. De igual forma se realizaron las mediciones experimentales de la cerámica con y sin presencia de los electrodos en el proceso de construcción de un transductor, comparando ambas respuestas.

Resultados

En la figura 1, se presenta la solución de la simulación con la geometría utilizada en la simulación mediante el MEF.

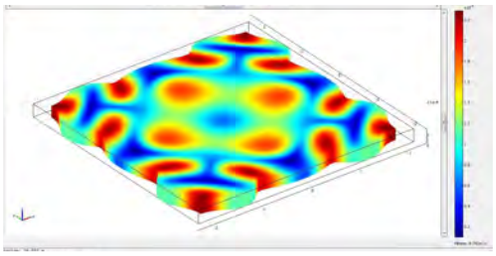

Figura1.- Resultado de la simulación usando el método de los elementos finitos, para una cerámica piezoeléctrica.

Posteriormente en la figura 2, se presenta la curva para esta simulación.

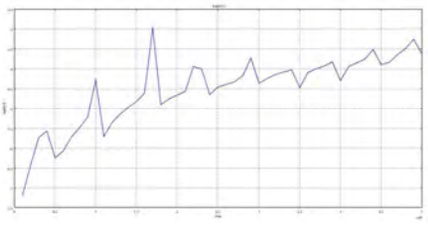

Figura 2.-Curva de la admitancia, para una cerámica piezoeléctrica.

En la figura 3, es mostrada una cerámica con los electrodos soldados, en ella es posible observar que se trato de limitar el punto de soldadura a máximo el 10% del área efectiva de la cerámica piezoeléctrica.

Posteriormente en la figura 4, es presentada la curva que se obtuvo de manera experimental para esta misma cerámica.

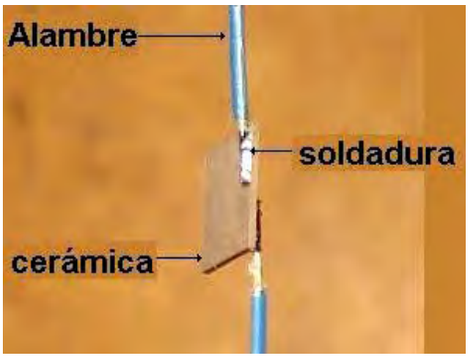

Figura 3.-Colocación de los electrodos soldados una cerámica piezoeléctrica

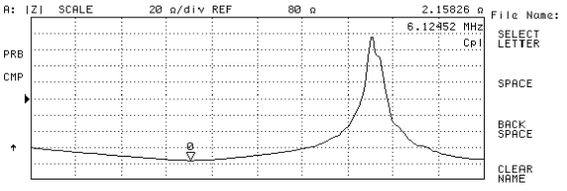

Figura 4.—Curva experimental de una cerámica piezoeléctrica

Resultados

Se puede concluir que la respuesta de un transductor ultrasónico dependerá de la forma en la que se trabaje con la cerámica piezoeléctrico y que esta presentará corrimientos en frecuencia, cuando se le coloquen elementos físicos que modifiquen el comportamiento natural de la cerámica. Razón por la cual es necesario contar con procedimientos que sean capaces de determinar de manera cuantitativa la variación que se presenta en la cerámica.

Referencias

[1] Sánchez, I., Faustmann, H, Acevedo, P. Fuentes, M Smith, Design and construction of ultrasonic Doppler transducers for blood flow measurement using Finite Element Analysis. IBERSENSOR 2008 24-26 Noviembre, São Paulo, Brasil

[2] Sánchez, I., & Acevedo, P. & Contreras, J.; Simulación y caracterización de un transductor ultrasónico utilizando Rexolite como acoplamiento acústico, 29th Annual Meeting International Conference on Materials, Surfaces and Vacuum, San Luis Potosí, San Luis Potosí, México del 21 al 25 de Septiembre de 2009.

Chapter 7: Intelligent Sensors and Wireless Networks

A Field Measurement Approach for LTE (4G) Wireless Networks Performance Monitoring

J. Nascimento[1], P. Vieira[1,2], M. Vieira[1,3]

[1]Electronics Telecommunication and Computer Dept. ISEL, Lisbon, Portugal
[2]Instituto de Telecomunicações (IT), Lisbon, Portugal
[3]CTS-UNINOVA, Quinta da Torre, Monte da Caparica, 2829-516, Caparica, Portugal
30582@alunos.isel.pt, pvieira@deetc.isel.pt, mv@isel.ipl.pt

Abstract

This paper presents a structured approach for 4G (LTE) wireless networks performance monitoring, using field measurements. This is achieved using specific equipment with multiple sensoring capabilities, which enables full layer LTE data capture. A measurement campaign in partnership with a Portuguese mobile operator was produced, which focused on areas where a LTE pilot network has been implemented. The proposed approach allowed to validate LTE's performance targets, set by 3GPP. The obtained performance results are rather promising, foreseeing a strong kick-off for 4G LTE based wireless networks.

Keywords: Wireless Communications, 4G, LTE, Field Measurements.

Introduction

The Long Term Evolution (LTE) of Universal Mobile Telecommunications System (UMTS) is just one of the latest steps in an advancing series of mobile telecommunications systems, being known as the '4th Generation' (4G).

The first mobile communication systems to see large-scale commercial growth arrived in the 1980s and became known as the 'First Generation' systems. The First Generation comprised a number of independently-developed systems worldwide using analogue technology.

Global roaming first became a possibility with the development of the digital 'Second Generation' (2G) system known as GSM (Global System for Mobile Communications). Fuelled by advances in mobile handset technology, which resulted in small, fashionable terminals with a long battery life, the widespread acceptance of the GSM standard exceeded initial expectations and helped to create a vast new market. The resulting near-universal penetration of GSM phones in the developed world provided an ease of communication never previously possible, first by voice and text message, and later also by more advanced data services boosted by the next 3rd generation of mobile communications, the UMTS.

LTE is now an emerging commercial reality in several countries worldwide. Being completely specified under the 3rd Generation Partnership Project (3GPP), the main performance targets are:

- spectral efficiency two to four times more than UMTS;
- enables round trip time <10 ms;
- packet switched optimized;
- high level of mobility and security;
- optimized terminal power efficiency;
- frequency flexibility with from below 1.5 MHz up to 20 MHz allocations;
- peak rates exceed 100 Mbps in downlink and 50 Mbps in uplink.

These LTE performance targets should be validated in initial live networks. Considering that network statistics are not yet strong enough for performance monitoring, due to the shortage of new LTE mobile users, the field measurement approach is the obvious solution.

This paper presents a structured approach for LTE performance monitoring, using field measurements. This is achieved using specific equipment with multiple sensoring capabilities, which enables LTE field data capture (Layer 1 to Layer 3 measurements) and merge them with Global Positioning System (GPS) data.

The Field Measurement Setup

A measurement campaign in partnership with a Portuguese mobile operator was produced, which focused on areas where a LTE pilot network has been implemented.

In carrying out field sensoring, a USB data card category 3 was used, which allows for LTE packet traffic with speeds up to 100 Mbit/s and 50 Mbit/s in downlink and uplink, respectively, within a 20 MHz bandwidth.

In conjunction with the card data, it was implemented a specific software to collect real time data. This software enables the main LTE parameter analysis, such as positioning (GPS sensoring), transmission, and signal quality. Additionally, it allows to plot the wanted parameters into a lat/long referenced map, in order to facilitate the real time visual parameter analysis, see Fig. 1.

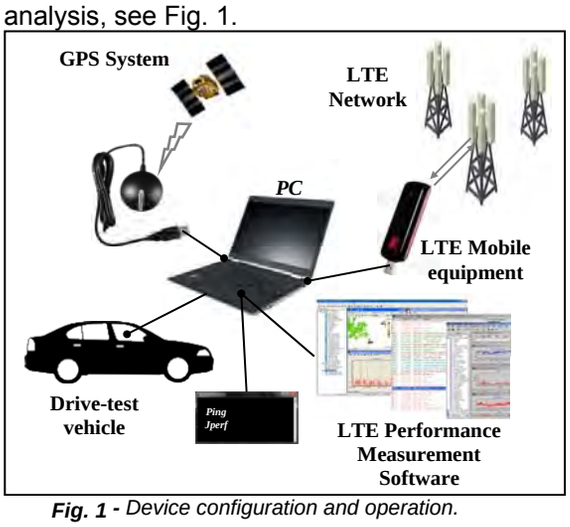

Fig. 1 - *Device configuration and operation.*

Four types of measurements were collected: static (hot spot oriented) and dynamic, in order to validate LTE mobility performance. Additionally, the two LTE mobile operation modes were tested: idle and connected mode.

In connected mode, and given that LTE is a packet switched network, User Datagram Protocol (UDP) data traffic was generated and transmitted. Received data was recorded in uplink and downlink in terms of bit rate, and also user plane latency. Other relevant measures were also collected, namely the Reference Signal Received Power (RSRP), the Reference Signal Received Quality (RSRQ) and Signal to Interference-plus-Noise Ratio (SINR).

Measurement Data

In this extended abstract, a few preliminary results are presented. The full data approach and analysis will follow, in the full paper version.

The drive test paths (dynamic mode) as well as the location of static measurements (blue stars) are shown in Fig. 2. LTE base station locations are also presented, with a tri-sectorized configuration.

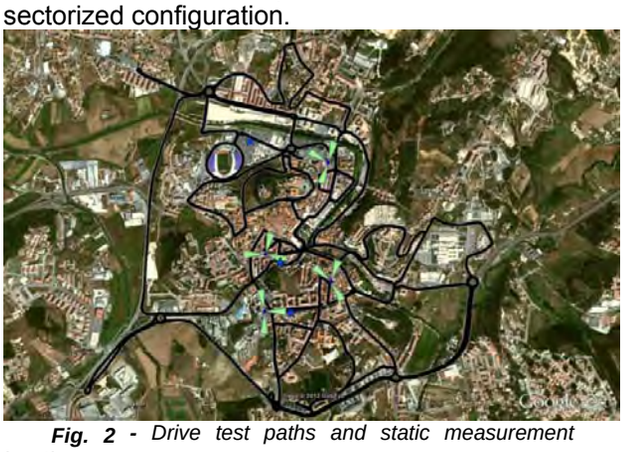

Fig. 2 - *Drive test paths and static measurement locations.*

Table 1 presents an overview about the performed LTE static and dynamic field measurements. The presented values are averaged over all static locations and also performed drive test paths.

Table 1 *LTE static and dynamic field measurements.*

Measurement type	Static		Dynamic	
Downlink (DL) / Uplink(UL)	DL	UL	DL	UL
Number of Sessions	10		-	
Service accessibility [%]	100.00	100.00	94.24	97.15
Average RSRP [dBm]	-71.50	-73.00	-92.83	-92.67
Average RSRQ [dB]	-9.57	-5.86	-10.18	-5.83
Average SINR [dB]	22.61	-	13.90	14.66
Average bit rate [Mbit/s]	81.60	41.10	47.27	21.37
Max. bit rate [Mbit/s]	93.88	47.54	100.11	48.66
Ping [ms]	19.33	-	-	-
Average Wideband CQI	12.27	-	10.00	-
Average speed [km/h]	-	-	11.00	

The proposed field measurement approach allowed to validate LTE's performance targets set by 3GPP. The obtained performance results are rather promising, foreseeing a strong kick-off for 4G LTE based wireless networks.

Conclusions

This paper presents a structured approach for LTE (4G) performance monitoring, using field measurements. This is achieved using specific equipment with multiple sensoring capabilities, which enables LTE field data capture with positioning information.

A measurement campaign in partnership with a LTE Portuguese mobile operator was produced and data was obtained. This process allowed to validate most of 3GPP's performance targets for LTE, foreseeing a strong kick-off for 4G LTE based wireless networks.

HSense: A High Performance Framework for Distributed Weather Sensor Networks

Jose A. Ortiz , Nayda Santiago, Jose G. Colom
University of Puerto Rico – Mayagüez
00680, Mayagüez, Puerto Rico
jose.ortiz19@upr.edu, nayda.santiago@ece.uprm.edu, colom@ece.uprm.edu

Abstract

HSense is a framework designed for aggregating sensor networks. It uses web technologies like REST (Representational State Transfer) and JSON (JavaScript Object Notation) to integrate networks to distributed databases. This allows a simple web interface for data distribution which eases the integration and management of heterogeneous sensors. This framework is currently being tested at the University of Puerto Rico at Mayagüez for managing distributed weather radars.

Keywords: sensors, networks, weather, environment, REST, web services, distributed, radars

Introduction

In recent years, development and integration of distributed sensor networks have dramatically increased [1]. From web services on the social net to environmental sensor networks, both intend to solve similar problems with different approaches. A hybrid approach has been developed at the University of Puerto Rico in Mayagüez. This method combines the REST capabilities of modern web services into the management and aggregation of sensor networks [3]. Sensor networks then can be accessed from the Internet through distributed databases across the globe. Web services provide the researchers the ability to query, monitor and manipulate the sensors. This approach permits the integration of heterogeneous networks into a single interface, allowing developers to create applications based on the sensors indexed by the databases. The Puerto Rico Weather Radar Network of UPRM is being used as a test bed to implement this framework.

Puerto Rico Weather Radar Network

The Puerto Rico Weather Radar Network is an initiative that started in the Electrical and Computer Department of the University of Puerto Rico in Mayagüez. The network consists of small portable weather radars spotted across the west coast of the Puerto Rico Island. It provides rain reflectivity measurements of the lower atmosphere. As the network intends to expand, it becomes ideal candidate for the testing of the HSense framework.

HSense Framework

The HSense framework aims to provide a better integration with current sensor networks while allowing users, developers and researchers to take advantage from the sensor data currently available but not accessible to the scientific community [1].

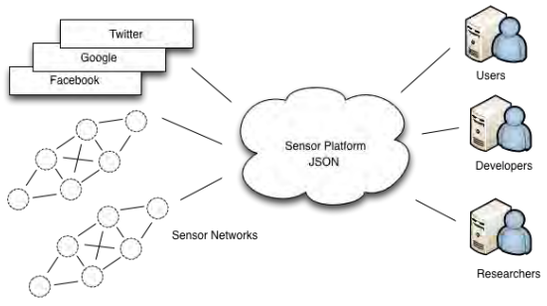

Figure 1: HSense framework

Server Module

The server module works as an interface to the distributed databases that contain the sensor data which in our case, consists of rain reflectivity. It also provides sub modules for processing and visualizes data. A management console monitors the individual networks and each of its sensors. A REST API (Application Programming Interface) is provided to developers so they can build applications on top of the framework.

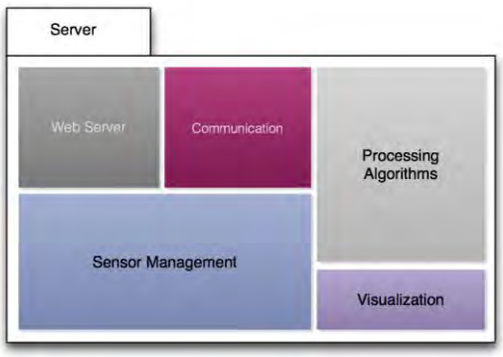

Figure 2: Server sub modules

Communication Module

The communication module is a piece of software which uses web technologies to connect sensors to the framework. This provides the data transformation needed for non-web capable sensors. Web capable sensors will still benefit from the approach of using HTTP based JSON communication. Using JSON for transferring data maintains a low overhead for the communications [4], allowing low powered sensors to transfer only the information required. The server module based on the characteristics of the sensor will dictate the verbosity of the communications.

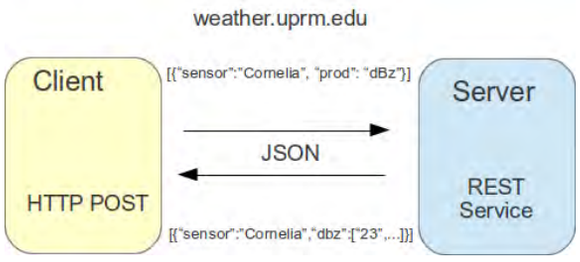

Figure 3: REST Protocol

Performance

HSense framework is built on top of the Haskell programming language and the Yesod web framework which is one of the fastest web frameworks available [5]. The framework is designed to process queries of hundreds of sensors simultaneously while processing sensor data in parallel. The host language of the framework allows the work to be shared among multiple processors [6].

Conclusion

Sensor management and integration is in a very active development phase. Multiple approaches to managing the data have been taken [2]. As presented in here, an approach for aggregating heterogeneous sensors in order to ease the development of applications was discussed and is been tested. At UPRM researchers can visualize data and download it to use their own tools or integrate their tools. Other sensors as well are being integrated providing a better way for research collaboration.

References

[1] Luca Mottola and Gian Pietro Picco. 2011. Programming wireless sensor networks: Fundamental concepts and state of the art. *ACM Comput. Surv.* 43, 3, Article 19 (April 2011), 51 pages.

[2] Nils Glombitza, Dennis Pfisterer, and Stefan Fischer. 2009. Integrating wireless sensor networks into web service-based business processes. In *Proceedings of the 4th International Workshop on Middleware Tools, Services and Run-Time Support for Sensor Networks* (MidSens '09). ACM, New York, NY, USA, 25-30.

[2] Luca Mottola and Gian Pietro Picco. 2011. Programming wireless sensor networks: Fundamental concepts and state of the art. *ACM Comput. Surv.* 43, 3, Article 19 (April 2011), 51 pages.

[3] M.Lee, T.Lee, “Middleware for Sensor Networks” 2003

[4] Sleman, A.; Moeller, R.; , "Micro SOA Model for Managing and Integrating Wireless Sensor Network into IP-Based Networks,"*Computational Intelligence, Communication Systems and Networks (CICSyN), 2010 Second International Conference on*, vol., no., pp.137-142, 28-30 July 2010

[5] Snoyman, M.; , "Warp: A Haskell Web Server,"*Internet Computing, IEEE* , vol.15, no.3, pp.81-85, May-June 2011

[6] Don Jones, Jr., Simon Marlow, and Satnam Singh. 2009. Parallel performance tuning for Haskell. In *Proceedings of the 2nd ACM SIGPLAN symposium on Haskell* (Haskell '09). ACM, New York, NY, USA, 81-92.

Sensor de temperatura multipunto empleando rejillas de Bragg con interrogación multiplexada en tiempo

A. Santiago-Toledo, Y. Bracamontes-Rodríguez, J. Castillo-Mixcóatl[1], G. Beltrán-Pérez, S. Muñoz-Aguirre
Facultad de Ciencias Físico Matemáticas, Benemérita Universidad Autónoma de Puebla
Av. San Claudio y 18 Sur, Col. San Manuel, C.U., Puebla, Pue. C.P. 72570, México.
[1]jcastill@fcfm.buap.mx

Abstract

Las rejillas de Bragg en fibra óptica son dispositivos muy versátiles que pueden ser empleados en una amplia variedad de aplicaciones. En particular son extremadamente útiles en el desarrollo de sensores. En este trabajo se presenta la implementación de un sensor multipunto con interrogación multiplexada en el tiempo, empleando rejillas de Bragg en fibra óptica. En particular se presentan los resultados para la interrogación de dos rejillas. El sistema propuesto es capaz de evaluar cambios de temperatura de hasta 0.01 °C.

Keywords: Sensores, FBG, Fibras Ópticas,

Introducción

Las fibras ópticas han revolucionado las telecomunicaciones en las últimas décadas. Mucho de este éxito se debe a las características ideales de las fibras: bajas pérdidas de trasmisión, alto nivel umbral de daño óptico, inmunidad a la interferencia electromagnética etc. [1]

Actualmente las fibras ópticas no solo permiten el guiado de luz para los sistemas de comunicaciones, sino que además han abierto nuevos caminos, como son aplicaciones en medicina o en sistemas de sensado.

Uno de los elementos más importantes son las llamadas Rejillas de Bragg (FBG por sus siglas en inglés). La característica principal de este dispositivo es su capacidad de filtrado, en su espectro de reflexión, la cual lleva a cabo con una alta eficiencia y muy bajas pérdidas [2].

Las FBG´s son elementos ópticos que tienen una aplicación importante en comunicación, instrumentación y sensores en el área de sensores se aprovecha la cualidad de corrimientos espectrales, y en función de la reflexión, se pueden evaluar diferentes parámetros físicos como son tensión, presión, temperatura entre otros [3]. Este es un dispositivo simple y que en su forma elemental es sencillamente una modulación periódica del índice de refracción del núcleo de una fibra óptica. En este trabajo se presenta un sensor de temperatura multipunto cuya interrogación de la respuesta de los sensores es multiplexada en el tiempo.

Desarrollo experimental

En la Fig. 1 Se muestra el sistema de sensado el cual monitorea la temperatura en distintos puntos. Este sistema consta básicamente de un diodo láser sintonizable marca Yenista, dos FBG con longitudes de onda Bragg en 1533 y 1539 nm aproximadamente, fibra SMF28 para separar las FBGs, un medidor de potencia PM100 de Thorlabs y una computadora para controlar el diodo láser y obtener las medidas de potencia mediante el PM100. Para determinar el comportamiento del corrimiento espectral del perfil de reflexión de las FBGs empleadas, fueron sometidas a cambios de temperatura y se determinó el espectro de reflexión para cada FBG.

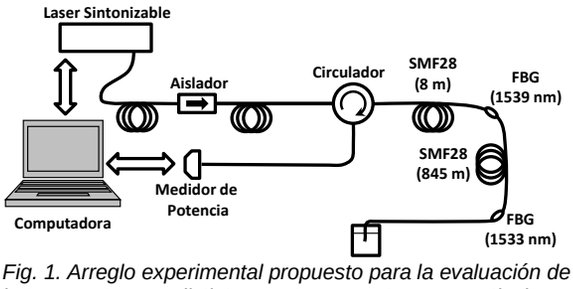

Fig. 1. Arreglo experimental propuesto para la evaluación de la temperatura en distintos puntos, en este caso particular solo se mide en dos lugares distintos separados por 845 m.

Una vez que se obtuvo el corrimiento espectral como función de la temperatura se procedió a determinar la región lineal en el espectro de reflexión de la FBG y mediante un programa elaborado en Matlab se eligió esta longitud de onda en el láser sintonizable. Los

cambios de potencia que se obtienen cuando existe un corrimiento en el espectro son cuantificados por el medidor de potencia y enseguida se determina la temperatura de las FBGs a través de las caracterizaciones previas.

Resultados

La Fig. 2 presenta el corrimiento espectral de una de las FBGs empleadas. La longitud de onda de Bragg a los 18 °C fueron de 1533 y 1539 nm aproximadamente. Solo por referencia la FBG a los 1539 nm mantiene su espectro de reflexión sin corrimiento debido a que se mantiene a temperatura constante.

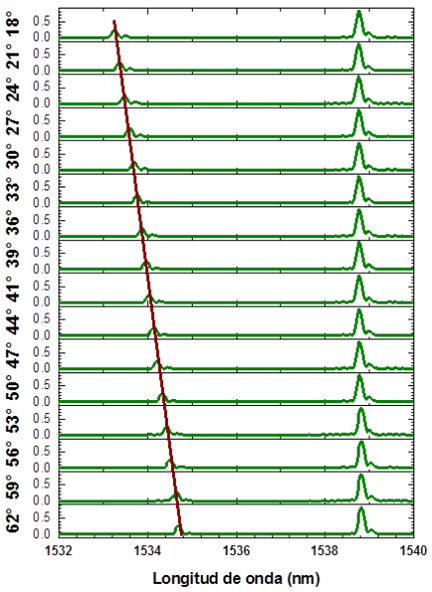

Fig. 2. Corrimiento espectral de la FBG_2 como función de la temperatura. Solo por referencia se muestra el espectro de la FBG, estable pues no se cambia su temperatura.

El corrimiento de la longitud de onda de Bragg como función de la temperatura para cada una de las FBG fue calculado, en la Fig. 3 solo se presenta el corrimiento de la longitud de onda de Bragg para la FBG entrada en 1533 nm.

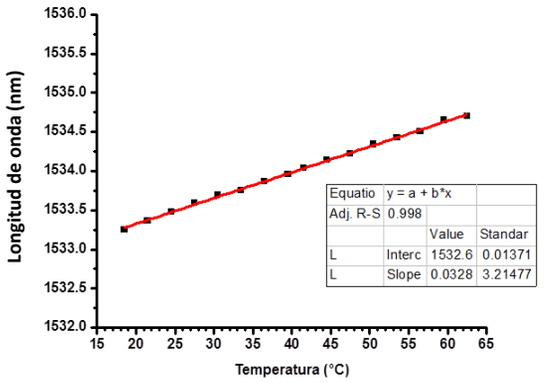

Fig. 3. Corrimiento de la longitud de onda de Bragg como función de la temperatura en la FBG. La sensibilidad de esta FBG fue de 32 pm/°C.

Una vez caracterizadas las FBGs, se procede a determinar la región de respuesta lineal del espectro de reflexión para cada FBG.

Fig. 4. Determinación de la región lineal del espectro de reflexión de la FBG centrada en 1533 nm.

En la Fig. 4 presenta el intervalo de longitudes de onda en la región lineal de la FBG alrededor de 1533nm.

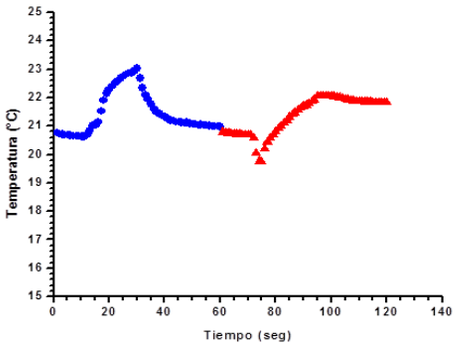

Fig. 5. Señal obtenida con el sensor funcionando plenamente, los cambios de temperatura se generan cuando uno de los autores coloca la mano sobre cada sensor.

Una vez determinadas las regiones lineales mediante un programa en Matlab se procede a interrogar cada FBG y con las sensibilidades de cada FBG se determina la temperatura de cada de ellas. En la Fig. 5 se muestra una curva obtenida en el tiempo cuando uno de los autores coloca la mano sobre cada un de las FBG en instantes distintos.

Conclusiones

Se desarrolló un sensor multipunto de temperatura empleando FBGs. Este sensor es capaz de evaluar cambios de ± 3 °C con una resolución de 0.01 °C. El sistema es completamente funcional y puede ser rápidamente modificado para evaluar tensiones sobre las FBG.

Referencias

[1] Govind P. Agrawal, “Fiber-Optic Commuincation Systems”, Wiley-Interscience, Chapter 1, pp. 1-4, 2002.
[2] A. Othonos, K. Kalli. “Fiber gratings and their applications” Artech House, pp. 9-10,21,60-70,1999.
[3] M. Durán-Sánchez, G. Beltrán-Pérez, J. Castillo-Mixcóatl, S. Muñoz-Aguirre, M. Méndez-Otero, Sensors and Actuators B, Vol 123, No. 2, pp. 816-821, May, 2007.

.

Electronic Design of Mandragora's Wireless Sensor Networks Motes

Francisco G. Flores García, Víctor D. Velasco Martínez, María de J. Flores Medina
Instituto Tecnológico de la Laguna
27200, Torreón, Coahuila, México

fflores@faraday.itlalaguna.edu.mx,
vvelasco@faraday.itlalaguna.edu.mx,
mflores@faraday.itlalaguna.edu.mx

Abstract

The hardware design of a Wireless Sensor Network mote, called Mandragora, is presented. The architecture was designed with modularity in mind. The primary modules functionality is described. Measuring tests of differently timed signals by some motes are done. Results comparing star and mesh topologies, and results of delays of sensed data by different motes are shown. Results are analyzed and discussed to describe the characteristics of the devices as data acquisitors.

Introduction

Wireless Sensor Networks (WSN) are one of the top trends in research. As WSN are complex systems of many autonomous devices, for larger deployments, cheaper devices are better. Mandragora is a project created to monitor agricultural fields [1]. The first revision was used to monitor soil's moisture. When prototypes were manufactured, some design flaws were found, thus a redesign was needed.

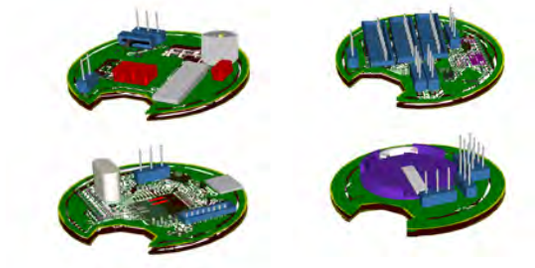

Figure 1 – New version mote's units in 3D View

Device Hardware and Description

Processing Unit

The processing unit has a PIC18F4550 micro-controller, a 512Kb EEPROM, and micro USB circuitry.

The micro-controller takes care of controlling the protocol and the hardware in all modules. It also has the user program in charge of data sensing: if it should be timed, by event, or by request.

It also exposes other internal peripherals of the micro-controller, as two PWM outputs, and three 10 bit ADC, and many general purpose digital input/output pins.

Transceiver Unit

The transceiver unit uses a MRF24J40, an 802.15.4-2003 compliant transceiver. It has both PHY and MAC stack on board.

The module also has a CSMA-RP connector for an antenna, and LEDs for monitoring mote's status.

Power Unit

One of the crucial features of WSN motes are power supply duration. This power unit uses a CR232 button battery. By the use of an AS1320 power regulator and elevator, mote's voltage supply is set on 3.3V.

It sports a regulator turn-off function, so the micro-controller can turn off the 3.3V output, effectively turning off the transceiver. This helps in power saving.

Acquisition Unit

This unit has one ADS8201 ADC. It is a 12 bit, 8 channel ADC. It has programmable gain, and the voltages references can be changed by two analog pins.

It has also an MCP4802, an 8 bit dual channel DAC. Each channel is an input of the voltage references pins of the ADS8201.

Both, programmabble gain, and the ability to control the voltage references through the MCP4802, enable sensing of small voltages much below the 12 bit resolution of the ADC. This is done directly from the microcontroller.

ADC's input channels are grouped in three blocks of three, and each block's voltage can be turned on and off from the microcontroller by using an FP1206. It also has configurable jumpers to set the voltage supply of each bank.

Firmware & Protocol

The motes are running a custom made operating system, to make it multi-tasking. It has control of the hardware and the communication protocol. The user application is embedded in the operating system.

Two protocols are used. First the 802.15.4-2003 star topology, done in hardware by the transceiver unit. Each mote communicates directly with the coordinator. Packets not directed to them by the coordinator are discarded.

The second protocol in use, is a simple flooding mesh protocol, used in the first version of Mandragora. All the motes can connect directly with the coordinator, but each mote has the promiscuous mode of the transceiver enabled, permiting them receiving data for other motes. If they find the data is not for them, they'll retransmit it in hope sometime they'll answer. This invalidates the hardware processing from the motes, and thus, times should be different.

Tests

A signal generator is put in sinusoidal wave mode, 3Vpp, +1.5V offset. The frequency of the generated signal is swept from 1Hz to 10KHz.

Three motes are prepared to sense the generated signal in the same channel. The coordinator issues requests every 100us to all motes to sense and transmit. This testbench is shown in Figure 2. The star topology is used.

The data received by the coordinator is sent to a computer through a serial port, and recorded in files. This test is repeated with the flooding mesh protocol.

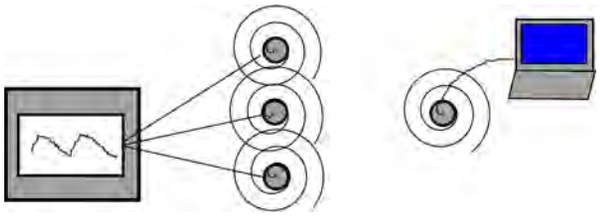

Figure 2 – Testbench

Results

All signals obtained in the first test are presented vs time, and compared between them. For the low frequency signals, the measurements recorded are almost the same between them, and similar to the original. When going up in frequency, a small offset is observed. In high frequencies the signal presents aliasing.

For the second protocol data, the same graphs are presented, showing a bigger offset, and aliasing at lower frequencies. Results of both protocols are contrasted.

Conclusions

The motes can be used to test signals in the sub-sonic frequency ranges. Heavy protocols can distort the instant when the mote starts sensing. Syncronization, and a tag indicating the time of the capture is good for signal reconstruction.

References

[1] M. de J. Flores M. et al. “Red Inalámbrica de Sensores para Monitoreo de Humedad Enterrada”. Proc. of the 7th Ibero-American Congress on Sensors, Lisbon, Portugal. November 9-11. November 2010

Implementación de un Sistema de Adquisición de Datos con comunicación inalámbrica para tres microsensores tipo CHEMFET

F. Pérez[1], C. Jiménez[2], E. Valdés[3], O. Arias de Fuentes[4§]
[1]Empresa Industrial para la Informática, las Comunicaciones y la Electrónica (GEDEME)
Callejón de Andrade y Prensa Latina, km 1 ½, Marianao, La Habana, Cuba.
[2]Instituto de Microelectrónica de Barcelona
Campus-UAB, 08193 Bellaterra, Barcelona, España
[3]Centro de Investigaciones en Microelectrónica Instituto Superior Politécnico José Antonio Echeverría
Apartado Postal 8016, Habana 8, Cuba.
[4]Instituto de Ciencia y Tecnología de Materiales, Universidad de La Habana
Zapata y G, Vedado CP 10400, C. Habana, Cuba.
§ E-mail: oarias@imre.oc.uh.cu; oarias@fisica.uh.cu

Abstract

En este trabajo se presenta el diseño e implementación de un Sistema de Adquisición de Datos para el monitoreo remoto de la concentración de iones en soluciones acuosas, basado en microsensores del tipo CHEMFET (Chemically Modified Field Effect Transistor). El sistema está formado por una Estación de Adquisición de Datos y una Estación de Procesamiento Central. La primera está constituida por un microcontrolador PIC, circuitos acondicionadores de señal y los sensores. La segunda la integran una microcomputadora y un instrumento virtual diseñado específicamente para esta aplicación, que permite el procesamiento, el almacenamiento y la presentación de la información adquirida por los sensores. Cada estación cuenta con un módulo para garantizar la comunicación inalámbrica entre ellas.

Palabras clave: SAD, CHEMFET, red inalámbrica de sensores, instrumentación

Introducción

La contaminación de los acuíferos debido a la agricultura y a la explotación minera es una problemática, cada vez más acuciante, que afecta a muchos países de Iberoamérica y Europa [1]. Por ello, la implementación de sistemas para determinar la presencia en el agua de elementos contaminantes, constituye una prioridad para la comunidad científica internacional.

La necesidad de disponer de sistemas de medición robustos, de bajo costo, que posibiliten una rápida respuesta y que funcionen ininterrumpidamente durante largos periodos de tiempo sin un gran mantenimiento, ha llevado hacia el desarrollo de sistemas multisensores que se puedan controlar remotamente mediante la implementación de redes de sensores inalámbricas.

Un aspecto importante para la optimización del funcionamiento de estas redes es la miniaturización de los sensores, ya que con ello es posible la reducción del consumo de energía, el incremento en la rapidez de la respuesta, el empleo de volúmenes pequeños de muestra y la compactación de los sistemas de detección, entre otros [2, 3, 4].

El objetivo de este trabajo está dirigido al diseño e implementación de un sistema de Adquisición de Datos (SAD) -para su utilización en lugares de difícil acceso- con el empleo de microsensores del tipo transistores de efecto de campo modificados químicamente (CHEMFET, por las siglas de su denominación en inglés; Chemically Modified Field Effect Transistor), que asegure el monitoreo remoto, con comunicación inalámbrica, de la concentración en soluciones acuosas de iones de interés medioambiental.

Concepción general del SAD

El Sistema de Adquisición de Datos que se diseña está constituido por dos módulos diferentes: la Estación de Adquisición de Datos (EAD) y la Estación de Procesamiento Central (EPC). La primera, ubicada en el sitio donde se necesita tomar las muestras, está formada por tres canales de medición para determinar la concentración de iones diferentes y otro para medir la temperatura. La segunda se sitúa en el lugar donde se procesa centralmente la información recibida, se muestra al usuario y se toman las decisiones. El sistema garantiza la comunicación bidireccional por radio entre las dos estaciones.

Diseño del hardware

La EAD está integrada por los tres microsensores, un sensor de temperatura, los circuitos acondicionadores de señal, un microcontrolador y un módulo de comunicación inalámbrica.

Como circuito acondicionador de señal para los CHEMFETs se seleccionó una variante simplificada de la topología denominada seguidor de drenaje y fuente [5].

Para la digitalización de las señales analógicas entregadas por los circuitos acondicionadores, así como el acoplamiento con el módulo de comunicación inalámbrica, se utiliza el microcontrolador PIC 16F877A, que constituye el elemento fundamental de la EAD.

Como dispositivos de comunicación inalámbrica, se seleccionaron los del tipo XBee, fabricados por MaxStream y basados en la tecnología ZigBee 802.15.4 [6].

La EPC está constituida por una microcomputadora personal, un instrumento virtual soportado en LabVIEW y otro módulo XBee acoplado a la microcomputadora por medio de la interfaz serie RS-232.

Diseño del software

Se implementan dos aplicaciones de software.

Una, el instrumento virtual diseñado en LabVIEW, que se ejecuta en la EPC y mantiene el control y la dirección de todo el proceso de medición. Este tipo de instrumentación con el ambiente gráfico que ofrece el LabVIEW constituye una interfaz con el usuario económica y de fácil empleo, que permite el procesamiento, visualización y almacenamiento de la información [7].

La otra, diseñada con el empleo del *PIC C Compiler,* que se ejecuta en el microcontrolador, y que permite adquirir y digitalizar el valor de tensión analógica que se recibe de la salida del circuito de polarización y su envío hacia la EPC mediante el módulo de comunicación inalámbrica. Por otro lado, esta aplicación facilita el procesamiento de las indicaciones recibidas desde la EPC y su ejecución.

Simulación de la comunicación entre la EAD y la EPC

En la Fig. 1 se muestran los resultados de la simulación realizada de la comunicación entre la EAD y la EPC. Para ello se empleó el Proteus 7.7 de Labcenter Electronics.

En la ventana ubicada en la parte inferior derecha se muestra la cadena de caracteres (b6a) enviada por el PC al microcontrolador para solicitar la medición de los canales en uno de los tres modos de trabajo establecidos.

A partir de esta orden se ejecuta entonces por el PIC la adquisición de las señales, su digitalización y su transmisión. Los caracteres transmitidos por el PIC y recibidos por el PC (valores de voltaje de RV0, RV1, RV2 para calcular la concentración de iones en tres canales y el valor diferencial de RV3 y RV4 para la temperatura) pueden observarse en la ventana ubicada en la parte inferior izquierda.

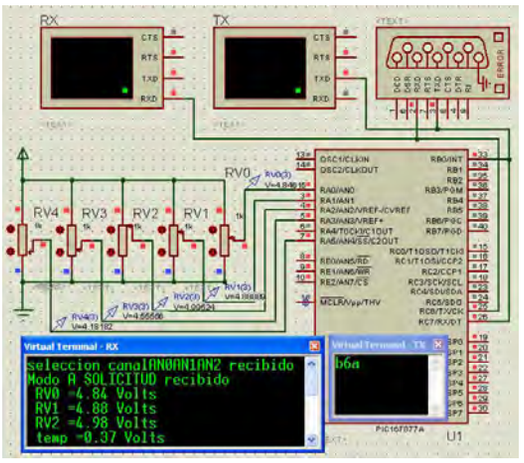

Fig.1: Simulación en Proteus de la comunicación entre la EAD y la EPC.

Agradecimientos

Los autores desean expresar su agradecimiento al Proyecto CYTED 510AC0408 "REDSENS" por las posibilidades de colaboración que ha brindado para la ejecución de este trabajo.

Referencias

[1] Redes de Sensores y Microsistemas para el Control del Impacto de la Producción Agrícola y la Minería en los Acuíferos, disponible en http://redsensa.ibersensor.org/. Consultado en: abril 2012.

[2] O. Arias de Fuentes; "Sensores electroquímicos fabricados con tecnología microelectrónica: ISFET y CHEMFET. Aplicaciones en el control del medio ambiente", Curso CYTED "Microsistemas y sensores", Montevideo, 2006.

[3] C. Jiménez, C. Domínguez, O. Arias de Fuentes, A. Lastres, E. Valdés; "Microsensores de estado sólido tipo ISFET: Estructura y fundamentos", Sensores y Microsistemas, Buenos Aires, Vol. II, 2006.

[4] C. Jiménez, J. Orozco, A. Baldi; Sensors, Vol. 10, pp. 61-83, 2010.

[5] P. Bergveld; Sensors and Actuators B, Vol. 88; pp. 1–20, 2003.

[6] MaxStream; "XBee/XBee-PRO OEM RF Modules"; Product manual v1.06, UK, 2005.

[7] E. Valdés; "Desarrollo de una instrumentación virtual para la caracterización de dispositivos ISFET", Tesis doctoral, Universidad Autónoma de Barcelona, 1998.

Aplicación de puertas de enlace en topologías de redes Zigbee

Hesner Coto-Fuentes[1], Francisco Valdés-Perezgasga[2], Enrique E. Valdés-Zaldivar[1]
[1]Instituto Superior Politécnico José Antonio Echeverría,19390, La Habana, Cuba
[2]Instituto Tecnológico de la Laguna, 27000, Torreón, Coahuila, México
hesnercf@gmail.com

Resumen

Las topologías utilizadas en redes Zigbee necesitan que coordinadores y ruteadores permanezcan encendidos para garantizar la gestión e integridad de la red. En el presente trabajo se describe una primera aproximación a la implementación y aplicaciones de una red Zigbee, donde al elemento coordinador y a los ruteadores se les ha incorporado la electrónica necesaria para interconectarse con equipos portátiles u otras redes operando con protocolos diferentes (gateway), extendiendo las prestaciones y operatividad de sistema donde se integre a los sensores la comunicación.

Palabras claves: zigbee, coordinador, ruteadores, interconectar, equipos portátiles, redes

Introducción

Las redes de sensores son principalmente utilizadas en ambientes industriales, permitiendo el monitoreo y control de los procesos productivos que en ellas se llevan a cabo [1]. El desarrollo de la industria electrónica ha permitido la integración y disminución de los costos, justificando junto a las ventajas de un estudio extensivo de variables de interés, la expansión de las redes de sensores a ramas como la meteorología, la domótica, la salud y la agricultura.

En el presente trabajo se describe una primera aproximación a la implementación y aplicaciones de una red Zigbee, donde al elemento coordinador y a los ruteadores se les ha incorporado la electrónica necesaria para interconectarse con equipos portátiles u otras redes operando con protocolos diferentes (gateway). La posibilidad antes descrita, junto a la necesidad de dichos dispositivos (coordinador y ruteadores) de mantenerse encendidos para garantizar la integridad de la red Zigbee, permite la extensión de las redes y sus prestaciones, así como su consulta y configuración a partir de dispositivos portátiles como teléfonos celulares, laptop y computadoras de escritorio.

Zigbee

El Zigbee es un protocolo de la capa de red que comúnmente utiliza módulos digitales de baja potencia basados en el estándar de hardware 802.15.4, diseñado para aplicaciones inalámbricas de baja transferencia de datos (<250 kbps) y operar en las bandas ISM (Industrial, *Scientific and Medical*) permitidas. Toda red Zigbee está compuesta por: un coordinador, encargado de iniciar y gestionar la red; un número opcional de ruteadores y un número opcional de dispositivos finales [2,3].

Entre las topologías que permite el protocolo se encuentran:

- Topología estrella
- Topología malla
- Topología árbol

La figura 1 muestra un ejemplo de red Zigbee utilizando topología de árbol.

Figura 1. Estructura de una red Zigbee utilizando topología de árbol.

Desarrollo

Partiendo de las características y los elementos de una red Zigbee a los nodos coordinadores y ruteadores se les han extendido las funciones al añadirle los componentes de *hardware* necesario para servir de puerta de enlace con otros protocolos, como podría ser: Bluethooth, Wifi, GSM, RS232, etc. Debido a que deben estar siempre energizados también se les incorporó la capacidad de almacenamiento en memoria externa, por lo que

dado el caso de perderse la conexión humana con la red, o de ser necesario su funcionamiento aislado, el sistema no perdería datos.

La figura 2 muestra a la izquierda el impreso de un nodo con puerta de enlace Zigbee – Bluetooth, a la derecha ambas capas de un nodo *de dispositivo final*. Los elementos más importantes que lo componen son los módulos de comunicación inalámbrica, una memoria y un microcontrolador, encargado de controlar el enlace entre módulos, el almacenamiento en la memoria, etc.

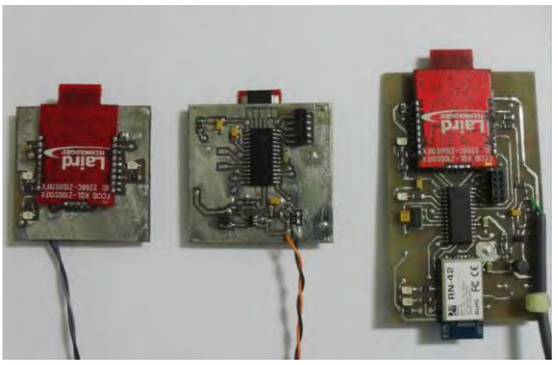

Figura 2. Nodo coordinador (izquierda) y de dispositivo final.

La inserción espacial correcta de nodos como el descrito en una red permite, por ejemplo: la consulta de datos, configuración, y actualización de todos los nodos de la red utilizando un equipo portátil como podría ser un *Smartphone* o una *Notebook*. En el caso que se analiza se utilizo durante la implementación y puesta a punto de los nodos una Galaxy Tab de Samsung con sistema operativo Android 2.2, para el cual fue necesario desarrollar el *software* correspondiente.

Aplicaciones

La figura 3 muestra un esquema donde se representa una variante de red utilizando las características antes mencionadas.

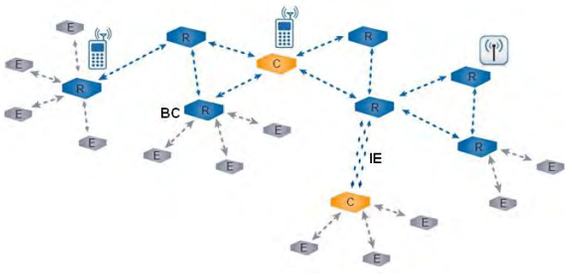

Figura 3. Red Zigbee utilizando topología de árbol y nodos con puerta de enlace.

En la figura, el coordinador, así como el ruteador de la izquierda realizan la función de enlace a través de Bluetooth, permitiendo la conexión, consulta y modificación de los nodos en la red utilizando dispositivos móviles. Con líneas cruzadas se representa una extensión de la red atravesando una zona de interferencia electromagnética (IE) utilizando un estándar cableado. Por último otro de los nodos realiza el enlace utilizando Wifi.

Una aplicación actualmente en progreso y precursora del presente trabajo es la colocación de nodos en pozos urbanos con la instrumentación necesaria para medir diferentes parámetros en el agua. La operatividad de la red, manipulación y configuración de los datos podría realizarse desde distintas localidades tomando en cuenta el área que abarcaría la red, utilizando según la locación un dispositivo portátil o una PC de escritorio.

Conclusiones

La utilización de puertas de enlace en los elementos ruteadores y en el coordinador permite extender las prestaciones de las redes Zigbee al facilitar la consulta, configuración y actualización de los integrantes de la red. Permite también diversificar las aplicaciones de dichas redes, incidiendo en el alcance, compatibilidad y condiciones de trabajo según el sistema donde se inserten.

References

[1] Labiod, H., “Wi-fi, Bluetooth, Zigbee and WIMAX”, Springer, 2007.

[2] Laird Technologies, “ZB2430 WIRILESS MODULE User manual”, v2.1, 2009.

[3] Gratton, Dean A., “Developing Practical Wireless Applications”, Elsevier, 2007.

Sistema Inalámbrico de Medición de CO con Interfaz sobre Teléfono Inteligente.

David Santiago Flechas, Nestor Misael Peña, Fredy E. Segura-Quijano
Universidad de los Andes
Bogotá, Colombia
{ds.flechas72}{npena}{fsegura}@uniandes.edu.co

Abstract

En este trabajo se presenta el diseño de un sistema inalámbrico el cual permite adquirir señales de un sensor de monóxido de carbono (CO) comercial, y transmitir su información por medio de bluetooth a un teléfono inteligente. Adicionalmente en el teléfono inteligente se pueden visualizar las concentraciones de CO y la localización geográfica del sensor, Con este esquema el sistema busca medir de manera más eficiente los niveles de contaminación de la ciudad de Bogotá-Colombia teniendo una mayor trazabilidad; la cual dependerá de la cantidad de sensores que se puedan tener funcionando en un determinado momento.

Keywords: Contaminación, CO, Monitoreo ambiental, Redes de sensores, Andorid.

Introducción

Actualmente la medición del aire en la ciudad de Bogotá-Colombia está a cargo de la Secretaría de Ambiente por medio de una Red de Monitoreo de Calidad del Aire (RMCAB) [1]. Esta red basa su funcionamiento en un sistema de monitoreo ambiental en tiempo real y cuenta con 15 estaciones distribuidas a lo largo de la ciudad. De las 15, 12 estaciones son mixtas para monitoreo de contaminantes y meteorología, dos son estaciones para medida de variables meteorológicas, otra es una estación móvil y la estación central de datos.

El objetivo principal de la RMCAB es la verificación del cumplimiento de las normas de calidad del aire con el fin de determinar las áreas críticas responsables de los niveles de contaminación de la ciudad, dado que Bogotá está entre una de las ciudades más contaminadas del mundo [2].

En el desarrollo de este proyecto se estudia la utilización de plataformas móviles como herramienta de desarrollo. Actualmente ya hay aplicaciones en el campo de la salud, el transporte y el control ambiental que se basan en este tipo de plataformas para su funcionamiento. La utilización de sensores sobre una red inalámbrica (WSN) para la medición de parámetros ambientales se describe en [3,4]. En el área de la salud existe extensiva documentación respecto a aplicaciones que integran el sistema operativo Android sobre redes de sensores; por ejemplo un sistema de recolección, procesamiento y almacenamiento de datos vitales de personas, al igual que estadísticas espacio-temporales integrado con dispositivos inalámbricos y sensores ambientales y biológicos [5]. También se han desarrollado y validado interfaces de control cerebro-musculo-computador basadas en Android, destinadas al uso de personas severamente paralizadas [6].

El objetivo de este trabajo es el diseño de un sistema de medición de CO distribuido, de bajo costo y basado en la plataforma móvil Android que permita complementar la infraestructura existente en el campo del control ambiental en la ciudad de Bogotá

Materiales y Metodología

El prototipo del sistema consta de el modulo del sensor, el dispositivo móvil con la aplicación sobre la plataforma Android, y el servidor WEB. Además se las interfaces de comunicación entre los componentes del sistema es mediante bluetooth e internet respectivamente.

En la fase actual del proyecto solo se contempla el desarrollo de la funcionalidad del sensor y el dispositivo móvil. La aplicación sobre el servidor WEB es parte del desarrollo futuro.

A. Módulo Sensor

La referencia utilizada para el sensor es: Sparkfun MQ7. Este es un sensor de CO de bajo costo, utilizado previamente en proyectos similares [7,8]. Es un sensor de tipo resistivo. El control del MQ7 se realiza mediante dos ciclos

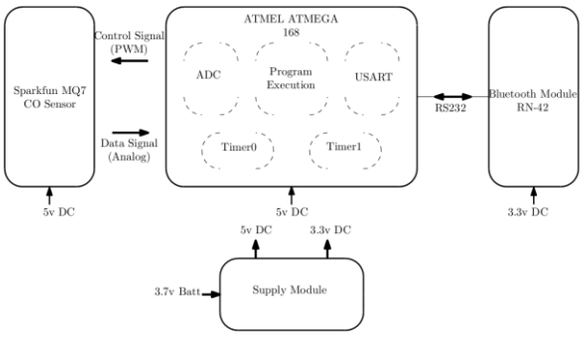

Figura 1. Diagrama de Bloques Tarjeta Sensor.

de funcionamiento: Purga y Estabilización. En el primero se aplica un voltaje de 5V durante 60s, con lo cual se eliminan residuos de CO mediante calentamiento. Durante la estabilización el voltaje aplicado es de 1.4V durante 90s; al cabo de este tiempo es posible realizar la lectura del sensor.

La integración del este sensor al sistema se realiza a partir de una tarjeta, cuyo diagrama de bloques se muestra en la Figura 1. Dicha tarjeta este compuesta por el sensor mencionado, un micro-controlador ATMEGA 168A, encargado de el control y la lectura del sensor MQ7, adicionalmente envía los datos al modulo bluetooth por medio del protocolo RS232. El modulo Bluetooth RN42 es una interfaz RS232-Bluetooth. Por ultimo el esquema de alimentación se basa en una batería recargable Li-Po de 3.7V(1000mAh) y un cargador/elevador USB a 5V.

B. Aplicación en Android

Dadas las características y facilidades que de la plataforma Android es posible el diseño de aplicaciones complejas soportadas por cada vez un mayor número de dispositivos móviles, menos costosos y con mejor desempeño. [3]

La aplicación diseñada consiste en dos interfaces de usuario cada una con una funcionalidad específica. En la primera (Fig.2) se observa la localización del sistema (Modulo Sensor – Dispositivo Móvil) marcada por un punto. El color del punto esta determinado por el nivel de concentración de CO en el lugar. En la segunda interfaz (Fig. 3) es posible visualizar los niveles de CO a través del tiempo en una grafica dinámica lineal.

Resultados y Conclusión

En las figuras 2 y 3, se muestran las funcionalidades de los sistemas asociadas a la visualización de los niveles de CO y a la localización geográfica del mismo respectivamente.

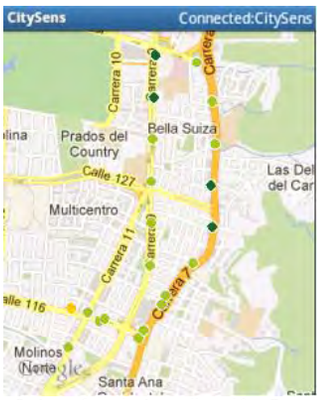

Figura 2. Interfaz de Localización Geografica.

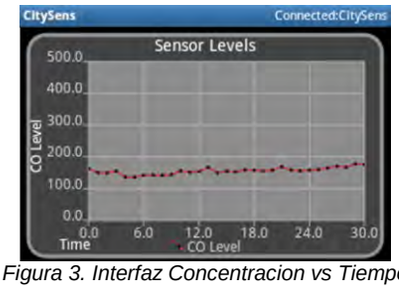

Figura 3. Interfaz Concentracion vs Tiempo

Es posible mejorar el desempeño del sistema mediante la adquisión de sensores de CO con mejor desempeño en cuanto a precisión y tiempos de medición.

Con este primer prototipo se ha podido validar la efectividad de las plataformas móviles como herramientas tecnológicas viables para el diseño de aplicaciones. Tanto el software como el hardware de estas plataformas son adecuados para su integración con sensores y redes de sensores.

Referencias

[1] Secretaria Distrital de Ambiente Bogotá D.C.," Red de monitoreo de calidad del aire (RMCAB)." [Online] http://ambientebogota.gov.co/red-de-calidad-del-aire

[2] Andrea Niño Penagos, "Red de monitoreo de calidad del aire de Bogotá (RMCAB)," 2011.

[3] L. Shum, P. Rajalakshmi, A. Afonja, G. McPhillips, R.Binions, L. Cheng, and S. Hailes, "On the development of a sensor module for real-time pollution monitoring," in Information Science and Applications (ICISA), 2011 International Conference on, pp. 1-9, april 2011.

[4] N. Moreira, M. Venda, C. Silva, L. Marcelino, and A. Pereira, "@sensor - mobile application to monitor a wsn," in Information Systems and Technologies (CISTI), 2011 6th Iberian Conference on, pp. 1-6, june 2011.

[5] M. Mitchell, F. Sposaro, A.-I. Wang, and G. Tyson, "Beat: Bio-environmental android tracking,"in Radio and Wireless Symposium (RWS), 2011 IEEE, pp. 402-405, jan. 2011

[6] S. Vernon and S. Joshi, "Brain-muscle-computer interface: Mobile-phone prototype development and testing," Information Technology in Biomedicine, IEEE Transactions on, vol. 15, pp. 531

Qualitative Analysis of Brandies by Means of a Voltammetric Electronic Tongue

Xavier Cetó[1], Matias Llobet[2], Joan Marco[2], Salvador Alegret[1], Manel del Valle[1]
[1] Sensors and Biosensors Group, Department of Chemistry, Universitat Autònoma de Barcelona, Edifici Cn, 08193, Bellaterra, Barcelona, SPAIN
manel.delvalle@uab.cat
[2] Miguel Torres SA, Vilafranca del Penedès, Barcelona, SPAIN

Abstract

This work reports the application of an Electronic Tongue (ET) in the analysis of brandies. For this, a voltammetric ET formed by an array of epoxy-graphite sensors, bulk-modified with different electrochemical catalysts, was used. Departure information was the set of voltammograms generated with the sensor array and Linear Discriminant Analysis (LDA) was used for building the classification model. Good discrimination was prediction ability was attained, therefore permitting the correct classification of the different samples under study.

Keywords: Electronic Tongue, Linear Discriminant Analysis, voltammetric sensors, classification, brandy

Introduction

Over the last years, a promising approach to analyze liquid samples is arising; this consists in the use of Electronic Tongues (ETs) [1,2]. Such systems are formed by an array of sensors where several sensing units, which exhibit different responses to various compounds, are coupled with advanced signal processing methods based on pattern recognition or multivariate models, which allow the qualitative or quantitative analysis of different samples parameters.

Classification of brandy samples is usually performed by a skilled sensory panel, given the difficulties to perform this classification using a classical analytical instrument. The obtaining of an automated method would allow to significantly reduce brandy tasting by the panel, even not replacing the panel, but increasing the number of samples that can be analyzed and allowing its use as screening method either to asses they guarantee quality control standards or to detect any adulteration or contamination.

The main goal of this work was the development of an ET that could be useful for recognizing and discriminating the different types of brandies, in a similar way a sensory panel would do and also adulterations in the production process. To this end, samples were measured using an array of modified voltammetric sensors, evaluating its response with a pattern recongnition method that will allow the discrimination of the different samples.

Experimental and Methods

An array of 6 voltammetric graphite-epoxy sensors made with different modifiers added to the bulk mixture were constructed according to our group methodology and based on previous studies [3]. Among those, five of them were modified by adding components such as cobalt phtalocyanine, conducting polymer as polypyrrole and metallic nanoparticles such as those of copper, platinum and silver to the bulk mixture – one component per electrode.

The ET was formed by the 6-sensor voltammetric array and a reference double junction Ag/AgCl electrode plus a commercial platinum counter electrode. Cyclic Voltammetry measurements were taken in a multichannel electrode configuration in quiescent conditions and room temperature (25 ºC).

The preprocessing of the data was based on extracting the selected features from the voltammogram of each sensor by means of Fast Fourier Transform (FFT) and entering those as the input information in an LDA model.

A total of 74 brandy samples, which were divided into two different sets, were analyzed. In the first case (41 samples), taste attributes were taken into account; while in the second (33 samples), the effect of the use of pieces of wood in the aging of brandy was studied.

Results

Evaluation of ET discrimination capabilities was attempted by the use of LDA. In this way,

two different classification models were built (one for each of the sets of samples) and i ts prediction performance was evaluated employing leave-one-out cross validation method.

Taste Attributes

Firstly, discrimination of brandies according to the scores obtained from a sensory panel was attempted. In this manner, samples were divided into three classes which correspond to the scores given by the expert's panel according to its organoleptic profile. As can be seen in Figure 1, clear discrimination was achieved for the three classes.

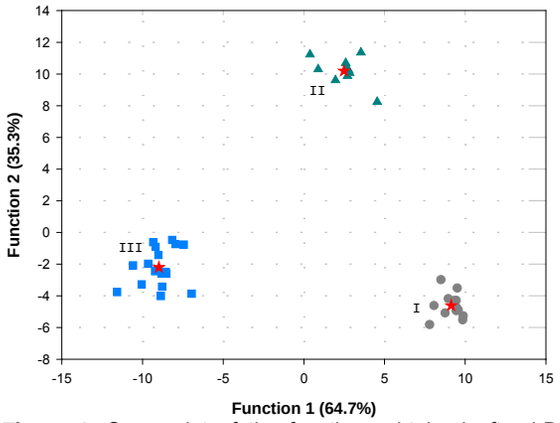

Figure 1. Score plot of the functions obtained after LDA analysis of the brandy samples, according to its taste category.

Aging of the brandy

In a second attempt, the effect of the use of pieces of wood in the aging of brandy was evaluated. That is, if the ET was capable to distinguish traditional aged samples from those using alternatives methods such as those using chips or staves to faster the rate of ageing. As before, Figure 2 shows the LDA score plot where clear discrimination between different aging methods could be seen.

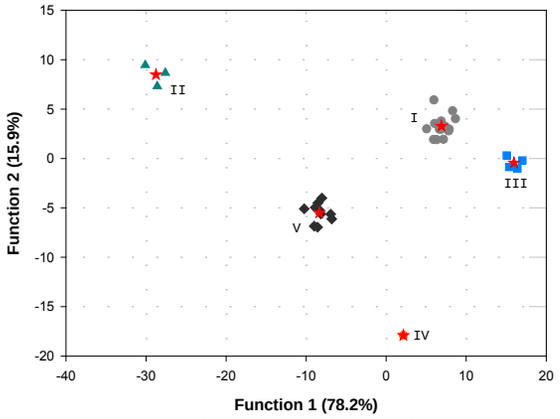

Figure 2. Score plot of the functions obtained after LDA analysis of the brandy samples, according to the aging method used.

Conclusions

Electronic Tongues have proved to be a useful analytical tool able to provide information of either the detection of the use of alternative ageing practices such as the use of pieces of wood or to asses a quality index of brandy samples according to skilled sensory panel results.

In this sense, ET represent an alternative to traditional methods with advantages over those such as being a fast-response and low-cost method for its characterization, really suitable for screening analysis.

Acknowledgments

This work was supported by MICINN trough the project CTQ2010-17099. X.Cetó thanks the support of AGAUR for the predoctoral grant.

References

[1] P. Ciosek and W. Wroblewski, Analyst, Vol. 132, No. 10, pp. 963-978, 2007

[2] M. del Valle, Electroanalysis, Vol. 22, , pp. 1539–1555, 2010

[3] X. Cetó, J.M. Gutiérrez, M. Gutiérrez, F. Céspedes, J. Capdevila, S. Mínguez, C. Jiménez-Jorquera and M. del Valle, Analytica Chimica Acta. doi: 10.1016/j.aca.2012.02.026

Chapter 8: Microfluidics and Micro-Total-Analysis-Systems

PAN/starch composite nanofibers as a selective membrane for sensors and microTAS

A. N. R. da Silva[a,b], M. L. P. da Silva[a,b] R. N. R. Dias[b], L. Sayuri[b] and E. R. Fachini[c]

[a]Department of Engineering of Electronic Systems, University of São Paulo,
São Paulo 05508-090, SP, Brazil
[b]Materials, Process, and Electronic Components Course, College of Technology of São Paulo
São Paulo 01124-000, SP, Brazil
[c]College of General Studies, University of Puerto Rico at Río Piedras
San Juan 00931, PR, USA
neilde@lsi.usp.br, malu@lsi.usp.br

Abstract

A composite material made of PAN (polyacrylonitrile) and starch granules using dimethylformamide as solvent was electrospinned to produce fibers and used as a selective membrane for volatile organic compounds (VOCs) and water in gaseous phase. Tests revealed that fibers incorporated starch granules and also that the composite are sensible for water but not VOCs; therefore, it is a good choice as selective barrier on sensors or microTAS protection.

Keywords: PAN, starch, electrospinning, composite, VOCs, water

Introduction

Membranes can merge different functions in one material, i.e. are useful not only for microTAS (micro total analysis system) devices [1] but also as sensitive layers in sensor devices [2]. Due to the small dimension on such devices, these membranes must be thin and able to cover rough topography, which make nanofibers good candidates for these functions. Moreover, whereas a continuous membrane will show diffusion effects [3] the small diameter of nanofibers will prevent it. The nanofibers can be produced by several different methods, but electrospinning is an ease and cost-effective process [4]. Furthermore, these fibers can be modified by the incorporation of active particles, which is a promising route to increase sensibility and/or to protect sensitive surfaces. An example is starch granules protected by fluorinated film for controlling of volatile organic compounds (VOC's) contamination [5]. Thus, this work proposes for the first time the production of PAN fibers modified with starch electrospun over a sensitive structure and test the material for water or VOCs air contamination.

Experimental

Fibers were produced by electrospinning using dispersion of starch granules from Cassava (*Manihot esculenta* Crantz, 5 μm diameter) [5] and polyacrylonitrile (PAN, Sigma Aldrich) in dimethylformamide (Sigma Aldrich). PAN/starch mass ratio was: 1:0.1; 1:1; 1:3, 1:5 and 1:7. The electrospinning setup was described elsewhere [6]. Films were obtained by spinning the same solutions, 6000 rpm, 1 minute. Silicon was used as substrate during fiber deposition. Fiber characterization uses optical and Scanning Electron microscopy (SEM). Chemical characterization was performed by Infrared spectroscopy to determined starch presence. Adsorption of VOCs and water was verified using Quartz crystal microbalance [5]. Relative viscosity of starch/PAN dispersions was measured in order to provide a model of composite fiber formation.

Results and Discussion

This composite material was produced in two different forms: as a thin film and as a fiber, but optical microscopy did not show any sensible difference. Moreover, film layer did not peel during several weeks, which pointed out that the composite material presents low stress. Figure 1a shows typical results for fiber obtained from optical analysis; as can be seen some of starch granules just rely on the surface of the fiber i.e without a strong connection between them. Otherwise, the SEM analysis shows that the addiction of starch granules increase the bead formation (Figure 1b) and the cluster

formation (Figure 1c). The fiber diameter is quite dependent on starch concentration, as evaluated by SEM and presented in the graph in Figure 2a.

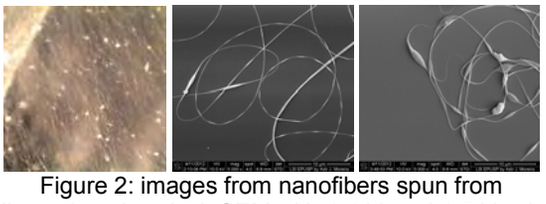

Figure 2: images from nanofibers spun from dispersion a) optical, SEM with 1:1 b) and 1:5 b) w/w PAN/starch.

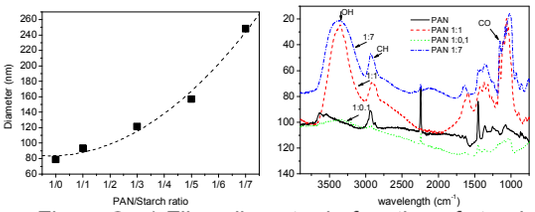

Figure 2: a) Fiber diameter in function of starch concentration, b) FTIR spectra for PAN and PAN/starch granules

The increase on diameter is owing to particle insertion on the fiber (see FTIR results). The increase in diameter is also correlated with bead formation due to the strong interaction, probably by hydrogen bond formation, between polymer molecule and starch surface. Thus, during the fiber formation, the flow is hindered by the surface charges present on the starch particle and bead formation is favored. FTIR shows that fibers are impregnated with starch granules in all mass ratios, as can be seen in Figure 2b. In this figure, bands for PAN spectrum (black line) are consistent with the assignment made by Serkov [7], furthermore bands are well defined indicating a high ordered structure. However, even for mass ratio of 1:0.1, the inclusion of starch granules leads to broader bands, i.e. interaction between the molecule and the environment, and the appearance of CO (1190-950cm^{-1}) and OH (3600-3000cm^{-1}) species, characteristic of cassava starch [8]. Moreover, CH bands (2933 and 2881 cm^{-1}) are merged, also due to strong interaction between granule and polymer molecule. For PAN, there is a direct correlation among viscosity, concentration and fiber diameter [9]. The inclusion of starch granule in the dispersion decreases the relative viscosity probably due to the adsorption of the polymer molecules on the surface of the granule. However, the fiber diameter did not diminish due to the starch presence, which is consistent with the starch insertion inside the fiber, as obtained by FTIR.

QCM analysis was provided simply electrospinning the fiber on the piezoelectric quartz crystal. The deposition decreases the QCM signal in approximately 100 Hz, i.e. just low amount of material is deposited on the surface. The exposure to n-hexane or 2-propanol did not change the signal whereas the presence of water (10% of relative humidity) also changes the signal, reversibility and in approximately 10 Hz. Therefore water molecule can permeate PAN fiber, probably due to hydrogen bond formation, but not the 2-propanol molecule, probably owing to the molecule size. A strong hydrogen bond linking nylon-6 nanofibers was already proposed [10], which reinforces the idea of water selective permeation from PAN fibers. Inside the fibers, starch will act as a scaffold and will retain a large amount of molecule, which explains the 10Hz variation. This effect can be used in several different manners, such as preconcentration on microTAS or as a sensible layer on a sensor device. The behavior of cassava starch granules was different on PAN fibers if compared with fluorinated composite obtained by Lima [5]. On such case, the permeable thin film also allows the concentration of 2-propanol. However, the use of fibers are more advantageous since avoids diffusion effects that delay QCM measurements, as obtained by Macagnano with Zn-porphyrin film [3].

Conclusions

Tests revealed that fibers incorporated starch grains and also that the composite are sensible for water but not VOCs. The results suggest that the PAN/starch nanofibers mat is a good choice as selective membrane on sensors or microTAS protection.

Acknowledgments

FAPESP and CNPq for financial support.

References

[1] M. Ulbricht, Polymer, vol. 47, pp. 2217–2262, 2006.
[2] C. Elosua, et. al., Sensors vol. 6, pp. 1440-1465, 2006.
[3] A. Macagnano, et al, Thin Solid Films Vol. 516, No. 21, September, pp. 7857-7865, 2008.
[4] S. K. Nataraj, et al., Progress in Polymer Science, Vol. 37, No. 3, March, pp. 487-513, 2012.
[5] R. R. Lima, et al., Sensors and Actuators B, vol. 141, July, PP. 349–360, 2009
[6] A. N. R. da Silva, et.al., II SBPMat, Brazilian MRS Meeting 2003, Rio de Janeiro, Brazil, 26-30 oct. 2003.
[7] A. T. Serkov, Fibre Chemistry Vol. 39, No. 1, pp. 60-63, 2009
[8] K. Kaewtatip, V. Tanrattanakul, Carbohydr. Polym., Vol. 73, No. 4, pp. 647–655, 2008.
[9] J-H. He, et al., Fibers and Polymers Vol.9, No.2, pp. 140-142, 2008.
10 H. R. Pant, et al., Colloids and Surfaces A, Vol. 370, No. 1–3, November, pp. 87–94, 2010

Continuous Flow Analytical Microsystem for Ammonium Determination Incorporating a Gas-Diffusion Membrane and Potentiometric Detection

A. Calvo, O. Ymbern and J. Alonso
Group of Sensors and Biosensors
Autonomous University of Barcelona, 08193, Bellaterra, Spain
antonio.calvo@uab.cat

Abstract

A potentiometric microsystem based on the polymer technology, selective for ammonium ion detection, was developed. The device integrates in a single substrate, comparable in size to a credit card, microfluidics, gas-diffusion module and working electrode. The working electrode consists in an ion selective electrode (ISE) built by an epoxy-graphite transducer and an ammonium polymeric membrane. The results shows that the microsystem developed can be used to monitor on-line ammonium ions in treated water samples.

Keywords: Ammonium detection, COC, Analytical microsystem, Gas-diffusion membrane, Potentiometric detection, Ion-selective electrode.

Introduction

Ammonium ion is a parameter to take into account to control the water quality. To date, on-line ammonium analyzers have been developed by incorporating a gas-diffusion membrane to improve their selectivity [1]. However, their large size prevents their use in certain applications that require robust, portable and low cost on-line analytical microsytems with low detection limits and with low sample and reagent consumption [2].

In this sense, our group has a large experience in the miniaturization of this type of analyzers [3], by means of Low Temperature Co-fired Ceramics (LTCC) technology. However, this technology is not optimal for the case of ammonium ion microanalyzers construction, due to the incompatibility between the high temperatures reached during the sintering step in the LTTC construction process and the plastic gas-diffusion membrane integrity.

In order to overcome this drawback, the polymer technology has been selected, using as a substrate Cyclic Olefin Copolymer (COC). This technology shares with LTCC technology the advantages of easy prototyping, economic production and the ability to perform tridimensional structures [4]. Furthermore, it is perfectly compatible with the integration of gas-diffusion membranes. These benefits are attached to those provided by continuous flow analysis technique like versatility, speed of analysis, simplicity, connectivity and automation of the analytical procedure, among others [5].

Moreover, Ion Selective Electrodes (ISEs) are potentiometric sensors based on permselective membranes, which can be easily integrated in automated devices for continuous water samples monitoring [6].

The present work proposes a COC-based ammonium potentiometric microanalyzer, using the technique of flow injection analysis (FIA). The device integrates in a single substrate, comparable in size to a credit card, microfluidics, gas-diffusion module and working electrode.

Experimental

The sensor was built using the multilayer approach of the polymer technology [7]. The fabrication process follows three steps. Firstly, it starts with the design of the device using a computer-aided design (CAD) software. Secondly, the microstructuring of the device (channels, mixers and detection chambers construction) takes place using a computer numerical control (CNC) micromilling machine. Finally, there are the back-end operations, as the gas-diffusion membrane integration, the working electrode fabrication and the encapsulation to obtain the finished device

Cyclic Olefin Co-polymer (COC) sheets and foils, used for the fabrication of the device, were purchased from Topas Advanced Polymers in different grades and thicknesses.

The gas-diffusion membrane is made of polyvinylidene fluoride (PVDF) (Millipore).

The working electrode consists of an ion selective electrode (ISE) built by an epoxy-graphite transducer and an ammonium polyvinyl chloride (PVC) membrane.

The epoxy-graphite transducer was made of graphite powder with a particle size of 50 µm Merck), epoxy resin Araldite-M (Ciba Geigy) and hardener HR (Ciba Geigy).

The composition of the ammonium membrane [1] consisted of 1 wt % nonactine, 65.5 wt % BBPA (bis(1-butylpentyl)adipate) and 33.5 wt % polyvinyl chloride (PVC). All these reagents were purchased from Fluka. The membrane components were weighed out and dissolved in THF. The membrane was deposited drop by drop onto the epoxy-graphite transducer and dried overnight prior to use.

Other reagents used were ammonium chloride (Fluka), sodium hydroxide (Panreac), tris(hydroxymethyl)aminomethane (Panreac) and hydrochloric acid (Sigma). Standard solutions were prepared by serial dilution of a stock solution.

In the Figure 1.A we can see the resulting device. The microsystem has three inlets (a, b, c) and two outlets (d and e). According to the balance $NH_4^+ + OH^- \rightleftharpoons NH_3 + H_2O$ (Ka = $5.5 \cdot 10^{-10}$), when sample and NaOH are mixed, all ammonium is converted to ammonia gas, which diffuses through the PVDF membrane. Then, a TRIS acceptor solution, adjusted to pH 7.4 with HCl, reversed the balance, obtaining ammonium without interferents.

The experimental set up is shown in Figure 1.B. The flow system consisted of a four channel peristaltic pump (Gilson) and an injection valve (Hamilton MVP). As a reference electrode was used a commercial Ag/AgCl electrode (Orion). Signal acquisition and digital processing was performed by means of a potentiometer (TMI).

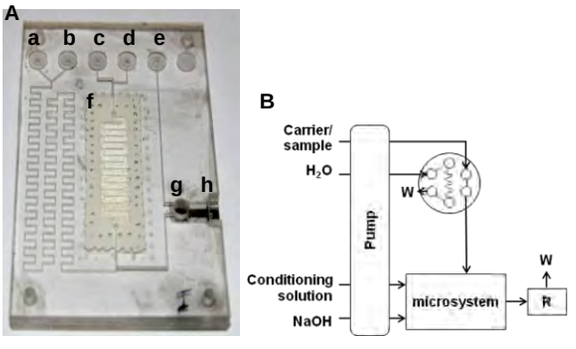

Figure 1: ***A:*** *Picture of the device.* ***a)*** *carrier/sample solution inlet;* ***b)*** *NaOH inlet;* ***c)*** *conditioning solution inlet;* ***d)*** *waste outlet;* ***e)*** *to external reference electrode outlet;* ***f)*** *gas-diffusion membrane;* ***g)*** *detection chamber with the ammonium selective membrane;* ***h)*** *electrical connection.* ***B:*** *Scheme of experimental set up.* ***R:*** *External reference electrode;* ***W:*** *waste.*

Results and discussion

The main issue of this study was to establish the compatibility between the materials used in the construction of both microfluidic platform and detection subsystem. After some problems of adhesion between the polymeric substrate and the transducer material, it was observed that the best results were obtained by fabricating a low-relief in the substrate and filling it with epoxy-graphite resin.

The hydrodynamic conditions for the employed ISE were evaluated and optimized in terms of sensibility, time of analysis and detection limit. In this sense, the flow rate was fixed at 0.4 ml/min and the injection volume in 225 µl. Meanwhile, the concentration of the conditioning solution (TRIS pH 7.4) and sodium hydroxide was set at 0.01 M and 0.1 M respectively. The robustness of the proposed microsystem allows changing the hydrodynamic variables depending on the application without losing its operational features.

The obtained calibration plot is shown in Figure 2. The working range is from 0.1 to 500 ppm of ammonium ion and the detection limit is abc

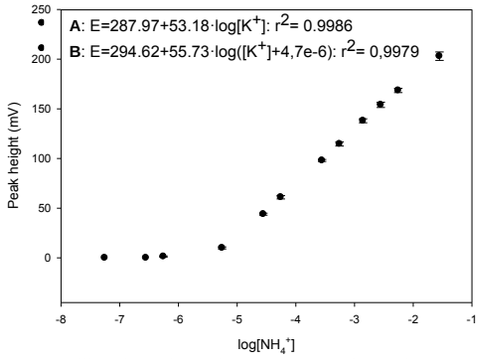

Figure 2: calibration plot. ***A)*** *Linear set;* ***B)*** *Nonlinear set.*

Conclusion

The results shows that the microanalyzer developed can be used to monitor on-line ammonium ions in treated water samples. In the near future the aim is to integrate also the reference electrode.

References

[1] S. Alegret; *et.al.,* Analyst, Vol. 114, pp. 1443-1447, 1989.
[2] N. Ibáñez-Garcia; *et al*., Electroanalysis, Vol. 22, pp, 2376-2382, 2010.
[3] N**.** Ibáñez-Garcia, Doctoral Thesis. Autonomous University of Barcelona, Spain, 2007.
[4] J.M.K. Ng,; *et.al.,* Electrophoresis, Vol. 23, pp. 3461-3473, 2002.
[5] J. Ruzicka; *et.al.,* Trends in Analytical Chemistry, Vol. 27, pp. 390-393, 2008.
[6] E. Arasa-Puig; *et al*., Proc. of the Ibersensor 2010, Lisbon, Portugal, November 9-11, 2010.
[7] H. Becker and C. Gärtner, Analytical and Bioanalytical Chemistry, Vol. 390, pp. 89-111, 2008.

Construction and characterization of ceramic optical detection flow cells based on the Low Temperature Co-fired Ceramics technology

Pedro Couceiro, Sara Goméz-de Pedro, Ana Dias, Julian Alonso-Chamarro
Grup de Sensors i Biosensors, Universitat Autònoma de Barcelona
08193 Cerdanyola del Vallés, Catalonia, Spain
Pedro.Couceiro@uab.es

Abstract

The use of optical detection in microfluidics devices fabricated in Low Temperature Co-fired Ceramics (LTCC) devices where, until now, limited to post-processed integration of glass windows. In this study, it has been fabricated and characterized with colorimetric samples different optical detection flow cells with different window thickness in ceramic material. Lambert-Beer linear range and detection limits for each device are presented.

Keywords: Low Temperature co-Fired Ceramics, Microfluidics, Optical detection, Flow cells

Introduction

Miniaturization of the components needed to design micro Total Analysis Systems (mTAS) is nowadays one of the most active areas in analytical chemistry research field, since development of μTAS would dramatically reduce reagents and sample consumption, and analysis time.

LTCC (Low Temperature Cofired Ceramics) technology, originally conceived for electronic purposes, emerges as an excellent material for the construction of such devices [1]. This technology is well established for both low-volume, high-performance (military, spatial) and high-volume, low-cost (portable wireless, automotive) applications [2]. Its multilayer approach and compatibility with screen printing techniques, could enable the development of highly integrated devices, including many stages of specific analytical process. Using this technology, devices integrating fluidic operations such as pretreatment steps, sample injection, manipulation, filtration, reaction, separation, and detection have been presented [2-7].

However, until know the use of optics detection in LTCC based devices was limited to post-processed integration of glass windows [7]. This has been a major drawback of the technology, since most of the detection systems used in this field are based on optics.

In this work, all LTCC optical detection flow cells with different window thickness where fabricated and characterized with colorimetric samples.

Experimental

DuPont 951 green tape where used as substrate for the fabrication of the devices. The LTCC tapes where cut using a LPKF Protolaser 200 and a LPKF ProtoMat C100\HF. The different LTCC layers were aligned in aluminum plates and laminated at 30 bar and 70ºC for 5 minutes. Finally, the devices were sintered in a programmable box furnace (Carbolite CBCWF11/ 23P16, Afora, Spain).

The fluidic LTCC devices were placed in a in-house built optical detection module based on a modulated Light Emitting Diodes (LEDs) with emission peak at 505 nm mounted in PCB (Printed Circuit Boards), where a photo detector is integrated.

The continuous flow system set-up consisted of a Gilson Minipuls 3 peristaltic pump equipped with flexible Tygon pumping tubes (1.2 mm internal diameter) connected to the microfluidic inlets through 0.8 mm internal diameter Teflon tubing.

For the colorimetric characterization, the simple reaction of iron (II) with 1,10-phenanthroline in water was selected, since its complex generates a strong colored complex

with its maximum absorbance wavelength located in 510 nm. For this purpose, stock solutions of reagents were prepared in the concentrations of 1500 ppm for $Fe(NO_3)_2$, 3330 ppm for 1,10-phenanthroline and 80000 ppm for hydroxylamine. Solutions with different concentrations of the complex were freshly prepared, taking into account the reaction stoichiometry (1:3), obtaining 15 different solutions from 0,1 to 80 ppm.

Results and Discussion

The fluidic part of the optical detection flow cells was constructed using Dupont 951 AX (254 µm thickness). The fluidic part consists of 600 µm width and 400 µm deep inlet channel and a 400 µ m width and 400 µ m deep channel. The LTCC layers were laser cut and laminated. The laminated devices where then aligned in a CNC machine, and the detection channel was cut using a 400 µm diameter drill bit. In order to obtain optical detection flow cells with different window thickness, Device 1 was then laminated with Dupont 951 AX (254 µm), Device 2, was laminated with Dupont 951 PT(114 µm thickness), and Device 3 was laminated with Dupont 951 C2 (50 µm thickness).

Since during sinterization the Dupont 951 tapes suffers 15% shrinkage in Z plane, the window thickness of the sintered Device 1 was 213 µm, 97 µm thickness for Device 2 and 43 µm thickness for Device 3.

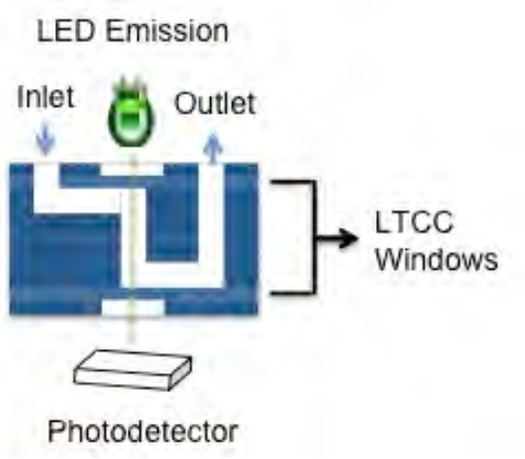

Fig 1 Continuous flow system and optical detection system set-up

Each dispositive was then aligned with the in-house built optical detection system and colorimetric solutions where injected at 0,89 mL/min.

As seen in Fig 2, the range of linearity of the Lambert-Beer equation increases with the decrease in the LTCC window thickness, as expected. Device 3 with 43 µ m thick LTCC window presented a linear range from 0 to 10 ppm of Fe^{2+}, while Device 1 with 213 µm thick LTCC windows presents a linear range an order of magnitude lower.

Detection limits of 0,16 ppm of Fe^{2+} where obtained for Device 3, 0,23 ppm for Devices 2 0,89 ppm for Devices 1.

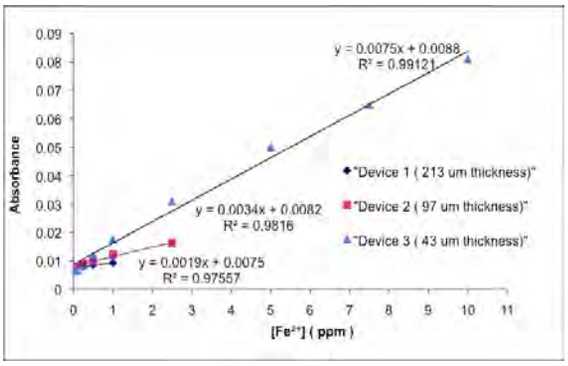

Fig 2 Graphic of Absorbance vs Fe^{2+} concentration for the Dispositive 1, Dispositive 2 and Dispositive 3

Conclusion

LTCC windows with different thickness were constructed and optically characterized. For the first time, all LTCC optical detection flow cells were constructed and characterized according to its window thickness.

References

[1] N. Ibáñez-García, C.S. Martínez-Cisneros, F. Valdés and J. Alonso, *TrAC-Trends in Anal. Chem.*, 2008, **27 (1)**, 24-33.

[2] L. J. Golonka, T. Zawada, J. Radojewski, H. Roguszczak and M. Stefanow, *Int. J. Appl. Ceram. Technol.*, 2006, **3(2)**, 150-156.

[3] M. Baeza, C. López, J. Alonso, J. López-Santin and G. Alvaro, *Anal. Chem.*, 2010, **82(3)**, 1006-1011.

[4] C. S. Martinez-Cisneros, Z. daRocha, M. Ferreira, F. Valdes, A. Seabra, M. Gongora-Rubio and J. Alonso-Chamarro, *Anal. Chem.*, 2009, **81**, 7448-7453.

[5] C.S. Martinez-Cisneros, N. Ibanez-Garcia, F. Valdes and J. Alonso, *Sens. Actuator A-Phys.*, 2007, **138**, 63-70.

[6] G. Fercher, A. Haller, W. Smetana and M.J. Vellekoop, *Analyst*, 2010, **135**, 965-970.

[7] S. Gómez-de Pedro, M. Puyol, J. Alonso, *Nanotechnol.*, 2010, **21**, 415603.

3-D LTCC Microfluidic device as a tool for studying nanoprecipitation

Schianti, J. N.[1] , Cerize, N. P. N.[2], Oliveira, A. M. [2], Derenzo, S.[2], Góngora-Rubio, M. R.[2]
[1] University of São Paulo, Integrated System Laboratory, Polytechnic School.
[2] Institute for Technological Research of the State of São Paulo, Center for Processes and Products Technology.
Av. Prof. Almeida Prado,532 – 05508-901, São Paulo, São Paulo, Brazil
junovais@ipt.br and juliana.schianti@usp.br

Abstract

Nanoparticles have been used to improve the properties of many cosmetic products, mainly the sunscreens materials using nanoencapsulation or nanosuspensions, improving the contact with active molecules, enhancing the sun protection effect and facilitating the formulation of industrial products. Microfluidic devices offer an important possibility to produce nanoparticles in a simple way, in an one step bottom up technique, in a continuum process with low polidispersivity, low consumption of reagents and additives. In this work, we microfabricated an 3-D LTCC microfluidic device to study the nanoprecipitation of Benzophenone-3, a substance used as a sunscreen in cosmetic and pharmaceutical industries. It was observed that some parameters influence on the particle size such as total fluid flow on device, the ratio between phases, and the Benzophenone-3 initial concentration. It was tested also the influence of applied voltages on particle sizes. The high voltage was applied in a Kovar tube inserted in the 3D device. The use of microfluidic device resulted in particles with 100 up to 800 nm of size, with polispersivity index below 0.3 and offers an interesting way to obtain nanoparticles. These studies are still in development but indicate the possibility to obtain B-3 nanostructured.

Keywords: nanoprecipitation, microfluidic device, Benzophenone-3, LTCC

Introduction

Anti-solvent precipitation is one of the technique used to obtain nanoparticles and can be improved by microfluidic devices [(i)]. With microfluidic devices is possible obtain a high supersaturation degree with a uniform spatial concentration distribution resulting in particles with a smaller size [(ii)]. The microfluidic devices offer micro or nanoparticles produced in only one step, in a continuum process with low polidispersivity, low consume of reagents and additives[(iii)]. Besides, the use of high voltages, producing an eletrospray, could reduce the particle size[iv]. Many kinds of materials could be synthesized in microfluidic devices resulting in nanoparticles, such as polymers, inorganic materials, hydrophobic drugs, etc.

Benzophenone-3 has been used in topical application as sunscreen in cosmetics industry and have properties improved in nanoscale [(v)]. In this work is presented the results of study of Benzophenone-3 nanoprecipitation using a 3-D LTCC microfluidic device. The influence of some parameters in the particle size such as total fluid flow on device, the ratio between phases, the Benzophenone-3 initial concentration were analyzed. It was tested also the influence of applying high voltages in the cross junction device on the particle size.

Materials and Experimental

The microfluidic device was microfabricated in LTCC 951 (DuPont), using a CO_2 Laser (Versalaser, ULS) and lamination and sintering standard process. In the cross junction a Kovar (TAI) tube is inserted to obtain a 3D structure. The device also displays two electrical conductors for High Voltage (HV) connection to fluids in order to observe nanoparticle size modification. This 3D device, with the scheme showed in Figure 1, is operated in the flow focusing regime in order to carry out the nanocrystallization process.

A high voltage source (GAMMA) with values ranging from 0 to 10KV to observe the influence in the nanoprecipitation. Two syringe pump (Harvard Apparatus) were used to control the fluid flow with values ranging from 500 up to 1000 µL/min. Benzophenone 3 (B-3) was solved

in two different solvents, isopropilic alcohol (IPA) and methanol (MTH), to observe the effect of the type of solvent in the particle size. It was observed also the influence of total fluid flow rate, the ratio between fluid flows ($R = Q_{water}/Q_{B-3}$) and the B-3 concentration. The B-3 nanoparticles were analysed by SEM-FEG to observe the morphology, and the particle sizes were obtained by DLS (Delsa NANO).

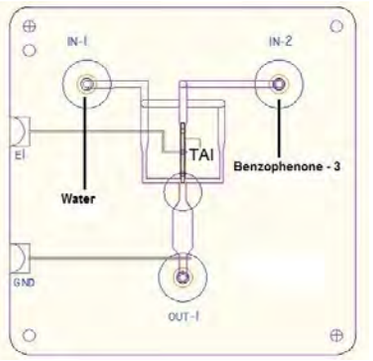

Figure 1. 3-D microfluidic device scheme for B-3 nanoprecipitation.

Results and Discussions

In Figure 2 is depicted the influence of ratio between flows on the particle sizes for the two different solvents: methanol and isopropyl alcohol. It can be observed that for higher values of R is possible to obtain small particles. The differences in size obtained for the two solvents were not so high. Since MTH have more toxicity, the use of IPA presents a better strategy for this nanoprecipitation.

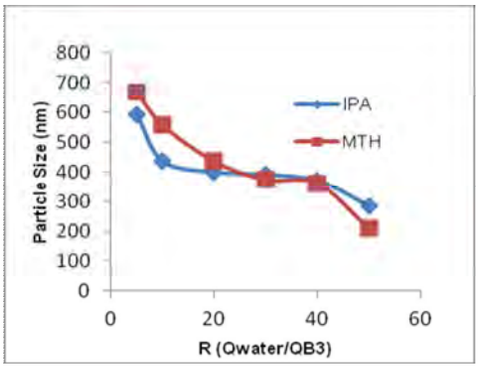

Figure 2: Particles sizes versus ratio between Water phase and B-3 phase using two different solvents: IPA and MTH.

Figure 3 shows the influence of applied voltage in particle size for two different total fluid flow rates (500 and 1000µL/min). In these studies, B-3 was solved in IPA, with a concentration of 7,5 mg/mL. In both cases the application of the high voltage in the process results in an increase of B-3 particle size. To observe the particle morphology a SEM-FEG analysis was done and the results are shown in Figure 4.The nanoparticles was obtained for a total fluid flow rate of 500 µL/min, and 500 V of voltage. It is possible to note that the B-3 have an spherical shape.

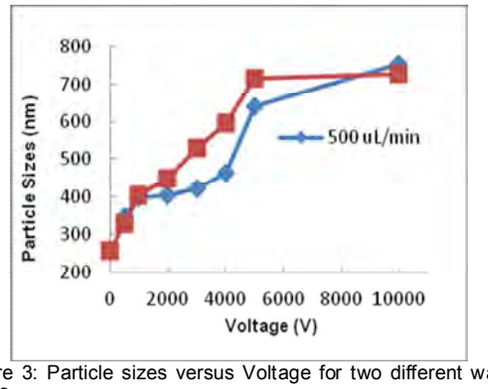

Figure 3: Particle sizes versus Voltage for two different water fluid flow.

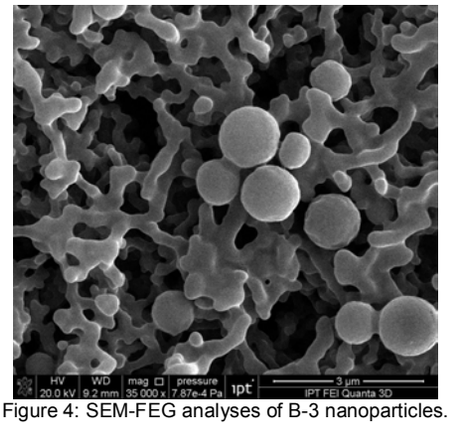

Figure 4: SEM-FEG analyses of B-3 nanoparticles.

Conclusions

The use of microfluidic device resulted in particles with 100 up to 800 nm of size, with polispersivity index below 0.3 and offers an interesting way to obtain nanoparticles. The increase of relation between phases (water and B-3) results in a decreasing of particles sizes. However, the use of high voltages results in an increasing of sizes.

References

[i] PANAGIOTOU,T. et. al. , NSTI-Nanotech 2007, ISBN 1420063766 ,Vol. 4, 2007

[ii] DESPORTES, S. et. al. , Chemical Physics Letters ,446, 212–216, 2007

[iii] LO, C. T. et. al., Langmuir, Vol. 26, n.11, 8559–8566, 2010

[iv] Kim, H. *et al.,* Appl. Phys. Lett. **91**, 133106 , 2007.

[v] Gonzalez, H. G. et al., Clinical and Experimental Dermatology,Vol. 27, 691–694, 2002.

Towards the Development of Vacuum Pressure Sensor Based on CNT-Si Field Emission Devices

Michel O. S. Dantas[1], Elisabete Galeazzo[2], Henrique E. M. Peres[2], Francisco J. Ramirez-Fernandez[2]
[1] Centro de Engenharia, Modelagem e Ciências Sociais Aplicadas (CECS) – UFABC
Rua Santa Adélia, 166, CEP 09210-170, Santo André - SP – Brazil
[2] Laboratório de Microeletrônica (LME) - Escola Politécnica – Universidade de São Paulo – EPUSP
Av. Prof. Luciano Gualberto, trav. 3, 158, CEP 05508-010, São Paulo - SP – Brazil
E-mail Address: michel.dantas@ufabc.edu.br

Abstract

The association of Si microtips with multiwalled carbon nanotubes was implemented to explore the development of vacuum pressure sensors based on field emission devices. It is reported that N_2 introduction into the vacuum chamber causes a considerable field emission current decrease. This effect was explored to demonstrate the promising application of miniaturized fabricated devices as gas or pressure sensors, obtained from low complex processes.

Keywords: Silicon field emission devices, Carbon nanotubes, Vacuum pressure sensors.

Introduction

Although Field Emission (FE) devices have been studied since 1970s, they are still a matter of great interest for developing applications in vacuum microelectronics. These devices offer the possibility of obtaining ionization sources constructed with the so-called “cold cathodes”, which have advantages in comparison with usual technologies, since no heat is necessary to promote electron extraction from a material. Applications of FE devices include flat panel displays, pressure and gas sensors, for example.

Silicon (Si) microtips are applied for the development of FE devices since it is the base-material of the microelectronics industry, the fabrication techniques of which are very well established for obtaining miniaturized signal conditioning and integrated circuits. Besides, Si has good mechanical and electrical properties for manufacturing microelectromechanical systems (MEMS), which includes microtips that are applied as emitters (or cold cathodes) in FE devices.

Another point of interest in Si is the possibility to improve their emitting characteristics by coating the emitters with other materials, such as Carbon Nanotubes (CNTs), which are showing remarkable properties in several fields. For field emission applications, CNTs are interesting due to their small tip apex size and negative electron affinity, which facilitates the field emission phenomena in comparison with other materials.

From the exposed before, this work aims at the combination of silicon microstructures and carbon nanotubes for the development of vacuum pressure sensors based on field emission devices.

Experimental Procedure

Si microtips emitters were obtained by HI-PS technique [1]. Next, multiwalled carbon-nanotubes (MWCNT) were deposited over Si emitters by electrophoresis technique [2]: an electrical current of 0.5 mA was applied between two electrodes (one of which contains the Si sample) for 4 minutes. The morphology of the devices was characterized by scanning electron microscopy (SEM-FEG, FEI NanoSEM 400).

To analyze the emission/ionization performance in a controlled environment, the devices were mounted in a diode configuration (CNT-Si microtips sample (cathode) and stainless steel planar disc (anode), spaced 250 μm), and placed inside a high vacuum chamber. Thus, the current was measured along time, at the fixed applied potential of 2700V, while the vacuum pressure was periodically switched between $2x10^{-7}$ Torr (for 400 s intervals) and $2x10^{-5}$ Torr (for 100 s intervals) by N_2 injection controlled by a MFC.

Results and discussion

Figure 1 shows a selective MWCNTs deposition over the Si microtips array area achieved after the electrophoretic process.

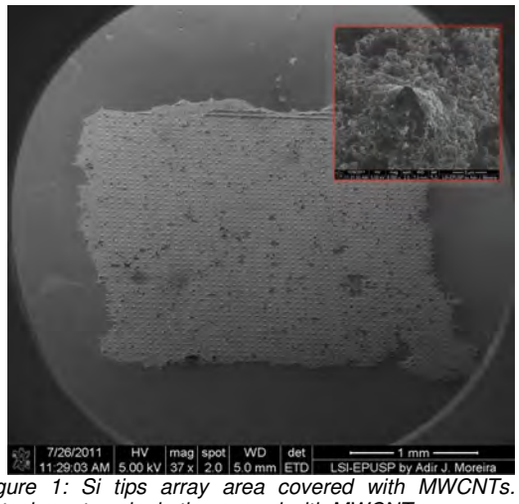

Figure 1: Si tips array area covered with MWCNTs. In detachment, a single tip covered with MWCNTs.

Figure 2 shows the effect of N_2 pressure in the emission current (*I-t* curve), which decreases as the pressure increases. The emission current is partially recovered upon each gas exposure, measured during an interval of 400 s before the next gas exposure. This effect might be associated with mechanisms of N_2 gas adsorption by the emitters, changing their intrinsic characteristics (such as effective work function at the localized sites [3]) and, consequently, reducing their efficiency. It is important to mention that, in this experimental characterization, not pronounced ionization processes were noted.

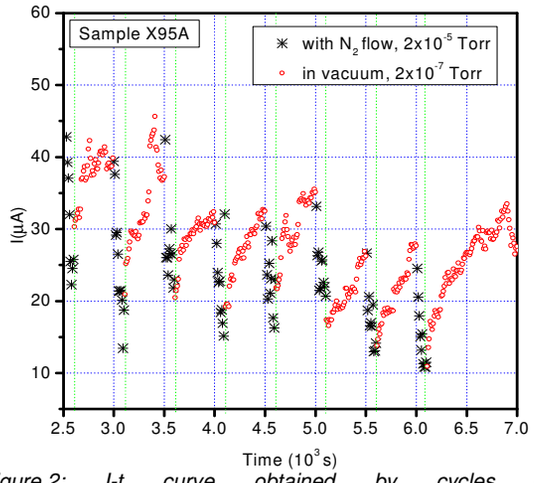

Figure 2: I-t curve obtained by cycles of increasing/decreasing pressure ($P = 2x10^{-5}$ Torr - N_2 flow (100 s); $P = 2x10^{-7}$ Torr - vacuum environment (400 s)).

Figure 3 illustrates *I-V* curves of the device before and just after all the tests with gas exposure. In the inset, the corresponding Fowler-Nordheim (FN) plots are shown. These curves show a considerable worsening (about 40 %) of field emission performance after gas exposure tests, since to obtain the same emission current level, it is necessary to apply a higher potential than before. The FN plots show that there is a little change in the slope of the straight line after gas tests, which can be attributed to the presence of some N_2 molecules adsorbed in the emitters.

These molecules can promote the formation of additional states in the electronic structure of CNTs, changing their electron work function and, consequently, making it difficult to recover their characteristics as before the gas exposure. Degradation of emitters after the test with gases might contribute to this result, too.

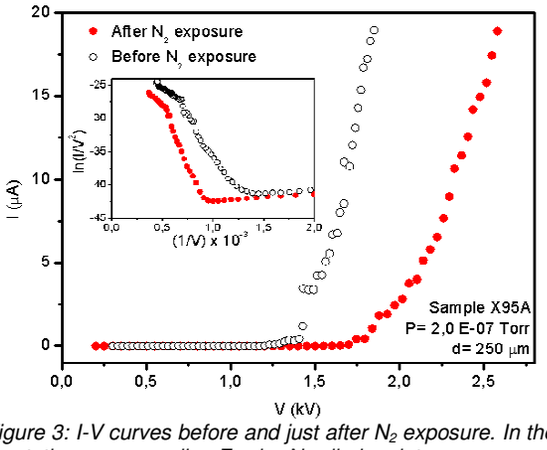

Figure 3: I-V curves before and just after N_2 exposure. In the inset, the corresponding Fowler-Nordheim plot.

Conclusions

The device developed showed pronounced changes in its electrical response related to gas injection into the vacuum chamber, which indicates a promising application as a miniaturized vacuum pressure sensor based on MEMS technology. Our results allow us to suppose that adsorption/desorption mechanisms have strong influence on the device current measurements. To confirm this hypothesis, we intend to implement desorption procedures, such as heating the samples after N_2 exposure. Also, other gas species will be experimented in order to analyze the behavior of the CNT-Si Field Emission Device as a vacuum sensor.

References

[1] M.O.S. Dantas, E. Galeazzo, H.E.M Peres, M. Kopelvski, F.J. Ramirez-Fernandez, Journal of Microelectromechanical Systems, No. 17, pp. 1263-1269, 2008.

[2] M.O.S. Dantas, E. Galeazzo, H.E.M Peres, F.J. Ramirez-Fernandez, Proc. of the 14th International Meeting on Chemical Sensors (IMCS-14), Nuremberg, Germany, May 20-23, 2012.

[3] S. Dardona, A. Peles, G. Wrobel, M. Piech, P.X. Gao, Journal Of Apllied Physics, No. 108, pp. 124318, 2010.

Mixing Platform for the Control of Magnetic Beads in Microfluidic Applications

Miguel Berenguel, Julián Alonso and Mar Puyol
Group of Sensors and Biosensors, Universitat Autònoma de Barcelona
08193, Bellaterra (Cerdanyola del Vallès), Catalunya, Spain
miguel.berenguel@uab.cat

Abstract

This communication presents a mixing platform, consisting of a rotary base with permanent magnets, which aims to use the magnetic beads both as active mixing agents as well as a solid support for the bioassays. To characterize the mixing and reaction processes of the system, two experiment sets are performed: on the one hand, we analyze the movement of the magnetic particles inside de microfluidic device; on the other hand, we study a model reaction between EDTA-coated MBs and a metal complex, monitoring the color change. The mixing platform enables the tuning of the MBs' movement within the microfluidic device, and the reaction time required is severely decreased. Further studies will be addressed to apply this mixing process to the implementation of *on-chip* immunoassays.

Keywords: Magnetic Mixing, Magnetic Beads, COC, Microfluidics, Immunoassay.

Introduction

Bioassays are very powerful analytical techniques, which benefit of the specificity of the recognition element. Particularly, immunoassays benefit of the unique properties of the antibodies, namely, their specificity, strength of binding (affinity) and the wide range of possible analytes to be determined [1]. Magnetic beads offer several advantages as solid support for the immunoassay [2], such as their long surface-to-volume ratio or the possibility to be manipulated using external magnetic fields. This latter fact enables the preconcentration of the analyte and its separation from the sample matrix, as well as the retention of the analyte during the washing steps of the procedure.

In spite of these advantages, heterogeneous immunoassays suffer from labor- and time-consuming procedures, including series of washing and incubation steps. Moreover, the immunoreagents used are relatively expensive [3].

Microfluidics emerges as the potential solution for these drawbacks, since it provides the basis for obtaining miniaturized (bio)analytical devices that are portable, very simple to use, with low reagent consumption and cost-effective (lab-on-a-chip). Furthermore, the control of the MBs by means of external magnets provides a way to improve the mixing efficiency [4], thus lowering the required incubation times.

The present study deals with the fabrication and characterization of an automated mixing platform containing permanent magnets. It is designed to improve the mixing efficiency of a system containing MBs in a microfluidic device.

Experimental

The mixing platform (see Figure 1) is designed as two separate parts: on the one hand, a support moiety, which fixes the motor and the microfluidic device; on the other hand, a rotary CD-shaped mobile moiety, which contains the permanent external magnets that control the MBs. It has been fabricated with PMMA using a Computer Numerical Control (CNC) micro-milling machine.

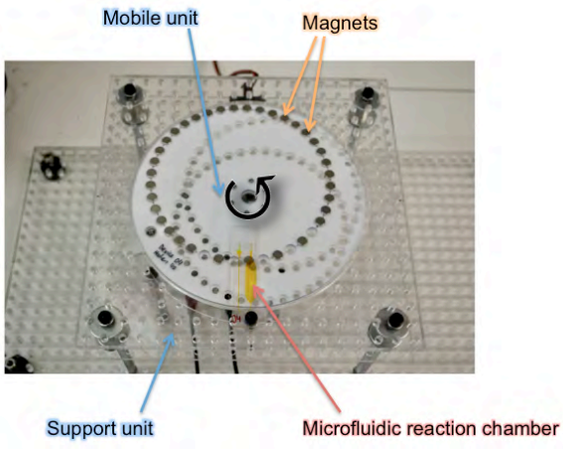

Figure 1. Top view of the mixing platform.

The microfluidic device is fabricated on Cyclic Olefin Copolymer (COC) following three basic steps: design, using Computer-Aided Design (CAD) software; microstructuring, by means of a CNC micro-milling machine; and back-end operations, namely encapsulation by thermal bonding and dicing.

Results

The rotation of the mobile moiety makes the particles move back and forth the microfluidic reaction chamber, as schematically seen in Figure 2.

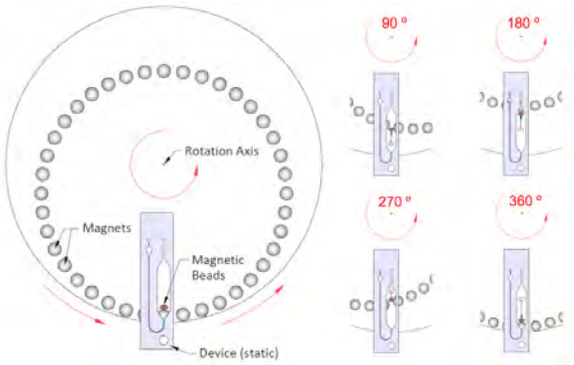

Figure 2. Working principle of the mixing platform. As the mobile moiety rotates, the MBs move back and forth along the reaction chamber.

Firstly, a qualitative study is carried out to analyze the movement of the MBs within a microfluidic chamber. Depending on the rotational speed, and the number and disposition of the magnets, three different types of movement are achieved when using magnetic particles with a 6,5 µm diameter: linear, zigzag and spread linear (occupying the whole width of the chamber).

Secondly, a model reaction between EDTA-modified MBs and a metal complex is studied, monitoring the color change of the solution (Figure 3). The blood red color of an iron (III) thiocyanate solution disappears when the EDTA-coated MBs react with iron (III), yielding a colorless complex.

Figure 3. Model reaction between EDTA-modified MBs and ferric thiocyanate.

When using the magnetic mixing platform, the movement of the MBs fosters the color change, since the reaction is not limited by diffusion anymore. This leads to the severe decrease of the reaction time required, as seen in Figure 4.

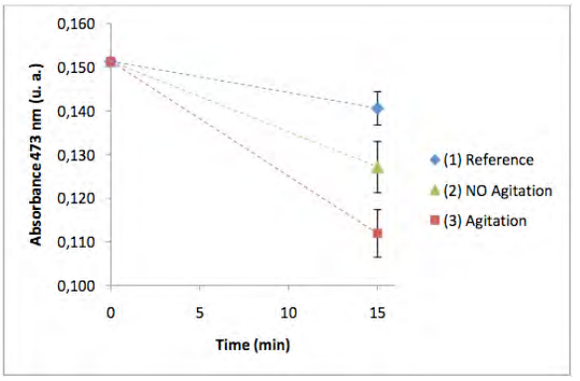

Figure 4. Absorbance decrease of the ferric thiocyanate solution: (1) reference, (2) without mixing and (3) mixing.

Conclusions

The mixing platform presented in this communication is simple, robust and low cost. Furthermore, it can be straightforwardly integrated with microfluidic systems and easily controlled.

The mixing platform proves to be versatile, since the movement of the MBs can be tuned by modifying the rotational speed, the disposition and number of magnets. The model reaction studied shows an effective improvement of its kinetics when carried out in the mixing platform. The interaction between the molecules is not limited by diffusion, and therefore, the reaction times are severely decreased.

References

[1] D. Wild, “The Immunoassay Handbook”, Elsevier Science, 3rd Edition, 2005.

[2] M.A.M. Gijs, F. Lacharme and U. Lehmann, Chemical Reviews, Vol. 110, No. 3, pp, 1518-1563, 2010.

[3] C.-C. Lin, J.-H. Wang, H.-W. Wu and G.-B. Lee, Journal of the Association for Laboratory Automation, Vol. 15, No. 3, pp. 253-274, 2010.

[4] M. Herrmann, E. Roy, T. Veres, M. Tabrizian, Lab on a Chip, Vol. 7, No. 11, pp. 1546-1552.

Colorimetric Determination of Free Sulfur Dioxide in a Centrifugal Microfluidic Disk with Integrated Gas-Diffusion Membrane and Integrated LED Optical Detection

O. Ymbern, N. Sández, T.M. Guimarães and J. Alonso-Chamarro
Group of Sensors and Biosensors
Universitat Autònoma de Barcelona, 08193, Bellaterra, Spain
oriol.ymbern@uab.cat

Abstract

A centrifugal microfluidic platform prototype designed to perform colorimetric determinations by the use of a simple miniaturized optical system based on an LED and a photodetector was fabricated evaluated for its application as a future analytical microsystem for multiparametric wine determinations. As a proof of concept the determination of free sulfur dioxide in wines was carried out. The centrifugal microfluidic platform allows multiple parallel analysis on a single disk. It integrates at least ten independent microfluidic systems which allows both calibration and sample determination (p.e. two blank and eight samples). To avoid interferences from colored samples, the microfluidic platform also permited the integration of a gas diffusion pretreatment step using a hydrophobic membrane permeable to gases to separate free sulfur dioxide from sample matrix.

Keywords: Lab-on-a-Disk, Centrifugal Microfluidics, Gas-diffusion membrane, Free Sulfur Dioxide

Introduction

Sulfur dioxide is typically used as an antioxidant and antiseptic in winemaking. The total and free SO_2 contents of wine are key analytical parameters for must and wine quality control; the amounts added to wine should ensure adequate protection while complying with prevailing legislation. Processing of a large number of samples calls for the use of automated methods minimizing analytical times and costs in addition to providing major advantages over the typically laborious classical methods [1,7]. It is well known the growing interest and high demand for the construction of devices featuring the integration of the total sequence of lab processes to perform chemical analysis. The benefits Lab-on-a-chip or μTAS (micro total analysis systems) include portability, reduction of sample and reagents consumption, as well as the integration on a single chip of different stages of the analytical process reducing the user-interference and human error in experimental operation [2]. In this way, centrifugal microfluidic platforms are of particular interest [3,4] resulting in the new technological component to be known Lab-on-a-CD. The most basic unit consists of a rotary engine in order to achieve a rotational speed and acceleration very stable, and its control electronics. By this simple device is possible the manipulation of liquids into the microfluidic platform. This solution is generally cheaper and allows a higher degree of integration to cause movement of fluids in microfluidic all subunits simultaneously. Due to symmetry of rotation of the discs, drastically simplifies the measurement of multiple units or subsystems integrated microfluidic in parallel. Two major advantages of the centrifugal microfluidics platform is the system's modular configuration, based on disposable plastic cartridges easily exchangeable, and multiple operational units that can be integrated microfluidics in parallel on a single platform or disk. This allows for a simultaneous handling, and high precision, multiple small aliquots of reagents and sample. In this work, the sulfur dioxide was determinated by a colorimetric method using p-aminoazobenzene (PAAB) as colorimetric reagent [1,7,8]. The analytical basis for the method is the reaction between SO_2 and PAAB and formaldehyde in an acid medium, which is monitored colorimetrically.

Experimental

The microfluic systems of the centrifugal microfluidic platform (Figure 1) for multiple and parallel analyisis were designed using a computer-aided design (CAD) software. Cyclo olefin copolymer (COC) was applied on the construction of microfluidic platforms [5]. A Polyvinylidene fluoride (PVDF) membrane was also mechanized and integrated into the device without fluidic leakage. Micromilling technique

with a CNC (Computer Numerically Controlled) machine was applied to construct microfluidic devices and thermo compression process was applied as a bonding method to seal hermetically the microfluidic system. Different devices were fabricated and evaluated.

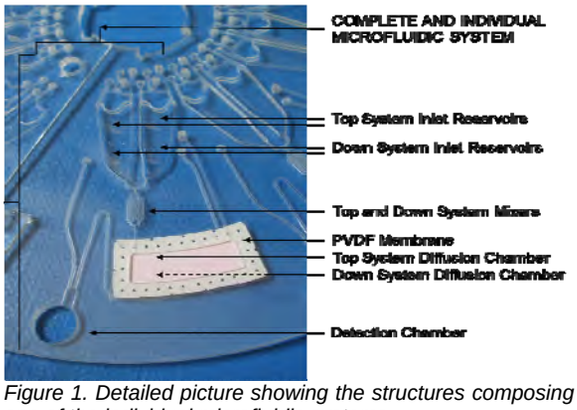

Figure 1. Detailed picture showing the structures composing one of the individual microfluidic systems.

The principle of operation inside the microfluidic system consists on the acidification of the sample containing the analyte in sulphite form. Sulphur dioxide generated passes through the PDVF membrane in gas state and is collected at the acceptor (Channel) chamber situated at the top of microfluidic system. Sulphur dioxide combines in situ with PAAB in the presence of formaldehyde to give a pink dye with an absorption maximum at 505 nm. The product of the reaction is automatically monitored in each of the ten individualized microfluidic systems integrated on the disk by a miniaturized optical detection system based on a LED an a photodetector (Figure 2). The signal measured in each microfluidic system is then processed in order to obtain both calibration curves o sample measurements.

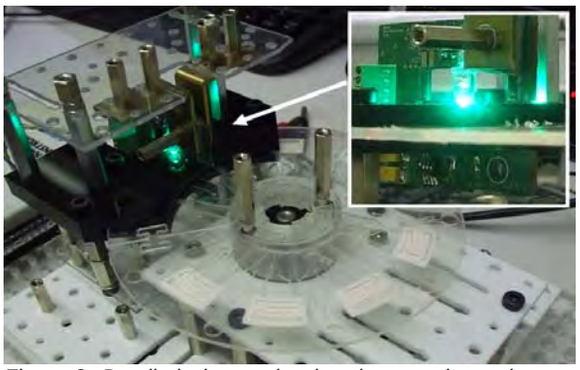

Figure 2. Detailed picture showing the experimental setup for automated and parallel colorimetric determination.

Results and Discussion

The main issue of this study was to demonstrate the possibility to integrate a PVDF membrane inside a microfluidic platform without leakage in order to eliminate the interference of coloured sample matrix. As well as, the possibility to carry out multiple analysis in a single disk in order to automatize parallel analysis. Promising results were obtained in the first experimental test of the microsystem. A linear dependence between the absorbance signal obtained by the detection system and the concentration of free sulphur dioxide of each sample was observed (Figure 3). The free sulphur dioxide was also determinated in a complex matrix using the wine samples evaluated. A study of PAAB concentration in the acceptor reagent solution was conducted in order to maximize sulphur dioxide diffusion through hidrofobic membrane and hence the magnitude of the signal measured.

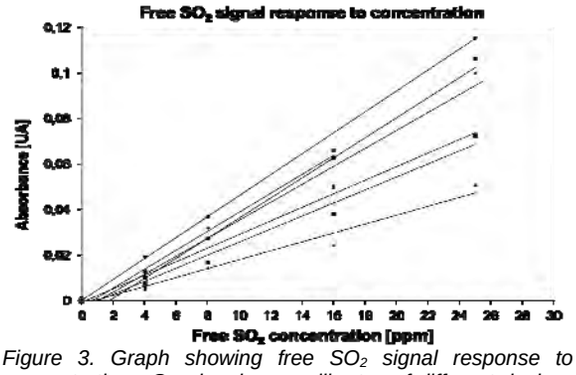

Figure 3. Graph showing free SO_2 signal response to concentration. Graphs shows calibrates of different devices constructed and evaluated.

Conclusions

The centrifugal microfluidic platform constructed and integrated to a miniaturized optical detection system demonstrated the possibility to monitor important parameters involved in wine making using colorimetric reagents. Although, further studies must be carried out to optimize the centrifugal microfluidic platform, its enormous potential has been shown.

References

[1] J. Bartroli, M. Escalada, C. . Jorquera and J. Alonso, Anal. Chem, 63, 2532-253, 1991.
[2] S. Haeberle, R. Zengerle, Lab. Chip., Vol.7, 1094 – 1110, 2007.
[3] J. Ducrée, S. Haeberle, S. Lutz, S. Pausch, F. v. Stetten, and R. Zengerle, Journal of Micromechanics and Microengineering, Vol.17, no. 7, S103-S115, 2007.
[4] M. Madou, J. Zoval, G. Jia, H. Kido, J. Kim, N. Kim, Annu. *Lab on a cd*, Annual Review of Biomedical Engineering, Vol. 8, 601-628, 2006.
[5] J. Steigert, S. Haeberle, T. Brenner, C. Muller, C. P. Steinert, P. Koltay, N. Gottschlich, H. Reinecke, J. Ruhe, R. Zengerle and J. Ducree, Journal of Micromechanics and Microengineering, 17, 333–341, 2007.
[6] *S. Chatterjee, A. K. Pillai and V. K. Gupta,* Journal of the Chinese Chemical Society*, 50, 257-260, 2003.*
[7] J. B. Pate, J. P. Lodge Jr., A. F. Wartburg, Anal. Chem., Vol. 34, no. 12, 1660-1662, 1962.
[8] P. W. West, G. C. Gaeke, Anal. Chem., 28, 1816, 1956.

Technological process for a silicon/glass microsystem fabrication towards cell culture applications

Cecilia Jiménez-Jorquera[a], Estrella González[b], Isabel Burdallo, Jose Antonio Plaza[a]
[a]Instituto de Microelectrónica de Barcelona (IMB-CNM), CSIC, Campus UAB, 08193 Bellaterra, Barcelona, Spain [b] Centro de Investigaciones en Microelectrónica (CIME), Carretera de Vento, Km 8, Capdevila, La Habana, Cuba
joseantonio.plaza@imb-cnm.csic.es, cecilia.jimenez@csic.es

Abstract

On line monitoring of metabolism in cell cultures is increasing in interest for cell biology studies. In this work we present a new technological process for the fabrication of a silicon chip with integrated biochemical sensors combined with a microfluidic glass chip to obtain a high functional Micro Total Analysis System (μTAS). The whole system includes a chamber for cell culture, fluid channels for liquid transport and managing and four electrodes plus a reference electrode for culture monitoring. The technology process is based on standard microfabrication processes for silicon wafers and on the anodic bonding of the silicon chip to the glass chip.

Keywords: μTAS, anodic bonding, cells culture, biochemical sensors, metabolism control

Introduction

The development for μTAS for cell biology studies is one of the most promising research activities regarding analytical microsystems.
Nowadays the assays with cells are followed mostly by means of fluorescence microscopy [1]. But this technique does not provide information about cells viability during the assay. Monitoring of extracellular parameters such as pH, potassium, oxygen and temperature in cell cultures using different kind of sensors mainly microelectrodes and micro-optodevices is reported in the literature [2-5]. A more advanced systems based on multisensor arrays fabricated with microelectronic technology placed at the bottom of a culture well were first described at the end of the nineties. The most significant examples are the Bionas 2500 [6-7] containing a multisensory chip and the Cytosensor Microphysiometer (Molecular devices) [8] based on a pH Light addressable potentiometric sensor (LAPS) technology.

But an interesting alternative is the use of a fluidic multisensory array separated from the cell culture. In that way the blocking of electrodes due to adhesion of cells is avoided and calibration and maintenance of sensors during measurement for long-live cells is possible.

Regarding to μTAs for cells assays, the most applications are based on microfluidic devices for cell culture, separation of cells according to their size and assays of drug citotoxicity [9]. Most of them are using silicon/polymer technology [10] or PDMS technology [11-12]. However, the combination of sensors and microfluidics for metabolism cells monitoring is still a key issue.

The most common substrate for transducer fabrication is silicon, mostly due to the huge variety of microfabrication processes available for the mechanization of structures on this material and the chance to integrate microelectronic circuits in the same substrate. On the contrary, traditionally glass substrates have been used for cell cultures since glass is a biocompatible material and able for microscopy inspection. Thus, in order to get high performance devices it should be desirable to combine both materials for the biochemical study of cell cultures.

In this work the technology for the fabrication of a μTAS containing a biosensor array and a cell chamber for cell culture and microscopy inspection is described.

Design of the proposed μTAS

In figure 1 a scheme of the designed μTAS to study in vitro cell cultures is depicted. It consists of a silicon substrate and a glass cover. In the silicon substrate the electrodes and metallic contacts are patterned**.** Three amperometric cells with the working electrode and the counter electrode, a conductimetric electrode based on 4-bars and a reference electrode are defined. The reference electrode is separated from the rest in order to use a polymeric liquid junction and a reference solution system that could be renewable. Also

the Ag/AgCl material of the reference electrode is separated from the sample.

The definition of the channels and cavities is performed on the glass substrate. The glass substrate is fabricated in a way it is optically transparent. The thickness of the glass at the bottom of the cell culture chamber is 180-200 µm. This value corresponds to the standard thickness of the glass plates used in cell biology for microscopy inspection. Thus the proposed devices offer the possibility to measure biochemical parameters at the same time that the cells can be observed in an Optical Microscopy or even in a Confocal Scanning Laser Microscopy using molecular probes.

The chamber containing the cell culture is placed separately from the electrodes. The idea is to measure different parameters of the culture media (glucose, pH, conductivity, DO, etc.) by transporting the media from the cell culture chamber to the sensors chamber. Under these conditions, sensors can be calibrated and maintained without affecting the cells as well as they are not blocked by the cells.

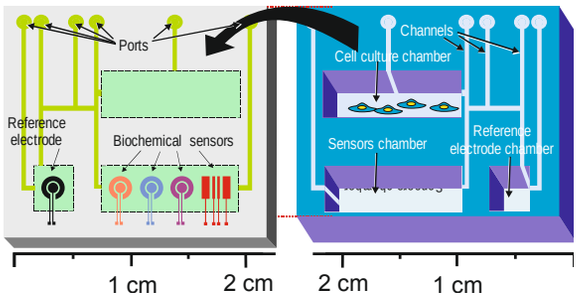

Figure 1. Schemes of the silicon chip showing the reference electrode and the 4 biochemical sensors (left) and the glass chip with the microfluidic parts (right).

Technological procedure

Briefly, a silicon wafer is used as substrate for the electrodes and a glass wafer is used as cover and fluidic substrate. The technology used for the fabrication is microelectronic based processes for the silicon substrate and sand blasting processes for the cover.

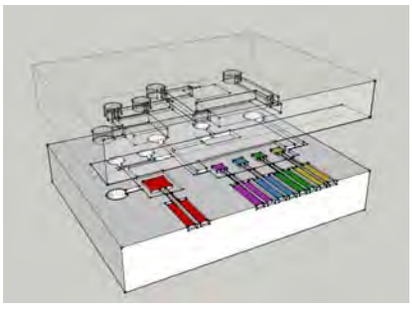

Figure 2. Scheme of the integrated µTAS concept

Silicon wafers are processed according to standard photolithographic processes. Deep reactive ion etching processes are used to define holes through the silicon wafer for fluidic connectors to the macroscopic fluidic system. The glass wafer is designed to contain the cavities and channels for fluid handling. Glass wafers were manufactured by Little Things Factory GmbH [4] following our design. To get the complete device, the pair of wafers are anodically bonded and the individual chips are diced by mechanical sawing.

Acknowledgements

The fabrication of the silicon devices is acknowledged to the clean room staff of the IMB-CNM. Funding from the CYTED project 510AC0408 for a stage of Dr. Gonzalez is acknowledged. We also thank the financial support of the project MINAHE4 (Ref. TEC2011-29140-C03-01).

References

1. Guez, J.S., et al., *The viability of animal cell cultures in bioreactors: Can it be estimated online by using in situ microscopy?* Process Biochemistry, 2010. **45**(2): p. 288-291.
2. Amatore, C., et al., *Electrochemical monitoring of single cell secretion: Vesicular exocytosis and oxidative stress.* Chemical Reviews, 2008. **108**(7): p. 2585-2621.
3. Bradley, P.M.J., et al., *A micro-optrode for simultaneous extracellular electrical and intracellular optical recording from neurons in an intact oscillatory neuronal network.* Journal of Neuroscience Methods, 2008. **168**(2): p. 383-395.
4. Lee, S., et al., *Measurement of pH and dissolved oxygen within cell culture media using a hydrogel microarray sensor.* Sensors and Actuators B-Chemical, 2008. **128**(2): p. 388-398.
5. Male, K.B., et al., *Assessment of cytotoxicity of quantum dots and gold nanoparticles using cell-based. impedance spectroscopy.* Analytical Chemistry, 2008. **80**(14): p. 5487-5493.
6. Thedinga, E., et al., *Online monitoring of cell metabolism for studying pharmacodynamic effects.* Toxicology and Applied Pharmacology, 2007. **220**(1): p. 33-44.
7. http://www.bionas.de/en/Home.html.
8. Hafner, F., *Cytosensor® Microphysiometer: technology and recent applications.* Biosensors and Bioelectronics, 2000. **15**(3-4): p. 149-158.
9. Kim, M.S., J.H. Yeon, and J.K. Park, *A microfluidic platform for 3-dimensional cell culture and cell-based assays.* Biomedical Microdevices, 2007. **9**(1): p. 25-34.
10. Chang, W.J., et al., *Poly(dimethylsiloxane) (PDMS) and silicon hybrid biochip for bacterial culture.* Biomedical Microdevices, 2003. **5**(4): p. 281-290.
11. Pereira Rodrigues, N., Y. Sakai, and T. Fujii, *Cell-based microfluidic biochip for the electrochemical real-time monitoring of glucose and oxygen.* Sensors and Actuators B: Chemical, 2008. **132**(2): p. 608-613.
12. Mehta, G., et al., *Quantitative measurement and control of oxygen levels in microfluidic poly(dimethylsiloxane) bioreactors during cell culture.* Biomedical Microdevices, 2007. **9**(2): p. 123-134.

Chapter 9: Sensors for Agricultural and Environmental Applications

Wireless sensor network based on green tape technology for in-soil nutrients monitoring

C.S. Martínez-Cisneros[1]*, A. Torre-Neto[2], A.R. Araujo[2], A. Parra[1] and J. Alonso-Chamarro[1]

[1]Grup de Sensors i Biosensors, Universitat Autònoma de Barcelona, Spain.
[2]Empresa Brasileira de Pesquisa Agropecuaria, Brazil.

*Corresponding author: Cynthia Martínez, +34 93 581 18 36, email: cynthia.martinez@uab.es

Abstract

In this work, the design and development of a series of miniaturized multiparametric probes for in soil nutrients monitoring under unattended conditions is presented. The devices are based on the green tape technology and include three ion-selective electrodes for the simultaneous and direct determination of nitrate, potassium and phosphorous. Taking advantages of the green tape compatibility with screen-printing techniques, the electronics regarding signal conditioning were monolithically integrated, increasing the devices reliability and robustness. The miniaturized probes were used to implement a wireless sensor network in order to obtain continuous and distributed information.

Keywords: nitrate, potassium, phosphorous, ion-selective electrodes, green tape technology, wireless sensor network.

INTRODUCTION

Grand efforts on the field of sustainable agriculture have been focused on the development of innovative practices that allow not only to optimize economical costs but also to minimize possible negative environmental impacts through appropriate and controlled fertilization processes. Chemical sensors are one of the most promising fields for in-soil analysis systems.[1] They are simple devices, compared with other analytical techniques, which provide a robust, versatile and low cost methodology for *in-situ* determinations.[2-4]

In this work, a set of miniaturized multiparametric probes based on the green tape technology was applied to implement a wireless sensor network for in-soil macro nutrients monitoring (K^+, NO_3^-, HPO_4^{2-}). Taking advantage of the compatibility presented by the green tape technology with screen-printing techniques, both the polymeric-based ion-selective and the reference electrodes were embedded into the ceramic body using silver-based paste. This compatibility was also profited to integrate monolithically all the electronics associated to signal conditioning, providing the device with a higher integration level, robustness and reliability.

EXPERIMENTAL

Probe fabrication. DuPont 951 green tapes were used as substrate for the fabrication of the miniaturized probes. Electrical conductors were printed using DuPont 6146 for solderable tracks, DuPont

[1] Lemos, S.G; et al. *Commun. Soil Sci. Plant Anal.* **2009**, 40, 1282.
[2] Artigues, J; Jiménez, C; Lemos, S. G; Nogueira, A. R. A; Torre-neto, A. *Sens. Actuators, B*, **2003**, *88*, 337.
[3] Lemos, S. G; Nogueira, A. R. A; Torre-neto, A; Parra, A; Artigues, J. Alonso, J. *J. Agric. Food Chem.* **2004**, *52*, 5810.
[4] Van Raij, B; Quaggio, J. A.; Silva, N. M. *Commun. Soil Sci. Plant Anal.* **1985** 16 (3), 245.

6142D for internal tracks and DuPont 6141 for via filling (Du Pont, UK). All the electronic components were carefully selected to improve the system response and reduce noise effects in signals. Surface Mount Devices (SMD) were used to reduce the dimensions of the electronics. The fabrication process regarding green tape technology was described elsewhere.[5] The design included 6 layers as depicted in figure 1.

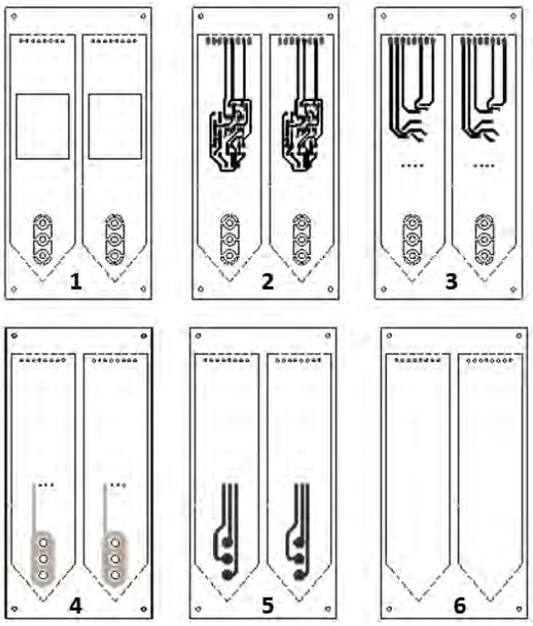

Figure 1. Layer by layer design. **1:** general top layer; **2:** top layer of the electronic circuit; **3:** bottom layer of the electronic circuit; **4:** reference electrode; **5:** paths over which the PVC membranes will be deposited; **6:** general bottom layer.

Once the device was burned-out, the pair Ag/AgCl (reference electrode) was formed by means of an anodization procedure. This process consisted on immersing the probe in a KCl 0.1M solution and applying a fixed potential of 1.2V during 10 minutes to the corresponding electrical terminal. The PVC-based ion-selective membranes were deposited by dropping the sensing cocktail into the previously defined cavities. The composition of the membranes for nitrate and potassium was that described on the bibliography.[6,7] Regarding phosphorous, its ionophore was synthesize in our research group.

The electronic circuit embedded in the probes avoids that cross-talking or electrical noise may mask signals through a proper impedance coupling. To ensure a proper analytical behavior of the probes, a calibration process was performed both, in solution and in-soil. Analytical features such as sensitivity and limit of detection were obtained from the calibration plots. Once prepared, the miniaturized probes were coupled to tailor-made wireless transmitters based on ZigBee technology, which enable communications with a personal computer in the vicinity.

RESULTS AND DISCUSSION

As a first approach, devices have been installed in at the EMBRAPA (*Empresa Brasileira de Pesquisa Agropecuária*) facilities in Sao Carlos, Brazil. Figure 2 presents one monitoring point were two wireless probes were installed.

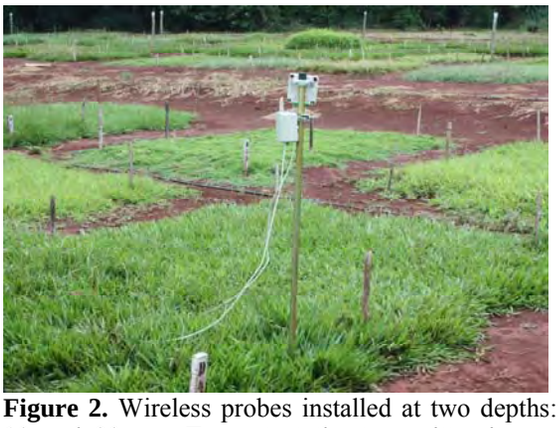

Figure 2. Wireless probes installed at two depths: 10 and 20 cm. To protect the transmitter it was enclosed in an IP68 protection code box.

First results demonstrated the viability of the system proposed to provide understanding information about soil processes in which K^+, NO_3^- and HPO_4^{2-} ions are implied.

[5] Ibáñez-García, N.; Alonso, J. Martínez-Cisneros C.S. et al., *Trends in Analytical Chemistry*, **2008**, 27, 24.

[6] Alegret, S.; Alonso, J.; Bartroli, J.; Paulis, J.M.; Lima, J.L.F.C.; Machado, A.A.S.C.; *Anal. Chim. Acta*, **1984**, 164, 147.

[7] Alegret, S.; Alonso, J.; Bartroli, J.; Lima, J.L.F.C.; Machado, A.A.S.C.; Paulis, J.M.; *Anal. Lett.*, **1985**, 18, 2291.

A Silver Ion LTCC-based Microanalyzers for the Control of Water Reutilization Processes in Manned Aerospace Missions

E. Arasa-Puig, J. Andrade, C.S. Martinez-Cisneros, J. Alonso-Chamarro
Universitat Autònoma de Barcelona, 08193, Bellaterra, Barcelona, Spain
eva.arasa@uab.es

Abstract

The challenge to achieve appropriate disinfection procedures without producing harmful wastes, as well as the growing demand for decentralized or point-of-use water treatment and recycling systems calls for new technologies for efficient disinfection and microbial control. This could be the case of manned aerospace missions which are raising the use of silver nanoparticles (nAg) as antimicrobial agent. Thus, a silver microanalyzer which allows to know the Ag^+ concentration in the recycled water and that fulfills the requirement to be sent in manned missions would be desirable.

Keywords: silver detection, potentiometric detection, LTCC analytical microsystem, manned aerospace missions.

Introduction

The use of sand filtration and chlorine disinfection marked the end of waterborne epidemics more than one century ago. Although the disinfection methods (chlorine, chloramines, ozone, etc.) currently used in drinking water treatment can effectively control microbial pathogens, they generate harmful disinfection byproducts (DBPs), many of which are carcinogens. Therefore, there is the need to reconsider the use of conventional disinfection methods and to take into account new approaches which avoid DBP formation.

Nanomaterials have experienced a rapid growing in the last decade and they are expected to revolution the water treatment process. They are excellent adsorbents, catalyst and sensors due to their large specific surface area and high reactivity. More recently, nanomaterials have also shown to have strong antimicrobial properties, including silver nanoparticles (nAg), photo catalytic TiO_2, aqueous fullerene nanoparticles (nC_{60}) and carbon nanotubes (CNT). Unlike conventional disinfectants, they are not expected to produce harmflul DBPs.[1]

Another potential application of antimicrobial nanomaterials is their use in decentralized or point-of use water treatment and reuse system. It is envisioned that functional nanomaterials, including those with antimicrobial properties, can be used as point-of-use systems to increase the robustness of water supply networks for emergency following catastrophic events and manned aerospace missions.

Space Agencies, such as European Space Agency (ESA), are promoting the use of nAg as antimicrobial agent in manned aerospace missions. Its antimicrobial mechanism consists on releasing Ag^+ ions which disrupt cell membrane and electron transport. Hence, it is mandatory to know if the concentration of released Ag^+ ions in the recycled water is suitable for human consumption. For this reason, it is necessary to develop a miniaturized Ag+ analyzer that fulfills the aerospace requirements such as low size, weight and reagent consumption and long operational life time. To attain this goal, some miniaturization techniques using substrates such as silicone and glass, polymers and green tape ceramics can be applied. This last technology, also known as LTCC (Low Temperature Co-fired Ceramics) has spread out its application in the microsystems field. The remarkable features of this technology allow the integration of detectors (optical, electrochemical, etc.), complex microfluidic structures and electronic circuits, all in the same device. [2]

Electrochemical detection (potentiometric, voltammetric) systems are an attractive alternative in microfluidics due to their small sample and reagents requirements, their low detection limits and their viability to be integrated in LTCC-based devices. [3,4]

Hence, in this work we proposed the development of an automated Ag^+ microanalyzer based on the LTCC technology with potentiometric detection using crystalline electrodes of Ag_2S, which fulfill the ESA

requirements in order to be actually applied to space missions.

Experimental

Figure 1 shows the Ag^+ microanalyzer. The reference Ag/AgCl electrode is placed in an auxiliary channel (c) through which a Cl^- ion solution flows continuously. The experiments are carried out using the flow injection analysis (FIA) technique.

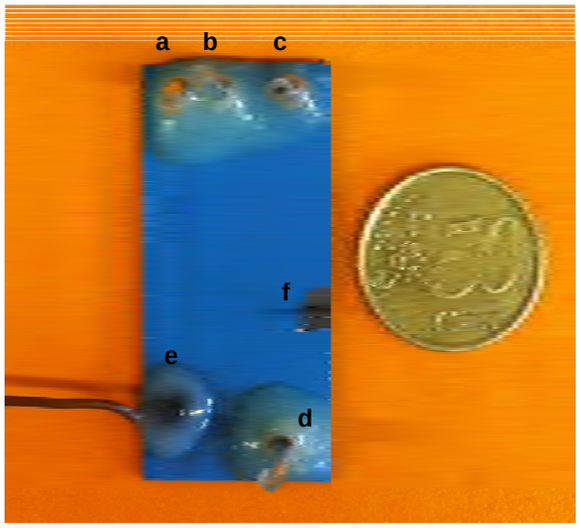

Figure 1. Ag+ microanalyzer where a is the conditioning solution inlet, b is the carrier solution/sample inlet, c is the Cl^- inlet and d is the waste outlet. e is the Ag_2S crystalline membrane with the electrical contact to the external set-up and f is the electrical contact of the reference electrode to the external set-up.

Results and discussion

The analytical features needed are a linear range of 80-8000 ppb Ag+ with a precision of 20%.

The linear range obtained with the proposed microanalyzer is 80-10000 ppb Ag^+ (see Figure 1 A). Figure 1 B shows the successive injections of the same stock solution. In this case, the calculated precision (% RSD) are less of 2.5%. Hence, this microanalyzer fulfill the prefixed requirements.

Since the device is expected to work autonomously in manned space missions, a long life-time is required (1 year at least). The life time study of the microanalyzer is currently under test. However, the electrode response has demonstrated to be stable at least during 5 months.

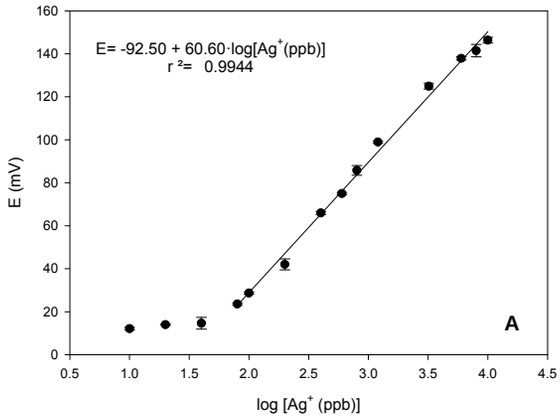

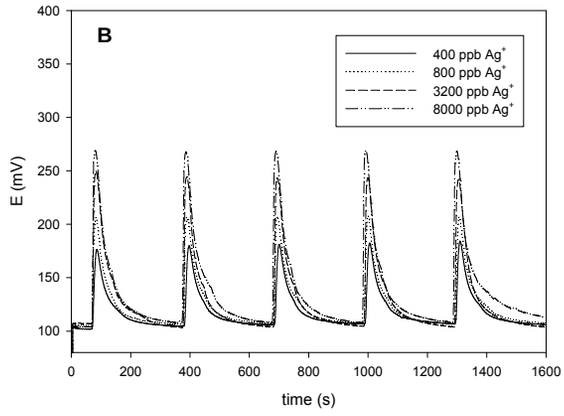

Figure 2.A) Calibration plot and B) successive injections of different concentrations of stock solutions ($AgNO_3$). Hydrodynamic conditions: 0.9 mL/min 0.05M Na_2SO_4 on a background of 2.5x10^{-7}M $AgNO_3$ (27 ppb) as conditioning solution; 0.9 mL/min of Milli-Q water as carrier solution; injection volume of 225 µL.

On the other hand, due to weight restrictions during space missions, the reagent consumption needs to be minimized as possible. In this case, a protocol which requires 4 analyses per day and a calibration procedure (2 points) per week will be acceptable if annual waste generation is maintained below 200 ml. The attainment of this requirement will be studied in the near future.

References

[1] Q.Li ; S. Mahendrea ; D. Y. Lyon ;et al:; Water Research, Vol. 42, pp. 4591-4602, August 2008.

[2] N. Ibanez-Garcia, J. Alonso.; C.S. Martinez-Cisneros; et al; Trends in Analytical Chemistry, Vol. 27, Nº 1, pp. 24-33, January 2008.

[3] N. Iba nez-Garcia; R.D. Man chado Gonçalves; Z.M. d a Rocha; et al.; Sensors and Actuators B, Vol. 118, Nº 1-2, pp. 67-72, May 2006.

[4] M.R. Gongora-Rubio; M.B.A. Fontes; Z.M. da Rocha,; et al.; Sensors and Actuators B. Vol. 103, Nº 1-2, pp. 468-473 , July 2004.

Determinação de Sulfato e Cloreto em Águas de Consumo com um Sensor Acústico

L. V. L. Venâncio, M. T. S. R. Gomes*
CESAM & Departamento de Química, Universidade de Aveiro
3810-193 Aveiro, Portugal
*mtgomes@ua.pt

Resumo

Um novo sensor baseado num cristal piezoeléctrico de quartzo foi desenvolvido para determinar sulfato. O sensor demonstrou possuir uma boa sensibilidade e ser bastante estável, mas responde a outros aniões. Apesar dos coeficientes de selectividade para diversos outros aniões terem sido muito inferiores ao do sulfato, a interferência dos cloretos e carbonatos na análise de águas sulfatadas comerciais não pôde ser ignorada, o que obrigou a um procedimento experimental mais trabalhoso, que incluiu a precipitação selectiva de alguns aniões. O novo sensor constituiu no entanto um passo importante na área dos sensores para aniões, dada a escassez de ionóforos e à dificuldade em conseguir determinar aniões na cauda da série de Hofmeister.

Palavras-chave: Sensor Acústico, Cristal Piezoeléctrico de Quartzo, Sulfato, Cloreto.

1. Introdução

Os sensores para aniões, independentemente do princípio transdutor, são escassos [1] e têm a sua selectividade ditada pela série de Hofmeister. Assim, a análise das águas de consumo e termais tem que ser normalmente realizada por métodos convencionais, recorrendo a instrumentação dispendiosa.

Neste trabalho apresenta-se um sensor novo, muito sensível ao ião sulfato, que por ser bastante hidrofílico se torna difícil de determinar. Este sensor foi testado na análise de águas sulfatadas.

O sensor, baseado num cristal piezoeléctrico de quartzo revestido com um composto orgânico, uma ftalocianina, especialmente sintetizado para o efeito, responde preferencialmente ao sulfato, mas apresenta um coeficiente de selectividade de 0,382 para o cloreto, que está presente em concentrações apreciáveis nas águas analisadas. Os carbonatos tiveram que ser eliminados por precipitação, uma vez que também interferiam na análise dos sulfatos. Recorrendo-se à precipitação selectiva dos sulfatos, foi possível conhecer a concentração individual dos cloretos e sulfatos nas amostras.

Os resultados foram comparados com os valores do rótulo das garrafas.

2. O Sensor Acústico e o Sistema de Análise

Foram utilizados cristais de quartzo piezoeléctrico de 9 MHz, corte AT, HC-6/U, polidos, com eléctrodos de ouro (ICM).

O cristal revestido foi introduzido numa célula de fluxo. Água MilliQ foi obrigada a mover-se com um caudal de 0,9 mL/min pela pressão exercida pelo azoto numa garrafa. As amostras foram injectadas numa válvula com uma serpentina de 0.5 mL, e transportadas pelo caudal de água até ao sensor. Na Fig.1 está representado o sistema de injecção em fluxo usado nas análises.

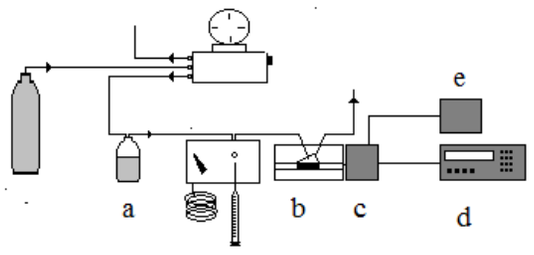

Fig. 1 – Sistema de injecção em fluxo: a) água MilliQ, b) célula com o sensor, c) oscilador, e) fonte de alimentação, d) frequencímetro.

A célula foi construída em PVC e pode ver-se em detalhe na Fig. 2.

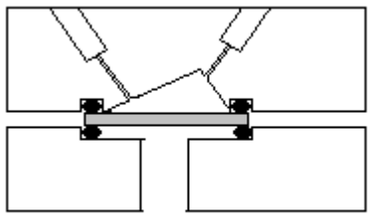

Fig. 2 – Célula do cristal em PVC..

O cristal está apertado entre duas anilhas, o que impede o líquido de molhar a face inferior do mesmo.

A frequência do sensor foi medida por um frequencímetro.

3. Resultados e Discussão

A resposta do sensor é rápida e completamente reversível. 45 s são suficientes para responder ao analito e recuperar. Na Fig.3 está representada a recta de calibração do sensor construída com os decréscimos de frequência obtidos injectando no sistema 0,5 mL de cada solução padrão de sulfato.

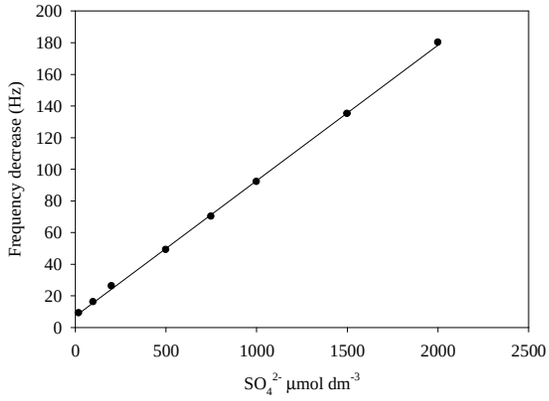

Fig. 3 – calibração do sensor.

A zona de calibração linear está entre 20 e 2002 µmol $dm^{-3,}$ e a sensibilidade ao sulfato foi de 85678 Hz dm^3 mol^{-1}. O tempo de vida útil do sensor foi de 8 semanas. A resposta variou com o pH, o que exigiu o ajuste do mesmo nas amostras.

O sensor foi usado na análise de águas sulfatadas comerciais. Aproveitando o facto do sensor ser também sensível ao cloreto, este anião também foi determinado. Apresentar-se--ão posteriormente os resultados dessas análises. Foram ainda feitas algumas análises por volumetria. A comparação dos resultados obtidos com o sensor com os valores do rótulo e com os resultados volumétricos permitiram apontar as vantagens e inconvenientes deste novo método de análise.

Agradecimentos

Os autores agradecem o apoio financeiro recebido do CESAM.

Referências

[1] Valente, N. I. P; Muteto, P. V.; Farinha, A. S. F.; Tomé A. C.; Oliveira, J. A. B. P.; Gomes, M. T. S. R. An acoustic wave sensor for the hydrophilic fluoride. *Sens. Actuators B* 2011, 157, 594-599.

Determination of Heavy Metals Contamination Using Optoelectronic Techniques

M. Aceves-Mijares, J. M. Ramírez, J. Pedraza, C. Chávez.
Instituto Nacional de Astrofísica, Óptica y electrónica,
Apdo. 51, Puebla, Pue. México72760
maceves@inaoep.mx, jmram@inaoep.mx, jpch@inaoep.mx

Abstract

The environmental contamination currently is a big problem for the life in the earth. So, the need for simple and economical ways of detection of different contaminants is an important area of research. In this paper, an intent on determine heavy metals in water is shown. The preliminary results are promising. However, much more research and experiments have to be done.

It is not necessary to mention the serious problems that we are facing up with water in our nowadays world. What is more, environmental contamination is a common problem not only in big cities but in rural areas also. Researchers, all around the world, are trying to find out simple methods of detecting and measure it. In particular, heavy metals in water are a big health problem because these metals are very toxic and the human body cannot eliminate them, causing irreversible diseases. Then, efforts to determine this contamination in a simple, reliable and cheap way are mandatory.

The development of new electronic light sources and detector in concurrence of new and more efficient ways of handle optical and electronic data, opens the possibility of analyze different compounds by optoelectronic methods. Instead of traditional techniques such as atomic absorption spectrometry and Inductively Coupled Plasma Optical Emission Spectrometry, simpler techniques are under developing. Optical characteristics as absorption, transmittance, reflectance, scattering and fluorescence are now easy and precisely measured. Some of these characteristics are now used to determine water contamination. The optoelectronic equipment used in those analyses is cheaper, transportable, simple to use and precise.

There are several experimental reports of optoelectronic sensors that use the principles mentioned. References [1, 2, 3, 4] are just some examples that can be found in the literature. Also, sensor and equipment using the principles mentioned are commercially available [5]. However, the use of optoelectronic properties to detect contaminants needs a lot of research efforts to be a common technique.

In this paper, the measurement, and data processing, of the transmittance of the UV radiation of pure water contaminated with heavy metals is proposed as an optoelectronic method to determine the contamination. Cadmium, Zinc, Lead, Cupper and Manganese are used in a preliminary experiment to explore the feasibility of the method.

The experimental set up is shown in figure 1(a), for more detail on the experimental procedure refer to [6]. The relative transmittance, Tr, was measured in the wavelength range of 200 to 400 nm. The results show clearly discernible curves for the different metals and concentrations. Figure 1(b) show the transmittance curves for the different metals used with a concentration of 5000 ppm. 100 ppm was the minimum quantity clearly determined. In this wavelength range, the Tr and the concentration is determined by quadratic relationship. In a simple way this relationship can be used to determine the metal and its concentration, experimentally an error of less than 5% was found.

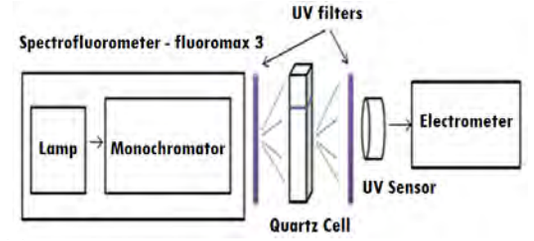

(a)

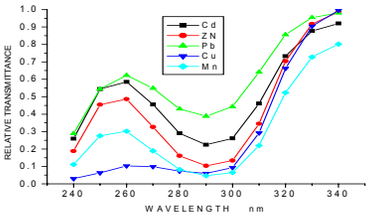

(b)

Fig. 1. (a) Experimental setup, the Xe lamp and the Monochromator of the spectrofluorometer is used as a monochromatic light source. (b) Relative transmittance as function of incident wavelength for the five metals used with 5000 ppm.

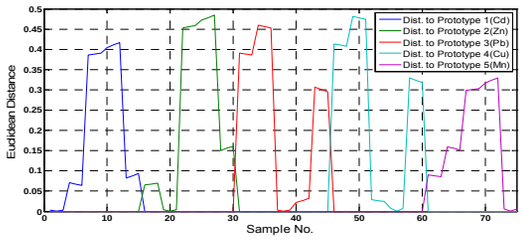

Figure 2. Euclidean distance from database samples to the five prototypes

In order to automatically classify the different contaminated solutions, a data base was created with the relative transmittance obtained at five different wavelengths in the range 250-300 nm, which were found to give the most discriminative values associated to the greatest variances. Separability on data clustering was tested through Euclidean distance classification, which is a well-known pattern recognition technique. The object under test is assigned to the nearest prototype among the p classes, using the minimum-Euclidean-distance criteria, equation 1, where each prototype is obtained as the mean vector of the m samples in each class, equation 2. In this work, the number of classes corresponds to p=5 (five contaminating metals), and m=3 (number of samples associated to each contaminating metal). Figure 2 shows the Euclidean distance obtained from the samples in the database to each prototype. Inter and intra-class statistical analysis indicates that an adequate data clustering with good data separability can be obtained through the described method. Further experimentation using non linear classification based on neural networks is currently in progress.

$$d_{ip} = \sqrt{\sum (\bar{X}_p - \vec{x}_i)^2} \qquad (1)$$

$$X_p = 1/m \sum_{j=1}^{m} x_j \qquad (2)$$

Additional experimentation aiming to the generation of a comprehensive database should be carried out in order to come up with a complete technique evaluation. Those experiments should include more contaminants at different concentrations, as well as combinations of them, which could take advantage of the non linear classification capabilities of the neural network.

In conclusion, heavy metals dissolved in water were determined using an optoelectronic method. Been aware that more research has to be done, it was possible to detect the type of contaminant, and the concentration up to 100 ppm, using the optical transmittance of light in the UV range and the statistical manipulation of the data.

Acknowledgements. The author appreciate the support of CONACyT.

References

1 Chuqun Chen; Fenfen Liu; Quanjun He; Heyin Shi "The possibility on estimation of concentration of heavy metals in coastal waters from remote sensing data" Geoscience and Remote Sensing Symposium (IGARSS), 2010

2 Herlina Abdul Rahim, Bashirun Che Morat, Ruzairi Abdul Rahim. "Non-Invasive Evaluation of Hydrogen Peroxide Concentrations in a Drinking Bottle by Near-Infrared Spectrometry" Sensors & Transducers Journal, Vol. 131, Issue 8, 2011, pp. 83-90

3 Mounir Boukadoum, Abdelaziz Trabelsi, Christian Fayomi. "FPGA-Based Multispectral Fluorometer using CDMA and Embedded Neural Network" International Conference on Microelectronics, pp 205 to 208, 2009.

4 A. Trabelsil, M. Boukadouml, C. Fayomil, E.M. Aboulhamid. "Blood Glucose Sensor Implant Using NIR Spectroscopy: Preliminary Design Study" International Conference on Microelectronics (2010)

5 S. Y. Yurish "Smart Optoelectronic Sensors and Intelligent Sensor Systems" Sensors & Transducers Journal, Vol. 14-1, (2012), pp. 18-31

6 César Chávez-Vallarino, Mariano Aceves-Mijares, Jorge Pedraza-Chávez. "Transmittance of Aqueous Solutions with Heavy Metals in The Uv Range" 8th International Conference on Electrical Engineering, Computing Science and Automatic Control. Merida, pp. 1066-1069, Yucatan, México. 2011

Efectos estacionales en los niveles de arsénico de pozos urbanos de la Comarca Lagunera.

Aldo Uriel Aguilar-Muñiz[1], Francisco Valdés-Perezgasga[1], Gonzalo G. García-Vargas[2]
[1]Instituto Tecnológico de la Laguna, 27000, Torreón, Coahuila, México
[2]Facultad de Medicina, Universidad Juárez del Estado de Durango, 35050, Gómez Palacio, Durango, México
doal86@hotmail.com

Resumen

En el presente trabajo se analizarán los cambios en los niveles de arsénico en el agua de varios pozos urbanos de la Comarca Lagunera al principio y al final del ciclo de riego agrícola. Este análisis es realizado utilizando un Sistema de Información Geográfica (SIG), el cual nos proporciona un panorama del comportamiento estacional de los niveles de arsénico de manera fácil de comprender. El trabajo se presenta como un precursor de un sistema basado en sensores, automatizado e inalámbrico.

Palabras Clave: Arsénico, Hidroarsenicismo, Sistemas de Información Geográfica.

Introducción

El arsénico (As) es un elemento tóxico para el cuerpo humano. Puede llegar a causar problemas de salud cuando se ingiere en pequeñas cantidades durante un periodo de tiempo considerable (por ejemplo en el agua de bebida). Los efectos sobre la salud son múltiples, y van desde simples alteraciones en la piel hasta cáncer de diversos órganos como piel, vejiga, riñones, pulmones, hígado y próstata [1].

Hidroarsenicismo

Las investigaciones que se han realizado apuntan a que el origen del arsénico en el agua subterránea de la Comarca Lagunera se debe a la sobreexplotación del acuífero dada por la disminución de los aportes de los ríos por causa de su desvío por canales de riego y la extracción inmoderada de agua del subsuelo [2].

Desarrollo

Para observar el efecto que tiene el ciclo de riego agrícola en los niveles de arsénico durante 2010, se realizaron muestreos de agua potable antes y después de dicho ciclo en 50 puntos distribuidos en toda la zona objeto de estudio. Las muestras fueron georreferenciadas y luego se les midió la concentración de arsénico y la conductividad. Una vez que se obtuvieron los resultados de dichos estudios, estos se analizaron con un sistema de información geográfica (SIG) para observar la probable distribución del arsénico en el subsuelo de la región.

El SIG es capaz de realizar una representación de los datos georeferenciados sobre el planeta a través de un mapa, una fotografía aérea o satelital.

Resultados

Las imágenes que se muestran son el resultado del análisis de datos usando el SIG. Dichas imágenes corresponden al análisis de muestras antes y después del ciclo de riego agrícola respectivamente.

El estudio se realizó únicamente en la zona urbana de la Comarca Lagunera, la fotografía satelital que aparece como fondo en las imágenes corresponde a dicha zona. Encima de esta fotografía se ubica la capa de resultados, donde las áreas rojas corresponden a una concentración superior a los 25 µg/L de arsénico en agua, el cual es el límite superior permisible por la Norma Oficial Mexicana [3], aún cuando la Organización Mundial de la Salud establece como limite 10 µg/L [4].

En la Imagen 1 se muestra el análisis realizado en el mes de abril 2010 (antes del ciclo agrícola).

Imagen 1 Niveles de arsénico en tomas de agua potable de la zona urbana en la Comarca Lagunera (abril 2010)

En la Imagen 2 se muestra el análisis realizado en el mes de octubre 2010 (después del ciclo agrícola).

Imagen 2 Niveles de arsénico en tomas de agua potable de la zona urbana en la Comarca Lagunera (octubre 2010)

Conclusiones

El ciclo de riego agrícola tuvo un efecto de disminución de los niveles de arsénico en el área oriente de nuestra zona de estudio y un efecto de aumento de niveles en el área poniente. Cabe mencionar que el límite derecho de la zona roja coincide en gran cantidad con el cauce seco del río Nazas, el cual experimentó también una avenida extraordinaria en el mes de agosto. Las avenidas del Nazas son muy poco frecuentes ya que en los últimos años solo se han tenido tres (1992, 2008 y 2010).

Esta avenida del Nazas pudo haber provocado una recarga violenta del acuífero. La recarga súbita pudo haber revuelto el arsénico depositado en forma de sales en el fondo del acuífero mezclándolo con estratos más superiores. En sitios más alejados del cauce (ubidados al oriente) la recarga fue menos violenta reflejándose en una disminución de lso niveles de arsénico.

El SIG tiene la ventaja de dar imágenes que posibilitan una comprensión mejor de fenómenos complejos. Esta comprensión sería mucho más difícil si la información permanece en una forma tabular y no gráfica.

Referencias

[1] López Uriostegui Zelene. Determinación de arsénico en aguas subterráneas de la Comarca Lagunera. Tesis de Ingeniería. Instituto Tecnológico de Mazatlán. Mazatlán, Sinaloa, México; Mayo 2007.

[2] M.A. Ortega-Guerrero. “Origin of high concentrations of arsenic in groundwater at the “La Laguna Region”, northern Mexico, and implications on aquifer management”. Memorias del 32 Congreso Internacional de Geología, Florencia, Italia, p. 1486.

[3] MODIFICACION a la Norma Oficial Mexicana NOM-127-SSA1-1994, Salud ambiental. Agua para uso y consumo humano. Límites permisibles de calidad y tratamientos a que debe someterse el agua para su potabilización. México, D.F., a 20 de octubre de 2000.
http://www.salud.gob.mx/unidades/cdi/nom/m127ssa14.html
[Consulta: 30 de Junio del 2011]

[4] Organización Mundial de la Salud. Guías para la calidad del agua potable.Vol.1: Recomendaciones. Tercera edición. ISBN: 92 4 154696 4.
http://www.who.int/water_sanitation_health/dwq/gdwq3_es_full_lowsres.pdf
[Consulta: 23 de Agosto del 2011]

DEMUTOX-SENSOR: KITS FOR MULTI-TOXIN DETECTION

Georges ISTAMBOULIE, Gaëlle CATANANTE, Audrey SASSOLAS, Yohann DAVIDDI and Jean Louis MARTY
Université de Perpignan Via Domitia, IMAGES EA 4218, 52 Avenue Paul Alduy, 66860 Perpignan Cedex, France
contact@demutox-sensor.fr

Abstract

In this work, two categories of pollutants are analyzed: Neurotoxins (in particular organophosphate insecticides and carbamates), and biotoxins (in particular microcystins and Okadaic acid, which is responsible for important economic losses in shellfish farming). We develop detection kits for precise targets and more generic kits to measure a global toxicity, the originality of our technological development is in the use of genetically-engineered enzymes: Acetylcholinesterase and Protein Phosphatases. The advantage of these recombinant enzymes is their stability (multiplied by 20) and their selective sensitivity for the several targets (which can be multiplied by 300,000 for dichlorvos for example).

Keywords: Colorimetric kits, Biosensor, mutant enzymes, neurotoxins, biotoxins

Problems

The International efforts aimed at environmental protection, allowed to bring to light a contamination by anthropological (pesticides) and natural pollutants (biotoxins), these toxins are observed in all the elements of a biosphere: water, ground, air, vegetation, animal and Man. Recent efforts led to the identification of known and emergent toxins, as well as the development of new detection methods, to measure their real toxicity and to evaluate the risks to the consumer. However, several analytical techniques have been criticized by the market players of the food-processing industry and the environmental protection agencies because of their low sensibility and their high costs. In December 2009, the French ministry of agriculture ended the “Mouse Bioassays”, which were used as a routine assay for the detection of toxic microalgae, leading regularly to ban the bivalve’s sale. The initiative of stopping this assay was based on ethics as well as its poor efficiency. The current conventional methods, (HPLC / SM, CL-SM / SM) allow a very sensitive detection of the possible presence of toxins, but they require heavy and expensive instruments. It has now become urgent to develop reliable, fast and low cost detection methods to insure the products safety and for environmental protection.
DEMUTOX-sensor project aims for the development of a multicriteria colorimetric kit for the detection of antropic and natural toxins, in animal and human foodstuffs, likewise in water and soil. The detection principle is based on the inhibition of highly stable and sensitive recombinant enzymes (acetylcholinesterases and protein phosphatases). This principle will subsequently be used to develop a portable and reliable amperometric screening kit.

Genetically-engineered enzymes

In this project, two categories of pollutants will be analyzed: Neurotoxins, in particular organophosphate insecticides and carbamates, and biotoxins, specifically microcystins and Okadaic acid, which is responsible for important economic losses in shellfish forming. The originality of our technological development is in the use of genetically-engineered enzymes. These enzymes, developed for several years by our group, have been improved upon and stabilized, to display optimum activity. Acetylcholinesterase (AChE) is an enzyme found in all animals, from insects to humans. It is essential to nerve cell function through its mechanism of breaking down the neurotransmitter acetylcholine into acetate and choline. This enzyme, which is the target of neurotoxic agents (organophosphorus and carbamates), can also be inhibited by heavy metals and natural neurotoxic compounds produced by cyanobacterias (Aphanizomenon and Oscillatoria). We will develop detection kits for precise insecticides and more generic kits to measure a global neurotoxicity. We have worked with a range of recombinant AChEs, whose performances allowed us to design

innovative biosensors for pesticide detection. The advantages of the recombinant enzymes are their stability (multiplied by 20) and their selective sensitivity for the organophosphate insecticides (which can be multiplied by 300,000 for dichlorvos for example). The Protein Phosphatases (PP1A, PP2A) are enzymes, which play an essential role in numerous aspects of the cellular physiology. They are inhibited by several biotoxins produced by algaes in sea and fresh water. In this project, we will develop detection kits for:

The microcystins are endotoxins that those preserve their toxicity for several weeks and carry a serious sanitary risk. The presence of endotoxins in blood is called Endotoxemia; it can lead to septic shock if the immune response is severely pronounced.

The Okadaic acid and its analogues, dinophysistoxines (DTX1, DTX2 and DTX3), form together the group of toxin AO. These toxins, lipophilic and thermostable, are produced by dinoflagellates (Dinophysis and Prorocentrum). They are responsible for syndromes of DSP (Diarrheic Shellfish Poisoning). These food poisonings are relatively common and have strong repercussions for food safety and on investment in seafood production zones.

Kits and biosensors

Colorimetric Kits:

This multicriteria kit will be based on recombinant acetylcholinesterases and protein phosphatases (PP2A, PP1A). It will be able to detect specifically: a wide range of neurotoxic agents (pesticides and heavy metals), okadaic acid and different kinds of microcystins. Technologically, the tests will be microplate kits. A hundred micro-liters of the sample will be sufficient to analyze and to obtain highly sensitive results, approximately a thousand times more sensitive than the commercial kits, (according to laboratory tests). This kit will allow analyses within one hour and will be adapted to in field measurements. There will be two methods for reading the results: visually (with decreasing sensibility), or using a low-cost portable colorimeter.

Portable Amperometric Kits :

In order to miniaturize the device, the target enzymes will be immobilized onto a transducer, leading to biosensors. During the last years, IMAGES laboratory has optimized the design and the composition of the transducer, using screen-printing technology. We are able to realize mass production of electrodes with good reproducibility and minimal cost. The developed biosensors, obtained after enzyme immobilization on these electrodes, allows for very sensitive detection of insecticides and toxins. The biosensors will be supplied with a portable and easy to use potentiostat, according to the following figure:

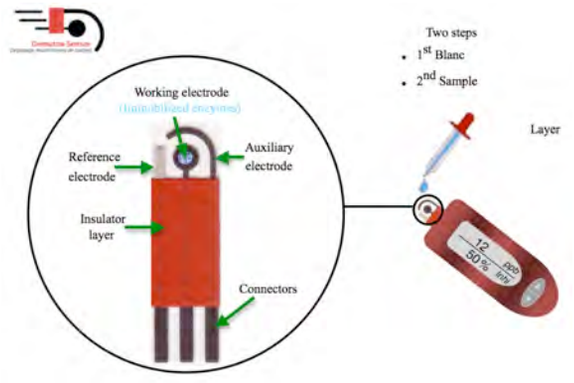

References

G. Istamboulie, S. Andreescu, J.-L. Marty, T. Noguer, Biosensors and Bioelectronics, Vol. 23, No 4, pp. 506-512, 30 November 2007.

G. A. Alonso, G. Istamboulie, A. Ramírez-García, T. Noguer 2, J-L Marty, R.Muñoz, Computers and Electronics in Agriculture, Vol. 74, pp. 223–229, November 2010.

A. Sassolas, G. Catanante, A. Hayat, J-L Marty, Analytica Chimica Acta, Vol. 702, No 2, pp. 262-268, September 2011.

A. Sassolas, G. Catanante, D. Fournier, J-L Marty, Talanta, Vol. 85, No 5, pp. 2498-2503, October 2011.

Chemical Wireless Sensor Network for pH Remote Monitoring

Claudia Manjarrés*, David Garizado*, Maria Calle*, Cecilia Jiménez**
*Department of Electrical and Electronics Engineering, Universidad del Norte, Barranquilla, Atlántico, Colombia **Instituto de Microelectrónica de Barcelona (IMB-CNM), CSIC, Campus UAB, 08193 Bellaterra, Barcelona, Spain

claudian, dgarizado, mcalle (@uninorte.edu.co), cecilia.jimenez@csic.es

Abstract

The use of microsensors for in-field monitoring of environmental parameters is gaining interest due to their advantages over conventional sensors. Among them, microsensors and specifically Ion Selective Field Effect Transistors (ISFETs) based on semiconductor technology offer additional advantages such as small size, robustness, low output impedance and rapid response. ISFETs sensors can be integrated into a wireless network in order to monitor pH from different locations and transmit information to a central point. The paper proposes a Chemical Wireless Sensor Network (CWSN) for pH monitoring through long distances, showing the general system and preliminary results.

Keywords: pH, ISFET, Chemical Wireless Sensor Network, Long Range

Introduction

Environmental monitoring often requires measuring a variable in different points simultaneously, since concentration of these variables often change with time or location. Examples include pollutants in a city or pH in a water source. One possible solution is to employ Wireless Sensor Network concepts to transmit chemical variables, defined as CWSN [1] combined with ISFET based sensors that have demonstrated to be a good alternative for environmental monitoring [2]. The proposed system includes hardware and software for a three-node network, scalable up to 65535 nodes. Hardware section allows for signal adaptation, analog to digital conversion, calibration and radio transmission. The software receives information from the network and shows an alert when pH value is out of range. Results show pH maximum error of 2.7% when compared to a WTW Multi3420 pHmeter.

Related Work

Although there is some literature concerning CWSN, such as [1], [3] and [4], these studies include short distance communication. Additionally, fewer studies include quantitative data on system accuracy.

System Description

Figure 1 presents a block diagram of the system. Each node includes a data acquisition board, Arduino Uno module for processing and one Xtend modem (by manufacturer Digi) as wireless Interface.

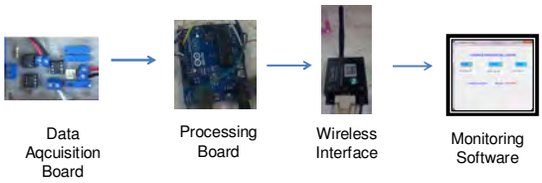

Figure 1. Block Diagram of CWSN. The prototype includes three nodes

Data acquisition board includes a circuit for providing the ISFET with a constant current of 100 µAmperes similar to [5]. ISFET output voltage may be negative and it depends upon pH values, thus the signal requires further conditioning to be processed. After conditioning, maximum output voltage is 1 V, connected to processing board's 10-bit Analog to Digital Converter (CAD), embedded in Arduino microcontroller. The device computes pH measurements and transmits data using a serial port to Xtend modem, whose transmission power ranges from 1 mW to 1 W. Figure 2 shows a schematic diagram of the data acquisition board.

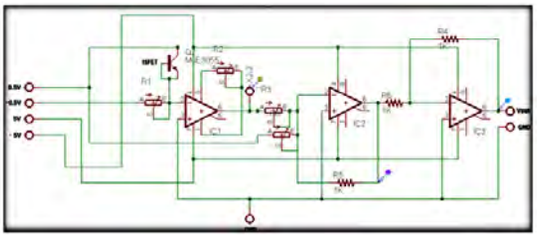

Figure 2. Detail on data acquisition board. The first op-amp provides a constant current to the ISFET; others create an inverter-adder to convert output voltage to a 0-1V signal

Chemical sensors require calibration that is measurement of signal/pH ratio with at least two standard solutions. The processing board implements a manual two-point calibration routine, to maintain accurate readings. Arduino also implements wireless communication protocols for CWSN. MAC layer uses a TDMA scheme to avoid collisions. CWSN uses a star topology, where all nodes can transmit directly to the final destination. Receiver modem is connected to a PC where resident Java software gathers information from the network and shows historical values. If pH values fall out of range, software will generate an alarm.

pH Measuring Results

The system was tested in laboratory for three solutions with different pH values: 4, 7 and 9. Each node uses one specific ISFET, and it is measured at least three times during 30 minutes. Table 1 shows average values obtained in each node, compared to pH values measured with a WTW Multi3420 pHmeter.

Table 1. Measurements taken by each node compared to readings with WTW Multi3420

Node	WTW pH	Calibrated pH	%Error
1	4,13	4,20	1,64
1	7,13	6,95	2,57
1	8,89	9,01	1,30
2	4,13	4,06	1,72
2	7,13	7,32	2,70
2	8,89	8,77	1,37
3	4,13	4,15	0,38
3	7,13	7,09	0,60
3	8,89	8,92	0,30

Table 1 show measurements agree, with maximum error 2.7 percent. Node 3 shows the best results, even though nodes are implemented with the same design described in Figure 2.

Figure 3 shows calibration curves for the three nodes employed.

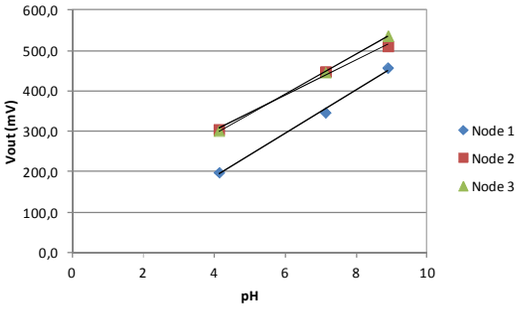

Figure 3. Calibration curves for the three nodes in CWSN

According to Figure 3, slopes for different nodes are: node 1 = 54 mV/pH, node 2 = 44 mV/pH and node 3 = 49 mV/pH. Values obtained for the three nodes are acceptable for silicon nitride ISFETs

Conclusions

A three node CWSN prototype was presented. The reproducibility of measurements between the three nodes is acceptable, although future work may improve on this metric. Wireless communication has been tested in a point-to-point Line of Sight setup, finding adequate transmission up to 4 kilometers. The next step includes integration of these wireless links to each node and measuring network performance.

References

[1] J. Hayes, S. Beirne, K. Lau and D. Diamond, “Evaluation of a low cost Wireless Chemical Sensor Network for Environmental Monitoring”, IEEE Sensors 2008 Conference, Lecce, Italy, October 26-29, pp 530-533, 2008.

[2] C. Jimenez-Jorquera, J. Orozco and A. Baldi, “ISFET Based Microsensors for Environmental Monitoring”, Sensors 2010, 10, 61-83

[3] S. De Vito et al, “Wireless Sensor Networks for Distributed Chemical Sensing: Addressing Power Consumption Limits With On-Board Intelligence”, IEEE Sensors Journal, Vol. 11, No. 4, pp. 947-955, April, 2011.

[4] V. Devan, “pH Wireless Sensor Network for the meat tenderizing process”, Master Thesis, Auckland University of Technology, Auckland New Zealand, 2010.

[5] F. Valdés-Perezgasga, “Intramyocardial pH Measurements using Ion-Sensitive Field-Effect Transistors”, Ph. D. Thesis, University of Newcastle upon Tyne, 1990.

Sensor de temperatura basado en un láser de fibra óptica

M. Durán Sánchez[a], E. Kuzin[b], B. Ibarra Escamilla[b], A. González García[b]
[a]Universidad Tecnológica de Puebla
Antiguo Camino a la Resurrección N°1002-A Parque Industrial, Puebla, Pue.72300,
México, tel/fax +52 222 3098825
[b]Instituto Nacional de Astrofísica, Óptica y Electrónica, Óptica,
Luis Enrique Erro No. 1, Puebla, Pue. 72000, México, tel/fax +52 222 2472940
mdurans.utp@gmail.com

Abstract

Presentamos resultados experimentales de un láser de fibra óptica. Con una simple detección de potencia óptica, presenta aplicaciones potenciales como sensor temperatura. La cavidad láser está formada por un espejo de lazo de Sagnac (sensor) y una rejilla de Bragg Sintonizable. El principio de operación se basa en medir la potencia óptica del láser para monitorear los cambios de temperatura en el interferómetro de Sagnac y determinar la temperatura del sistema.

Keywords: Fiber optics sensor, fiber interferometer, fiber optic laser, Sagnac interferometer

Introducción

En los últimos años, las fibras ópticas han sido utilizadas ampliamente en el ámbito de las telecomunicaciones, en sensores de fibra óptica, etc., debido a sus características únicas, tales como la multiplexión, la alta flexibilidad, bajas perdidas en la propagación, la alta sensibilidad, el bajo costo, su tamaño reducido, la alta precisión, la capacidad de detección simultanea y la inmunidad a las interferencias electromagnéticas. Hasta la fecha, una serie de estudios se han hecho para utilizar fibras ópticas como sensores de temperatura, tensión, presión, rotación, desplazamiento, índice de refracción, polarización, ultrasonido, y así sucesivamente [1-4]. De hecho, en algunas aplicaciones se han utilizado para el control real en la deformación de aviones, barcos, puentes y construcciones. A pesar de las investigaciones crecientes se extienden áreas de aplicación, principalmente debido al alto costo, solo pocos de ellos se han comercializado. Incluso en el mercado de sensores, los sensores de fibra óptica representan sólo una pequeña porción. Sin embargo, hasta ahora no se ha estudiado detalladamente el comportamiento de la potencia de salida del laser de fibra óptica utilizando para ello un interferómetro de Sagnac.

En este trabajo se evalúa dicho efecto y se muestra que puede ser aplicado al desarrollo de sensores, en particular se muestran resultados que permiten medir la temperatura mediante cambios de la potencia óptica en el sistema propuesto. Aunque solo mostraremos resultados respecto a la medición de temperatura, es claro que se puede utilizar para otra variable física. Finalmente, analizamos el espectro del interferómetro de Sagnac con un fotodetector, identificando de esta forma, los cambios de temperatura y acotando en un rango para ser utilizado como sensor.

Arreglo Experimental

La configuración experimenta del láser propuesto se muestra en la Figura 1. La cavidad lineal del láser está formada por un espejo de lazo de fibra óptica (FOLM) compuesto de un acoplador 50/50 cuyos puertos de salida se conectan 28 cm de fibra de alta birrefringencia (Hi-Bi), 3 m de fibra dopada con erbio y una rejilla de Bragg (FBG). La FBG tiene una longitud de onda central a 1537 nm. La reflexión máxima es de 55 %. La FBG se sintoniza mediante la deformación axial aplicada por un dispositivo mecánico. La EDF se bombea con un diodo laser cuya señal es introducida a la fibra atraves de un multiplexo por división de longitud de onda (WDM-980/1550) con una potencia máxima de 70 mW . El puerto libre del acoplador 50/50 se usa como salida del láser (Salida). La emisión laser en salida es enviada a un Monocromador con una resolución de 0.2 nm, después de ser detectada por un fotodetector y monitoreada mediante un osciloscopio digital para observar el espectro óptico. Posteriormente se coloca directamente un fotodetector para observar la potencia óptica de salida del láser.

El FOLM con fibra de Hi.Bi presenta una longitud de onda periódica dependiente de la reflectividad. Nosotros informamos de un análisis más detallado del comportamiento del FOLM en la aplicación laser con doble longitud de onda en la ref. [5]. La fibra de Hi-Bi se colocó en un Peltier para aplicar cambios de temperatura, donde se puede ajustar en un rango de temperatura de 15-30 °C. La fibra de alta birrefringencia es altamente sensible a cambios de temperatura que provocan un desplazamiento en el espectro óptico del FOLM y consecuentemente en la lectura del medidor de potencia óptica. Un sistema de medición y control electrónico se diseño para tener un control de temperatura de hasta 0.1 °C.

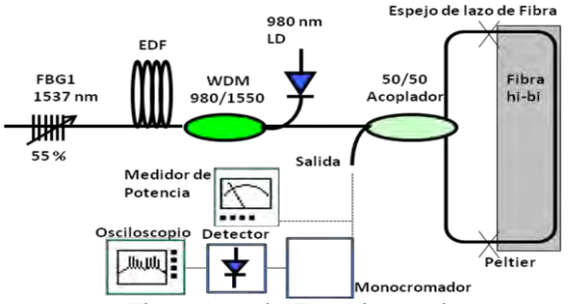

Fig. 1 Arreglo Experimental

Resultados y discusiones

La Figura 2 muestra el espectro óptico del laser cuando es bombeado a 70 mW junto con la sintonización del láser, esta sintonización se logra cuando se le aplica compresión a la rejilla de Bragg mediante un dispositivo mecánico. La compresión aplicada en la FBG generada por el desplazamiento de un tornillo micrométrico es de aproximadamente 1nm/10µm tomada a temperatura ambiente.

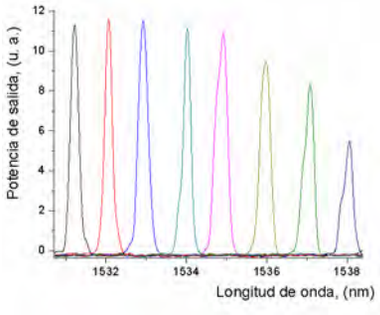

Fig.2 Laser Sintonizable

La Figura 2 se muestra la potencia óptica de salida con respecto a cambios de temperatura en el FOLM. La longitud de onda de la rejilla se encuentra fija a 1531.4 nm y los cambios de temperatura son de 15 °C a 30 °C mostrando una potencia máxima de salida de 1.8 mW a 17.2 °C y 19 °C, además se observa que para cada cambio de temperatura corresponde una potencia óptica de salida diferente de ahí su aplicación como sensor.

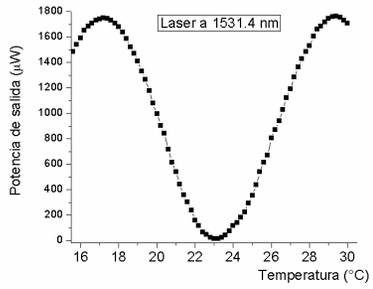

Fig.3 Potencia de salida con cambios de temperatura

La Figura 3 muestra las mediciones de potencia óptica a la salida para láser con diferentes longitudes de onda, se muestra el comportamiento del FOLM como sensor laser.

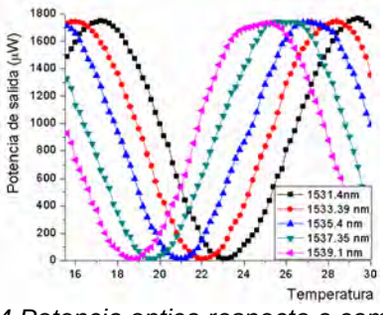

Fig.4 Potencia optica respecto a cambios de temperatura para diferentes sintonizaciones

Los resultados muestran que la relación de la potencia de salida con la variación de la temperatura tiene un comportamiento regular, con lo que es posible realizar las mediciones relacionando directamente éste valor de potencia con el de la variable física. El hecho de que la intensidad de salida del láser se comporte de ésta manera, se puede atribuir al espectro del Sagnac, lo que puede ser utilizado para modificar las características de la respuesta del sensor, es decir, modificar la sensibilidad y rango dinámico. Para esto, sería suficiente con elegir un perfil adecuado del FOLM.

Actualmente se está diseñando un FOLM con un periodo más grande para que el rango de temperatura sea mayor y se sustituirá el medio activo por un simple diodo laser a longitud de onda fija.

Este trabajo es soportado por Proyecto Conacyt 151434

Referencias

[1] Eric Udd, et. al. Fiber Optics Sensors,John Wiley, second edition, Chapter 1 and 9. pp. 1-8 and 199-230, 2011.
[2] M. Durán-Sánchez, et.al., Sensor and Actuators B, Vol. 123, pp. 816-821, 2007.
[3] F. Yu, S. Yin, “Fiber Optics Sensors”, Marcel-Dekker 2002.
[4] Byeong Ha Lee, et. al., Sensors 2012, Vol. 12, pp. 2467-2486, February 2012.
[5] R. I. Alvarez Tamayo, et. al., Applied Optics, Vol. 50, pp. 253-260, January 2011.

Fabrication of Phosphorus Doped Polysilicon Thin-Film Strain Gauges Using a 50 Microns Silicon Substrate Thickness

Acácio Luiz Siarkowski and Nilton Itiro Morimoto
LSI - Integrated Systems Laboratory / EPUSP - Polytechnic School of University of São Paulo
Av. Prof. Luciano Gualberto, Trav. 3, 158, São Paulo, SP, Brazil. CEP 05508-900
acacio@lsi.usp.br; morimoto@lsi.usp.br

Abstract

The strain gauges fabrication, using phosphorus doped polysilicon thin-film resistors, has been performed. Strain gauges transducers were designed to measure the strain in load cells, using a Wheatstone bridge circuit configuration. The strain and sensitivity measurements results for load cells application are described. A linear response and excellent repeatability were obtained.

Keywords: silicon substrate, strain gauges, polysilicon, thin-films, load cells and Wheatstone bridge.

Introduction

Typical strain gauges are made from a heat-treated metallic foil bonded to a dielectric layer [1, 2]. However, phosphorus doped polysilicon layer is used as a piezo-resistive material, mainly because the temperature coefficient of resistance (TCR) can be set as zero by suitable adjustment of the doping concentration [3, 4]. Phosphorus doped polysilicon thin films strain gauges technology is used as sensor for precision mass measurement. Polysilicon thin films strain gauges have high accuracy, repeatability, and reliability and low cost. These characteristics become very suitable to apply it in load cells elements. The strain gauges are positioned onto the areas, where the highest deformation is located onto the load cells (usually aluminum). The strain gauges are connected into a Wheatstone bridge circuit configuration. When a load is applied in the load cell, the strain gauge detects the strain and an unbalance in the Wheatstone bridge is observed, the resistance variation of the strain gauge is proportional to the mass of the load [3, 5]. This paper shows the fabrication process of phosphorus doped polysilicon thin film strain gauges and the optimization of phosphorous diffusion procedure to enhance the sensor sensitivity. The fabricated devices were tested in load cells used in commercial mass measurement equipment.

Fabrication and Bonding of Strain Gauges

Polysilicon thin films have sensitivity in between of a metal foil and monosilicon. However, the temperature coefficient of resistance, (TCR), which represents the extent of the effect of temperature changes, is significantly lower than of monosilicon strain gauges; it is typically less than 500 ppm/^{o}C [6].

A 100 oriented, p type, 10-20 Ω.cm, 50μm thick silicon wafer was used as substrate. It was processed with the following steps:

1. Chemical cleaning: The wafers were cleaned by standard RCA cleaning procedure.
2. Thermal oxidation: The wafers were thermally oxidized to grow a silicon oxide layer of 1μm thick.
3. Polysilicon Deposition: A polysilicon thin-film of 0.6μm thickness was deposited by Low Pressure Chemical Vapour Deposition (LPCVD) technique at 630ºC.
4. Phosphorus doping: A SOG (Spin on Glass) layer, with 1% or 3% phosphorus concentration, was deposited on the polysilicon film and the diffusion process temperature was carried out at 1150ºC. The SOG layer was removed using a 1% HF solution.
5. Patterns definition: The patterns of the designed strain gauges were defined by optical lithography and the polysilicon film was etched by a SF_6 plasma process. The photoresist was removed by O_2 plasma etching process.
6. Metallization: An aluminum layer of 1μm thick was deposited by thermal evaporation. This aluminum layer was annealed at 420ºC in inert gas ambient for 2 hours to improve the electrical contacts.
7. Contacts definition: The contacts patterns were defined by optical lithography and etched in a H_3PO_4 solution. The photoresist was removed by acetone and 2-propanol solvents.
8. Strain gauges dicer: The silicon wafer was diced by a disco saw to detach the individual strain gauges.

The electrical contacts of the strain gauges can be made using a solder paste or wiring-bond processing. The Figure 1 shows an image of one strain gauge (1.2 x 3.0mm) bonded using a high-performance epoxy resin and the electrical contacts were bonded using a silver conductive paste.

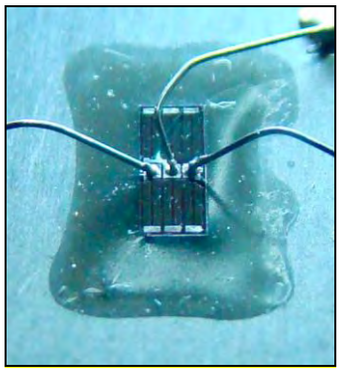

Figure 1. Strain gauge bonded on aluminum cantilever beam using an epoxy resin and a silver conductive paste was used to perform the electrical contacts.

Experimental Results

Measurements of sheet resistance: The diffusion process changes the sheet resistance of the polysilicon film and it was characterized by a four-probe-meter. The main results of sheet resistance as a function of diffusion time and the concentration of phosphorus are shown in Table I.

Table I. Values of sheet resistance (Rsheet) of doped polysilicon films.

SOG Phosphorus Concentration	Processing Time (min)	Rsheet (Ohms/square)
1%	20	150 ± 16
1%	30	42 ± 7
1%	40	14,4 ± 0,5
3%	70	10,7± 0,2

The variation of sheet resistance depends mainly on the thickness and doping uniformity of the polysilicon film, but is within acceptable values for the strain gauge designed.

Measurements of electrical resistance: The electrical resistance of the fabricated strain gauges were measured by an analyzer, where it was applied a voltage of 1V in strain gauges distributed in the silicon wafer. The average values for the fabricated devices are shown in Table II.

Table II. Values of electrical resistance of fabricated strain gauges.

Strain gauge identification	Resistance - Designed	Resistance - Measured
A	2 kΩ	2,10 ± 0,03 kΩ
B	1.2 kΩ	1,27 ± 0,02 kΩ
C	1.3 kΩ	1,34 ± 0,02 kΩ

The electrical resistance values were close to the designed resistance values, indicating that the polysilicon film deposition and phosphorus SOG difusion process results can be reproduced.

Electrical characterization of Wheatstone bridge in the load cell: In the experimental arrangement it was used aluminum cantilever beam as a load cell. The arrangement was mounted on a stable and vibration free table. The input voltage was 5V and output voltage was monitored by a precision voltmeter in function of the force (mass) applied on the structure. The results are shown in Figure 2.

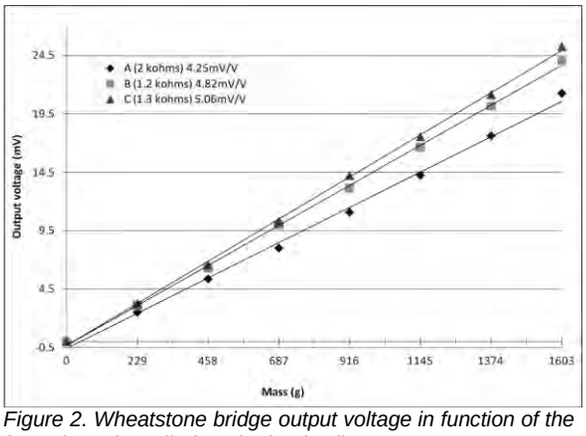

Figure 2. Wheatstone bridge output voltage in function of the force (mass) applied on the load cell.

It is observed a linear variation of Wheatstone bridge output voltage in function of the force applied to the structure with good correlation ($R^2 > 0.996$). So, the resistance of each strain gauge increased linearly with the tensile stress while it decreased with the compressive stress. In all cases, the sensitivity (output rating) for loads of 1.6 Kg were higher than 4.25 mV/V (2.41 μV/V.g). The design of strain gauge C had longer lines in the same device and it was doped with a high phophorus concentration, resulting in 5.06 mV/V (3.00 μV/V.g) of sensitivity.

References

[1] A. L. Window, Strain Gauge Technology, Elsevier, Applied Science, 2nd ed. London (1992).
[2] A. S. Khan and X. Wang, Strain Measurements and Stress Analysis. Upper Saddle River, Prentice-Hall, NJ (2001).
[3] K. Sivakumar, et al; in Sensitivity Enhancement of Polysilicon Piezo-resistive Pressure Sensors with Phosphorus Diffused Resistors, International MEMS Conference 2006, Journal of Physics: Conference Series 34, pp. 216-221(2006).
[4] S. C. Kim and K. D. Wise, Temperature Sensitivity in Silicon Piezo-resistive Pressure Transducers, IEEE Transactions on Electron Devices, vol. EE-30, N0.7, pp 802-810, (1983).
[5] P. Ciureanu and S. Middelhoek, “Thin film resistive sensors”; Bristol: Institute of Physics, (1992).
[6] S. Beeby, et al, MEMS Mechanical Sensor, Artech House, Norwood, MA (2004).

Sistema de sensado ultrasónico para la medición de la evaporación de agua con transmisión sin cables (inalámbrica)

Francisco G. Flores García[1], Julio Vladimir Castañeda García[1]
[1] Instituto Tecnológico de la Laguna, Torreón, Coahuila, México.
fflores@itlalaguna.edu.mx, juliovladimir.castaneda@gmail.com

Resumen

Se diseñó un sistema capaz de medir la cantidad de agua que se evapora en el ambiente de la región, las unidades de milímetros por día mm/día de evaporación y a su vez permite hacer un cálculo del volumen de agua usada en determinada área en caso de que el dispositivo sea montado en campo. Este prototipo está basado en la adquisición de datos de un sensor ultrasónico con un rango de medición de 50 mm hasta los 500 mm. Envía una señal de 4 a 20 mA al sistema de adquisición de datos (circuito), el cual está diseñado mediante un PIC16F876 que procesa los datos convirtiendo la variación de voltaje en milímetros, estos datos son enviados a un transmisor de datos Xbee por medio del puerto serie y serán recibidas con otra tarjeta Xbee la cual transfiere los datos a una interfaz de visualización LabView. Se realizaron varias pruebas de medición y comparación de voltaje para checar su correcto funcionamiento, así como pruebas de monitoreo junto con otras estaciones ya ubicadas en la región Laguna de Coahuila las cuales cuentan con monitoreo manual de la evaporación, arrojando resultados similares de medición en las cantidades de agua evaporada en cada una de las estaciones de monitoreo. Las ventajas del dispositivo son que se puede programar la cantidad de datos muestreados en tiempo real y el bajo costo en su fabricación.

Palabras clave: Prototipo, evaporación de agua, medición sin cables, Xbee.

Introducción

El agua es esencial para la vida, por lo que su uso y cuidado es primordial. Se estima que aproximadamente el 84% del volumen disponible en el acuífero de la región Laguna se destina a la agricultura. [1]. En la actualidad, los productores e ingenieros agrónomos han buscado diversas formas para elevar la producción de forraje, hortalizas y huertos. Una de las tareas a las que se han enfocado es la medición, relación, y aplicación de variables climáticas las cuales se sabe que determinan directamente el crecimiento de los productos del campo [2]. El presente proyecto muestra el diseño e implementación de un sistema de medición de evaporación de agua ya que este es un factor de importancia en el área de cultivo ya que ayudan a determinar ciclos de riego (agua necesaria), fertilización y fumigación.

Comúnmente se utiliza para la medición de la evaporación el tornillo milimétrico el cual es de uso fácil y rápido, así como también es de diversas formas y tamaños para cualquier necesidad en especifico, es fácil de trasladar y los calibres mecánicos presentan una buena durabilidad resistentes a golpes y desgastes además que es muy recomendable en cuanto a precio y calidad. Este método además tiene la desventaja de ser inferior en rendimiento frente a un micrómetro, requiere de elementos costosos para su calibración, y los calibres digitales de estos mismos tienen menor durabilidad.

El prototipo diseñado plantea la utilización de un sensor ultrasónico que no es intrusivo (no tiene contacto con el medio) para evitar problemas de corrosión y contaminación. Adicionalmente, estos sensores tienen una medición continua y puntual, no poseen partes móviles los cuales generan un menor mantenimiento y se utiliza para líquidos y sólidos conductivos y no conductivos. Las desventajas de estos sensores es que la medición puede ser afectada por el movimiento del material en el tanque, la espuma del líquido puede absorber la señal transmitida y la presencia de partículas o vapor en el aire puede interferir la señal de los sensores no intrusivo.

Materiales y Métodos

Se utiliza un tanque cilíndrico de lámina galvanizada, de 1,21 m de diámetro y 25 cm de profundidad. Se coloca sobre una plataforma de madera de 10 cm de alto, perfectamente horizontal. El volumen de agua consumido se transforma en mm de agua evaporada por unidad de tiempo.

Para la medición de evaporación del agua del tanque, se adecuó un sensor ultrasónico de la marca Peperl+Fuchs Modelo: UC500-30GM-IUR2-V15 (Alemania 2003) el cual tiene un rango de detección de nivel de 30 a 500 milímetros, el tiempo de respuesta aproximada es de 50 milisegundos y una frecuencia de conmutación de 10Hz, su resolución máxima es de 0.13 milímetros lo cual ofrece la ventaja de tener un sistema con precisión de medida en milímetros. El sensor opera con una tensión de entrada que va desde los 15 hasta los 30 VDC, y su salida se puede manejar con 2 opciones, de 0 a 10VDC o de 4 a 20 Ma. El circuito de adquisición e interfaz electrónica se diseño con un microcontrolador el tipo PIC 16F876 y la transmisión inalámbrica con módulos Xbee.

Resultados y Discusión

Los resultados obtenidos del sistema se muestran en la tabla 1. Estos resultados fueron obtenidos entre las etapas experimentales en laboratorio y las de campo donde se probó el circuito en condiciones de intemperie y funcionó de manera continua y correcta. Los alcances de transmisión del sistema fueron de aproximadamente 90 mts. en vía libre.

Tabla 1.- Resultados de evaporación por mes en la Comarca Lagunera utilizando el sistema diseñado.

	Milimetros acumulados de evaporacion mensual
Enero 2011	114
Febrero 2011	136
Marzo 2011	206
Abril 2011	244
Mayo 2011	280
Junio 2011	272
Julio 2011	265
Agosto 2010	245
Septiembre 2010	205
Octubre 2010	175
Noviembre 2010	135
Diciembre 2010	109

Adicionalmente el sistema genera gráficas y archivos de los datos obtenidos para tener un historial que permita generar programas de riego eficiente. La figura 1 muestra la pantalla de la interfaz diseñada.

Conclusiones

El sistema funcionó adecuadamente utilizando un emisor ultrasónico para medir la diferencia de distancias respecto de un componente líquido con una precisión de milímetros. Su funcionamiento en condiciones de intemperie fue correcto y en tiempos de monitoreo extendidos. Los valores se compararon contra los estándares de medición de la SAGARPA, México.

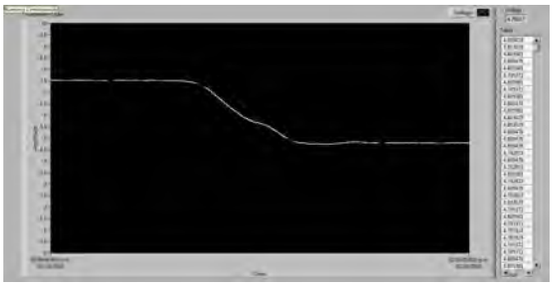

Figura 1.- Gráfica y tabla de datos del sistema-

Agradecimientos

Agradecemos al CONACYT por la beca otorgada al estudiante para la realización de este proyecto y al Instituto Tecnológico de Torreón por facilitarnos las instalaciones,

Referencias

[1] Aguilera, C. y R. Martínez E. Relaciones Agua, Suelo, Planta, Atmósfera. 4a ed. Universidad Autónoma Chapingo. Chapingo, México, 1996

[2] Bowen, I.S. The ratio of heat losses by conduction and by evaporation from any water superface. Phys. Rev. 2: 779-787, 1926.

[3] Lopez E., J., L. Tijerina Ch., G. Haro A. y R. Arteaga R.; Calibración de fórmulas de evapotranspiración mediante un cultivo de alfalfa como referencia en el área de Montecillo, Estado de México. Agrociencia 2: 55-72. 1991

[4] Peña P., E.; Proyecto y construcción de un lisímetro de pesada y estructura inalterada. Tesis de Maestría. Colegio de Postgraduados. Chapingo, México, 1974.

[5] Thornthwaite, C.W. y B. Holzman. Measurement of evaporation from land and water surfaces. US Dept. Agr. Tech. Bull. 817: 75. 1975

[6] Tijerina Ch., L. Uso eficiente del agua en unidades de riego para el desarrollo rural. Diplomado. Colegio de Postgraduados. Montecillo, México; 1992.

[7] Al-Ghobari H.M. Estimation of Reference Evapotranspiration for Southern Region of Saudi Arabia. J. Irri ga tion Science, 19(2):81-86. 2000 b.

[8] Allen G.R., Pereira L.S., Raes D., Smith M. FAO Irrigation and Drainage Paper No. 56 , Crop Evapotranspiration (guidelines for computing crop water requirement). ISBN 92-5-104219-5., 290 pp. 1998.

[9] Amatya D.M., Skaggs R.W., Gregory J.D. Comparison of Methods for Estimating REF-ET. J. Irrig. and Drain. Engrg. ASCE, 121(6):427-435. 1995.

[10] Braunworth W.S., Mack H.J. Evapotranspiration and Field Comparisons Among Soil-Water-Balance and Climate-Based Equations for Irrigation Scheduling of Sweet Corn. Agron. J., 79:837-841. 1987.

Chapter 10: Biomedical Applications

A PVDF transducer array to measure temperature gradients in a soft tissue *phantom*

Mónica Vázquez Hernández, Pedro Acevedo Contla,
Adalberto J. Durán Ortega, Josué J. Méndez Martínez.

Universidad Nacional Autónoma de México, DISCA-IIMAS, Apdo. Postal 20-726 Admon. No. 20, Del. Alvaro Obregón, 01000 México D.F.

Abstract

The objective of this work is the measurement of temperature gradients to the interior of a soft tissue phantom simulator in a total volume of 500 ml; the algorithm used for detecting temperature changes is based on the detection of phase shifts. The chosen exploration mode was **through transmission**, a commercial ultrasonic PZT transducer (21 mm in diameter) was used as a transmitter and a linear array of PVDF ultrasonic transducer (9 μm thickness) as a receiver, obtaining a spatial resolution of 4 mm in width by 4 mm in height.

Keywords: PVDF, transducer, temperature, through transmission.

Introduction

The objective of this work is the measurement of temperature gradients through the determination of phase shifts, i.e. time shifts of the waveform of the echo due to a change in the speed of propagation of ultrasound as a result of a change in temperature, they can be interpreted as phase shifts in the frequency domain. Making it possible to determine the change in temperature from the phase shifts; in a medium of propagation previously characterized [1].

On the other hand, PVDF has shown that is a material that can be used in the construction of ultrasonic transducer for a variety of medical applications, it is physiologically safe, lightweight, flexible, low-cost, available in thin films of different dimensions and it has a wide bandwidth. Contact PVDF transducers have a good performance in tissue, because its acoustic impedance is similar to the tissue impedance [2].

Methodology

The construction of the array was made using a thin PVDF film (9 μm thickness), uniformly polarized (Piezo Film sheet), it was cover using a conductive layer of epoxy (Conductive Epoxy CW2 400J) on each of the faces. As shown in Figure 1.

The connections of the wires on both sides of the PVDF film were made using conductive epoxy, then these wires were connected to a coaxial cable, and in order to have a more robust insulation, Scotch 3M laminar tape 3311 was used.

To carry out tests inside a water tank, a layer of electrical insulation was bonded to the contacts and the faces of the transducer Linear arrays of 4 elements were designed; with two variants in the backing; one using acrylic and another using only air.

The responses of the home-made arrays were compared against the response of a LDT1 - 028 K commercial transducer (28 μm thickness).

The sample (water or phantom with an area of Hydrogel) was tested using a transducer as transmitter and the PVDF array as a receiver, the through transmission technique was used (see figure 1)

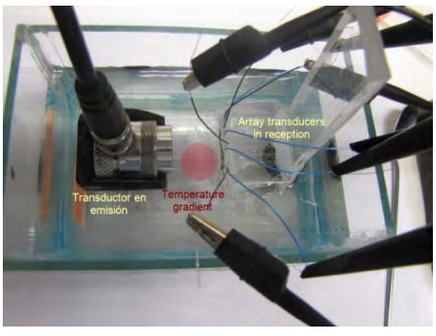

Figure 1. Top view of experimental set-up in water.

A 3.5 MHz Aerotech (Gamma series) transducer was used as a transmitter to radiate to the medium, commercial transducers and home-made arrays were used as receivers. In the water tank a volume of water or soft tissue phantom was immersed with a small spherical volume (Hydrogel) incorporated at a different

temperature (temperature gradient) which was kept at a constant temperature, using a small control system. To determine the temperature gradient, echoes from each one of the elements of the array were capture using a four-channel Tektronic DPO3014 oscilloscope, the acquired signals were conditioned and then processed in a PC using the method of phase change in a Matlab platform.

The evaluation of the response of the arrays was first conducted in water (see Figure 1) and later on a soft tissue phantom. In both cases the Hydrogel sphere contains the volume of water at a higher temperature than the rest of the water and/or soft tissue phantom.

Results

The signals were acquired using a 100 MHz sampling frequency; they were subsequently pre-processed. A segment of interest (the first echo area) was chosen, they were subsequently filtered using a fifth Chebyshev order filter and finally the phase spectrum was calculated.

Figure 2 shows different signals corresponding to the array with backing of acrylic and it also shows different zooms of the signals corresponding to the first echo of channel one acquired at different temperatures.

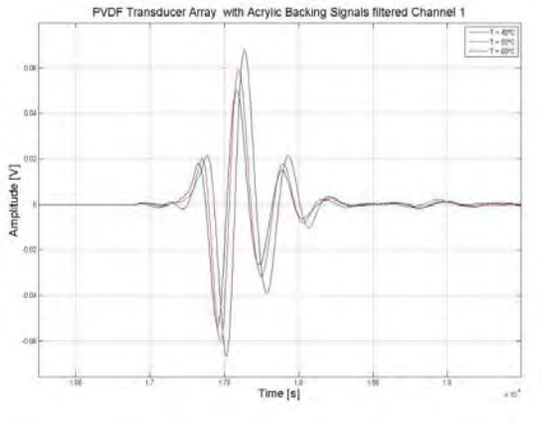

Figure 2. Zoom of the first echo from channel one of the PVDF array with backing of acrylic.

Figure 3 shows the comparison of three echoes at different temperatures from a zoom of the echoes obtained from a PVDF array with backing of acrylic using a commercial transducer.

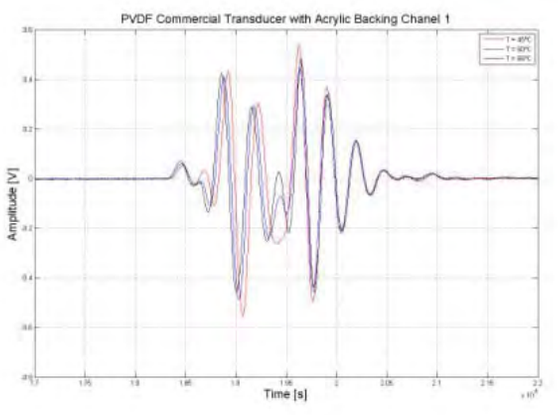

Figure 3. Zoom of the first echo from channel one using the PVDF commercial transducer.

Discussion

Experimental results show a linear relationship between temperature and phase changes, which is equivalent to that reported by other authors whom had used other methods or techniques such as time delays or the spectral power density to measure temperature changes. The disadvantage of the signal processing technique used is that it is not robust against noise, since it has a high sensitivity to phase transitions.

Conclusion

The results are very promising on noninvasive measurement of temperatures using spatial-temporal resolution, our method relates phase shift to temperature variation. The variation of temperature with respect to time is an area of interest to explore. As future work is planned to process signals using wavelets and its evaluation on real biological tissue (in vitro and in vivo).

References

[1] Vázquez M., Ramos A., Leija L., Vera A. Non-Invasive Temperature Estimation in Oncology Hyperthermia by Using Phase Changes in Pulse-Echo Ultrasonic Signals. Japanese Journal of Applied Physics. Vol. 45. No.10 A, 2006, pp.7991-7998. ISSN: 0021-4922

[2] Brown, Lewis F., Mason L Joel . Disponsable PVDF Ultrasonic Transducers for Nondestructive Testing Applications. IEEE Transactions on Ultrasonics, Ferroelectrics and Frequency Control, Volume: 43, Issue: 4, pp.560– 568, July 1996.

Un nuevo concepto de Imunosensor Piezoeléctrico (QCM) para plaguicidas, basado en la detección de cambios de fase a alta frecuencia

A. Montoya[1] *, J.V. García-Narbón[2], A. Sánchez[1], A. Arnau[2], Y. Jiménez[2], C. March[1]

[1]Instituto Interuniversitario de Investigación en Bioingeniería y Tecnología Orientada al Ser Humano (I[3]BH) and [2]Grupo de Fenómenos Ondulatorios (GFO)
Universitat Politècnica de València.
46022 Valencia, España.
amontoya@ginmuno.i3bh.es

Resumen

Para resolver las limitaciones de sensibilidad asociadas a los biosensores QCM basados en la detección de pequeños cambios de frecuencia, se propone un nuevo concepto de biosensor piezoeléctrico. El nuevo biosensor se basa en la detección de cambios de fase, trabajando a frecuencia alta y constante. Sobre esta base, se ha desarrollado un inmunosensor QCM de 50 MHz para la determinación de plaguicidas con alta sensibilidad.

Palabras clave: Inmunosensor piezoeléctrico. Detección de fase. Alta frecuencia. Plaguicidas.

La detección de cambios de masa muy pequeños mediante la Microbalanza de Cristal de Cuarzo (Quartz Crystal Microbalance, QCM) es una de las técnicas de transducción más ampliamente utilizadas en el diseño de sensores y biosensores para aplicaciones bioquímicas en medio líquido. Así, recientemente se ha descrito su utilización en el desarrollo de inmunosensores para la determinación de plaguicidas en frutas y productos derivados [1]. A pesar de las indudables prestaciones analíticas de los biosensores basados en QCM, existen todavía aspectos mejorables, tales como el aumento de la sensibilidad y la disminución de los límites de detección, que permitirían extender la utilización de estos inmunosensores a aplicaciones más exigentes, tales como el análisis de plaguicidas en aguas potables.

El aumento de la frecuencia de vibración fundamental del sensor piezoeléctrico se traduce en un aumento efectivo de la sensibilidad (relación frecuencia/masa), tal como predice la ecuación de Sauerbrey [2]. Sin embargo, este aumento de sensibilidad no se ha podido transferir en la misma medida a una mejora en los límites de detección. La progresiva desestabilización de la frecuencia como consecuencia del aumento del ruido de fase, particularmente en los dispositivos osciladores, parece ser la causa más probable que impide alcanzar la resolución deseada a concentraciones de analito muy bajas.

Para intentar resolver estas limitaciones, se propone un nuevo concepto de biosensor piezoeléctrico. A diferencia del QCM clásico, en el cual se detectan cambios de frecuencia asociados a pequeños cambios de masa, el nuevo biosensor se basa en la **detección de cambios de fase, trabajando a frecuencia alta y constante**. Sobre esta base, se ha desarrollado un **inmunosensor QCM de 50 MHz para la determinación de plaguicidas**. Con el objetivo de asegurar la estabilidad mecánica, facilidad de manipulación y robustez del dispositivo, los cristales de alta frecuencia fundamental (High Fundamental Frequency, HFF) se anclaron permanentemente a un soporte de chips PEEK (Fig. 1) diseñado y construido expresamente. Se ha desarrollado también el sistema automático de inyección de flujo (Fig. 2), que consta de: la celda de flujo para el chip sensor, el circuito de flujo con bombas de jeringa y válvulas de distribución e inyección automáticas, y el sistema de caracterización electrónica, basado en la medida de fase/masa a frecuencia constante [3,4].

El plaguicida modelo escogido para el desarrollo del inmunosensor fue el insecticida carbaryl, para el cual ya se había desarrollado un biosensor QCM clásico [1]. Como molécula de biorreconocimiento se utilizaron anticuerpos monoclonales específicos de carbaryl, en un inmunoensayo competitivo en el formato de conjugado inmovilizado. El conjugado hapténico de carbaryl se unió covalentemente a la superficie de oro del elecrodo del sensor, mediante monocapas autoensambladas (SAM) de ácido mercaptohexadecanoico.

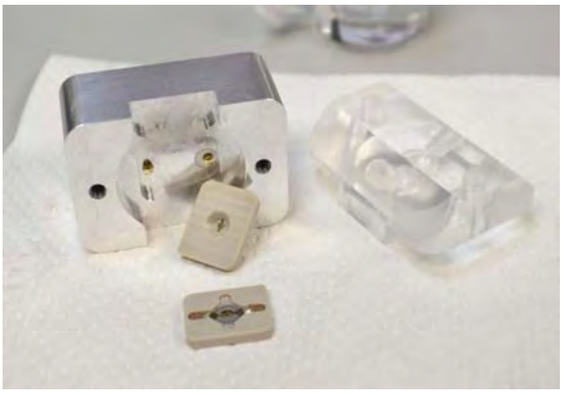

***Figura 1**. Chips y celda de flujo del sensor HFF-QCM*

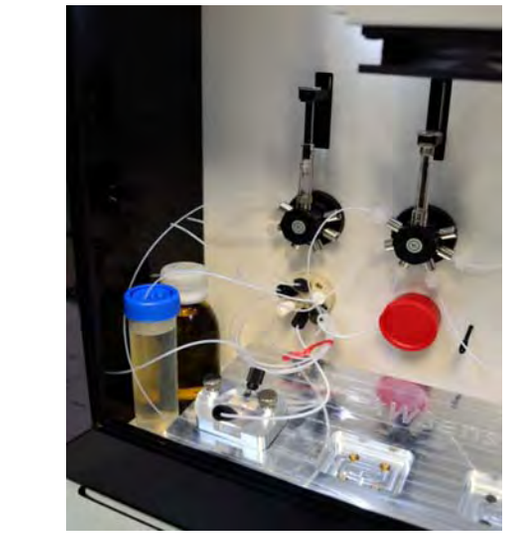

***Figura 2**. Sistema automátizado de medida para el inmunosensor de alta frecuencia*

En la Fig. 3 se muestra la curva patrón de carbaryl obtenida con el nuevo inmunosensor. El análisis automatizado permitió alcanzar una excelente reproducibilidad. Se obtuvo una mejora de más de un orden de magnitud en la sensibilidad (I_{50} = 1,2 µg l^{-1}) y de dos órdenes de magnitud en el límite de detección (LOD = 0,16 µg l^{-1}), comparados con los resultados previamente obtenidos con el biosensor QCM clásico de 10 MHz [1,4]. Además, se disminuyó el consumo de inmunorreactivos entre 5 veces (anticuerpo) y 1000 veces (conjugado de ensayo).

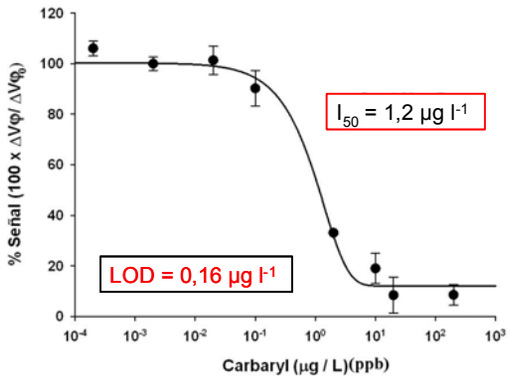

***Figura 3**. Curva patrón de carbaryl obtenida con el inmunosensor de detección de fase a 50 MHz*

La sensibilidad alcanzada por este inmunosensor permite la determinación del plaguicida a concentraciones cercanas a los límites máximos de residuos (LMR) establecidos por la regulación europea para aguas potables. Todavía pueden esperarse mayores aumentos de la sensibilidad mediante la utilización de sensores de más alta frecuencia fundamental (100-150 MHz).

Referencias

[1] C. March, J. J. Manclús, Y. Jiménez, A. Arnau, A. Montoya. A piezoelectric immunosensor for the determination of pesticide residues and metabolites in fruit juices. Talanta, 78 (3), 827-833, 2009.

[2] G. Sauer brey. Verwendung von Schwingquarzen zur Wägung dünner Schichten und zur Mikrowägung. Zeitschrift für Physik, 155 (2), 206-222, 1959.

[3] A. Arnau, Y. Montagut, J. V. García, Y. Jiménez. A different point of view on the sensitivity of quartz crystal microbalance sensors. Measurement Science and Technology, 20 (12) 124004, 2009.

[4] Y. Montagut, J. V. García, Y. Jiménez, C. March, A. Montoya, A. Arnau. Validation of a Phase-Mass Characterization Concept and Interface for Acoustic Biosensors. Sensors, 11 (5), 4702-4720, 2011.

Multi-parameter measurement system for an in-vitro characterization of the hemodynamics in carotid arterial bifurcations +

[1] Laboratorio de Acústica Ultrasonora, Instituto de Física, Facultad de Ciencias, UDELAR, Montevideo, Uruguay.
[2] Departamento de Fisiología, Facultad de Medicina, UDELAR, Montevideo, Uruguay.
[3] Departamento de Electrónica, Facultad Regional Buenos Aires, Universidad Tecnológica Nacional, Argentina.
Contacts: dsb@ieee.org; carlosn@fisica.edu.uy

Keywords: biomedical measurements, multi-parameter measurement system; hemodynamic simulator; ultrasound; parameter estimation.

Introduction

Arterial behavior is influenced by the interaction between blood flow and the arterial wall endothelium, and arterial wall biomechanics. This interaction plays an important role in pathogenic mechanisms of cardiovascular diseases, such as atherosclerosis and arteriosclerosis. To quantify these interactions both from biomechanical and hemodynamical standpoints, a complete characterization and modeling of the arterial wall, blood flow, shear wall and circumferential wall stresses are needed. This characterization can be done in-vitro by means of a hemodynamic work-bench simulator in which arterial segments are intercalated in closed fluid circuit that emulates main features of systemic arterial circulation [1] [2] [3] [4]. A specific experimental set-up is needed in order to be able to work with arterial bifurcations. This set-up is presently under development and poses several interesting problems related with signal acquisition using a variety of sensors.

Objetives

Describe the development of a new multi-paramater measurement system for an in-vitro characterization of the biomechanics and hemodynamics in carotid arterial bifurcations. Measurements obtained from cryopreservated and fresh carotid arterial bifurcations subjected to different hemodynamical regimes allowes us to characterize the biomechanical properties of arterial segments. These are obtained by parameter estimation and will be employed in a model for the numerical simulation of the interaction between structure and fluid. Velocity profiles obtained in the work-bench will be compared with the ones obtained by CFD simulations with moving wall.

Materials and Methods

We developed a new specific experimental set-up based on our existing hemodynamic work-bench simulator, in order to be able to work with arterial bifurcations. The hemodynamic closed circuit is composed by: a pump, the tubing between the pump exit and the entrance to the arterial bifurcation, the arterial bifurcation being studied, tubing between each branch of the bifurcation exit and the entrance to a fluid reservoir, a fluid reservoir with mean pressure adjustment, and a returning tubing from the reservoir to the pump. An artificial heart (Jarvik 5 and Cardiobot) was used as the pulsatile pump, with frequency and ejection volume adjusted at demand. The output load impedance distal to each branch of the arterial bifurcation was adjusted by means of a variable restriction in each branch. In each experimental configuration, the artificial heart was operated at constant frequency. The measurements were done after a steady regime of pulsatile flow was attained in the circuit.
Samples were mounted on an arterial bifurcation fixing system which was submerged in a physiological solution pool. The circuit was filled with physiological solution or blood treated with EDTA sodic (rheological properties previously obtained with Brookfield, LVDT –II+ plate-cone viscosimeter). Temperature control was done in the reservoir and in the pool. Set-up point was 37°C (measured using one thermistor in each of the above mentioned recipients). The reservoir is a tank containing blood or physiological solution and air. Its mean pressure can be adjusted at constant values by means of a pump and a differential pressure sensor.
With no flow in the circuit, measurements where done over the bifurcations in A-Scan mode (Panamerics 20 Mhz ultrasonic transducer) in

+ Grant by Agencia Nacional de Investigación e Innovación (ANII), Montevideo, Uruguay.

order to obtain lengths, internal and external diameters and wall thickness (usefull to construct a simplified finite-element grid for a CFD model).
After that, several hemodynamic conditions where simulated adjusting the pump frequency and the air volume applied to Kolff´s diaphragm or the programmed flow pattern of the Cardiobot, reservoir pressure and the variable restrictions. External diameter measurements were taken at suitable points in the segment of common carotid artery and at each segment corresponding to internal and external carotid branches using a gold-standard System 6 Mainframe equipped with sonomicrometer ultrasonic modules [5] and ultra resolution techniques [4]. Sonomicrometer ultrasonic crystals (5 MHz, 2mm diameter) where hand-crafted, fixed to synthetic fabric, and sutured to the outer face of the arterial wall (adventitia). Pressure waveforms were obtained using Königsberg P2,5-S sensor located near diameter measurement points. The sensing surface pointed to the lumen in order to obtain the hydrostatic component of the pressure. Velocity profiles at different locations were obtained using a multigate Doppler system (DOP, Signal Processing SA). Flow was also measured using transit time flowmeters (Triton flowmeters). In order to give a time reference for the measurements of the different sensors, a periodic pulse signal was generated related with pulsatile pump function.
Signals where acquired using 12-bit data acquisition modules (NI USB-6009 and LabJack U3-HV). Pressure and diameter samples were processed on-line in a computer running a specific developed algorithm. Biomechanical properties of the wall were obtained by means of model parameter adjustment. The biomechanical properties of the arterial segment obtained by parameter estimation will be employed in the model for the numerical simulation of the interaction between structure and fluid. Velocity profiles obtained in the work-bench will be compared with the ones obtained by CFD simulations with moving wall. To validate the experimental results obtained using the new multi-paramater measurement system, we studied the performance of each sensor in the framework of the whole measurement system, taking into account possible external influences. The generalized static and dynamic characteristics of the sensors [6] used in the new system were checked as well as the interoperability in the framework of the whole system. Before operating the system with arterial samples, suitable phantom models where used for sensor calibration and error estimation. A survey of possible external influences was done. The influence of noises of the same physical nature as the input signals to the sensors and the EMC aspects were studied.

Results and conclusions

A- The static and dynamic characteristics of the sensors used were suitable for the attaining of the posed objectives. B- However some systematic errors were found and their effects on measurements were taken into account. C- The effects of delays in temperature control response were not significant. D-Working in a steady pulsatile regime with a time reference signal allowed us to take different physical measurements in the same point of the arterial sample locating there different type of sensors and relating the signals recorded to the same phase of the periodic regime. This allowed us to overcome the difficulties due to the size of the different sensors. E-Some radiated and conducted electromagnetic interference was detected and reduced by the implementation of a shield to isolate the workbench from its external environment. Sonomicrometer measurements are sensitive to external perturbations. They generated spurious triggering at the RF processing stage, altering the stability of the measured distances.
F-Obtained measurements allowed: 1-Grid construction for CFD modeling using ultrasonic measurements and morphometric arterial sample data. 2-Parameter estimation of the biomechanical properties of the arterial wall, suitable to be employed in a model for the numerical simulation of the interaction between structure and fluid. 3-Assessment of velocity profiles in order to make a comparison with the ones obtained by CFD simulations of the arterial carotid bifurcation sample, taking into account the movement of the arterial wall. Estimation of the endothelial wall shear stress for a carotid arterial bifurcation, at different points under a periodic pulsatile flow can be done by CDF simulation.

References

[1] J Brum, D Bia, N Benech, G Balay, RL Armentano, C Negreira, “Setup of a cardiovascular simulator: application to the evaluation of the dynamical behavior of atheroma plaques in human arteries”, PhysicsProcedia, vol. 3, pp.1095-1101, 2010.

[2] G. Balay, J, Brum, D. Bia, R.L. Armentano, C.A. Negreira, “Improvement of artery radii determination with single ultra sound channel hardware & in vitro artificial heart system”, Conf. Proc. IEEE Eng. Med. Biol. Soc. 2010, pp. 2521-4, 2010.

[3] D. Bia, R.L. Armentano, Y. Zocalo, W. Barmak, E. Migliaro, E.I. Cabrera Fischer, “In vitro model to study arterial wall dymamics through pressure-diameter relationship analysis”, Latin American Applied Research, vol. 35, pp. 217-225, 2005.

[4] J. Brum, D. Bia, N. Benech, G. Balay, R. L. Armentano y C. Negreira, “Medición de diámetros arteriales utilizando ultrasonido de alta resolución: validación in vitro”, CLAIB2011, La Habana, Cuba, mayo de 2011.

[5] Triton Technology Inc, System 6 Manual, 1997.

[6] J. Webster, “Medical instrumentation: application and design”, J. Wiley & Sons Inc, 4ed, NJ, chapter 1, pp 19-25, 2010.

Difusão de Fármacos Monitorizada em Tempo Real por um Sensor de Ondas Acústicas

Cláudia A.M. Oliveira, Marta I.S. Veríssimo, J. A. B.P. Oliveira, M. Teresa S.R. Gomes*
CESAM/Departamento de Química, Universidade de Aveiro, 3810-193 Aveiro, Portugal
*mtgomes@ua.pt

Resumo

Foi desenvolvido um novo método analítico, baseado num sensor de ondas acústicas, para monitorizar em tempo real a difusão de fármacos. O sensor de ondas acústicas consiste num cristal piezoeléctrico de quartzo revestido com uma camada sensível ao composto farmacêutico em estudo (diclofenac de sódio). Para estes estudos foi desenvolvida uma nova célula de difusão que permite a incorporação do sensor de ondas acústicas na câmara receptora. A utilização de um sensor em vez da amostragem discreta a partir da célula de Franz permite seguir em tempo real a permeação do composto através da membrana. A aplicação deste novo método para outros compostos farmacêuticos é simples e de baixo custo, bastando para tal a substituição do sensor de ondas acústicas por outro com um revestimento sensível ao composto de interesse.

Palavras-chave: permeação, diclofenac de sódio, sensor de ondas acústicas

Introdução

A administração de medicamentos através da pele pode ser uma alternativa à administração oral. A necessidade de controlar as dosagens dos medicamentos e as suas formulações, exige que sejam realizados testes de permeação através da pele.

Os estudos de permeação de medicamentos através da pele podem ser realizados *in-situ*, directamente no ser humano, ou *in-vitro*, com soluções simulando os fluidos corporais.

Idealmente os testes de permeação deveriam ser feitos *in-situ*. No entanto, muitos compostos são tóxicos, e os testes estão sujeitos a restrições éticas. Os testes *in-vitro* permitem verificar o comportamento dos princípios activos do medicamento, sendo utilizada a pele de cadáveres humanos, a pele obtida após cirurgias plásticas ou a pele de alguns animais. Membranas naturais (pele de pêssego, de tomate, de cebola) ou sintéticas, (celofane), também podem ser usadas, visto apresentarem poros e canais com propriedades hidrofílicas capazes de permear compostos de diferentes tamanhos, de maneira similar à da pele humana [1].

Nos estudos de permeação através da pele *in-vitro* são geralmente utilizadas as células de Franz [2], que permitem criar as condições necessárias para simular a passagem percutânea do composto, controlando a temperatura, a dose, a agitação e a natureza da membrana. A célula de Franz consiste em duas câmaras, a dadora, onde o composto é depositado, e a receptora, onde o composto se difunde, passando através da pele/membrana entre as duas câmaras. Na câmara receptora existe uma abertura que serve para retirar periodicamente aliquotas da solução, sendo o volume reposto com a solução inicial. As alíquotas são analisadas posteriormente para determinar a quantidade de composto difundido através da pele/membrana. São utilizadas diversas técnicas analíticas na quantificação do composto farmacêutico em estudo, tais como: espectrofotometria de UV, espectroscopia FT-Raman, potenciometria, HPLC entre outras. No entanto, continua a existir uma procura por métodos mais eficazes, baratos e simples.

O sensor de ondas acústicas baseia-se na utilização de um cristal piezoeléctrico. Estes sensores de ondas acústicas têm sido largamente usados para medir variações de massa e ainda, em menor escala, para detectar variações nas propriedades viscoelásticas de filmes poliméricos [3] e a sorção de proteínas [4], entre muitas outras aplicações. A deposição de uma membrana selectiva a um determinado analito numa das faces do cristal permite fabricar sensores muito sensíveis [5]. Os sensores de ondas acústicas têm sido usados com sucesso para monitorizar uma grande variedade de analitos, mas não há ainda registo

na literatura de sensores de ondas acústicas utilizados para monitorizar em tempo real a difusão de fármacos.

O objectivo deste trabalho foi o desenvolvimento de um novo método analítico, baseado num sensor de ondas acústicas, para monitorizar em tempo real a permeação do diclofenac de sódio. Para tal foi necessário revestir um cristal piezoeléctrico com uma membrana sensível ao diclofenac. Foi desenvolvida uma nova célula de difusão que permite a incorporação do sensor na câmara receptora, sendo possível deste modo monitorizar em tempo real a quantidade de composto difundido.

Metodologia Experimental

Foram utilizados cristais de quartzo polidos de 9 MHz com corte AT, com eléctrodos de ouro (ICM). Os cristais foram revestidos com uma membrana sensível ao diclofenac [6]. A nova célula de permeação foi desenhada e fabricada, tendo em conta a incorporação do sensor de ondas acústicas na câmara receptora e o controlo da temperatura e da velocidade de agitação. O sensor foi também acoplado a um oscilador, que estava ligado a uma fonte de alimentação e a um frequêncímetro, controlado remotamente por um computador. A temperatura foi controlada com uma estufa FrioCell e a agitação da câmara receptora e dadora foi feita com agitadores magnéticos, controlados independentemente por dois motores.

Resultados e Discussão

O sensor foi calibrado na célula de difusão. Para tal encheu-se a célula (sem membrana) com um volume de água Milli-Q rigorosamente medido e após a frequência estabilizar, foram adicionadas quantidades sucessivas de 40 µL de solução padrão de diclofenac a 8000 mg L^{-1}. Cada adição de 40 µL de solução padrão levava ao decréscimo de frequência, proporcional à massa adicionada. Cada adição era efectuada apenas após a estabilização da frequência. Com a variação da frequência correspondente a cada adição de solução de diclofenac, construiu-se a recta de calibração.

Após a calibração do sensor, este foi usado para monitorizar a permeação de uma solução de diclofenac através de uma membrana. Para tal. utilizou-se uma membrana sintética (celofane) que foi colocada entre as duas câmaras, sendo estas preenchidas com volumes rigososamente medidos de água Milli-Q.

A Fig. 2 apresenta a resposta do sensor à permeação do diclofenac através da membrana de celofane, para uma concentração de diclofenac na camara dadora de 225.14 mg L^{-1}.

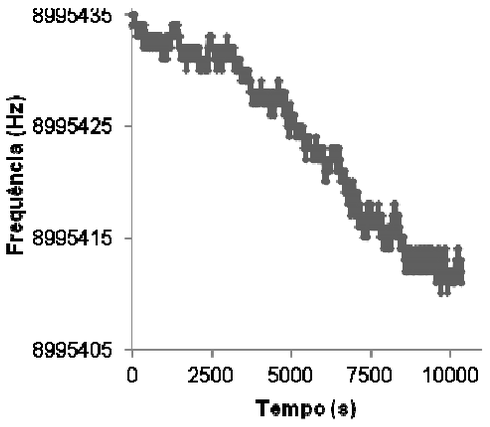

Figura 2– Resposta do sensor à permeação do diclofenac através da membrana de celofane.

Como podemos observar na Fig. 2, a frequência decresce à medida que o diclofenac se vai difundindo através da membrana, até estabilizar. Através deste decréscimo de frequência, e com a utilização da recta de calibração obtida anteriormente, é possível representar a concentração de diclofenac em função do tempo. A aplicação da 1º Lei de Fick a estes resultados permite obter o coeficiente de difusão, o tempo de latência e o fluxo. Estes valores para a membrana sintética (celofane) e para outras membranas naturais irão ser apresentados posteriormente, sendo os coeficientes de difusão comparáveis aos valores que se encontram na literatura para estudos de difusão em pele.

Agradecimentos

Os autores agradecem o apoio financeiro recebido do CESAM e da FCT (BPD/30134/2006).

Referências

[1] M. Ansari, M. Kazemipour, M. Aklami, International Journal of Pharmaceutics, Vol 327, pp 6-11, 2006.
[2] T.J. Franz, Journal of Investigation Dermatology, Vol 64, pp 190-195, 1975.
[3] C. Behling, R. Lucklum, P. Hauptmann, Sensors and Actuators A, Vol. 68, pp 388-398, 1998.
[4] B.A. Čavić, G.L Hayward, M. Thompson, The Analyst, Vol. 124, pp 1405-1420, 1999.
[5] M.I.S. Veríssimo, M.T.S.R. Gomes, Analytica Chimica Acta, Vol. 617, pp 162-166, 2008.
[6] M. Shamsipur, F. Jalail, S. Ershad, Journal of Pharmaceutical and Biomedical Analysis, Vol. 37, pp 943-947, 2005.

Implementación de un sistema de tomografía óptica coherente

éxiFacultad de Ciencias Físico Matemáticas, Benemérita Universidad Autónoma de Puebla
Av. San Claudio y 18 Sur, Col. San Manuel, C.U., Puebla, Pue. C.P. 72570, México.
jcastill@fcfm.buap.mx[1]

Abstract

La tomografía óptica coherente es una aplicación muy interesante de la óptica con la cual es posible establecer mediciones de tejidos de manera no invasiva. En esencia esta técnica se basa en el empleo de fuentes de luz de muy baja coherencia, lo que permite analizar las muestras bajo análisis con resoluciones de algunos micrómetros. En este trabajo se presentan resultados experimentales de un sistema de tomografía óptica coherente empleando un diodo superluminescente como fuente de luz y un interferómetro de michelson en fibra óptica.

Keywords: OCT, Fibras Ópticas

Introducción

La tomografía óptica coherente tiene características que son comunes tanto con el ultrasonido como con la microscopia. Por otra parte en el ultrasonido clínico la resolución es del orden de 0.1 – 1mm [1-3], mientras que para la microscopia confocal esta puede llegar hasta algunos μm, sin embargo su profundidad de penetración no supera los cientos de μm. Por otro lado la OCT puede llegar a tener resoluciones algunas micras con profundidades de varios mm [4, 5]. Estas características hacen de la OCT una técnica con prometedoras aplicaciones sobre todo en el área clínica. La idea de la OCT es trabajar con los "ecos de luz" para evaluar las muestras de interés.

La Fig. 1 muestra un arreglo típico para establecer una medida de los ecos de luz. Los interferómetros son precisamente poderosos sistemas que permiten evaluar la magnitud y retraso de los ecos de luz. La OCT emplea estos instrumentos y se basa en la técnica clásica de medición óptica llamada interferometría óptica de baja coherencia.

El concepto fundamental del funcionamiento de la OCT radica básicamente en la idea de hacer interferir haces de luz con pequeñas longitudes de coherencia. Con esto uno puede esperar señales interferométricas siempre que las diferencias de caminos ópticos no superen los caminos ópticos.

En esta técnica se lleva a cabo la correlación o interferencia entre la luz que es esparcida por la muestra bajo análisis la luz que ha viajado una distancia conocida la que se ha "retrasado" por viajar este camino, el cual es conocido como camino de referencia. En particular en la Fig. 2 puede reconocerse que el sistema forma esencialmente un interferómetro de Michelson. De aquí que el campo a la salida de sistema (en el detector de luz) uno espera una intensidad

$$I_0 \propto |E_r|^2 + |E_s|^2 + 2E_r E_s Cos(2k\Delta L) \qquad (1)$$

donde ΔL es la diferencia de camino entre los brazos de los haces señal, E_s, y de referencia, E_r. Si la longitud del brazo de referencia fuese cambiada (barrida en alguna distancia) la intensidad de salida del sistema mostraría una dependencia cosenoidal que variaría en el tempo. Para detectar los ecos de luz es necesario emplear fuentes de luz de baja coherencia (amplios anchos de banda).

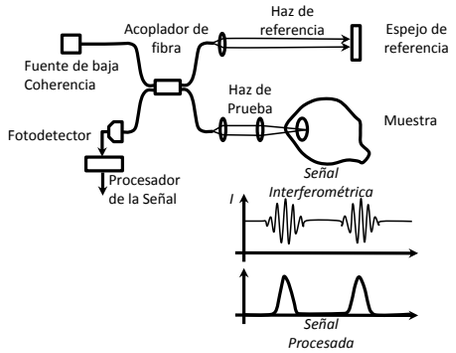

Fig. 1. El concepto fundamental del funcionamiento de la OCT radica básicamente en la idea de hacer interferir haces de luz con pequeñas longitudes de coherencia. Con esto uno puede esperar señales interferométricas siempre que las diferencias de caminos ópticos no superen los caminos ópticos.

De esta forma cuando se emplea este tipo de fuente solo se observará interferencia cuando las longitudes de camino óptico sean tales que su diferencia no supere a la llamada longitud de coherencia de la fuente empleada. De esta forma el interferómetro efectivamente

evalúa la correlación de los “trenes de luz”. La magnitud del eco retrasado de la luz puede ser medida mediante el escaneo del brazo de referencia y demodulando la señal de interferencia. De esta forma la longitud de coherencia determina la resolución axial de la imagen generada.

Desarrollo experimental

Con el arreglo de la Fig. 1 a la salida del sistema normalmente se obtiene una señal como la que se observa en la Fig. 2.

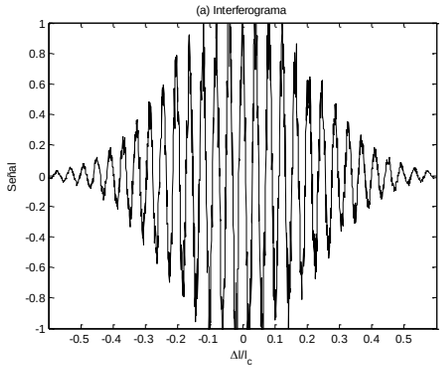

Fig. 2. Interferograma de salida como función de la diferencia de camino óptico normalizado con la longitud de coherencia de la fuente de luz.

Como puede observarse la señal de interferencia es máxima cuando la diferencia del camino óptico Δl es cero. Dado que normalmente uno barre la posición del espejo de referencia, para determinar la posición del máximo de la señal envolvente ($\Delta l = 0$) uno puede hacer un filtraje de la señal interferométrica en el dominio de Fourier, para esto primero se rectifica la señal interferométrica como se observa en la Fig. 3

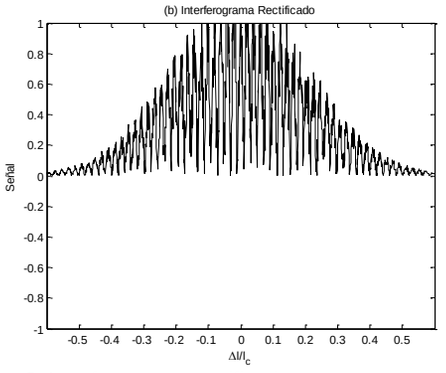

Fig. 3. Interferograma rectificado.

Una vez que la señal se ha rectificado, puede llevarse a cabo la transformada de Fourier de ésta, los resultados se observan en la Fig. 4. Una vez que se ha hecho esto basta con eliminar las componentes que en este caso se encuentran en las frecuencias -4 y 0, para enseguida desplazar el pico de frecuencia 4, al origen. Con esto y aplicando la transformada de Fourier inversa es posible determinar el perfil de la señal envolvente. Tal y como se muestra en la Fig. 5.

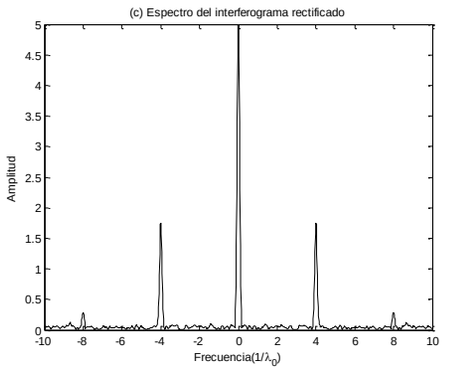

Fig. 4. Espectro del interferograma rectificado, para obtener la envolvente basta con eliminar los picos en frecuencias -4 y 0, y desplazar al centro el pico en la frecuencia 4.

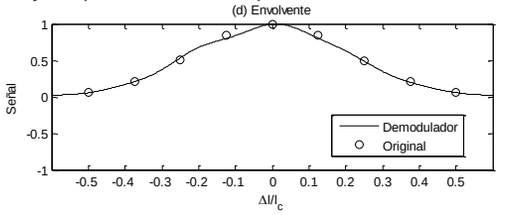

Fig. 5. Perfil de la señal envolvente, con ésta es posible determinar con facilidad la posición del máximo y por lo tanto la posición cuando $\Delta l = 0$.

Conclusiones

En este trabajo se presentan resultados de un sistema de tomografía óptica coherente. Este sistema esta conformado por un interferómetro de Michelson realizado en fibra óptica. Se presenta el desempeño de programas en matlab que son capaces de obtener las señales interferométricas así como el procesamiento de estas para establecer mediciones axiales de las muestras bajo análisis. Como fuente de luz se emplea un diodo superluminescente alrededor de los 1550 nm y con un ancho espectral de 90 nm.

Referencias

[1] R. Erbel, J.R.T.C. Roelandt, J. Ge, G. Gorge, “Intravascular Ultrasound”, Martin Dunitz, London, 1998.

[2] L. Szabo, “Diagnostic Ultrasound Imaging: Inside Out”, Elsevier, Burlington, MA, 2004.

[3] W.R. Hedrick, D.L. Hykes, D.E. Starchman, “Ultrasound Physics and Instrumentation”, 4th edn., Elsevier, Mosby, St. Louis, 2005.

[4] J.S. Schuman, C.A. Puliafito, J.G. Fujimoto, “Optical Coherence Tomography of Ocular Diseases”, 2nd end., Slack Inc., Thorofare, NJ, 2004.

[5] W. Drexler, J.G. Fujimoto, “Optica Coherence Tomography Technology and Applications”, Springer-Verlag, Berlin Heidelberg, 2008.

Diseño y construcción de una plataforma experimental para la caracterización de flujo sanguíneo.

Julio Solano González, Israel Sánchez Domínguez, Mónica Vázquez Hernández, Martín Fuentes Cruz, Eliseo Diaz Nacar, Fabián García Nocetti.
Universidad Nacional Autónoma de México, Instituto de Investigaciones en Matemáticas Aplicadas y en Sistemas, Departamento de Ingeniería en Sistemas Computacionales y Automatización.
04510, México, D.F., México
israel@uxdea4.iimas.unam.mx

Abstract

Es bien conocida la importancia que tiene el área de diagnóstico médico en el tratamiento y seguimiento de terapias de pacientes con diferentes enfermedades. En particular cuando se tratan padecimientos que tienen relación con enfermedades cardiovasculares; una de las principales causas de muerte en el mundo. Para ello es necesario contar con instrumentos y personal calificados para llevar a cabo estos diagnósticos, dar soluciones a los problemas y seguimiento a los tratamientos. Para lograr lo anterior se requiere de una gran inversión en investigación biomédica y en el desarrollo de plataformas experimentales de las cuales surgirán los instrumentos que serán llevados al campo de la medicina. Tal es el caso de los denominados “phantoms” de tipo biológico, mecánico e inclusive virtuales, que pueden ayudar a desarrollar y calibrar instrumentos, o bien a entrenar y capacitar al personal, permitiendo mejorar los diseños instrumentales. Este trabajo presenta el desarrollo de una plataforma experimental para la caracterización de instrumentos que miden la cantidad y calidad de flujo sanguíneo que en particular es utilizado para verificar el éxito de una revascularización coronaria, empleando el ultrasonido Doppler.

Keywords: phantom, flujo sanguíneo, estenosis, revasculación coronaria, sistema Doppler.

Introducción

La importancia que tiene el diagnóstico médico para el tratamiento y seguimiento de terapias en pacientes con diferentes enfermedades, en particular cuando se tratan padecimientos relacionados con enfermedades cardiovasculares (una de las principales causas de muerte en el mundo), es uno de los puntos claves para lograr una recuperación del paciente. Por ese motivo se ha desarrollado una plataforma experimental cuyo objetivo es que dicho dispositivo emule las principales características del flujo sanguíneo producido por el corazón, y en él se puedan incorporar variantes como ritmo cardiaco, pulso cardiaco y emular diferentes grados de “estenosis”, con lo cual es posible llevar a cabo investigación sobre el comportamiento del flujo sanguíneo tanto en condiciones “sanas” como “patológicas”, esto ultimo se logra al modificarse las características del flujo a través de dichas “estenosis” acumuladas en las paredes de las arterias en estudio, para la caracterización de instrumentos que midan la cantidad y calidad de flujo sanguíneo.

Desarrollo

El diseño del phantom es simple, pues consta de una bomba dosificadora lineal (figura 1), esto garantiza que el flujo entregado será constante durante todo el tiempo del experimento. Los vasos (venas o arterías) se emulan mediante el uso de mangueras de teflón o de silicón (silicona), estos materiales son flexibles y durables, inodoros. También son inertes y estables a altas temperaturas, lo que los hace útiles en gran variedad de aplicaciones (figura 2). Asimismo se emplea un soporte el cual permite sostener un transductor ultrasónico, este soporte posee dos grados de libertad, uno de estos grados permite desplazar el transductor en el rango de 20° a 160°, sobre el eje “x”, permitiendo medir el flujo que pase por las mangueras. El otro grado de libertad permite el desplazamiento de 0° a 180°, sobre el eje “y”, como se muestra en la figura 3.

Figura 1. Bomba dosificadora.

Figura 2. Mangueras de teflón.

Figura 3. Plataforma experimental para la medición de flujo sanguíneo.

El proceso de emulación de “estenosis” es realizado mediante un sistema en el cual se provocan diferentes grados de oclusión, permitiendo ir cerrando el paso de la luz en cada manguera. Se utiliza asimismo sangre sintética que cuenta con las características reológicas de la sangre humana, así como los reflectores necesarios para la medición del flujo a partir de un principio Doppler.

Resultados

Los resultados presentados en este artículo indican la efectividad de la plataforma, de tal forma que se pueda utilizar como marco de referencia para la calibración de instrumentos.

Se presentará un caso de estudio real en el cual se ha empleado la plataforma para la calibración de un Sistema Doppler de Medición de Flujo Sanguíneo, así como el sistema utilizado durante la revascularización coronaria (en quirófano)., así como avances de investigación.

References

[1] García-Nocetti, Fabián; Solano-González, Julio;Fuentes-Cruz, Martín, Design of a Pulsed Wave Doppler Ultrasound Blood Flow Detector for Cardiovascular Applications, 19th International Congress on Acoustics. Madrid, España, september 2007.

[2] García-Nocetti, Fabián; Solano-González, Julio; Fuentes-Cruz, Martín, Moreno-Hernández,Eduardo; Villar-Inclán, Alejandro; Prohias-Martínez, Juán, Doppler Ultrasound Blood Flow Measurement System, 19th International Congress on Acoustics, Madrid, España, September 2007.

[3] J. Solano, F. García, M. Vázquez, I. Sánchez, M. Fuentes, E. RubioSmith, Análisis de la Respuesta Espectral en la Medición de la Turbulencia causada en el Flujo Sanguíneo por la presencia de Estenosis en Vasos Ibersensor. 6to Congreso ibero- americano sobre sensores 2008, Sao Paulo. Brasil, Noviembre 24-26, 2008.

[4] David H. Evans, " Doppler Ultrasound", John Wiley and sons, second edition, 1989.

Experimental Approach on Measuring Sheep Coronary Arteries Vasomotricity

Leandro J. Cymberknop[1], Ricardo L. Armentano[1], Franco M. Pessana[1], Alejandro Furfaro[1] and Alberto J. Crottogini[2]
[1]Electronics Department, Buenos Aires Regional Faculty, National Technological University
[2]Department of Physiology, Favaloro University, Buenos Aires, Argentina
Contact: ljcymber@electron.frba.utn.edu.ar

Abstract

Coronary circulation is responsible for the blood supply to the heart muscle. Changes in large coronary arteries are fundamental in the pathogenesis of myocardial ischemia in coronary heart disease. It is widely known that the evaluation of arterial biomechanical behavior implies the analysis of the stress (applied pressure) vs strain (diameter variation) relationship. Consequently, the aim of this study was to design an experimental approach in order to measure sheep coronary arteries vasomotricity during in vivo experiences.

Keywords: coronary; pressure; diameter; vasomotricity; smooth muscle activation.

Introduction

Arterial stiffening is a common but highly variable disorder that is associated with advancing age and exacerbated by many known cardiovascular disease risk factors, including genetic factors. The cardiac muscle provides blood flow to the arterial system, exerting hemodynamic forces on the vessel walls. The main function of systemic circulation is to guarantee a continuous blood flow at capillary level. Excessive arterial pulsatility is associated with various common diseases of aging and hypertension [1]. In this sense, mechanic behavior of large arteries, denoted by its viscoelastic properties, plays a fundamental role [2]. Coronary circulation is responsible for the blood supply to the heart muscle. Changes in large coronary arteries are fundamental in the pathogenesis of myocardial ischemia in coronary heart disease. Traditionally, the diagnosis of coronary stenosis severity was based only on angiography methods. However, the clinical significance of a coronary stenosis cannot be fully characterized based on the geometry alone [3]. Evaluation of arterial biomechanical behavior implies the analysis of the stress (applied pressure) – strain (diameter variation) relationship [4]. In addition, smooth muscle activation alters the viscosity as well as the elasticity of the vessel wall [5]. The aim of this study was to design an experimental approach in order to measure sheep coronary arteries vasomotricity during in vivo experiences. Coronary elastic modulus was obtained by means of the slope of the coronary pressure (***CP***) vs. coronary arterial diameter (***CAD***) loop. Additionally, ***CP*** and central aortic pressure (***CAP***) were measured simultaneously, in order to demonstrate that either of them can be used in coronary arterial stiffness assessment. Experiments were performed under acute hypertension states, induced by the activation of smooth muscle cells, by means of the administration of a sympathomimetic drug.

Material and Methods

Four Corriedale castrated male sheep weighing 28.4±3.2 kg were operated. After premedication with intramuscular acepromazine maleate (0.2 mg/kg), anesthesia was induced with intravenous sodium thiopental (20 mg/kg) and maintained with 2% halothane in pure oxygen under mechanical ventilation (Neumovent 910, Córdoba, Argentina). The electrocardiogram, heart rate and oxygen saturation (Novametrix 515A pulse oxymeter, Wallingford, CT) were monitored during surgery and recovery. After a sterile minithoracotomy at the 4th intercostal space, the left anterior descending artery (***LAD***) was dissected just proximal to the origin of the second diagonal branch. To measure the external diameter, a pair of ultrasonic crystals (5 MHz) was sutured to the upper third of the ***LAD***. The ultrasonic signal transit time was converted into distance through a sonomicrometer (Triton Biosciences Inc., California, USA). A pressure microtransducer (Millar microtip catheter) was positioned in the upper third of the ascending aorta. In order to compare this pressure with

coronary arterial pressure, a Konigsberg P2.5 microtransducer (1200Hz, Pasadena, USA) was located in a lateral branch close to the upper third of the ***LAD*** (figure 1). Simultaneous aortic pressure and diameter were measured in control state and under VSM activation: ***PHE*** group (phenylephrine 5 µg/kg/min). All experimental procedures were performed in agreement with ethics norms and international recommendations about research in laboratory animals, ratified in Helsinki and actualized by the Physiology American Society (1981) [6]. Changes in coronary wall stiffness were estimated assuming that the arterial wall is an isotropic homogeneous elastic material with a pressure-strain elastic modulus (***E***) [7].

Results

Arterial pressure and ***LAD*** diameter measured signals, in control state and after smooth muscle activation, may be observed in figure 2, for a typical case. Similar morphology was found in the rest of the processed cases, for different phenylephrine states.

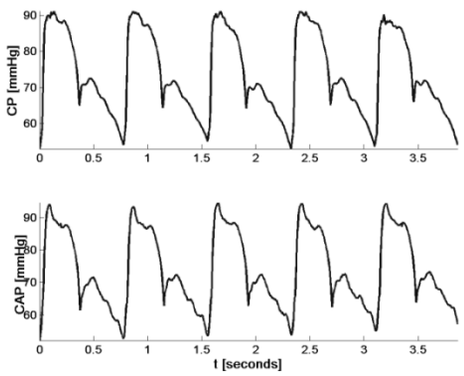

Figure 1. **Higher Panel**: In-vivo measured aortic pressure. **Lower Panel**: In-vivo measured coronary arterial pressure, for a single case.

Conclusion

With the present approach, aortic pressure, coronary pressure and coronary diameter waveforms were obtained simultaneously in control state and under smooth muscle activation. Phenylephrine administration produced arterial stiffening unrelated to the arterial vasomotricity state. Pulse pressure was observed to be highly dependent of the smooth muscle activation levels.

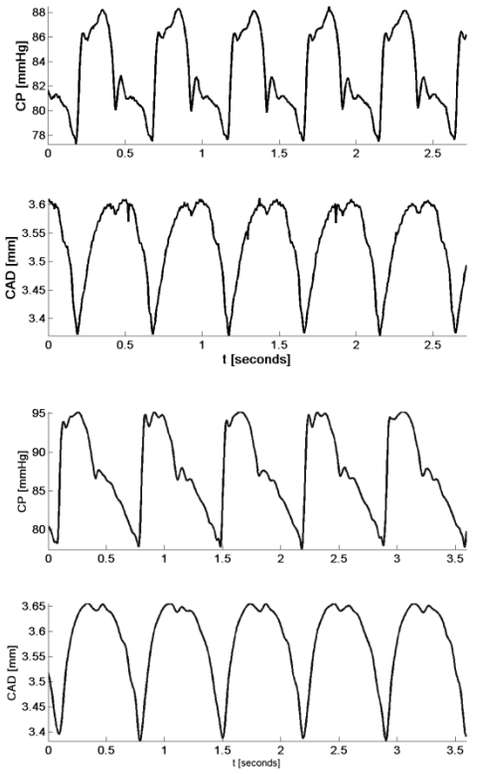

Figure 2. **Higher Panels:** In-vivo measured pressure and coronary diameter, under control state. **Lower Panels:** In-vivo measured pressure and coronary arterial diameter, after phenylephrine administration, for a typical case.

References

[1] Safar M. E., Levy B. I., and Struijker-Boudier H., “Current Perspectives on Arterial Stiffness and Pulse Pressure in Hypertension and Cardiovascular Diseases”, Circulation, vol. 107, no. 22, pp. 2864–2869, 2003.

[2] Armentano RL, Graf S, Barra JG, Velikovsky G, Baglivo H., Sanchez R, Simon A, Pichel RH, Lenvenson J, “Carotid wall visosity increase is related to intima media thickening in hypertensive patients”, in Stroke 35, 2004.

[3] Spaan J., Kolyva C., Van Den Wijngaard J., Ter Wee R., Van Horssen P., Piek J., y Siebes M., “Coronary Structure and Perfusion in Health and Disease”, Phil. Trans. R. Soc. A, vol. 366, no. 1878, pp. 3137–3153, 2008.

[4] Cabrera Fischer E, Bia D, Zócalo Y, Camus J, Forteza E, Armentano RL, “Effects of removing adventitia on the mechanical properties of ovine femoral arteries in vivo and in vitro”, in J. Circ., 74, 2010.

[5] Barra JG, Levenson J, Armentano RL, Cabrera Fischer E, Piehel RH, Simón A, “Assessment of smooth muscle contribution to descending thoracic elastic mechanics on concious dogs”, in Circ. Res, 73, pp. 1040-1050, 1993.

[6] Guide for the Care and Use of Laboratory Animals, National Institutes of Health (NIH Publication Nº 86-23, revisited 1985).

[7] Armentano R. L., Cabrera Fischer E. I., Barra J. G., Levenson J. A., Simon A. C., and Pichel R. H., “Single beat evaluation of circumferential aortic elastin elastic modulus in conscious dogs. Potential application in non-invasive measurements”, Med Prog Technol, vol. 20, no. 1–2, pp. 91–99, 1994.

ELECTRODES FOR BIO-APPLICATION: RECORDING AND STIMULATION

Marcelo Bariatto Andrade Fontes

MPCE/DSE – FATEC-SP – CEETEPS, São Paulo, Brasil
bariatto@fatecsp.br

Abstract

Recording and stimulation electrodes applied on excitable tissue are the basis of electrophysiological research, such as brain, muscles, peripheral nerves or sensory systems. Electrode-electrolyte impedance is one of important characteristic due to its influence on the signal/noise ratio, signal distortion and built-up voltage. Strategies to lowering and tuning the impedance is achieved by biasing iridium oxide modified platinum microelectrodes. Surface and impedance analysis after pulse stimulation are also addressed.

Keywords: electrode modification, bio-application, impedance spectroscopy, Iridium Oxide

Introduction

The bioelectric potentials carried in electrolytic media in form of ionic currents, are transduced by the electrodes in to electronic signals. This takes place by means of capacitive coupling (without net charge transfer), such as occurs during recording, and by charges transfer reactions in which the electrodes and ions in the physiologic environment exchange electrons through redox reactions, this process occurs manly during stimulation. Those reactions can be reversible or irreversible, usually generating gases at the electrode site (H_2, O_2, Cl_2), leading to damaging/poisoning of the tissue and electrode corrosion due to its oxidation [1-2].

Strategies to lower the impedance are of key importance in applications such as the recording of neural signals. Iridium Oxide (IrO_x), a biocompatible metallic oxide film, is an excellent candidate to accomplish this impedance reduction given its texture. Because it is an electroactive material, i.e., it forms a fast-kinetics redox system on the electrode surface, therefore allowing Faradaic charge transfer, it is also of particular importance in cases where electrical stimulation is required [3,4].

Iridium oxide is known to exhibit electrochromic behavior, i.e. the reversible change of color in response to the application of an electric charge). Electrochromism is also followed by a change in impedance, whose value is decreased for anodic potentials [5]. Once the impedance is set, it will stay at that value until a new potential is applied. The process is fully reversible within a time scale of milliseconds .

Electrode Modification

IrO_x coatings have been obtained by directly electroplating over platinum electrodes. The electroplating solution is water based containing iridium chloride ($IrCl_4 \cdot H_2O$), hydrogen peroxide (H_2O_2), oxalic acid $(COOH)_2.2H_2O$ and potassium carbonate to adjust the pH to 10.5 [6,7].

Several electroplating protocols were used both potentiostatic and galvanostatic, as previously reported [7]. We have utilized a CompactStat (Ivium Technologies) to realize such depositions, to perform electrochemical impedance spectroscopy (EIS) characterization and cyclic voltammetry on the obtained electrodes. For the stimulation studies an Autolab Potentiostat was used. All EIS characterization and stimulations protocols was performed in physiological solution (0.9% NaCl, pH=7.4).

Impedance Tuning

EIS measurements are usually performed at equilibrium potential (E_0) or at zero volts, but this value can be adjusted as a bias to which the AC signal is superimposed. No effect is observed for platinum electrodes when EIS is performed with a bias voltage ranging from 0 to 1 V in 100 mV steps. On the other hand, platinum electrodes plated with IrOx show bias dependent impedances for voltages above 500 mV, figure 1a. Impedance reduction up to two orders of magnitude at 1V can be observed at 1 kHz (figure 1b). Applying a 1V pulse train to the platinum electrodes shows no changes in impedance, as expected. Applying the same pulse train to IrOx coated electrodes, a reproducible and reversible impedance decrease was observed with a time response of less than 200 ms.

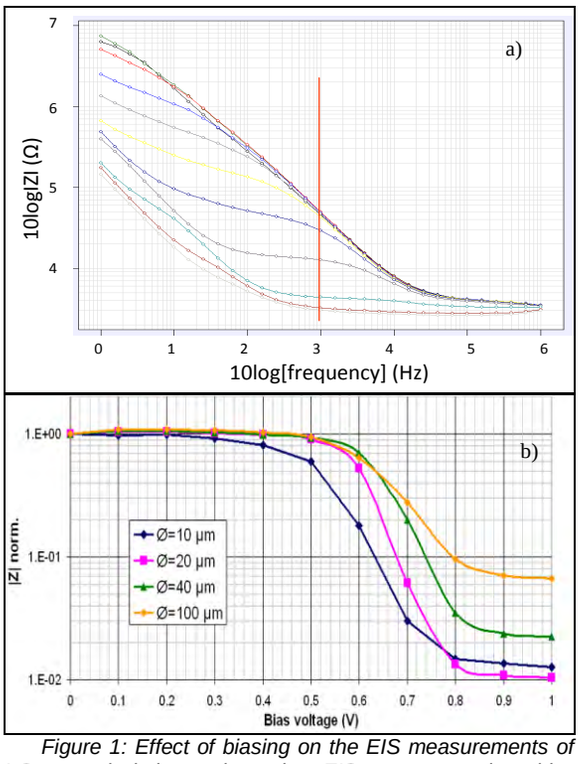

Figure 1: Effect of biasing on the EIS measurements of IrO_x-coated platinum electrodes: EIS scans at various bias voltages on a 100 µm diameter (a) and impedance versus bias voltage plots for various sample diameters (b).

Electrode Stimulation

The aim of the stimulation is to provide enough charge to trigger an action potential at a given spot. For example at the muscle, periferical nerve, cortical surface level, requires charges up to 0.2 to 5 µC / stimulation pulse and intracortical region needs only 8 to 64 nC / stimulation pulse. As the electrode area goes down the amount of charge density increases leading to a failure of the electrode. Optimize a parameter called Charge Store Capacity (CSC), leads to more charge per electrode area, therefore prevent the failure of the electrode. This parameter can be extract through the cyclic voltammetry wave, where the cathodic region (negative current) are related to the amount of the electrons that the electrode can supply at a given range of voltage [1].

Stimulation protocols are usually carried out in form of pulses of voltage or current, where the last one is more common. Several combinations can be used but charge balanced biphasic protocols are usually standard due to the fact that the net charge is zero [2].

Before and after stimulation, cyclic voltammetry and impedance for all electrodes were performed, figure 2. Results showed an improvement for platinum electrodes, most probably due to the electrode cleaning. Iridium oxide coverage presents a decreasing of their CSC along a decreasing of impedance. It was also optically observed changing in the electrode surface.

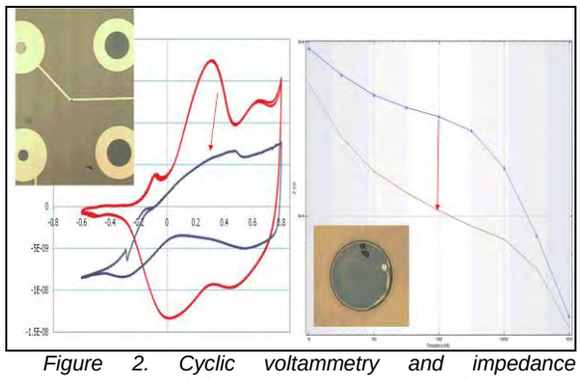

Figure 2. Cyclic voltammetry and impedance measurements for IrO_x modified electrode (Φ=40µm), before and after stimulation.

Conclusion

Impedance tuning of iridium oxide electrodes has been demonstrated. By applying a DC voltage between 0 and 1 V it is possible to vary electrode impedance by as much as two orders of magnitude, therefore enabling the electrode impedance to be electrically programmed. The process is fully reversible with a time response in the millisecond range. Iridium Oxide electrodes combines a low impedance and high charge storage capacity, therefore it is a superior candidate for recording and stimulation

Acknowledgments

The author wish to acknowledge Interuniversity Microelectronics Center (IMEC**),** Division of Neurophysiology at Catholic University of Leuven, Belgium and also the Department of Microsystems Engineering – IMTEK, University of Freiburg, Germany.
Finally the author acknowledge CNPq for the grant (201720/2007-8)

References

[1] R. Frölich, A. Rzany, J. Riedmüller, A. Bolz, M. Schaldach, "Electroactive coating of stimulating electrodes," *J. Mat. Sci. Materials in Medicine*, vol. 7, pp. 393-397 (1996).
[2] J.D. Weiland, and D.J. Anderson, "Chronic neural stimulation with thin-film, iridium oxide electrodes," *IEEE Trans. Biomed. Eng*., vol. 47, no. 7, pp. 911-918 (2000).
[3] R. D. Meyer, S. F. Cogan, T. H. Nguyen, and R. David Rauh, "Electrodeposited Iridium Oxide for Neural Stimulation and Recording Electrodes" *IEEE Trans. Neural Systems Rehab. Eng., vol. 9, no 1, pp. 2-11, March 2001*
[4] J. D.Weiland and D. J. Anderson, "Chronic neural stimulation with thin film, iridium oxide stimulating electrodes," *IEEE Trans. Biomed. Eng.*,vol. 47, pp. 911–918, July 2000.
[5] T. Pauporte, R. Durand, "Impedance spectroscopy study of electrochromism in sputtered iridium oxide films," J. Appl. Electrochem., vol. 30, pp. 35-41 (2000).
[6] K. Yamanaka, "Anodically electrodeposited iridium oxide films (AEIROFs) from alkaline solutions for electrochromic display devices," Jpn. J. Appl. Phys., vol. 28, pp. 632-637 (1989).
[7] Fontes, M.B.A; "In Situ Impedance Monitoring of Iridium Oxide Electrodeposition for Neural Recording", Proc. 7th IberoAmerican Sensors Conference, November 09th - 11th, 2010, Lisbon, Portugal.

Multiplex Electrochemical Genosensing of Pathogenic Bacteria by using Silica Magnetic Particles

S.Liébana[1], S. Campoy[2], P.Cortés[2], S.Alegret[1], M.I. Pividori[1]*

[1] Grup de Sensors i Biosensors, Departament de Química, Universitat Autònoma de Barcelona, Bellaterra, Spain.
[2] Unitat de Microbiologia, Departament de Genètica i Microbiologia, Universitat Autònoma de Barcelona, Bellaterra, Spain
* Tel: +34 93 581 4937, E-mail address: Isabel.Pividori@uab.cat

Abstract

A multiplex approach for the detection of the most common pathogenic bacteria in food safety (*Salmonella spp., E.coli* and *L. monocytogenes*) is presented. The method is based on the lysing and nuclease-inactivating properties of the chaotropic agent guanidinium thiocyanate together with the nucleic acid-binding properties of silica particles in the presence of this agent. After the lysis of the captured bacteria, further amplification of the genetic material by multiplex PCR with a labelled set of specific primers for each pathogen is performed. The amplicon, tagged with fluorescein, digoxigenin and biotin for *Salmonella, E.coli* and *Listeria* respectively, was then immobilized on silica magnetic beads. To confirm the identity of the three bacteria, three different electrochemical tags are used antiFluorescein-HRP, antiDigoxigenin-HRP and streptavidin-HRP conjugates for *Salmonella, E. coli* and *Listeria amplicons*, respectively. This method is able to clearly distinguish among pathogenic bacteria.

Keywords: multiplex pathogen detection, DNA, PCR, silica magnetic bead, electrochemical magneto genosensor, food safety.

Introduction

The control of food quality has become of growing interest for both consumer and food industry since the increasing incidence of food poisoning is a significant public health concern for customers worldwide. Among food pathogens, *Escherichia coli, Listeria monocytogenes* and *Salmonella typhimurium* have been the source –in the last decade– of many outbreaks [1].

In the last few years molecular techniques have appeared as promising alternatives in food microbiology. Nucleic acid based amplification techniques, of which the polymerase chain reaction (PCR) has been so far the most extensively employed, offer several advantages over the classical microbiological methods such as shorter time of analysis, low detection limits, specificity and potential for automation [2].

Several strategies of detection using *Salmonella* as a model have been developed previously in our group [3], [4]. In this work, a rapid and sensitive method for the multiplex detection of food pathogenic bacteria is reported. After the lysis of the bacteria, further amplification of the genetic material by multiplex PCR with a labelled set of specific primers for each pathogen is performed. The amplicon, tagged with fluorescein, digoxigenin and biotin for *Salmonella, E.coli* and *Listeria* respectively, was then immobilized on silica magnetic beads. The method is based on the lysing and nuclease-inactivating properties of the chaotropic agent guanidinium thiocyanate together with the nucleic acid-binding properties of silica particles in the presence of this agent, previously described by Boom et al. [5], [6]. To confirm the identity of the three bacteria a magneto genosensing strategy is performed using three different electrochemical tags, antiFluorescein-HRP, antiDigoxigenin-HRP and Streptavidin-HRP conjugates for *Salmonella, E. coli* and *Listeria* amplicons, respectively.

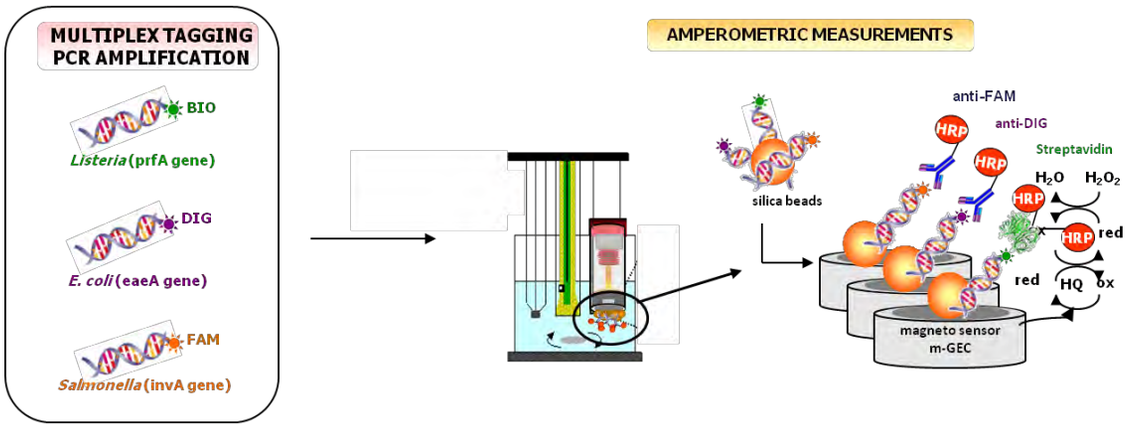

Figure 1. Schematic representation of the multiplex electrochemical genosensing approach.

Experimental section

A schematic procedure is outlined in Figure 1. In this approach a multiplex tagging PCR amplification based on the multiplex PCR system developed by A. Germini et al. was done [2], primers selected are detailed in Table 1.

Table 1. Primers pairs selected for the multiplex PCR [2]

	Primer name	Primer sequence	bp	Labelling	Amplicon size bp
Salmonella	Q-INVA-F	AATTATCGCCACGTTCGGGCAA	22	SH/FAM	284
	Q-INVA-R	TCGCACCGTCAAAGGAACC	19		
E.coli	Q-eaeA-F	GGCGGATAAGACTTCGGCTA	20	SH/DIG	217
	Q-eaeA-RV	CGTTTTGGCACTATTTGCCC	20		
Listeria	Q-PRFA-F	TCATCGACGGCAACCTCGG	19	SH/DIG	150
	Q-PRFA-RV	TGAGCAACGTATCCTCCAGAGT	22		

After the multiplex tagging PCR amplification further confirmation of the identity of each bacteria by electrochemical magneto genosensing of the amplicon was performed. The immobilization procedure of the amplicon on silica magnetic beads and the labeling step with three different electrochemical tags antiFluorescein-HRP, antiDigoxigenin-HRP and Streptavidin-HRP conjugates for *Salmonella, E. coli* and *Listeria* amplicons, respectively**,** have been optimized.

Results and discussion

Regarding the multiplex tagging PCR, the chosen set of primers amplified exclusively the invA, eaeA and prfA insertion sequences for *Salmonella, E.coli* and *Listeria* respectively, producing only the expected fragments in agarose gel electrophoresis.

The immobilization procedure of the amplicon on silica magnetic beads and the labeling steps with three different electrochemical tags have been optimized. The method is able to clearly distinguish among the three bacteria with an amperometric signal above 10 μA and with a signal-to-background ratio of 12, 10 and 7 for *Salmonella, E.coli* and *Listeria* respectively in a total assay time of 3 hours including PCR amplification time.

Conclusions

In the present work the setting of a multiplex electrochemical genosensing method for the simultaneous detection of *Salmonella spp., E.coli* and L_{278} *Monocytogenes* has been described. The method is able to clearly distinguish among theses pathogenic bacteria.

The amplicon immobilization on silica magnetic beads using guanidinium thiocyanate agent has been optimized and the capability of silica magnetic beads coupled with magneto electrodes (m-GEC) for the electrochemical detection of PCR amplicons has been proved.

This strategy can be considered as rapid alternative to the time consuming classical methodology by replacing the selective enrichment and biochemical/serological tests.

References

[1] M. Upmann, C. Bonaparte. “Rapid methods for food hygiene inspection. In Encyclopedia of Food Microbiology”; Academic Press, New York, p 1887, 2004.

[2] A.Germini, A.Masola, P.Carnevali, R.Marchelli. Food Control, 20, pp. 733–738, 2009.

[3] S.Liébana, A.Lermo, S.Campoy, J.Barbé, S.Alegret, MI. Pividori. Anal.Chem., 81, 5812-5820, 2009.

[4] S.Liébana, A.Lermo, S.Campoy, MP.Cortés, S.Alegret, MI. Pividori, Biosensors and Bioelectronics, 25, 510-513, 2009.

[5] R. Boom, C. J. A. Sol, M. M. M. Salimans, C. L. Jansen, P. M. E. Wertheim-Van Dillen, J. Van der Noordaa. Journal of Clinical Microbiology, 495-503, 1990.

[6] R. Boom, C. Sol, M. Beld, J. Weel, J. Goudsmit, P. Wertheim-Van Dillen. Journal of Clinical Microbiology, 615-619, 1999.

Phagomagnetic Separation and Electrochemical Detection of Pathogenic Bacteria

S.Liébana[1], D.Spricigo[2], P.Cortés[2], M. Llagostera[2], S.Alegret[1], M.I. Pividori[1]*

[1] Grup de Sensors i Biosensors, Departament de Química, Universitat Autònoma de Barcelona, Bellaterra, Spain.
[2] Unitat de Microbiologia, Departament de Genètica i Microbiologia, Universitat Autònoma de Barcelona, Bellaterra, Spain
* Tel: +34 93 581 4937, E-mail address: Isabel.Pividori@uab.cat

Abstract

A novel strategy for electrochemical biosensing of food pathogenic bacteria is reported. For the first time phages are used as biorrecognition element for the magnetic separation of pathogenic bacteria, coupled with electrochemical genosensing as a detection technique. The phage capabilities as biorrecognition element are explored by using the model phage nanoparticle P22 towards *Salmonella*. P22 nanoparticles are immobilized in an oriented way on activated magnetic beads. Different methodologies were used in order to study the yield of immobilization, such as: chemical methods (quantification of protein capsid by the Coomassie Bradford Protein Assay) and SEM microscopy. The correct orientation of the phage nanoparticles was studied by the classical phage plating technique and formation of plaques in semi-solid agar. The bacteria are then captured and preconcentrated by the phage-modified magnetic beads throughout the phage-host interaction. To confirm the identity of the bacteria, further double-tagging PCR amplification of the captured bacteria DNA and electrochemical magneto genosensing of the amplicon are performed as rapid alternatives to the time consuming classical selective enrichment and biochemical/serological tests.

Keywords: bacteriophage P22, *Salmonella*, magnetic bead, double-tagging PCR, magneto electrode, electrochemical genosensor.

Introduction

Several strategies of detection using *Salmonella spp.* as a model have been developed previously in our group [1], [2]. The strategy presented is based on the use of bacteriophages, which are biologic nanoparticles, offering several analytical advantages as biorecognition element, since they are inexpensive, highly specific and strong binders, resistant to high temperatures and environmental stresses. Phages are promising alternatives to antibodies as a biorecognition element in a variety of biosensing applications [3].

In this work, phages are used as biorrecognition element for the magnetic separation of pathogenic bacteria for the first time. The phage capabilities as biorrecognition element are explored by using the model phage nanoparticle P22 towards *Salmonella*. P22 nanoparticles are immobilized in an oriented way on activated magnetic beads. The bacteria are then captured and preconcentrated by the phage-modified magnetic beads throughout the phage-host interaction. To confirm the identity of the bacteria, further double-tagging PCR amplification of the captured bacteria DNA and electrochemical magneto genosensing of the amplicon are performed. The features of this approach are discussed and compared with classical culture methods and PCR-based assay.

Experimental section

A schematic procedure is outlined in Figure 1. Firstly, the covalent immobilization of P22 nanoparticles on tosylactivated magnetic beads was performed. Further evaluation of this immobilization was done by Coomassie Bradford Protein Assay, SEM microscopy and classical phage plating technique.

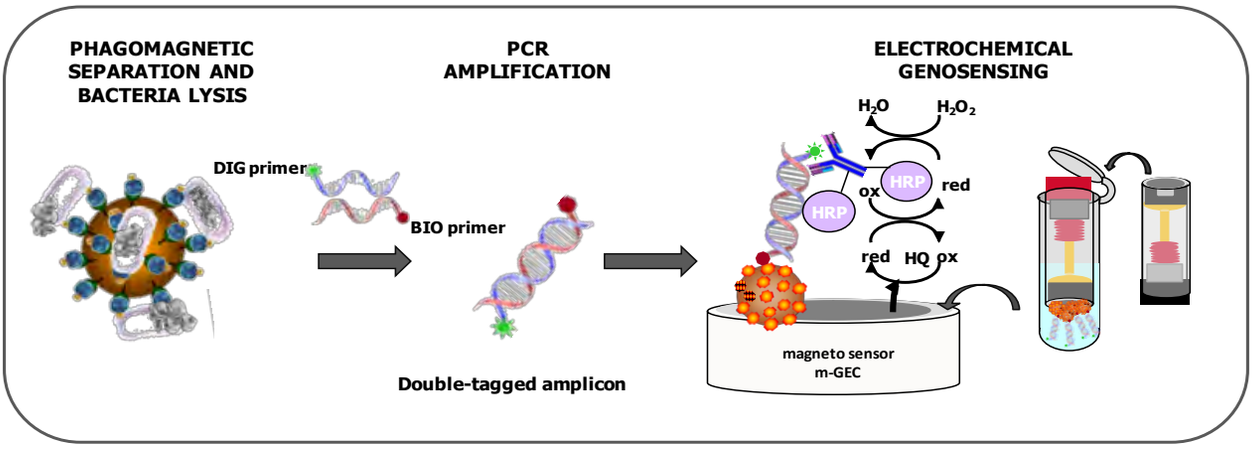

Figure 1. Schematic representation of the phagomagnetic separation and electrochemical detection approach.

Once the immobilization and correct orientation of the P22 nanoparticles was evaluated, the Phagomagnetic Separation (PMS) of *Salmonella* was performed and evaluated by SEM microscopy and classical culture methods.

To confirm the identity of captured bacteria, double-tagging PCR amplification of the bacteria DNA and electrochemical magneto genosensing of the amplicon were performed. After the PCR amplification the double-tagged amplicon was detected by electrochemical genosensing, using streptavidin-magnetic beads that were captured on m-GEC magneto electrodes for the electrochemical detection based on the enzymatic activity of the peroxidase.

In order to verify the specificity of this approach, the above procedure was performed with *Escherichia coli, Salmonella* and a mix containing both bacteria.

Results and discussion

The covalent immobilization of the P22 nanoparticles on tosylactivated magnetic beads has been achieved with 30% efficiency in Coomassie Bradford Protein Assay, which ensures more than 2000 P22 particles per bead. As can be seen in Figure 2, SEM microscopy images confirm the presence of P22 nanoparticles on magnetic beads. The correct orientation of these particles to be able of recognizing bacteria has been proved by classical phage plating technique.

Phagomagnetic Separation was evaluated by SEM microscopy, Figure 2, and classical culture methods.

Regarding the double-tagging PCR, the chosen set of primers amplified exclusively the IS200 insertion sequence, producing only the expected 201 bp fragments in the agarose gel electrophoresis for the concentration range from 10^6 to 10^3 cfu·mL^{-1} .

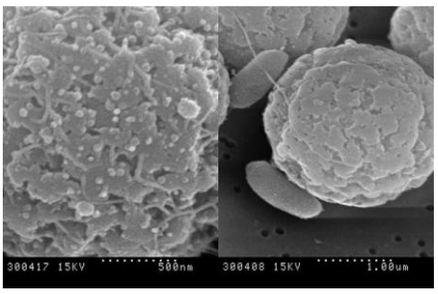

Figure 2. Evaluation of the PMS by SEM microscopy

The method has a LOD of 1 cfu·mL^{-1} in a total assay time of 3 hours including PCR amplification time and is able to clearly distinguish between *Escherichia coli* and *Salmonella.*

Conclusions

Phage capabilities as biorrecognition element have been proved with this rapid and sensitive assay which combines Phagomagnetic Separation (PMS), double-tagging PCR, and electrochemical magneto genosensing of the double-tagged amplicon for *Salmonella spp*. The method is able to detect as low as 1 cfu·mL^{-1} showing highly specificity in a considerable reduced assay time.

References

[1] S.Liébana, A.Lermo, S.Campoy, J.Barbé, S.Alegret, MI. Pividori. Anal.Chem., 81, 5812-5820, 2009.

[2] S.Liébana, A.Lermo, S.Campoy, MP.Cortés, S.Alegret, MI. Pividori, Biosensors and Bioelectronics, 25, 510-513, 2009.

[3] A.E. Smartt, S. Ripp. Anal Bioanal Chem., 400, 991-1007, 2011.

Multiplex Immunosensing Detection of Pathogenic Bacteria

D. Brandão[1], S. Liébana[1], S. Campoy[2], S. Alegret[1], M. I. Pividori[1,*]

[1] Grup de Sensors i Biosensors, Departament de Química, Universitat Autònoma de Barcelona, Bellaterra, Spain
[2] Unitat de Microbiologia, Departament de Genètica i Microbiologia, Universitat Autònoma de Barcelona, Bellaterra, Spain

* Tel: +34 93 581 4937, E-mail address: Isabel.Pividori@uab.cat

Abstract

The increasing incidence of food-borne illnesses is becoming an important public health concern for consumers worldwide. In recent years, many improvements have been made in order to replace time-consuming conventional culture detection methods by rapid methodologies, such as polymerase chain reaction (PCR), immunological assays and biosensors.
In the present work, a simple methodology for the simultaneous immunomagnetic detection of different bacteria using magnetic particles modified with specific antibodies is reported. *Salmonella enterica*, *Escherichia coli* and *Listeria monocytogenes* were selected as a model. The strategy is based on the detection of the whole bacteria by a double immunological recognition. The effects of the particles size, reaction time and bacteria concentration were studied. Finally, the bacteria detection was evaluated through electrochemical magneto immunosensing, as well as magneto-ELISA with optical detection.

Keywords: multiplex pathogen detection, electrochemical magneto immunosensor, food-borne, magneto-electrode, immunomagnetic separation, magneto immunoassay.

Introduction

The increasing incidence of food-borne illnesses is becoming an important public health concern for consumers worldwide. As a result, several tests in multiplex format have been developed for the rapid detection and quantification of more than one microbial species. [1]
Conventional methods for food pathogen detection depend upon microbiological culturing techniques combined with standard biochemical identifications. These methods are time-consuming, laborious and might introduce sampling and enumeration errors due to the low concentration of pathogenic bacteria in food samples. [2]
In this context, multiplexed electrochemical immunosensors offer promising solutions due to their high sensitivity, rapidity, low cost and possibility of being a hand-held platform for field applications. Furthermore, the integration of magnetic particles in immunoassays provides improved analytical performance, allowing miniaturization, development of integrated systems and also the reduction of reagent and sample consumption. [3]
In this methodology, the bacteria are captured and preconcentrated from food samples with magnetic particles by immunomagnetic separation (IMS). Then, the bound target is detected using an enzyme-labeled probe through optical and electrochemical approaches.

Experimental section

The multiplex immunomagnetic detection of *Salmonella enterica*, *Escherichia coli* and *Listeria monocytogenes* comprises the following steps, as detailed outlined in scheme 1: (A) Immobilization of specific antibodies for each bacteria on tosylactivated magnetic beads; (B) Immunomagnetic Separation (IMS); (C) Immunological reaction with a secondary polyclonal antibody labeled with peroxidase specific for each bacteria; (D) Electrochemical and optical detection.

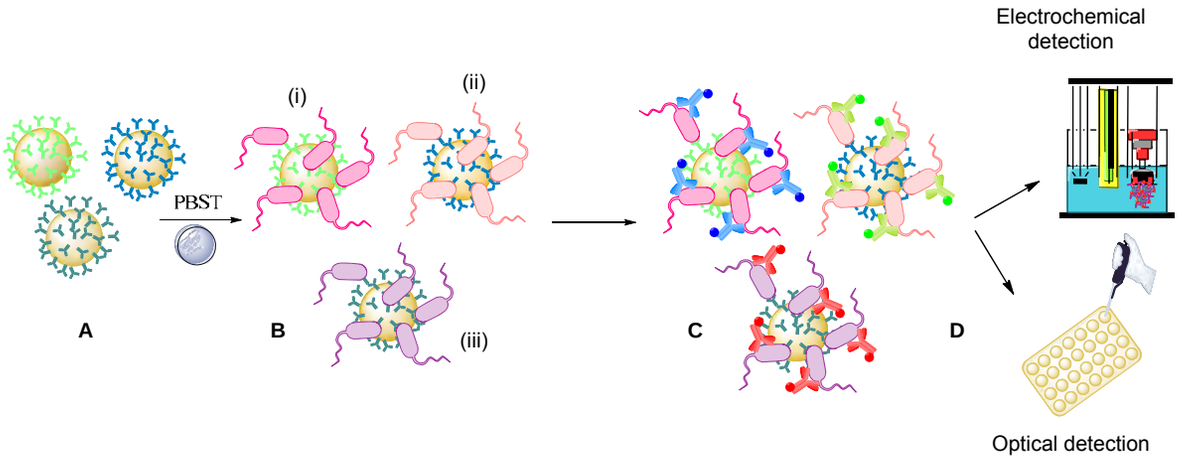

Scheme 1: *Schematic procedure of the multiplex detection of pathogenic bacteria. (A) MP-Ab complexes suspended in PBST. (B) Formation of (i) MP-Ab-E.coli complexes (ii) MP-Ab-Salmonella complexes (iii) MP-Ab-Listeria complexes . (C) Addition of an enzyme-labeled probe specific for each bacteria (D) Electrochemical detection based on a magneto-electrode and also magneto-ELISA.*

Results and discussion

The covalent immobilization of specific antibodies on tosylactivated magnetic beads was performed. Afterwards, the protein coupling efficiency was determined by Coomassie Bradford protein assay, with an average of 83% of the total antibody amount immobilized on the magnetic particles for both *Salmonella enterica* and *Escherichia coli.*

The IMS performance, expressed as percentages of captured bacteria, was evaluated using classical culture methods and Scanning Electron Microscopy (figure 1). In addition, the effects of the particles size, reaction time and bacteria concentration were also studied. Regarding the results from microbiological plating and also from Scanning Electron Microscopy, it was obtained an IMS average percentages of 98% and 80% for *Salmonella enterica* and *Escherichia coli*, respectively, suggesting that the capture of these pathogens with magnetic particles was well succeeded.

Further optimization of the optical detection has been done presenting promising results for the multiplex immunosensing detection by magneto-ELISA.

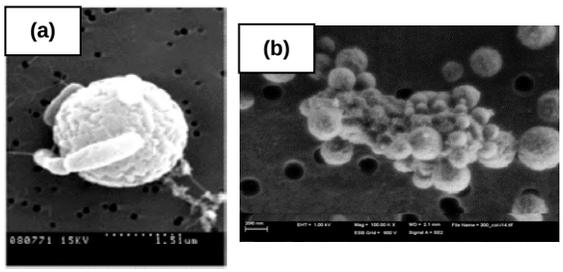

Figure 1: *SEM images of the bacteria capture of: a) Salmonella [3] and b)E.coli.*

Conclusions

According to the preliminary results, it is suggested that magnetic particles modified with specific antibodies can be successfully used to preconcentrate and capture pathogenic bacteria from food samples matrices by immunomagnetic separation. Thus, time-consuming conventional culture detection can be replaced by immunomagnetic separation, whereas the standard biochemical identification can be succesfuly replaced by electrochemical magneto immunosensor..

References

[1] B. Suo, Y. He, G. Paoli, A. Gehring S. Tu, X. Shi, Molecular and Cellular Probes, 24, pp. 77–86, 2010.

[2] S. Liébana, A. Lermo, S. Campoy, J. Barbé, S. Alegret, M. I. Pividori, Anal. Chem., 81, pp. 5812–5820, 2009.

[3] S. Liébana, A. Lermo, S. Campoy, J. Barbé, S. Alegret, M. I. Pividori, Bios Bioelec, 25, pp. 510-513, 2009.

Magneto biosensing of $CD4^+$ T cells for clinical diagnosis

S. Carinelli[1], C. Xufré Ballesteros[2], M. Martí[2], S. Alegret[1], M.I. Pividori1*
[1] Grup de Sensors I Biosensors, Universitat Autònoma de Barcelona, Spain
[2] Institute of Biotechnology and Biomedicine, Spain
08193, Bellaterra, Barcelona, Spain
E-mail Address: Isabel.Pividori@uab.cat

Abstract

A novel and sensitive method for diagnosis of AIDS and immunodeficiency based on electrochemical biosensor and magneto-ELISA in blood sample is described. $CD4^+$ T cells are separated from the sample and preconcentrated using one-step immunomagnetic separation based on the CD3 receptor and using magnetic particles modified with antiCD3 antibody. After the immunomagnetic separation, the captured cells are then labeled with a biotinylated antiCD4 antibody, followed by the reaction with the streptavidin-peroxidase conjugate. Finally, the electrochemical detection is performed using a magneto electrode based on graphite epoxy composite and compared with the optical detection in a magneto-ELISA procedure.
The results indicated that the limit of detection for magneto-ELISA assay is as low as 12 $CD4^+$ T cells per μL of human serum. The linear range was between 0 to 1000 cells/μL, which involves the whole medical interest range for $CD4^+$ T cell counting in HIV-1-infected patients. Moreover, the electrochemical biosensor is able to clearly distinguish between different levels of $CD4^+$ T cells, being a promising device for the HIV diagnosis.

Keywords: HIV diagnostic, $CD4^+$ T cells, magneto-ELISA, electrochemical magneto immunosensor, magnetic beads

Introduction

The incidence of human immunodeficiency virus (HIV) infection and clinical disease continues to increase rapidly in underdeveloped and developing countries. In a patient with HIV infection, $CD4^+$ T cells counting help determine the stage of infection, guide drug choices and indicate the response of the patients to the treatment as well as disease progression. Moreover, this indicator is also recommended for immune disorders, after an organ transplant or a graft. In developed countries, $CD4^+$ T cells counting for patient with HIV infection are usually determined every 3–6 months. Flow cytometry is the standard method for $CD4^+$ T cells counting, but the high investment of the instrument and costly reagents make it unaffordable to most of the centers in a developing country.
To solve the urgent need for improved diagnostic tools of HIV, electrochemical immunosensors offer an exciting alternative, especially in poorer populations, as a rapid, cost-effective, and high-sample-throughput analytical strategy that can be handled for unskilled personnel at the community and primary care level.

Recent advances allow the use of magnetic beads as a support in immunosensing strategies, which greatly improves the performance of the immunological reaction, due to (i) that they can be conveniently manipulated using well-controlled magnetic fields, (ii) the increased surface area, and (iii) the faster assay kinetics because the beads are in suspension. In addition, due to the improved washing and separation steps, the matrix effect is minimized in complex samples [1].
The high sensitivity conferred by the m-GEC electrode in connection with the use of magnetic nanoparticles and enzymatic labeling result in a rapid, inexpensive, robust, and hand-held device able to be used as an alternative diagnostic tool at the community and primary care level, especially in the least developed countries, for the detection of HIV virus as well as for cell counting [2].

Methods

The electrochemical immunosensing strategy is compared with a developed magneto-ELISA procedure.

Magneto-ELISA procedure. The magneto-ELISA procedure is based on a sandwich assay and

comprises the following steps: (a) Capturing of $CD4^+$ T cells from the sample and preconcentration using one-step immunomagnetic separation based on the CD3 receptor and using magnetic particles modified with antiCD3 antibody; (b) Enzymatic labeling by a biotinylated antiCD4 antibody, followed by the reaction with the streptavidin-peroxidase conjugate; (c) Enzymatic reaction by adding TMB (3, 3´, 5, 5´tetramethylbenzidine) and incubation for 30 min at room temperature; (d) Optical determination at 450 nm (Fig. 1).

b) Electrochemical immunosensing strategies. The electrochemical immunosensing strategy is based on a sandwich assay and comprises the following steps: (a) Capturing of $CD4^+$ T cells from the sample and preconcentration using one-step immunomagnetic separation based on the CD3 receptor and using magnetic particles modified with antiCD3 antibody; (b) Enzymatic labeling by a biotinylated antiCD4 antibody, followed by the reaction with the streptavidin-peroxidase conjugate; (c) Magnetic capture of the CD3-modified magnetic beads by the magneto electrode based on graphite epoxy composite; (d) Amperometric determination (Fig. 1) based on the activity of the peroxidase enzyme as electrochemical reporter by using hydroquinone as a mediator and hydrogen peroxide as the substrate for the enzyme.

Results

Magneto-ELISA procedure. The different steps of magneto-ELISA procedure were optimized. The optimal concentrations were: $8x10^6$ magnetic particles/mL, 36 ng/mL biotinylated antiCD4 antibody, and 2 mg/mL streptavidin-peroxidase. The limit of detection for magneto-ELISA assay was as low as 12 $CD4^+$ T cells per μL of human serum. The linear range is between 0 to 1000 cells/μL, which involves the whole medical interest range for $CD4^+$ T cells counting in HIV-1-infected patients.

Electrochemical immunosensing strategies. The electrochemical magneto biosensor is used for the rapid detection of $CD4^+$ T cells. Good results are obtained in all the tested concentration range.

Conclusions

Novel electrochemical magneto immunosensing and ELISA strategies for clinical diagnosis of AIDS and other immunodeficiency disorders were developed. The application of the bioassay strategies are demonstrated for the detection $CD4^+$ T cells.
The use of magnetic beads provided improved features regarding sensitivity and selectivity of the assays. Magnetic particles modified with antiCD3 antibody can easily immobilize the cells on the magneto electrodes, avoiding other time consuming immobilization procedures. Promising results have been obtained applying the electrochemical immunosensing strategies to $CD4^+$ T cells detection.

References

[1] J.E. Smith, K.E. Sapsford, W.H. Tan, F.S Ligler, Anal Biochem, 410:124-132, 2011

[2] M. De Souza Castilho, T. Laube, H. Yamanaka, S. Alegret, M.I Pividori, Anal Chem, 83: 5570-5577, 2011

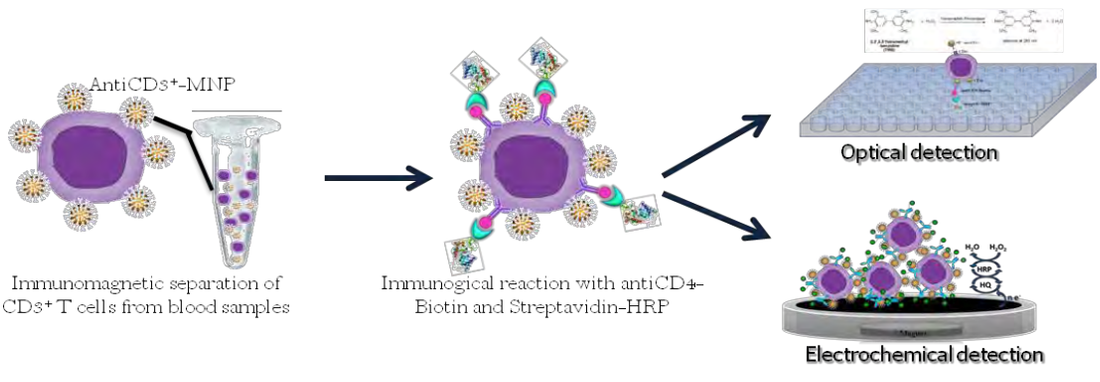

Fig.1. Schematic representation of the bioassay for the rapid $CD4^+$ T cell counting in peripheral blood by using magnetic particles for cells specific isolation based on optical and electrochemical readouts.

Development of an electrochemical biosensor for the detection of an ADP-Ribosylating Toxin, Exo A from *Pseudomonas aeruginosa*

Yanira Enríquez, Yashira Negrón and Ana R. Guadalupe.
University of Rico, Río Piedras Campus
Department of Chemistry, PO Box 23346, San Juan, PR 00931-3346
yanira.enriquez@gmail.com

Abstract

A free radical copolymerization of Styrene and NAS has been done in a range of 10:90 to 90:10 (Sty:Nas) molar ratios. These copolymers were used to generate a film on carbon surfaces to anchor a β-NAD^+ electroactive analog. Ferrocene-labeled $NAAD^+$ (Fc-$NAAD^+$) was prepared by attaching Ferrocene Succinimide (Fc-NHS) to the primary amine in the adenine moiety of the cofactor. The OSWV analysis of the new Fc-$NAAD^+$ showed an anodic peak in 320 mV and the CV analysis showed chemical reversibility and electrochemical quasi-reversibility.

Keywords: *Pseudomonas aeruginosa* (PA), Exotoxin A (Exo A), Ferrocene succinimide, Styrene, Acrylic Acid N-hydroxysuccinimide ester, beta-Nicotinamide adenine dinucleotide (β-NAD^+), Electrode area, Square Wave Voltammetry (SWV), Cyclic Voltammetry (CV).

Pseudomonas aeruginosa is an opportunistic pathogen and is considered one of the most common bacterium found in nosocomial infections. The capacity of *Pseudomonas aeruginosa* (PA) to infect a tissue depends upon the production of virulence factors like enzymes and toxins that damage host cells. One of the virulence factors, in fact the one we are interested in is Exotoxin A. This exotoxin inhibits the protein synthesis in a number of culture cells by catalyzing the transfer of the ADP-ribose of β-NAD^+ to eukaryotic elongation factor 2 (eEF-2). Apparently this "ADP-ribosylation" of EF-2 inhibits the translocation of ribosomes to mRNA and as a consequence avoids protein synthesis. We are interested in designing an electrochemical biosensor for the detection of PA.

A free radical copolymerization of seven copolymers of Sty:NAS with different molar ratios (10:90, 25:75, 40:60, 50:50, 60:40, 75:25, 90:10) was done using AIBN as the initiator.The polymerizationn was done under N_2 (g) reflux at approximately 70^0C - 75^0C for 24 hrs. The final product was purified in methanol and was characterized by FT-IR and HPLC-UV. These copolymers will be used to generate a film on carbon surfaces in order to anchor β-NAD^+ electroactive analog.

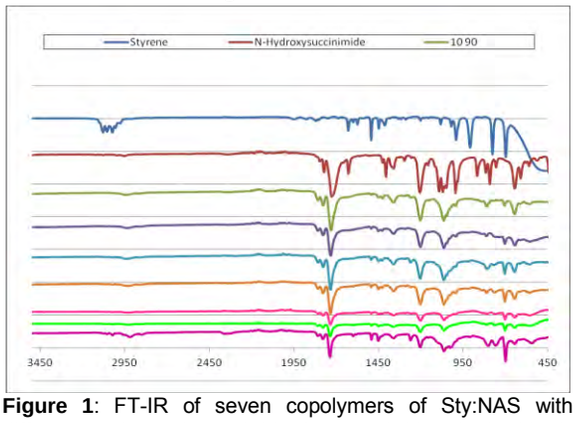

Figure 1: FT-IR of seven copolymers of Sty:NAS with different molar ratios (10:90, 25:75, 40:60, 50:50, 60:40, 75:25, 90:10).

A Ferrocene-labeled NAAD cofactor (Fc-NAAD) was prepared by attaching Ferrocene Succinimide (Fc-NHS) to the primary amine in the adenine moiety of NAAD. The NAAD and Fc-NHS solutions were mixed in a 1:1.2 molar ratio respectively and the synthesis was done in triplicate at room temperature.The final product was purified using a column of Sephadex G-15 and water as the mobile phase. The electrochemical characterization was done using a three electrode cell system with glassy C as the working electrode, Ag/AgCl (NaCl 3M)

as the reference electrode and Nichrome, as the counter electrode. The Cyclic Voltammetry (CV) analysis was done using a 1.00 X 10^{-3} M solution of Fc-NAAD in 0.020 M PBS buffer pH 7.09. The CV window potential was -100-750 mV going in the positive direction at 50, 100, 200, 500 and 1,000 mV/s. Our results clearly show the formation of a new electroactive derivate. The OSWV analysis showed an anodic peak in 320 mV. As expected the current increases with higher scan rate and our new product shows chemical reversibility (Ipa/Ipc = 1.00 ± 0.01 A at 200 mV/s) and electrochemical pseudo-reversibility.

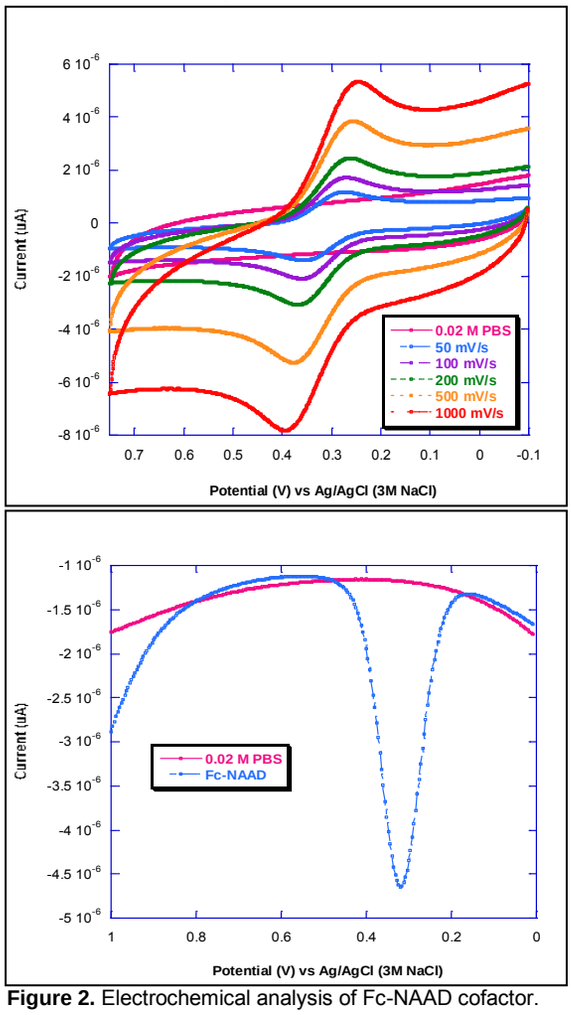

Figure 2. Electrochemical analysis of Fc-NAAD cofactor.

Our work is now focused on the full characterization of the Fc-NAAD cofactor. The carboxyl group in the nicotinic acid moiety of the Fc-NAAD will be used for the immobilization on the electrode surface through an amine linker and our final goal is the electrochemical monitoring of the ADP-ribosylation process mediated by Exo A in vitro.

References

1. Val Delden, C.; Iglewski, B. Cell to Cell Signaling and *Pseudomonas aeruginosa* Infections, ***Emerging Infectious Diseases***, **1998**, *4*, 551-560.
2. Cornelis, P. Pseudomonas: Genomics and Molecular Biology; Caister Academic Press, UK; **2008**, p.129-158.
3. Salyers, A. A.; Whitt, D. D. Bacterial Pathogenesis: A molecular approach; **1994**, p.260-269.
4. Leppla, S. Large Scale Purification and Characterization of the Exotoxin of *Pseudomonas aeruginosa*. *Infection and Immunity*, **1976**, 14, 1077-1086.
5. Iglewski, B.; Sadoff, J.; Bjorn, M.; Maxwell, E. Pseudomonas aeruginosa exoenzyme S: An adenosine diphosphate ribosylatransferase distinct from toxin A, *Proceedings of the National Academy of Science,* **1978**, *75*, 3211-3215.

Acknowledgments

Rise Program Award ID: 2R25GM061151-11

PENN-UPRH Partnership for Research and Education (NSF-DMR- 0934195)

.

Magneto Immunosensor for *Plasmodium Falciparum* Histidine-rich Protein 2 Related to Malaria

M. De Souza Castilho[1], T. Laube[2], H. Yamanaka[1], S. Alegret[2], M.I. Pividori[2*]
[1] UNESP, Laboratorio de Eletroanalítica, Instituto de Química, Universidade Estadual Paulista, Campus de Araraquara, Sao Paulo, Brazil
[2] Grup de Sensors i Biosensors, Universitat Autònoma de Barcelona, Campus UAB, Edifici Cn, 08193, Bellaterra, Barcelona, Spain.

Abstract

A recent study emphasizes the difficulty in making a presumptive diagnosis of malaria and highlights the urgent need for improved diagnostic tools that can be used at the community and primary care level, especially in poorer populations. Magneto immunoassay-based strategies for the detection of Plasmodium falciparum histidine-rich protein 2 (HRP2) related to malaria are described for the first time by using magnetic micro- and nanoparticles. The covalent immobilization of a commercial monoclonal antibody toward the HRP2 protein in magnetic beads and nanoparticles was evaluated and compared. The immunological reaction for the protein HRP2 was successfully performed in a sandwich assay on both kinds of particles by using a second monoclonal antibody labeled with the horseradish peroxidase enzyme (HRP). Then, the modified magnetic particles were easily captured by a magneto sensor made of graphite-epoxy composite (m-GEC) which was also used as the transducer for the electrochemical detection. The performance of the immunoassay-based strategy with the electrochemical magneto immunosensors was successfully evaluated and compared with a novel magneto-ELISA based on optical detection using spiked serum samples. The electrochemical magneto immunosensor coupled with magnetic nanoparticles have shown better analytical performance in terms of limit of detection (0.36 ng mL^{-1}), which is much lower than the LOD reported by other methods.

Keywords: immunosensor, Malaria, magnetic nanoparticles, clinical diagnosis.

Introduction

About 40% of the world's population living in the poorest countries is at risk of malaria infection. Microscopy, with an accuracy of only 70-75%, is considered to be the gold standard for malaria diagnosis, and it is generally available at hospitals. However, microscopy depends on well-maintained equipment, an uninterrupted supply of good quality reagents, trained staff, and good quality monitoring and supervisory systems, so it is not suitable for routine use at the community level.

Modern methods of malaria diagnosis include also fluorescent microscopy, flow cytometry, automated blood cell analysers, serology antibody detection, molecular methods, and laser desorption mass spectrometry. The main disadvantage, however, is their high cost. [1] Among these, the rapid diagnostic tests based on detection of Plasmodium-specific proteins as parasite biomarkers detectable in whole blood, serum, and plasma seem to be good candidates for the development of novel rapid and decentralized methods.[2] Some examples are the histidine-rich protein 2 (HRP2) (only found in *Plasmodium falciparum*), as well as the glycolytic lactate dehydrogenase (LDH) and the *Plasmodium* aldolase (both found in all *Plasmodium* species). However, better sensitivity was reported for *P. falciparum* HRP2-based assays compared with LDH and aldolase tests for the detection of *P. falciparum*.[3]

To solve the urgent need for improved diagnostic tools of malaria, electrochemical immunosensors offer a promising alternative as a rapid, cost-effective, and high-sample-throughput analytical strategy that can be handled by unskilled personnel at primary care level. Recent advances allow the use of magnetic beads as a support in immunosensing strategies, which greatly improves the performance of the immunological reaction based on the concept of magnetic bioseparation while minimizing matrix effect. [4]

An electrochemical immunosensing strategy based on a magneto sensor is presented in this work as a rapid, sensitive, inexpensive, and user-friendly analytical method compared with classical assays for the diagnosis of malaria based on the detection of P. falciparum HRP2 protein in serum. The assay relies for the first

time on a sandwich magneto immunoassay between P. falciparum histidine-rich protein 2 (HRP2) in the sample and two commercially available monoclonal antibodies that target two different epitopes of the antigen, one of them covalently coupled to magnetic particles and the other labeled with the enzyme horseradish peroxidase (HRP) to provide the electrochemical (or optical) signal. The procedure is schematically outlined in Fig. 1.[5]

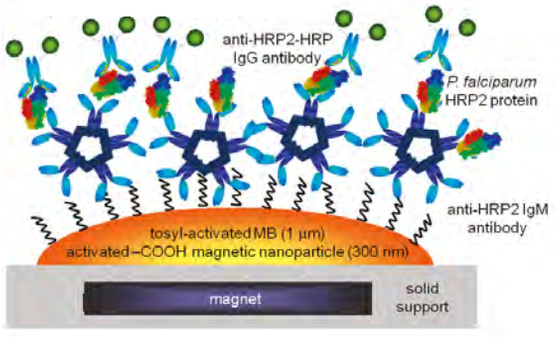

Fig. 1- Schematic representation of the sandwich immunoassay performed on the magnetic beads.

Experimental and Results

Binding of the Anti-HRP2 IgM Antibody on Magnetic Beads and Nanoparticles

The anti-HRP2 IgM antibody was covalently coupled for the first time to 300 nm active magnetic nanoparticles (MNPs) as well as to 1 µm tosyl-activated magnetic beads (MBs). The efficiency of the coupling strategies was evaluated by the Bradford test, analyzing the antibody concentration in the supernatant before and after the conjugation. The antibody binding efficiency to the magnetic beads was found to be 81.9%, while a higher immobilization rate was achieved for the magnetic nanoparticles, of around 94.5%.

Sandwich Magneto-ELISA Optimization and Matrix Effect Study

Two-dimensional (2D) serial dilution experiments were performed using the sandwich magneto-ELISA with optical detection to select optimal concentrations for the modified magnetic beads and nanoparticles as well as the specific HRP2 antibodies. Optimal combination was chosen to produce a signal up to 2 absorbance units with a low background adsorption value.

The results were analyzed for a concentration range from 0 to 250 mg mL^{-1} to cover the low, medium, and high concentration range of HRP2 protein. To study the matrix effect of human serum, the standard curve was performed in human serum diluted 1/5 in PBST and directly in buffer. For both kinds of particles, the absorbance values increased when the sandwich assay was performed in human serum compared with when it was performed in PBST buffer, showing higher matrix effect when using the nanoparticles.

Concentration Response and Accuracy Studies in Spiked Human Serum

Excellent results were obtained with the electrochemical magneto immunosensor using both the magnetic nanoparticles and the magnetic beads as solid support, performed with commercial human serum diluted 1/5 in PBST. However, improved sensitivity was obtained when using 300 nm magnetic nanoparticles, being the slope 4 times higher in this case. The electrochemical magneto immunosensor coupled with magnetic nanoparticles had the best analytical performance, showing the lowest limit of detection (0.36 ng mL^{-1}). Moreover, at a low level of HRP2 concentration of 31.0 ng mL^{-1}, a signal of 15.30 µA was reached with a cutoff value of 0.34 µA, giving a clear positive result with a nonspecific adsorption ratio of 51.

Human serum samples spiked with *P. falcifarum* HRP2 protein at a level of low (35.0 ng mL^{-1}), medium (125.0 ng mL^{-1}), and high (250.0 ng mL^{-1}) concentration were tested, and excellent recovery values were obtained in both methodologies and using both magnetic nanoparticles and magnetic beads as solid support.

Conclusion

Covalent immobilization of anti-HRP2 IgM antibodies was successfully performed, achieving excellent coupling efficiencies. Better LOD values were obtained with the nanoparticles, obtaining values 100 times lower than a concentration of 33.0 ng mL^{-1}, considered as a low-level of HRP2. Due to the high sensitivity, this novel strategy offers great promise for rapid, cost-effective, and on-site detection of *falciparum* malaria disease, but also to screen out at-risk blood samples for prevention of transfusion-transmitted malaria.

References

[1] Hanscheid, T. Clin. Lab. Haematol, 21, 235–245, 1999.
[2] C.K. Murray, D. Bell, R.A. Gasser, C. Wongsrichanalai, Trop. Med. Int. Health, 8, 87–83, 2003.
[3] C.M. Kifude, H. Rajasekariah, D.J. Sullivan, V.A. Stewart, E. Angov, S.K. Martin, C.L. Diggs, J.N. Waitumbi, Clin. Vaccine Immunol., 15, 1012-1018, 2008.
[4] Smith, J. E.; Sapsford, K. E.; Tan, W. H.; Ligler, F. S. Anal. Biochem. 2011, 410, 124–132.
[5] M. De Souza Castilho, T. Laube, H. Yamanaka, S. Alegret, M.I. Pividori, Anal. Chem., 83, 5570–5577, 2011.

Biotinylated Bacteriophages as Nano-labels for *Salmonella* Biosensing

T. Laube[1], M.P. Cortés[2], M. Llagostera[2], S. Alegret[1] and M.I. Pividori[1]*
[1] Grup de Sensors i Biosensors, Departament de Química, Universitat Autònoma de Barcelona.
[2] Unitat de Microbiologia, Departament de Genètica i Microbiologia, Universitat Autònoma de Barcelona
08193, Bellaterra, Barcelona, Spain
* Isabel.Pividori@uab.cat

Abstract

There is an urgent need for fast, competent, and reliable methods for direct detection and identification of foodborne pathogens. The development of biosensors is a growing area that offers an exciting alternative to the more traditional analytical methods, allowing rapid 'real-time', selective and low cost analyses. In this work, the development of a biosensor for *Salmonella* based on immunomagnetic separation is reported. A novel labeling strategy based on the use of biotin-modified bacteriophages is presented. Optimization of reagent concentration as well as matrix effect study and immunoassay performance were evaluated using magneto-ELISA with optical detection and promising results were also obtained by electrochemical detection through a magneto-electrode based on graphite-epoxy composite (m-GEC). In all cases a streptavidin-peroxidase (HRP) conjugate was used as enzymatic label. These strategies show great promise for rapid, simple, cost-effective and on-site analysis of food samples.

Keywords: immunosensor, biotin, bacteriophage, *Salmonella*, food safety.

Introduction

Detection of pathogenic bacteria is an area of prime interest for food safety since infectious diseases spreading every day through food have become a life-threatening problem for millions of people around the world. In recent years significant improvements have been made in order to reduce the analytical time and media requirements of the conventional culture-dependent techniques. Immunological detection of bacteria has become more sensitive, specific, reproducible and reliable with many commercial immunoassays available for the detection of a wide variety of bacteria [1]. Further improvement involves the use of "immunomagnetic separation" (IMS), that is, the use of magnetic beads to capture target bacteria through an immunological reaction, from contaminating microflora and interfering components, and to concentrate them into smaller volumes [2].

Our group (GSB) has been reporting many methodological improvements in immuno- and genosensors for the sensitive detection of pathogenic bacteria [3, 4]. The present proposal is going further to the use of bacteriophages for the improved detection of *Salmonella*.

Phages possess features such as specificity and rapid growth, which make them ideal agents for the rapid detection of bacteria. They are unique natural self-reproducing, and self-assembling nanostructured particles, extremely resistant and stable for long periods of time. Moreover, for each phage, all the naturally occuring nanoparticles are nearly identical, being mono-disperse in shape and size, a fact difficult to achieve by laboratory synthesis. Beside this, they provide a large amount of viral coat proteins with a big surface for further chemical modification [5]. Biotinylation of phage coat proteins [6], as well as genetic modifications to directly express biotin on the capsid [7], were reported for the immobilization on streptavidin-modified surfaces.

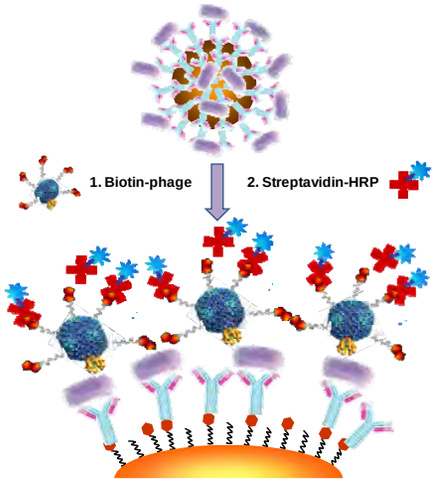

Fig.1- Schematic representation of the sandwich immunoassay performed on the magnetic beads.

Here, we report the biotinylation of P22, a model bacteriophage towards *Salmonella Thyphimurium*, in order to evaluate its capability as nano-tag for an immunosensor. After the IMS of the target bacteria, the biorecognition strategy was based on an indirect sandwich immunoassay using our biotin-modified phages as primary tag and a streptavidin- HRP conjugate as secondary enzymatic label. The procedure is schematically outlined in Fig. 1

Experimental and Results

Phage Biotinylation.

Different biotinylation strategies were evaluated, labeling primary amino groups or carboxylic groups of the phage coat proteins by using NHS- activated biotin or Amine- modified Biotin, respectively. Additionally, the biotin amount was also optimized. In order to analyze the best conditions, the phage titer was controlled by the classical phage plating technique and formation of plaques in semi-solid agar, and the biotin labeling efficiency was analyzed by magneto-ELISA. Best results were obtained by the reaction of 1 mg of biotin with the amino groups of P22 (in a concentration of around 10^{11} PFU/mL).

Phago-assay Optimization

IMS of *Salmonella* was performed using commercially available magnetic beads already modified with the specific antibody. Magnetic beads concentration as well as incubation time were optimized using the sandwich magneto-ELISA with optical detection.

Optimization experiments were also performed in order to determine the optimal biotin-phage conjugate dilution as well as the best streptavidin-HRP concentration. With this purpose the signal to non-specific adsorption ratio was evaluated to find the best conditions for achieving high positive signals related to low blank values. Beside the reagent concentrations, the incubation step with the modified bacteriophage was another important parameter to be optimized in order to improve the immunoassay. Incubation time, as well as temperature and shaking conditions were evaluated, obtaining the best results after incubating 20 minutes at 37ºC without agitation.

Matrix Effect and Concentration Response

The responses of the 'IMS/phagosensing' approach for artificially inoculated *Salmonella* (from 10^2 to 10^7 CFU mL^{-1}) in LB broth and in skimmed-milk diluted 1/10 in LB are shown in Fig.2. Similar behaviors were observed regardless the sample, suggesting that the matrix effect is not very significant in this case. The signal corresponding to the LOD was estimated by processing 10 negative control samples (0 CFU mL^{-1}) and adding three times the standard deviation to the mean value. The cut-off values obtained show that the system is able to detect around 10^3 CFUmL^{-1} in both cases.

Preliminary studies have been made with the magneto-immunosensor and promising results were also obtained, showing higher ratios between positive signal and negative control, in comparison with optical detection.

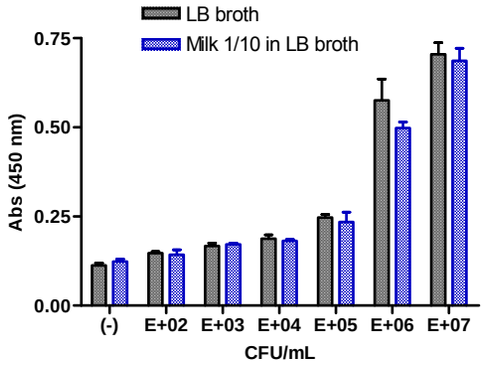

Fig.2- Results for the detection from 10^2 to 10^5 CFUmL^{-1} Salmonella cells in LB broth and skimmed-milk diluted 1/10 in LB. A biotin-phage dilution 1/100 and streptavidin-HRP 0.5 µg mL^{-1} was used. The error bars show the standard deviation for n = 3, except for the negative control (n = 10).

Conclusion

P22 was successfully biotinylated, providing a useful label for bacteria detection with the advantageous features of phages. The results of the IMS/phagosensing strategy are promising for the rapid and sensitive screening of food samples.

References

[1] M. Upmann, C. Bonaparte, "Rapid methods for food hygiene inspection", Robinson, R.K., Batt, C.A., Patel, P. Eds, Encyclopedia of Food Microbiology, Academic Press, pp 1887, 1999.
[2] K.S. Cudjoe, "Detection by Immunomagnetic Particle-based Assay", Robinson, R.K., Batt, C.A., Patel, P. Eds, Encyclopedia of Food Microbiology, Academic Press, pp 1968, 1999.
[3] A. Lermo, et. Al., Biosensors and Bioelectronics, Vol. 22, pp. 2010-2017, 2007.
[4] S. Liébana, et al., Biosensors and Bioelectronics, Vol. 25, pp. 510–513, 2009.
[5] A.E. Smartt, S. Ripp, Anal. Bioanal. Chem., Vol. 400, pp. 991-1007, 2011.
[6] W. Sun, L. Brovko, M.W. Griffits, J Ind Microbiol Biotechnol, Vol. 25, pp. 273–275, 2000.
[7] L. Gervais, et.al., Sens. Actuators B, Vol. 125, No. 2, pp. 615–621, 2007.

Citotoxicidad y Genotoxicidad de Nanoparticulas de SiO_2 y TiO_2 In Vitro

Fernando Pastrana[a], Diana Narvaez[b], Helena Groot[b], Alba Avila[a], Felipe Muñoz[c], Fabian Cuellar[d]

a. Facultad de Ingeniería Eléctrica y Electrónica, b. Laboratorio de Genética Humana, c. Facultad de Ingeniería Química, d. Facultad de Ingeniería Mecánica Universidad de los Andes, 111711, Bogota D.C. Colombia.
a-avila@uniandes.edu.co

Resumen.

Se estudio la citotoxicidad relacionada con nanopartículas de T_iO_2 y S_iO_2 con diámetro promedio de 32 nm en un cultivo de fibroblastos de hámster chino (CHOCK 1). El tiempo de exposición fue de 72 Horas para evaluar la citotoxicidad crónica utilizando concentraciones entre 0 y 60µg/ml. Mediante ensayos de MTT se determino que la viabilidad celular es inversamente proporcional a la concentración de nano partículas (NP).La prueba Cometa permitió identificar daños genéticos en concentraciones desde 0.01µg/ml.

Palabras Clave: Nanopartículas, TiO2, SiO2, Citotoxicidad, Genotoxicidad

Introducción.

Según la definición de la Organización Internacional de Estandarización (ISO) los nanomateriales son aquellos materiales donde al menos una de sus dimensiones se encuentra a nanoescala (1 y 100 nm) [1]. En la última década se ha incrementado el interés por las aplicaciones de los nanomateriales [2-4]. Materiales como los óxidos metálicos (T_iO_2) [5, 6] y los no metálicos (S_iO_2) han encontrado una gran variedad de aplicaciones [7, 8]. Según datos obtenidos en la base de datos en línea Nanotechnology Project (2012) hay más de 1318 productos, basados en nanotecnología de consumo en el mercado. Entes reguladores y de control reconocen que los nanomateriales sintetizados químicamente tienen información limitada de su toxicidad o no la poseen [9-13].

El objetivo de este estudio fue evaluar la citotoxicidad NP de T_iO_2 y S_iO_2 (32 nm) en fibroblastos de hámster chino (Chock 1) con Metilo tiazolil tetrazolio (MTT) y Azul de tripan (T. Mosmann., 1983) y la genotoxicidad de estas mismas con la prueba de COMETA.

Materiales y Métodos

Nanopartículas

Se utilizaron partículas de T_iO_2 y S_iO_2 de 32 nm fabricadas por la empresa Millennium Chemicals. Se suspendieron en agua des ionizada, sonicaron a 42 kHz y fueron esterilizadas con UV por una hora

Cultivo celular y tratamiento con nanopartículas.

Se usaron fibroblastos de hámster chino (CHOCK 1) suministradas por el laboratorio de genética Humana de la Universidad de los Andes (Bogotá, Colombia).el medio de cultivo celular usado fue RPMI (Roswell Park Memorial Institute médium).

Resultados.

MTT S_iO_2

En el test de MTT concentraciones de S_iO_2 inferiores a 0.01µg/ml no presentaron reducción en la viabilidad celular. Concentraciones de 0.1 µg/ml a 3 µg/ml la viabilidad se redujo entre el 9% y el 19%. La LD 50 (Dosis letal 50%) se encontró en los 10 µg/ml aproximadamente. La viabilidad celular a la concentración de 60 µg/ml fue del 2%

MTT T_iO_2

Para las NP de TiO_2 el test de MMT también evidencio una disminución de la viabilidad celular asociada al incremento de la concentración. A 15 µg/ml la viabilidad fue del 66%, con concentraciones de 30 µg/ml la viabilidad fue del 40% y finalmente a la concentración de 60 µg/ml el 30% presento

viabilidad. Determinando una menor citotoxicidad en este tipo de células del TiO_2 que del SiO_2.

Resultados prueba de azul de tripan.

El conteo células realizado 3 horas después de la prueba MTT en azul de tripan (tabla III), demostró un promedio superior al 80% (Gráfica 3 y 4) de viabilidad. Descartando que los resultados obtenidos en la prueba de cometa fueran causados por toxicidad normal

Ensayo del Cometa.

Se observo que las partículas de T_iO_2 y S_iO2 en bajas concentraciones (0.01 y 0.1 µg) no generaron una diferencia significativa con respecto al control, aunque las células expuestas a las NPs de T_iO_2 mostraron mayores índices de genotoxicidad. En las concentraciones de 1 y 10 µg la diferencia con respecto al control fue significativa, teniendo como resultado daño alto y daño total. (Gráfica 1). En la concentración 10µg/ml se observa que Las NP de S_iO_2 son mas toxicas que las de T_iO_2. Lo cual se correlaciona con la prueba MTT donde SiO_2 tuvo una menor viabilidad que TiO_2 a concentraciones de 60µg/ml. Sin embargo a concentraciones menores de 0.1µg/ml el comportamiento es opuesto.

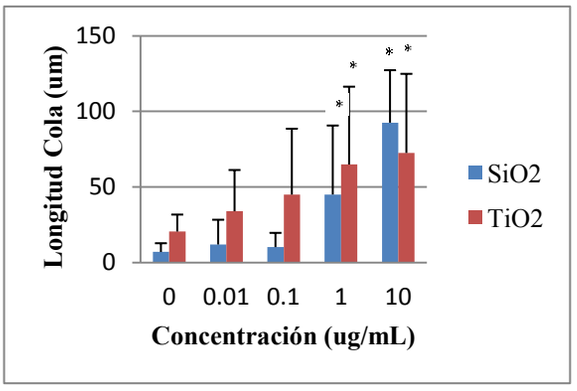

*Gráfica 1. Daño en el ADN inducido por la exposición a NPs, de acuerdo a la longitud de la cola en el Ensayo del Cometa. Barra de error igual a DE. * Diferencias significativas con respecto al control negativo (p < 0.01), prueba de Kruskal-Wallis.*

Conclusiones.

La utilización de NP de TiO_2 y SiO_2 en cultivos celulares de fibroblastos de ovario de ratón Chino, evidencio un comportamiento citotóxico y genotóxico por medio de la utilización de pruebas MTT y Cometa. Este comportamiento es dependiente de la concentración de NP que sean utilizadas.

Concentraciones altas superiores a 10µg/ml producen daños genéticos en cerca del 90% de las células para el caso de NP de SiO_2 y del 60% para el TiO_2.

En la evaluación de citotoxicidad y genotoxicidad es pertinente determinar las interacciones con otros factores: sistema inmune, proteínas plasmáticas entre otros. Se insta a realizar estudios para determinar límites de la exposición a estos materiales en productos comercializados. Que permitan garantizar la seguridad en la salud y el medio ambiente, previniendo efectos secundarios no deseados.

Al mismo tiempo, los investigadores también están expuestos y requieren Guías de Buenas Prácticas de Manipulación de Nanomateriales.

References

[1] I.-I. O. f. Standardization, "ISO/TS 80004-1:2010 - Nanotechnologies -- Vocabulary -- Part 1: Core terms," 2012.

[2] S. Parveen, R. Misra, and S. K. Sahoo, "Nanoparticles: a boon to drug delivery, therapeutics, diagnostics and imaging," *Nanomedicine: Nanotechnology, Biology and Medicine,* vol. 8, pp. 147-166, 2012.

[3] M. Cushen, J. Kerry, M. Morris, M. Cruz-Romero, and E. Cummins, "Nanotechnologies in the food industry – Recent developments, risks and regulation," *Trends in Food Science & Technology,* vol. 24, pp. 30-46, 2012.

[4] C. Underwood and A. W. van Eps, "Nanomedicine and veterinary science: The reality and the practicality," *The Veterinary Journal*.

[5] Y. Yu, J. Wang, and J. F. Parr, "Preparation and properties of TiO2/fumed silica composite photocatalytic materials," *Procedia Engineering,* vol. 27, pp. 448-456, 2012.

[6] R. Dastjerdi and M. Montazer, "A review on the application of inorganic nano-structured materials in the modification of textiles: Focus on anti-microbial properties," *Colloids and Surfaces B: Biointerfaces,* vol. 79, pp. 5-18, 2010.

[7] F. Iskandar, "Nanoparticle processing for optical applications – A review," *Advanced Powder Technology,* vol. 20, pp. 283-292, 2009.

[8] M. Boutonnet, S. Lögdberg, and E. Elm Svensson, "Recent developments in the application of nanoparticles prepared from w/o microemulsions in heterogeneous catalysis," *Current Opinion in Colloid & Interface Science,* vol. 13, pp. 270-286, 2008.

[9] U. S. EPA., "Nanomaterial Case Studies: Nanoscale Titanium Dioxide in Water Treatment and in Topical Sunscreen (Final).", U. S. E. P. Agency, Ed., ed. Washington, DC: U.S. Environmental Protection Agency, 2010.

[10] NIOSH, "Approaches to Safe Nanotechnology," D. o. H. a. H. Services, Ed., ed. Atlanta: DHHS (NIOSH), 2009.

[11] L. Ma-Hock, S. Brill, W. Wohlleben, P. M. A. Farias, C. R. Chaves, D. P. L. A. Tenório, A. Fontes, B. S. Santos, R. Landsiedel, V. Strauss, S. Treumann, and B. van Ravenzwaay, "Short term inhalation toxicity of a liquid aerosol of CdS/Cd(OH)2 core shell quantum dots in male Wistar rats," *Toxicology Letters,* vol. 208, pp. 115-124, 2012.

[12] E. R. Observatory, "Workplace Exposure to Nanoparticles," E. A. f. S. a. H. a. Work, Ed., ed, 2009.

[13] FDA. (2012, 24 Abril 2012). *Press Announcements > FDA issues draft guidance on nanotechnology* [WebContent]. Available: http://www.fda.gov/NewsEvents/Newsroom/PressAnnouncements/ucm301125.htm[

Electrochemical magneto immunosensor for the detection of anti-TG2 antibody in celiac disease

S. Kergaravat[1], S. Alegret[2], M.I. Pividori[2], S.R. Hernández[1]

[1] Laboratorio de Sensores y Biosensores, Universidad Nacional del Litoral, Argentina
[2] Grup de Sensors I Biosensors, Universitat Autònoma de Barcelona, Spain

08193, Bellaterra, Barcelona, Spain

E-mail Address: skergaravat@fbcb.unl.edu.ar

Abstract

A simple and fast method for the detection of anti-TG2 antibody in blood serum samples was developed based on an electrochemical magneto inmunosensor. These antibodies are widely used in the detection of celiac disease. Anti-TG2 antibodies were separated from the samples and preconcentrated using immunomagnetic separation. TG2 was immobilized over magnetic particles and the anti-TG2 antibodies were captured. Then, they were revealed by adding anti-IgG antibody labeled with peroxidase. Finally, the electrochemical detection was performed using a magneto electrode based on graphite epoxy composite and the response was detected by square wave voltametry. The merit figures of method such as limit of detection (LOD), limit of quantification (LOQ), sensitivity (EC50) and dynamic range were calculated. Fifty serums were evaluated by the developed method, showed a good correlation with an optical ELISA kit.

Keywords: anti-TG2 antibody, celiac disease, serum sample, electrochemical magneto immunosensor, magnetic beads

Introduction

Celiac disease (CD) is one of the most prevalent genetically-determined clinical conditions. It is characterized by an excessive immunological reaction against dietary gluten, reaction that starts in the small intestine. This reaction triggers an autoimmune response against several auto-antigens, and results in the development of intestinal and extraintestinal manifestations. Recently, the availability of sensitive noninvasive serological tests has made possible screening for celiac disease in general population. Most of them concluded that the most realistic prevalence may be 1 in 200 individuals or greater [1]. The anti-endomysium antibodies (AEA) by indirect immunofluorescence are used as serological CD markers due to its highly specificity. In 1997, the transglutaminase (TG2) was identified as the major target antigen recognized by AEA in patients with untreated CD [2]. The common methodology for the detection of anti-transglutaminase antibodies (IgA-ATG2) is an enzyme-linked immunosorbent assay (ELISA) with optic detection due to its high sensitivity and specificity in the CD [3]. Other alternatives are the electrochemical immunosensors which are based on the capture of antibodies against transglutaminase by immobilization of TG2 onto electrode surface [4]. These dispositive have revolutionized the modern analysis because their simplicity and speed in the response by direct transduction to electronic equipment. In their development, the magneto graphite-epoxy composite electrodes (m-GEC) are widely employed as transducers. They are cheap, easy to prepare, use, renew and modify. Moreover, the inclusion of MP has improved the LOD, the signal-to-noise ratio, sensitivity and analysis time [5]. The present work is focused on the electrochemical detection of ATG2. Initially, TG2 is immobilized to magnetic particles (MP). Then, ATG2 is captured by MP-TG2 and revealed by the antiIgG conjugate. Finally, the electrochemical response of the enzymatic reaction with their substrates is measured over the m-GEC.

Methods

a) Magneto inmunosensor procedure
The electrochemical magneto inmunosensor procedure was based on an indirect assay: (a) Immobilization of TG2 to MP and then incubation of MP-TG2 with ATG2-IgG; (b) Addition of anti-IgG antibodies label with peroxidase (antiIgG-HRP) and incubation; (c)

Addition of o-phenilendiamine (OPD) and H_2O_2; (d) Electrochemical detection in the m-GEC by square wave voltammetry in the range from 0 to -400 mV. Ag/AgCl and Pt were used as reference and auxiliary electrodes, respectively.
b) Validation assays
The standard curve was fitted to a four-parameter logistic equation and the merit figures were extracted. The precision tests were performed to ATG2 titers of 1:9200, 1:4800 and 1:3200. The interassay test was evaluated by multiple analysis in one assay while the intra-assay was assessed by analysis in three separate analytical runs. The calibration curves for the ATG2 titers which ranged from 1:70000 to 1:300 were built in buffer, negative plasma diluted 1:25 and negative serum diluted 1:25 for evaluating matrix effect. Then, recovery tests were performed by three ATG2 titers (1:2000, 1:3540 and 1:5110) spiked in negative serum and plasma diluted 1:25. Fifty samples were analyzed by this methodology and correlated with an optical ELISA kit.

Results

Magneto inmunosensor procedure

An immunoassay for the ATG2 detection was performed by an indirect assay. The detection system, the MP-TG2 concentration and the antiIgG-HRP title were optimized. First, OPD was selected as cosubstrate due to its highest electrochemical efficiency as HRP cosubstrate in comparison with the other evaluated seven cosubstrates. Second, concentrations of MP-TG2 from 0.25 to 1 mg mL^{-1} were tested against dilutions of ATG2 from 1:20000 to 1:800 and antiIgG-HRP antibody of 1:20000. 0.75 mg mL^{-1} of MP-TG2 was chosen due to the fact that it presented higher electrochemical response with wider dynamic range. Third, the antiIgG-HRP title was optimized by incubation of 0.75 mg mL^{-1} MP-TG2 with dilutions of ATG2 from 1:20000 to 1:800 and antiIgG-HRP dilutions from 1:10000 to 1:30000. The antiIgG-HRP title of 1:20000 was selected due to the lower LOD and wider dynamic range obtained. The typical voltammogram of assay is showed in Fig. 1.

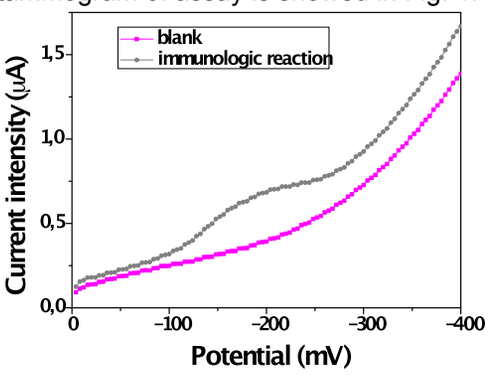

Fig. 1

Validation assays

The standard curve of ATG2 is showed in Fig. 2. EC50, LOD and dynamic range were 1:5715, 1:14223 and from 1:10328 to 1:3013 of ATG2 titers, respectively. Interassay and intrassay tests presented CV less than 20% (n = 3). Absence of matrix effect was observed. Recoveries of ATG2 in serum and plasma ranged from 94 to 123 % with CV less than 8% (n = 3). Fifty positive and negative serums were analyzed by electrochemical magneto inmunosensor and showed 94 % of correlation with optical ELISA kit.

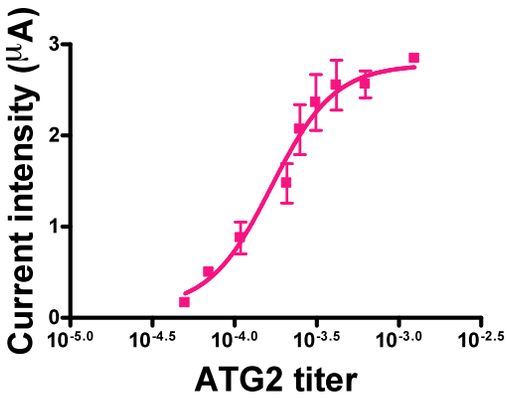

Fig. 2

Conclusions

A simple electrochemical magneto immunosensor have been developed. The utility of the bioassay was demonstrated for the detection of ATG2 in celiac patients.
TG2 was easily immobilized to the MP with a good efficiency of coupling and possible matrix interferences could be eliminated. Moreover, the use of magnetic beads and electrochemical detection provided improved features regarding sensitivity of the assays.

References

[1] J.C. Gomez, G.S. Selvaggio, M. Viola, B. Pizarro, G. la Motta, S. de Barrio, R. Castelletto, R. Echeverría, E. Sugai, H. Vazquez, E. Mauriño, J.C. Bai, Am. J. Gastroenterol., 96: 2700-2704, 2001.

[2] A. Mankaï, W. Sakly, H. Landolsi, L. Gueddah, B. Sriha, A. Ayadi, M.T. Sfar, K. Skandrani, A. Harbi, A.S. Essoussi, S. Korbi, N. Fabien, M. Jeddi, I. Ghedira, Pathol. Biol., 53: 204–209, 2005.

[3] A. Miller, W. Paspaliaris, P.R. Elliott, A. d'Apice, Aust. N.Z.J. Med., 29: 239-242, 1999.

[4] T. Balkenhohl, F. Lisdat, Anal. Chim. Acta, 597: 50–57 2007.

[5] E. Zacco, M.I. Pividori, S. Alegret, R. Galve, M.P. Marco, Anal. Chem., 78: 1788–1789, 2006.

Chapter 11: Research Networks and Education

Development of Microsensors and Applications under the INCT NAMITEC Network

Jacobus W. Swart[1], José A. Diniz[1,2], Stanislav Moshkalev[2], Jair F. de Souza[2,3]
[1]FEEC/UNICAMP, [2]CCS/UNICAMP, UNICAMP and [3]CTI
13.083-852, Campinas, SP, Brazil
jacobus@fee.unicamp.br

Abstract

INCT NAMITEC is the acronym for a research network on micro and nanoelectronics in Brazil. It has over 150 researchers from 25 participating institutions. It covers a broad spectrum of micro and nanoelectronics activities, including wireless sensor networks (WSN) and sensor development. This paper presents a general overview about the INCT NAMITEC network, with emphasis on the sensors and WSN applications.

Keywords: Sensors, Wireless Sensor Networks, ISFET, CNT, gas sensor.

The INCT NAMITEC Network

The INCT program or Institutos Nacionais de Ciência e Tecnologia, was launched through a public call by CNPq in Brazil at the end of 2008, as a continuation of the Millennium Institute Program. One of the over 120 approved projects in all the fields was the NAMITEC Network (Micro and Nanoelectronics Systems). This network was first created in 2001 under the Millennium Institute program and gradually increased in size and activities, starting with 60 researchers from 8 institutions to presently 155 researchers from 25 institutions.

The objectives of the INCT program is not only support for research, but also foster education, formation of human resources, transfer of knowledge to society and industry. So, NAMITEC is active in all these fields and the main results can be summarized as follows: publication of about 6 books, 100 peer reviewed journal papers, 270 papers at conferences and 3 patents, all in average per year; graduation of 50 master and 20 PhD degrees per year; participation on 3 expositions per year and interaction or collaboration with about 50 companies for knowledge transfer during the last 3 years [1].

The research areas within the network cover 5 main subjects: System-on-Chip and Wireless Sensor Networks (WSN); ICs and IP blocks library design and associated methodologies; development of Electronic Design Automation tools; semiconductor devices and materials and fabrication techniques [1]. In the area of semiconductor devices, many different sensors are worked-on. Similarly, many WSN applications are developed. In this paper the different WSN and sensor are summarized and two sensor types are presented in more detail.

WSN and Sensors

Different groups within the INCT NAMITEC are working on WSN architectures, including protocols, signal processing, energy harvesting, low power consumption and different applications. The applications are now grouped under two main sub-areas: ambient or ecological applications and agricultural and livestock applications. Also design of SoC and discrete WSN nodes are being developed. Examples of WSN being developed are now described. a) Detection and identification of the sound of frogs to identify the type, number and size of the frogs in the ambient. This helps biologists to monitor the environment and to study the animals. b) Air quality monitoring in an urban area, to monitor pollution emission by industry and traffic. c) Monitoring Free Air CO_2 Enrichment (FACE project) in open field areas. d) Ambient Monitoring applied to the Amazon forest areas, measuring relative humidity, temperature and ambient pressure. A low cost WSN was developed for this application. e) Monitoring leakage current at lightning protection for high voltage networks. By monitoring the 3td harmonic of the resistive component of the leakage current and its time evolution it is possible to predict the maintenance actions. An inductive magnetic sensor based on nanocrystalline alloy was developed for the MSN node. f) An instrumental sphere node to monitor fruit and other goods transportation to monitor acceleration,

temperature and humidity parameters. A specific low cost node was developed.

The sensor development works can be grouped under electrical sensors, optical sensors and electomechanical sensors. The electrical sensors include the Ion Sensitive Field Effect Transistor – ISFET, chemical sensors based on polymeric micro and nanofibers, CNT or grapheme, chemical sensors for hydrogen and acetylene and organic chemical sensors. The optical sensors include photometry and imaging at the THz band spectrum and a position sensitive multiple photodetector. The electrochemical sensors include microelectro-mechanical sensors, a photo-acoustic spectrometer using a camera with pressure chip to characterize biofuels, SAW sensors with nanostructured sensitive films and a silicon-polymer conductor flexible cantilever as a water vapor sensor. These devices are developed mainly at 4 different laboratories within the network with clean room facilities. Two of these sensors are described in more detail: a) The ISFET and b) a gas sensor based on CNT's.

ISFET Development

ISFETs have been developed, using different gate dielectrics (silicon nitride, aluminum nitride [3,4], tantalum oxide and titanium oxide [2]) to get: high sensibility, response linear, reduced thermal instability and robust devices. Figure 1 presents an overview of part of array with 78 ISFETs, where the gates are opened to detect the pH solution. These ISFETs are packaged in alumina substrate with polymer passivation, which was developed to resist the corrosion of chemical solution. In this period, these ISFETs have been tested using the packaging presented in Figure 1. One example is presented in the next item.

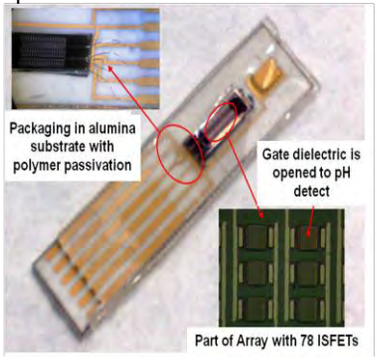

Fig.1 pH sensor with array of 78 ISFETs.

Silicon nitride (SiNx) films have been obtained by Low Pressure Chemical Vapor Deposition (LPCVD) at temperature of 720°C for 30 min, using different ratios of $[SiH_2Cl_2]/[NH_3]$ reagent gases. These films been used as ISFET gate dielectric. Using the packaging presented in Figure 1, these ISFETs were characterized, measuring current between source and drain (I_{DS}) versus time of immersion of device in three different pH solutions. The voltage of 2V between source and gate ($V_{GS} = V_{ref}$) was equal the voltage between source and drain (V_{DS}), in saturation region, for ISFETs. In this case, sensibility of S=1,24 mA/pH was estimated.

Low Power CNT gas sensor

Gas sensors were fabricated using decorated multi-wall carbon nanotubes (CNT) [5]. The CNT's are deposited between two contact electrodes using a dielectrophoresis process and a chemical process was used to decorate the CNT's with metal oxide nanoparticles [6,7]. Two structures were used, first with the CNT's deposited between the electrodes on top of the silicon-oxide surface and the second with the CNT's suspended over a deep trench between the electrodes, as shown in figure 2, together with the response to an oxygen gas, indication the superior sensitivity for the suspended structure, even without heating the substrate.

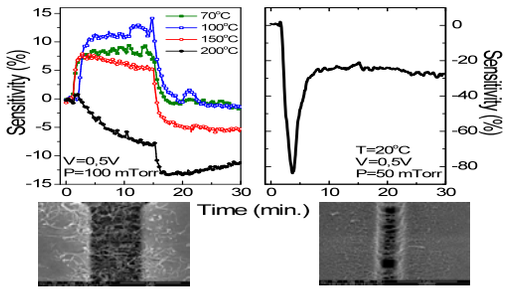

Fig.2 Sensor response to O2 pulses for Ti-decorated CNTs, in supported (left) or suspended (right) configurations.

Conclusion

Very promising results are obtained in the field of sensors and wireless sensor networks, besides other results obtained within the NAMITEC network. The 10 years experience of the network has resulted in great benefit for the member institutions located in the different regions in the country, including emerging areas and institutions, as in the northeast and north.

References

[1] http://namitec.cti.gov.br
[2] Barros, A.D., Albertin, K.F., Miyoshi, J., Doi, I., Diniz, J.A., Microelectronic Engineering, 87 (2010) 443–446.
[3] M.A. Moreira, I. Doi , J.F. Souza, J.A. Diniz, Microelectronic Engineering 88, 802–806, 2011.
[4] J. F. Souza, M. A. Moreira, I. Doi, J. A. Diniz, P. J. Tatsch, and J. L. Gonçalve, Physica Status Solidi C, in press.
[5]. Gelamo R.V., Rouxinol, F.P.M., Verissimo, C., Moraes, M. B., Moshkalev, S.A., Sensor Lett., 2010. v. 8. p.488-492.
[6]. Leon J., S.A. Moshkalev, C. Verissimo, A. Vaz, A. Flacker, M. B. de Moraes, J. Nanosci. Nanotechnol. 2010, v. 10. 6234 - 6239.
[7]. S.A. Moshkalev, J. Leon, C. Verissimo, A. Vaz, A. Flacker, M. B. de Moraes, J. W. Swart, J. Nano Research, v.3, p.25 - 32, 2008.

Portable, $5 Microfluidics Laboratory for Education and Outreach

R. Perez-Castillejos[1,*] A.B. Shrirao[1], A. Raman[1,2], E. Ryll[1], A. Disame[1], and H. Talasan[1]
[1] New Jersey Institute of Technology (NJIT), 07102, Newark, NJ, USA
[2] Marlboro High School, 07746, Marlboro, NJ, USA
* raquelpc@njit.edu

Abstract

Access to the design and use of microfluidic devices has been traditionally limited to those with access to a cleanroom or facilities for the fabrication of miniaturized devices. Here we present a method for inexpensively and easily implementing an educational laboratory for the design, fabrication, and test of microfluidic devices. For its simplicity, we base our developments on the well known process called *soft lithography*, which starts with a master that is typically made of photoresist micropatterned using conventional photolithography in a cleanroom. Our method to design, fabricate, and test microfluidic devices uses bench-top materials and tools: paper, drawing tool (pencil, pen, or printer), adhesive tape, scalpel, glass or plastic slides, commercially available uncured silicone (polydimethylsiloxane), containers (such as polystyrene Petri dishes), dyes (colored ink or food coloring dyes), and disposable pipettes. One tape-based master can be used for casting PDMS tens to hundreds of times. Differently than other pre-college educational approaches to microfluidics, which are limited to replicating and testing a prefabricated master, the method presented here allows students to design and fabricate their own devices. This method does not require the use of expensive apparatuses/materials, and can be implemented in any room simply equipped with tables.

Keywords: microfluidics, educational, outreach, teaching lab, portable, low-cost

Flow in the microscale is governed by viscous and capillary forces [1] whereas in the macroscale, flow is typically convective—i.e., governed by inertial forces. From a pedagogical perspective, microfluidic devices provide a unique window into the unintuitive fluidic conditions surrounding microorganisms such as bacteria, algae, or plankton [2]. Although the field of microfluidics and lab-on-a-chip has already reached adulthood [3], its integration into the educational curricula remains in its infancy [4] due to the challenges associated with taking all the steps of microfluidic creation (i.e., concept, design, fabrication, and test) into the classroom. One must note that even if your institution has a cleanroom, it is also very challenging to take into the cleanroom all the students registered for a course. Therefore, students interested in Lab on a Chip (LoC) need to join a microfluidics research lab (if available in their campus) that provides them with the required equipment and hands-on training. As a result, most engineers and scientists currently graduate with no or reduced knowledge of microfluidics, which is typically limited to introductory theoretical courses that follow specialized books and/or use simulation tools. The limited exposure of graduates to microfluidics translates into limited awareness of microfluidics in industry, and ultimately hinders the use of microfluidics by industry in cases when miniaturized approaches could optimize operations and minimize production cost. Here we introduce an educational protocol that would allow the easy implementation of a microfluidics teaching laboratory in any classroom for a minimal cost. In line with the STEAMD pedagogical philosophy [5]—which aims at integrating the learning of Science, Technology, Engineering, Art, Mathematics, and Design—this teaching laboratory will make it possible for the students to develop (from concept to characterization) simple microfluidic devices.

Two concepts are key in implementing the Teaching Microfluidics Lab presented here: (1) **cleanroom-free fabrication of microfluidic devices** based on soft lithography [6], and (2) **pump-free liquid transport of liquids for testing the microfluidic devices**.

Microfluidic devices will be produced by casting PDMS onto a master made of adhesive tape patterned manually with a blade; the blade-patterned tape substitutes the master made of UV-patterned photoresist of standard soft lithography. These microfluidic devices exhibit a height (distance between the substrate and the ceiling of the device) of ~ 60 µm, in agreement with the thickness of the tape, and will result in laminar flows (Fig. 1). The materials and tools needed for this technology kit are Scotch® tape,

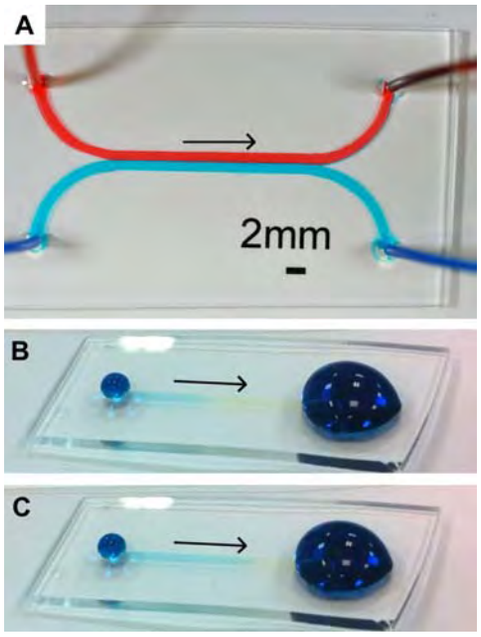

Figure 1. (A, B, C) Photos of microfluidic devices fabricated using tape-based soft lithography. Devices were tested by using (A) a syringe or (B, C) passive capillary-driven transport. Arrows show the direction of the fluid flow. The time elapsed between B and C was ~20 seconds. Co-authors E. Ryll, A. Disame, and H. Talasan designed, created, and tested the device in B, C in a teaching lab prototyping the procedures presented here.

blade, glass or plastic slides, commercial uncured PDMS, and Petri dishes—or another suitable container such as a baking mold. We have tested this fabrication route for different applications, including the patterning of mammalian cells for studying the collective processes conductive to wound healing [7-9].

In order for this microfluidics teaching lab to have minimal cost and maximal portability, we chose to induce liquid flow by capillary force from one inlet (with the smallest drop) to the other (with the largest drop) [10]. Notably, this approach eliminated the need for a syringe pump in order to test the devices (Fig. 1B,C).

We have tested the feasibility of this portable, $5 microfluidics lab as a pedagogical tool for students of different levels, from high school to undergraduates. We organized a 5-h workshop (2 sessions of ~2.5h each) in which undergraduate students produced their microfluidic devices and characterized them with food dyes and their digital cameras (e.g., their cell phones), as shown in Fig. 1B,C. In their assessment, the participating students stated that the workshop allowed them to understand concepts of microfluidics that were unclear after the introductory slides and movies. Additionally, one of the co-authors (A. Raman), a local high school student, was invited this past summer to record a video manual that could be used to guide the implementation of this teaching lab in high schools. *(If accepted for publication, this video manual will be published as supplementary material.)*

Figure 2. Photo showing the setup used for prototyping the microfluidics teaching lab described here.

We present here a pedagogical route to integrate hands-on microfluidics modules to pre-college and undergraduate curricula. The approach is committed to provide students with access to all the stages of the production of a microfluidic device (design, fabrication, and test) while keeping the practical requirements for implementing this teaching approach within the reach (in terms of cost and logistics) of most non-graduate educational settings. Despite we are limited in this abstract by the limited space, we look forward to go into the details of our approach in our presentation (and publication, if the manuscript gets accepted).

References

[1] H.A. Stone, A.D. Strook, A. Ajdari, Annu. Rev. Fluid Mech., Vol. 36, pp. 381-411, 2004.

[2] E.M. Purcell, Am. J. Phys., Vol. 45, pp. 3-11, 1977.

[3] A. Manz, N. Graber, H.M. Widmer, Sens. Act. B, *Vol.* 1, pp. 244-248, 1990.

[4] H. Becker, Lab Chip, Vol. 10, pp. 2497-2498, 2010.

[5] NSF/RISD Bridging STEM to STEAM Workshop, http://www.stemtosteam.org/archive/nsf-risd-workshop.

[6] D. Qin, Y. Xia, G.M. Whitesides, Nat. Prot., Vol. 5, pp.491-502, 2010.

[7] A.B. Shrirao, R. Perez-Castillejos, Mid-Atlantic ASEE conference, Easton, PA, 2010.

[8] A.B. Shrirao, R. Perez-Castillejos, Lab Chip: Chips & Tips, 2010.

[9] A.B. Shrirao, A. Hussain, C.H. Cho, R. Perez-Castillejos, Biotechniques Rapid Dispatches, 2012.

[10] G.M. Walker, D.J. Beebe, Lab Chip, Vol. 2, p.131, 2002.